

# Algebraic solutions to the dynamics of dissipative many-body quantum systems



Cameron Booker

Lady Margaret Hall

University of Oxford

A thesis submitted for the degree of

*Doctor of Philosophy*

Lent 2022

# Acknowledgements

Science is never completed in isolation, and I am indebted to many people for their assistance. Firstly I must recognise my two supervisors, Dieter Jaksch and Berislav Būca. To Dieter, I owe my begrudging transformation from a mathematician to a physicist. As painful as it has sometimes been, your guidance on making abstract maths applicable and exciting to a broad audience of physicists has been invaluable and has improved my work immeasurably. To Beri, I thank you for your endless enthusiasm, understanding and support throughout the last few years. I had no idea how to start a DPhil when I joined Oxford, but it is thanks to your continued advice and willingness to discuss that I have completed this thesis. I am incredibly proud of the work we have achieved together, and I wish you all the best in your future endeavours and ambitious research programme. I will forever remember that ‘theoretical physics is not an exact science’.

I would also like to thank Marko Medenjak. Although not my supervisor, your input as a collaborator has been incredibly valuable, and your tolerance with my slowness at times was much appreciated.

Beyond those I have directly worked with, I thank the rest of the Jaksch group, both past and present. Even though we have been working from all over the country/world for most of my DPhil, the weekly group meetings and ‘Corona Cafe’ have provided much needed social contact and some very stimulating discussions. Specifically, I am grateful to Ben, Nick and Joey for their help with my feeble attempts to write code, particularly understanding what on earth a pointer was, and to Lewis for opening the door and making me feel productive because at least I wasn’t asleep at my desk!

Throughout my DPhil, I have been very aware that it was the culmination of a journey that began long ago at Farnborough Sixth. As such, I must thank Kayoko Koyama, without whom it would never have even started. I cannot express how grateful I am for all the time and effort you dedicated to me as I applied for Cambridge maths. I hope I have been able to channel your enthusiasm and dedication to the student I have tutored myself.

I would also not have managed to make it to this point without the endless support of my family throughout my time at university, and of course, even before that. I’m not sure that any of us expected that when you dropped me off for the first time at Homerton that this is where I would end up. You always seem to put up with me discussing far more maths than is probably acceptable over the dinner table or while walking the dogs, especially during those long lockdown months. It has certainly been far from smooth sailing since leaving for Cambridge. Without your continued love, advice, support, and those termly trips to Trumpington Waitrose, I would never have been able to achieve anything near as much as I have.

Finally, and in many ways, most importantly, I must express my endless and limitless thanks to Rosie. This is almost as much your thesis as it is mine, as without you it would never have been started let alone finished. Your free python or git support has been essential several times, as well as being a willing guinea pig for my talks and presentations. You quite possibly know it better than me, especially after your tireless effort to correct my haphazard spelling of Hamilontian and Louvillan. You have shown impressive tolerance and patience with me when I struggled to keep going or worked at stupid hours. I hope you are as excited as I am to move on from this rather stressful few years and to enjoy life together in the real world with proper jobs and inevitably more pets!

# Abstract

From the motion of hurricanes to the cooling of a cup of tea, dissipative dynamics are ubiquitous in nature. Unfortunately, when studying lattice-based strongly correlated quantum systems, a common focus of experiments and highly relevant for material science, the curse of dimensionality prevents us from directly solving the exact equations describing the dissipative motion. We instead often use approximations and numerical analysis, as few analytical techniques currently exist which can provide useful insights.

This thesis studies the constraints that non-abelian algebraic structures place on the dynamics of such non-equilibrium many-body quantum systems. In doing so, we develop novel algebraic methods that provide previously absent analytic insight into a range of problems. We apply these new techniques to study dynamical phases of quantum matter that are of both theoretical and experimental interest.

We study how simple algebraic structures imply persistent non-stationarity in dissipative many-body quantum systems. These results enable us to develop a theory of quantum synchronisation based on symmetries and to explore a novel class of time crystals where order is induced by noise. These dynamical phases of matter have been gaining recent interest for their insights into thermalisation and their potential application in quantum technologies. We therefore use our results to explore experimentally realisable models.

We also use the general principles of prethermalisation to propose a new theory to potentially explain recent experiments studying light-induced superconductivity in terms of  $\eta$ -pairing and approximate symmetries. We discuss the merits and weaknesses of our proposal in relation to the experimental evidence. We also indicate techniques that, within our theory, stabilise superconducting states by harnessing the quantum Zeno effect

For certain systems, known as integrable, there are enough symmetries to allow for exact solutions using the Bethe ansatz. We demonstrate that Bethe ansatz techniques can be extended and applied to non-equilibrium problems. As an example, we use this method to analytically study the dynamical phase transitions of an XXZ spin chain with boundary loss.

# Contents

<b>Acknowledgements</b>	<b>ii</b>
<b>Abstract</b>	<b>iv</b>
<b>Contents</b>	<b>v</b>
<b>List of figures</b>	<b>ix</b>
<b>List of publications</b>	<b>xi</b>
<b>Resources and funding</b>	<b>xii</b>
<b>1 Non-equilibrium many-body quantum mechanics</b>	<b>1</b>
1 Many-body quantum mechanics and emergent dynamics . . . . .	2
1.1 Approximate numerical methods . . . . .	3
1.2 Thermalisation . . . . .	4
2 Open quantum systems . . . . .	6
2.1 Density operator formalism . . . . .	7
2.2 The Lindblad equation . . . . .	12
2.3 Solving the Lindblad equation . . . . .	19
3 Symmetries in quantum systems and their generalisations . . . . .	21
3.1 Groups and representations . . . . .	21
3.2 Symmetries and conservation laws . . . . .	22
3.3 Applications of symmetries . . . . .	26
4 Dynamical phases of matter and their technological applications . .	28
5 Summary . . . . .	30
<b>2 Integrable systems in the presence of dissipation</b>	<b>32</b>
1 Introduction to integrability . . . . .	33
1.1 Integrability of a quantum system and the Yang-Baxter equations . . . . .	33
1.2 Coordinate Bethe-ansatz . . . . .	37
1.3 Discussion . . . . .	38

2	Dissipative Bethe Ansatz . . . . .	39
2.1	Spectral solutions to models with loss . . . . .	40
2.2	Examples of dissipative quantum models solvable by the dissipative Bethe ansatz . . . . .	42
2.3	Application to a boundary loss XXZ model . . . . .	44
2.4	Extensions to the thermodynamic limit . . . . .	54
2.5	Discussion . . . . .	59
3	Generalised Hydrodynamics with dissipation . . . . .	59
3.1	Introduction to GHD . . . . .	60
3.2	Lossy systems . . . . .	63
3.3	Dephased systems . . . . .	64
4	Conclusions . . . . .	65
<b>3</b>	<b>Algebraic conditions for persistent non-stationarity in dissipative systems</b>	<b>66</b>
1	Solutions to long time dynamics of time homogeneous open systems	67
2	Conditions for persistent non-stationarity in quantum systems . . .	68
3	Perturbations to systems possessing purely imaginary eigenvalues .	76
3.1	Ultra-low frequency and Zeno dynamics . . . . .	76
3.2	Metastable dynamics . . . . .	77
4	Summary . . . . .	80
<b>4</b>	<b>Dissipative time crystals</b>	<b>82</b>
1	The origins of time crystals . . . . .	83
2	Definition of dissipative time crystals and their spectral requirements	85
2.1	Definition . . . . .	85
2.2	Spectral requirements . . . . .	86
2.3	Relation to boundary time crystals . . . . .	87
3	Dissipative time crystals in a heated Hubbard model . . . . .	89
3.1	Measures of time crystalinity . . . . .	89
3.2	Closed Hubbard model . . . . .	90
3.3	Two-body loss . . . . .	93
3.4	Two-body loss and gain . . . . .	95
3.5	Perturbations . . . . .	97
3.6	Discussion . . . . .	102
4	Dissipative Floquet time crystals in a heated Hubbard model . . . .	104
4.1	Periodically driven heated Hubbard model . . . . .	104
4.2	Stability to Gaussian noise . . . . .	105
4.3	Discussion . . . . .	107
5	Conclusions . . . . .	111

<b>5</b>	<b>Quantum synchronisation</b>	<b>113</b>
1	Introduction to synchronisation . . . . .	114
1.1	General synchronisation . . . . .	114
1.2	Quantum synchronisation . . . . .	117
1.3	Definitions . . . . .	118
2	Algebraic conditions for quantum synchronisation . . . . .	120
2.1	Stable synchronisation . . . . .	120
2.2	Metastable synchronisation . . . . .	125
2.3	Comparison between quantum and classical synchronisation	126
3	Examples . . . . .	127
3.1	Anti-synchronising two spin-1/2s . . . . .	128
3.2	Driven-dissipative spin-1 pair . . . . .	130
3.3	Lattice models with translationally invariant non-abelian symmetries . . . . .	136
4	Conclusions . . . . .	143
<b>6</b>	<b>Engineering superconductivity through symmetries</b>	<b>145</b>
1	Conventional vs. light-induced superconductivity . . . . .	146
2	Theoretical background . . . . .	148
2.1	ODLRO and superconductivity . . . . .	148
2.2	Prethermalisation . . . . .	149
3	Possible explanation of experimentally observed superconductivity .	150
3.1	Description of underlying Hamiltonian . . . . .	151
3.2	Microscopic description of the laser pulse and the induction of ODLRO . . . . .	152
3.3	Superconductivity following the laser pulse . . . . .	155
3.4	Predictions of the theory and agreement with experimental evidence . . . . .	161
4	Stabilising the superconducting state . . . . .	162
4.1	Stabilisation from the quantum Zeno effect . . . . .	162
4.2	Possible realisations . . . . .	165
5	Conclusions . . . . .	166
<b>7</b>	<b>Conclusions and outlook</b>	<b>168</b>
<b>Appendices</b>		
<b>A</b>	<b>The Jordan-Wigner transformation</b>	<b>173</b>
<b>B</b>	<b>Matrix product state calculations</b>	<b>175</b>
1	The MPS ansatz . . . . .	175

2	Matrix product operators . . . . .	177
3	Time evolution operators . . . . .	179
<b>C</b>	<b>Tensor network methods for the dynamics of open systems</b>	<b>181</b>
1	Quantum Monte-Carlo . . . . .	181
2	Ancilla MPS description . . . . .	182
	<b>References</b>	<b>184</b>



# List of figures

2.1	Liouvillian gap for boundary loss XXZ model . . . . .	47
2.2	Liouvillian spectrum of boundary loss XXZ model for increasing $\Delta$	50
2.3	Spin profile of boundary bound states . . . . .	51
2.4	Time evolution of boundary loss XXZ model in easy axes regime .	53
2.5	Time evolution of boundary loss XXZ model in easy plane regime	54
2.6	Comparison between dynamics and top-magnon decay rates . . .	55
2.7	Dynamical phase transition at $\Delta \approx 1$ . . . . .	56
2.8	Bethe roots of the Lieb-Liniger model with complex interaction .	58
2.9	Separation of scales for hydrodynamics . . . . .	60
4.1	Spectrum of a closed Hubbard model . . . . .	92
4.2	Dynamics of a closed Hubbard model . . . . .	93
4.3	Spectrum of a Hubbard model with pure two-body loss . . . . .	94
4.4	Dynamics of a Hubbard model with pure two-body loss . . . . .	95
4.5	Spectrum of a Hubbard model with two body loss and gain . . . .	97
4.6	Dynamics of a Hubbard model with two body loss and gain . . . .	98
4.7	Individual trajectories for a Hubbard model with two body loss and gain . . . . .	99
4.8	Spectrum of a Hubbard model with two body loss and gain and an inhomogeneous magnetic field . . . . .	100
4.9	Dynamics of a Hubbard model with two body loss and gain and an inhomogeneous magnetic field . . . . .	101
4.10	Behaviours of eigenvalues for a Hubbard model with two body loss and gain and an inhomogeneous magnetic field . . . . .	102
4.11	Dissipative Floquet time crystals in the heated Hubbard model .	106
4.12	Dissipative Floquet time crystals in the heated Hubbard model with additive Gaussian noise . . . . .	108
4.13	Dissipative Floquet time crystals in the heated Hubbard model with multiplicative Gaussian noise . . . . .	109
5.1	Illustration of a generic many-body open quantum system with finite dimension local Hilbert space . . . . .	118

5.2	Visualisation of the different definitions of synchronisation . . . . .	121
5.3	Illustration of 3 interacting spin-1/2 particles . . . . .	128
5.4	Antisynchronised spin-1/2 particles . . . . .	130
5.5	Bloch sphere representation of antisynchronised spin-1/2 particles	131
5.6	Evolution of inverted limit cycle model . . . . .	133
5.7	Evolution of the detuned inverted limit cycle model in the Zeno limit	135
5.8	Evolution of pure gain spin-1 model . . . . .	136
5.9	Synchronisation in the Fermi-Hubbard model with spin agnostic heating . . . . .	138
5.10	Comparison with experimental data for $SU(N)$ fermionic atoms in optical lattices . . . . .	142
6.1	Illustration of 1D ring geometry . . . . .	157
6.2	Meissner stiffness of a 1D Hubbard model . . . . .	159
6.3	Comparison between predicted resistivity and experimental data .	163
6.4	Stabilising $\eta$ -pairs through dissipation . . . . .	164
A.1	Jordan-Wigner ladder . . . . .	174

# List of publications

Many of the results in this thesis have been published in the works listed below. In each case, CB's specific contributions are detailed. Some passages written by CB in these works have been reproduced essentially verbatim in the chapters indicated.

**Chapter 2:** Bethe ansatz approach for dissipation: exact solutions of quantum many-body dynamics under loss. B Buča, C Booker, M Medenjak, D Jaksch - New Journal of Physics, 2020.

*CB performed all the numerical simulations and calculations, derived the Bethe equations for the boundary loss XXZ model, found and analysed the dynamical phase transition, derived expressions for the Liouvillian eigenstates and contributed substantially to the writing of the article.*

**Chapters 3 & 5:** Algebraic theory of quantum synchronization and limit cycles under dissipation. B Buča, C Booker, D Jaksch - SciPost Physics, 2022.

*CB stated and proved Thm 3 and Cor 5, classified the modes of metastable synchronisation, formulated the working definitions of synchronisation, contributed to the proofs of Thms. 1 & 2 and Cors. 2 & 3, performed all numerical simulations, studied the examples and wrote the majority of the manuscript.*

**Chapter 4:** Non-stationarity and dissipative time crystals: spectral properties and finite-size effects. C Booker, B Buča, D Jaksch - New Journal of Physics, 2020.

*CB performed the analytic and numerical calculations, explored the possible observables to detect dissipative time crystals and wrote the article with advice and contributions from BB & DJ.*

**Chapter 6:** Infinite Temperature Superconductivity. B Buča, C Booker, M Medenjak, M Buzzi, A Cavalleri, D Jaksch - In preparation, 2022.

*CB contributed to developing the fundamental ideas of the theory and connecting the theory with experimental evidence, performed extensive analytic calculations for various parts of the theory, performed most of the numerical simulations and contributed significantly to the writing of the manuscript.*

# Resources and funding

## Funding

The author gratefully acknowledges funding from the EPSRC Doctoral Training Programme awarded by the University of Oxford Physics Department.

## Computational resources

The simulations presented in this thesis were performed using the following libraries

- Qutip - <https://qutip.org/>
- TNT library - <http://www.tensornetworktheory.org/documentation/>
- ITensor - <https://itensor.org/>

The author would also like to acknowledge the use of the University of Oxford Advanced Research Computing (ARC) facility in carrying out this work - <http://dx.doi.org/10.5281/zenodo.22558>

# 1

## Non-equilibrium many-body quantum mechanics

The central aim of this thesis is to develop new analytic insights into the dynamics of non-equilibrium many-body quantum systems. Our approach will be to study the constraints that non-abelian symmetries place on the dynamics of non-equilibrium many-body quantum systems and, in doing so, develop novel algebraic methods that provide previously absent analytic insight to a range of problems. The key advantage of such methods based on the algebra of quantum mechanical operators is that they are generally independent of system size, making them easier to apply to many-body systems and have the additional advantage of being rigorously well defined in the thermodynamic limit through  $C^*$ -algebras. Our aim is motivated by the desire to understand dynamical phases in the types of lattice-based out of equilibrium quantum systems that are prevalent throughout experimental physics, material science and quantum technologies. Consequently, throughout this thesis we will use our theoretical results to study experimentally relevant models.

We will begin this thesis by providing a comprehensive introduction to non-equilibrium many-body quantum systems in order to explain the key results and highlight the numerous challenges in the field. This will further motivate our approach of using algebraic techniques. Our introduction will finish by discussing the types of systems and the particular dynamical phases of matter that we will focus on in the remainder of the thesis.

# 1 Many-body quantum mechanics and emergent dynamics

In 1972, Nobel Laureate Philip Anderson claimed in his essay “More is Different” [1] that the complex dynamics observed in the world around us cannot be explained and understood directly from a fundamental quantum theory. This view is at odds with the longstanding reductionist hypothesis that is prevalent throughout science. However, 50 years later, it would appear Anderson is correct as relatively little progress has been made towards connecting the quantum world of few particles and the classical world around us. This is despite the wide application of such an understanding to a diverse range of fields such as quantum chemistry, materials science, condensed matter physics and quantum technologies.

The central obstacle preventing us from understanding quantum systems of many strongly interacting particles is that the complexity of a such system increases dramatically with the number of interacting bodies present – the so-called ‘many-body problem’. This is not a challenge that is unique to quantum mechanics. Indeed in Newtonian mechanics there does not exist a general closed-form solution to the motion of three gravitationally interacting objects. Instead, one is required to solve the equations of motion numerically to find the objects’ trajectories which usually requires very high precision, and hence computationally expensive, numerical integration as the system of equations are known to exhibit chaos [2].

In quantum mechanics exact numerical integration of the equations of motion becomes almost impossible for systems of more than a handful of particles, even with state-of-the-art supercomputers. Here the problem is the exponential growth of Hilbert space with the number of particles since quantum mechanical systems are composed by taking tensor products. Focusing as we will throughout on lattice based quantum systems, suppose a single particle has a Hilbert space of dimension  $d$ , then a system of  $N$  such particle will have a Hilbert space of dimension on the order of  $d^N$ . If our unit system is a spin- $\frac{1}{2}$  particle with dimension 2 then fifty such particles will have a Hilbert space of dimension  $2^{50} = 1125899906842624$ . Describing a state vector with 1125899906842624 complex elements in double-precision floating-point arithmetic requires approximately 12.5 petabytes of computing memory. This exceeds the random access memory capacity of even the most powerful supercomputers [3, 4] and this is without considering performing any numerical operations. Unfortunately, most systems in the world around us are made up of on the order of  $10^{23}$  rather than on the order of 50 particles which leaves a substantial gap between the systems we can study exactly and the macroscopic systems we would like to describe quantum mechanically. Clearly, as supercomputers improve we will gain access to larger and larger systems. However, at the current rate of computational improvements, this is unlikely to bring us any closer to our target of  $10^{23}$  particles any time soon.

## 1.1 Approximate numerical methods

The exponential growth of Hilbert space, which is at the heart of the many-body problem, is closely related to entanglement. This manifestly quantum phenomenon is where the quantum state of individual particles cannot be described independently of the states of other particles. Much progress has been made over the last few decades in accessing larger systems through approximate numerical methods which limit the degree of entanglement that can be described. One of the most prominent of these are tensor network-based methods using matrix product state (MPS) [5, 6], matrix product operator (MPO) [7] and projected entangled pair states (PEPS) [8, 9] descriptions. This broad class of methods generally approximate the state of the system as a ‘train’ [10] of tensors connected by ‘bonds’ with a limited maximum dimension which controls the overall degree of entanglement that can be described. The first such method was the density matrix renormalisation group (DMRG) [11, 12] which proved very successful for studying low energy eigenstates of 1D Hamiltonians with short-range interactions. It was later shown that DMRG can be viewed as a variational method over the space of matrix product states [13], and in turn that because of their entanglement structure matrix product states are especially suited to describing 1D lattice systems with short-range interactions and an energy gap [14].

More pertinent to the focus of this thesis is the application of these methods for studying the dynamics of many-body systems. The main such methods are time-evolving block dissemination (TEBD) [15], time-dependent DMRG (t-DMRG) [16, 17], time-evolving matrix product states (t-MPS) [18], and the time-dependent variational principle (TDVP) [19, 20]. These are once again based on the suitability of MPSs to describe the states of 1D quantum systems, but use different methods to propagate the state in times. TEBD and tDMRG, which are mathematically identical though numerically different [18], both approximate the time-evolution operator,  $U(\delta t)$ , using a Suzuki-Trotter [21] decomposition which is particularly suited to systems with short-range interactions. They then update the matrix product state bond-by-bond for each timestep. The t-MPS algorithm is very similar but updates all bonds at once and does not necessarily require a Suzuki-Trotter decomposition, although the use of one can improve efficiency. On the other hand, TDVP uses Krylov subspaces [22] to directly approximate the action of  $U(\delta t)$  on the current state without explicitly calculating  $U(\delta t)$ . In-depth details of these methods can be found in reviews such as [18] or [23], while the specific methods used for the simulations in this thesis are outlined in the appendices.

These approximate numerical methods, and their numerous variants and refinements [8, 18, 24–31] have proven incredibly useful for studying many-body quantum systems and have provided great insights into various phenomena. However several serious limitations still exist. Firstly matrix product states are best suited to one

dimensional systems with short-range interactions which is quite a restricted class of problems. While alternative decompositions such as PEPS are more suited to higher dimensions, these are generally significantly more expensive computationally since exact contractions are  $\#P$ -Hard [32]. Secondly, by design, these methods can only study weakly entangled systems. This is not a significant issue when studying low-temperature, equilibrium properties when the systems are known to be weakly entangled, but can cause problems when studying dynamics as there is often no reason for the entanglement to remain low. Additionally, in most calculations, the ‘bond dimension’, often denoted as  $\chi$ , which controls the degree of entanglement is a user-defined variable that must balance providing a sufficiently accurate representation of the system while still remaining numerically tractable. While methods do exist, it is often difficult to predict a priori how large to take  $\chi$  and equally difficult to evaluate whether a sufficiently large value was used. Finally, calculating accurate long-time dynamics is incredibly computationally expensive. This is not a problem unique to quantum systems, but it is particularly relevant when the computational complexity of storing and performing basic operations on the state is already very high.

## 1.2 Thermalisation

In parallel to the progress made by developing approximate numerical methods, substantial efforts have been made to understand the dynamics of many-body systems analytically. This work has, for the most part, focused on the relaxation of isolated many-body systems to thermal equilibrium, in line with Anderson’s assertion that computing emergent dynamics is impossible. This focus has also been motivated by connecting the results of quantum mechanics with the long standing fields of statistical mechanics and thermodynamics.

The study of how quantum systems thermalize began with von Neumann in 1929 when he proved the *Quantum Ergodic Theorem* [33] in an attempt to explain how statistical mechanics could emerge from quantum theory. This theorem, in the words of Goldstein et al. [34], states

*For a typical finite family of commuting macroscopic observables, every initial wave function from a microcanonical energy shell evolves so that for most times, in the long run, the joint probability distribution of these observables obtained from the unitarily time-evolved wave function is close to their microcanonical distribution.*

The quantum ergodic theorem, which has since been understood through random matrix theory [35–37], can be seen as a precursor to the more recent *Eigenstate Thermalisation Hypothesis* (ETH) [35, 38, 39]. To briefly explain the ETH, consider



the evolution of a pure state  $|\psi_0\rangle$  under some Hamiltonian  $H$  in an isolated system. We can write

$$|\psi(t)\rangle = \sum_k e^{-iE_k t} c_k |k\rangle, \quad (1.1)$$

where  $|k\rangle$  are eigenstates of  $H$  with eigenvalue  $E_k$  and we have set  $\hbar = 1$  as we will throughout this thesis. The amplitudes  $c_k$  are determined by the initial state  $|\psi_0\rangle$ . The evolution of the expected value of some observable  $O$  can then be written as

$$\langle O(t) \rangle = \sum_k |c_k|^2 O_{kk} + \sum_{k \neq j} c_k c_j^* e^{i(E_k - E_j)t} O_{jk}, \quad (1.2)$$

where  $O_{jk} = \langle j|O|k\rangle$ . It is instructive to observe that as the size of the system increases the energies,  $E_k$ , will generically become dense and incommensurate, up to perhaps some finite gaps, and thus the second term begins to resemble an integral similar to

$$\sum_{k \neq j} c_k c_j^* e^{i(E_k - E_j)t} O_{jk} \sim \int d\varepsilon f(\varepsilon) e^{i\varepsilon t}. \quad (1.3)$$

Importantly, the Riemann-Lebesgue lemma [40] then states that under fairly relaxed conditions on  $f(\varepsilon)$  this integral vanishes as  $t \rightarrow \infty$ , indicating stationarity in the long time limit. This process, referred to as eigenstate dephasing, can be observed in systems of relatively small size, as we will see in Ch 4. Eigenstate dephasing can be viewed as the principle motivation for the ETH which asserts that

$$O_{jk} = O(\bar{E})\delta_{jk} + \frac{1}{2}e^{-S(\bar{E})}f_O(\bar{E}, \omega)R_{jk}, \quad (1.4)$$

where  $\bar{E} = \frac{1}{2}(E_j + E_k)$ ,  $\omega = E_k - E_j$  and  $S(\bar{E})$  is the entropy at energy  $\bar{E}$  [35]. The functions  $O(\bar{E})$  and  $f_O(\bar{E}, \omega)$  are smooth and  $O(\bar{E})$  is exactly the expectation value of  $O$  given by the microcanonical ensemble, which directly connect this hypothesis with classical statistical mechanics. Finally  $R_{jk}$  are independent random variables with zero mean and unit variance.

This ETH ansatz has direct consequences for the thermalisation of a many-body system. For instance, one can show that under the ETH long-time averages of temporal fluctuations of  $\langle O \rangle$  vanish exponentially with system size. Additionally, the temporal fluctuations of extensive observables satisfy the standard fluctuation-dissipation relations. However, as the name suggests, the above ansatz for the matrix elements  $O_{jk}$  is only a hypothesis. It is currently unknown exactly which observables it holds for and when it can be expected to be violated. One important class of systems which do not thermalise according to the ETH are integrable systems, although a generalisation of the ETH to integrable systems or those

under the influence of weak integrability breaking has been studied [41]. More discussion and the precise definition of integrable models will be given in Chapter 2. Numerical evidence currently indicates that the ETH holds for few-body observables, irrespective of locality, but not for eigenstate projectors [35, 42]. For more details about eigenstate thermalisation, the reader is directed to the excellent review of [35].

The ETH indicates that generic isolated quantum systems will thermalise so that any measurements will return the value associated with the microcanonical ensemble. However, it does not make direct predictions about the time scales involved. For instance, if one considered the whole universe to be the ‘system’ in question then our very existence is itself evidence that these time scales can be arbitrarily long. It is expected that the thermalisation time can be related to the energy scale of the system’s Hamiltonian but also that it generically grows with system size. We must also then consider what is meant by an ‘isolated’ system since one could argue that the only perfectly isolated system is the whole universe. At this point it is important to make the following experimental consideration: a system of interest can be considered to be isolated if the time scales on which it interacts with the environment are much longer than those on which it thermalises. This consideration allows us to separate what we mean by the ‘system’ and the ‘environment’, but raises the immediate questions: what happens when the system-environment interactions become stronger so that the interactions occur on time scales closer to those on which the system thermalises? Can we understand the dynamics of the system before the ETH predicts that the system and environment should thermalise? This brings us to the realm of non-equilibrium quantum mechanics, which will be the central focus of this thesis. As we will discuss in the following sections, non-equilibrium quantum systems can exhibit a range of interesting phenomena which bring us closer to understanding the emergence of complex dynamics. Additionally, there are a plethora of experimentally and technologically relevant models that are out-of-equilibrium. For example, the deep optical lattices commonly used in cold atom experiments are known to induce strong dephasing while the error inducing quantum channels found in qubit systems are also usually caused by interactions with the environment.

## 2 Open quantum systems

In this section we will discuss the dynamics of non-equilibrium quantum systems, also referred to as open quantum systems, where the system of interest interacts with an environment/bath [43, 44]. Before doing so, we will recap the density operator formalism for quantum mechanics in order to demonstrate how we arrive at the equations of motion for an open quantum system.

## 2.1 Density operator formalism

### 2.1.1 Properties and operations

In the density operator formalism, the state of a quantum system with Hilbert space  $\mathcal{H}$  is described by a bounded, self-adjoint linear operator

$$\rho : \mathcal{H} \rightarrow \mathcal{H} \quad (1.5)$$

which is positive semi-definite and has unit trace. Since the operator has non-negative eigenvalues and unit trace its spectral decomposition

$$\rho = \sum_k p_k |\psi_k\rangle \langle \psi_k|, \quad (1.6)$$

satisfies

$$\sum_k p_k = 1 \quad (1.7)$$

and hence the state  $\rho$  can be interpreted as a statistical ensemble of pure states,  $|\psi_k\rangle$ , which occur with probability  $p_k$ . In a general basis, such as the particle number, energy or computational bases, however, the state  $\rho$  will likely not be diagonal and the off diagonal components correspond to quantum coherences. Broadly speaking, as we discuss below, it is these off diagonal terms that contribute to quantum effects such as interference and entanglement, so when the system experiences decoherence and the off diagonal terms decay, the resulting dynamics become effectively classical.

Given positive operator-valued measure (POVM),  $\{M_a\}$  with  $\sum_a M_a^\dagger M_a = \mathbb{1}$ , the probability that a system in a state  $\rho$  returns the result  $a$  is

$$\mathbb{P}(a) = \text{Tr}(M_a \rho M_a^\dagger), \quad (1.8)$$

while the expected value of an observable  $O$  is given by

$$\langle O \rangle = \text{Tr}(O \rho). \quad (1.9)$$

The space of bounded linear operators acting on  $\mathcal{H}$ , to which both the states and observables belong is labeled  $\mathcal{B}(\mathcal{H})$ . This construction is known as the *Dirac-von Neumann axioms* of quantum mechanics. We will sometimes make a use of Fock-Liouville space [45] and ‘vectorise’ operators in  $\mathcal{B}(\mathcal{H})$  using double-kets,

$$\rho \longleftrightarrow |\rho\rangle\rangle, \quad (1.10)$$

which will allow us to write the Hilbert-Schmidt inner product as

$$\text{Tr}(A^\dagger B) \longleftrightarrow \langle\langle A^\dagger | B \rangle\rangle. \quad (1.11)$$

This notation will be useful when discussing superoperators that act on operators in  $\mathcal{B}(\mathcal{H})$ . Importantly, however, a state  $|\psi\rangle\rangle \in \mathcal{B}(\mathcal{H})$  is not necessarily a density operator describing the state of a quantum system. We will indicate where this could cause any confusion.

An important operation that can be performed on a density operator,  $\rho^{AB}$  which acts on a composite Hilbert space,  $\mathcal{H}_A \otimes \mathcal{H}_B$  is the *partial-trace*, defined as

$$\text{Tr}_B(a \otimes b) = a \text{Tr}(b), \text{ for } a \in \mathcal{B}(\mathcal{H}_A), b \in \mathcal{B}(\mathcal{H}_B) \quad (1.12)$$

which in turn defines the reduced density operator for the system  $A$  as

$$\rho^A = \text{Tr}_B(\rho^{AB}). \quad (1.13)$$

The reduced state,  $\rho^A$ , represents the state of the subsystem  $A$  if we have no knowledge of the subsystem  $B$ . The partial trace is the unique operation that gives the correct description of observable quantities for the reduced system in this sense.

For our purposes, the most important use of the partial trace will be to separate the system we are interested in from the environment. We will usually consider the full system-environment Hilbert space,  $\mathcal{H}_{SE}$ , as the tensor product of the separate environment and system Hilbert spaces,

$$\mathcal{H}_{SE} = \mathcal{H}_S \otimes \mathcal{H}_E, \quad (1.14)$$

and then describe the system using the reduced density operator obtained by tracing out the environment Hilbert space. By doing this, even if the full system-environment system is described by a pure state, the system on its own is described by a mixed state. Further, entanglement between the system and the environment causes the off diagonal elements of the reduced system density operator to decay, known as decoherence. As a simple example of this, consider the case of a two level system, with basis  $\{|j\rangle\rangle$  and a two level environment with basis  $|\epsilon_j\rangle$  where  $j = 0, 1$ . Suppose the full system-environment state is

$$|\Phi\rangle = \frac{1}{2\sqrt{1-\alpha+\alpha^2}} ((|0\rangle + |1\rangle)(|\epsilon_0\rangle - |\epsilon_1\rangle) + 2\alpha |0\rangle |\epsilon_1\rangle), \quad \alpha \in \mathbb{R}, \quad (1.15)$$

then the reduced density operator describing the system of interest is given in the  $\{|j\rangle\rangle$  basis by

$$\rho_S = \frac{1}{2(1-\alpha+\alpha^2)} \begin{pmatrix} 1-2\alpha+2\alpha^2 & 1-\alpha \\ 1-\alpha & 1 \end{pmatrix}. \quad (1.16)$$

We see that as  $\alpha \rightarrow 1$  the system is described by a classical probability distribution over the states  $|j\rangle\rangle$ , which is exactly the behaviour described as decoherence.

Computing the Renyi-2 entropy as a measure of the entanglement between the system and environment gives

$$S_2 = -\text{Tr} \log(\rho_S^2) = \log \left( \frac{2(1 - \alpha + \alpha^2)^2}{2 - 4\alpha + 5\alpha^2 - 4\alpha^3 + 2\alpha^4} \right). \quad (1.17)$$

This entanglement measure is maximised at  $\alpha = 1$ , in other words the system completely decoheres when it is maximally entangled with the environment. This simple example demonstrates the counterintuitive mechanism by which strong entanglement - a manifestly quantum phenomenon - effectively hides quantum mechanics from us in the classical world.

### 2.1.2 Evolution

The postulates of quantum mechanics state that the evolution of a closed quantum system from time  $t_0$  to  $t_1$  is described by a unitary transformation with operator  $U(t_0, t_1)$ . Thus we have

$$\rho(t_1) = U(t_0, t_1)\rho(t_0)U(t_0, t_1)^\dagger. \quad (1.18)$$

In the case that the evolution is smooth, this corresponds to the Schrodinger equation

$$i\frac{d}{dt}\rho(t) = [H(t), \rho(t)], \quad (1.19)$$

for some possibly time-dependent Hamiltonian,  $H(t)$ . However, we once again run into the problem of what is meant by “closed” as no system is ever completely isolated from the environment. Here we can be more rigorous and introduce the *system-environment model*. We divide our joint system into the system of interest,  $S$ , and the environment,  $E$  which can be arbitrarily large. When the joint system evolves under Eq. (1.18) from an initial state  $\rho_0^{SE}$  we have

$$\rho^{SE}(t) = U(t)\rho_0^{SE}U(t)^\dagger. \quad (1.20)$$

We then discard the environment by taking the partial trace so that the evolution of the system of interest is given by

$$\rho^S(t) = \text{Tr}_E \left( U(t)\rho_0^{SE}U(t)^\dagger \right). \quad (1.21)$$

The final assumption we must now make is that there are no initial correlations between the system and the environment, and thus we can write  $\rho_0^{SE} = \rho_0^S \otimes \tau_0$ . In this case we can write

$$\rho(t) = \text{Tr}_E \left( U(t)(\rho_0 \otimes \tau_0)U(t)^\dagger \right) = \Lambda_t(\rho_0), \quad (1.22)$$

where we have dropped the system index on the state. This equation now describes the evolution of the state of the system of interest in terms of a linear super-operator  $\Lambda_t$ . Written in this way, the Steinspring dilation theorem [46] immediately tells us that  $\Lambda_t$  is a completely-positive trace-preserving (CPTP) map.

**Definition** (CPTP Map). A map  $\Lambda(\rho)$  is CPTP if it preserves the trace of  $\rho$ , i.e.  $\text{Tr}(\Lambda(\rho)) = \text{Tr}(\rho)$  and for all  $n \in \mathbb{N}$  the map  $\Lambda \otimes \text{Id}_n$  is a positive map. Here  $\text{Id}_n$  is the identity operator on a Hilbert space of dimension  $n$ .

Importantly CPTP maps are exactly those maps that preserve the fundamental properties of density states we gave previously. It is often miss-interpreted that CPTP maps are the *only* maps which can describe the evolution of a quantum state. However, as the above discussion indicates, this is only true when there are no initial correlations between the system and its environment, [47]. Indeed there are notable examples of situations when non-completely-positive maps are necessary to describe the evolution of a quantum system, in particular quantum process tomography [48, 49]. While this is an interesting line of study, in the remainder of this thesis we will be concerned exclusively with CPTP evolutions as these are widely considered the standard.

### 2.1.3 $C^*$ -algebras

Before introducing the Lindblad equation, which will be central to this work, we give a brief discussion of  $C^*$ -algebras. This discussion is important to emphasise the importance of  $C^*$ -algebras for describing physical systems in a mathematically rigorous way and to motivate our use of symmetries and algebraic relations to study quantum dynamics.

Let us first define what is meant by a  $C^*$ -algebra.

**Definition** ( $C^*$ -algebra). A  $C^*$ -algebra,  $\mathcal{A}$ , is a complex vector space with an associative product which is linear in both arguments. The space is also endowed with a norm with respect to which the product is continuous, i.e.,

$$\|AB\| \leq \|A\|\|B\|, \quad \forall A, B \in \mathcal{A}. \quad (1.23)$$

Finally there also exists an involution operator,  $*$  :  $\mathcal{A} \rightarrow \mathcal{A}$ , such that for  $A, B \in \mathcal{A}$  and  $\lambda \in \mathbb{C}$ ,

$$(A + B)^* = A^* + B^*, \quad (\lambda A)^* = \bar{\lambda}A^*, \quad (AB)^* = B^*A^*, \quad (A^*)^* = A. \quad (1.24)$$

This involution operator must satisfy the  $C^*$ -condition

$$\|A^*A\| = \|A\|^2. \quad (1.25)$$

This structure provides a natural extension of matrix algebra to more abstract objects. As we will now illustrate, this is also the natural language with which to describe all physical systems, both quantum and classical, in an operational way.

Summarising the arguments presented by [50], consider any physical system that can be experimentally prepared. We can then describe this system mathematically as the collection,  $S$ , of all possible states,  $\omega$ , that we can prepare. A physical property of the system, or observable,  $A$ , is defined by some experimental procedure or apparatus which we use to measure the system. In practice we take many measurements on identically prepared states and then conclude that the expected value of an observable  $A$  on a system in a state  $\omega$  is defined as the average of these multiple measurements,  $\omega(A)$ . From an operational point of view, our only way of understanding the system is through the set of all possible measurements,  $\mathcal{O}$ , and so we must identify two states,  $\omega_1$  and  $\omega_2$  as the same physical state if they cannot be distinguished by any observable, i.e.

$$\omega_1 = \omega_2 \iff \omega_1(A) = \omega_2(A), \quad \forall A \in \mathcal{O}. \quad (1.26)$$

In a similar way, two observables,  $A_1$ ,  $A_2$ , must be identified if they return the same result for all states,

$$A_1 = A_2 \iff \omega(A_1) = \omega(A_2), \quad \forall \omega \in S. \quad (1.27)$$

It is also operationally possible, for instance by rescaling our ruler or taking powers of the measurement result, to define observables corresponding to real polynomials of  $A$ . This means that there exists for each  $A \in \mathcal{O}$  a commutative polynomial algebra of observables,  $\mathcal{O}_A \subset \mathcal{O}$ . This can, without loss of generality, be extended to a complex polynomial algebra  $\mathcal{A}_A$ . One can further argue, based on physical and operational considerations [50], that these complex polynomial algebras are in fact exactly  $C^*$ -algebras and that the states of our system define normalised positive linear functionals on them.

It is plausible to conjecture that the set of all observables of our system generate a  $C^*$ -algebra,  $\mathcal{A}$ , such that the states described by normalised positive linear functionals on the individual complex polynomial algebras,  $\mathcal{A}_A$ , now naturally extend to normalised positive linear functionals on  $\mathcal{A}$ . Although this structure of observables and states may be questioned, it is satisfied by classical systems, and is implied by the Dirac-von Neumann axioms through the Gelfand-Naimark theorem and the Gelfand–Naimark–Segal construction [50–54]. In this unified  $C^*$ -algebraic picture of physical systems, the only difference between a classical and quantum mechanics is that the algebra of operators,  $\mathcal{A}$ , is commutative in the classical and non-commutative in the quantum cases.

As a concrete example, consider the case of a single particle with spin  $s$  fixed in space. The  $C^*$ -algebra of observables is then generated by all possible linear combinations of the operators

$$(S_x)^\alpha (S_y)^\beta (S_z)^\gamma, \quad \alpha, \beta, \gamma \in \mathbb{N}, \quad (1.28)$$

where  $S_x$ ,  $S_y$ ,  $S_z$  satisfy the usual commutation relations

$$[S_a, S_b] = i\varepsilon_{abc}S_c. \quad (1.29)$$

The states of the particle can then be described as normalised positive linear functionals on this algebra, for example

$$\omega_\beta(A) = \frac{\text{Tr}(\exp(-\beta S_z)A)}{\text{Tr}(\exp(-\beta S_z))}. \quad (1.30)$$

Finally, we can fix the total spin of the particle by restricting to the representation in which

$$S_x^2 + S_y^2 + S_z^2 = s(s+1). \quad (1.31)$$

There are many results in the study of  $C^*$ -algebras and their consequences for quantum mechanics, although these will not be directly relevant to the rest of this thesis and the reader is directed to the works of [50, 52, 53, 55] for more details. The key relevance of  $C^*$ -algebras for our work is that they are manifestly well defined in the thermodynamic limit where the number of particles in our system is taken to infinity, since they make no a priori reference to the size of the physical system. In this limit, other techniques can be poorly defined unless treated carefully so  $C^*$ -algebras indicate that for many-body quantum mechanics, it is the operator algebra generated by observables that should be studied, thus motivating our focus on symmetries and algebras. In this thesis we will not work directly with  $C^*$ -algebras and assume that  $\dim(\mathcal{H}) = d < \infty$  is arbitrarily large but strictly finite unless explicitly stated. However, since many of our results are formulated in terms of operator algebra, especially those of Chs 3 - 5, future works should be able to extend them to the rigorous language of  $C^*$  algebras so that they can be formally applied in the thermodynamic limit. These extensions may also allow us to connect the results obtained here for quantum systems to classical systems through the unifying language of  $C^*$ -algebras

## 2.2 The Lindblad equation

### 2.2.1 The generator of CPTP maps

In Section 2.1 we demonstrated that the evolutions of quantum systems are almost always described by CPTP maps

$$\rho(t) = \Lambda_{t,\tau}[\rho(\tau)]. \quad (1.32)$$



Notice that  $\Lambda_{t,\tau}$  depends explicitly on both the initial,  $\tau$ , and final,  $t$ , times. This is important as we will now restrict ourselves to *Markovian* evolutions<sup>1</sup> where the maps  $\Lambda_{t,\tau}$  satisfy the inhomogeneous composition law

$$\Lambda_{t,s} \circ \Lambda_{s,\tau} = \Lambda_{t,\tau}, \quad \forall \tau \leq s \leq t. \quad (1.33)$$

For most evolutions it is also physically reasonable to assume that for each  $\tau$  the operators  $\Lambda_{t,\tau}$  form a one-parameter family of differentiable CPTP maps, with a generating equation

$$\frac{d}{dt}\Lambda_{t,\tau} = \mathcal{L}_t\Lambda_{t,\tau}, \quad \Lambda_{\tau,\tau} = \text{Id}. \quad (1.34)$$

Here it is again the Markovian assumption that restricts the generator  $\mathcal{L}_t$  to be  $\tau$  independent. This in turn gives us a time-local master equation for the evolution of the state

$$\frac{d}{dt}\rho(t) = \mathcal{L}_t[\rho(t)]. \quad (1.35)$$

We can now use the fact that  $\Lambda_{t,\tau}$  is a CPTP map to derive an explicit form for  $\mathcal{L}_t$ . To do so, following the standard route [45], we first recall the Choi-Krauss theorem [56]. This states that a map  $\Lambda : \mathcal{B}(\mathcal{H}) \rightarrow \mathcal{B}(\mathcal{H})$  is CPTP if and only if it has a Krauss decomposition

$$\Lambda[\rho] = \sum_{k=1}^{d^2} M_k \rho M_k^\dagger, \quad (1.36)$$

where  $d \leq \dim(\mathcal{H})$  and the Krauss operators,  $\{M_k\}$ , obey the completeness relation

$$\sum_{k=1}^{d^2} M_k^\dagger M_k = \text{Id}. \quad (1.37)$$

We can thus write the evolution equation as

$$\rho(t) = \sum_{k=1}^{d^2} M_k(t, \tau) \rho(\tau) M_k(t, \tau)^\dagger. \quad (1.38)$$

Now we choose an orthonormal basis,  $\{F_k\}_{i=1}^{d^2}$ , of  $\mathcal{B}(\mathcal{H})$ . Without loss of generality we can take the first element in the basis to be  $F_1 = \mathbb{1}/\sqrt{d}$  which then requires all other elements to be traceless. Next we expand Eq. (1.38) as

$$\rho(t) = \sum_{i,j=1}^{d^2} C_{i,j}(t, \tau) F_i \rho(\tau) F_j^\dagger, \quad (1.39)$$

---

<sup>1</sup>We will briefly discuss non-Markovian quantum evolutions in a separate section below, but the results in this thesis focus exclusively on Markovian dynamics.

where

$$C_{i,j}(t, \tau) = \sum_{k=1}^{d-1} \langle \langle F_i | M_k(t, \tau) \rangle \rangle \langle \langle M_k(t, \tau) | F_j \rangle \rangle. \quad (1.40)$$

We can compute the time derivative of  $\rho(t)$  as

$$\frac{d}{dt}\rho(t) = \lim_{\delta t \rightarrow 0} \frac{1}{\delta t} \left[ \sum_{i,j=1}^{d^2} C_{i,j}(t + \delta t, t) F_i \rho(t) F_j^\dagger - \rho(t) \right] \quad (1.41a)$$

$$\begin{aligned} &= \lim_{\delta t \rightarrow 0} \frac{1}{\delta t} \left[ \sum_{i,j=2}^{d^2} C_{i,j}(t + \delta t, t) F_i \rho(t) F_j^\dagger + \frac{1}{\sqrt{d}} \sum_{i=2}^{d^2} C_{i,1}(t + \delta t, t) F_i \rho(t) \right. \\ &\quad \left. + \frac{1}{\sqrt{d}} \sum_{j=2}^{d^2} C_{1,j}(t + \delta t, t) \rho(t) F_j^\dagger + \left( \frac{1}{\sqrt{d}} C_{1,1}(t + \delta t, t) - 1 \right) \rho(t) \right] \end{aligned} \quad (1.41b)$$

$$= \sum_{i,j=2}^{d^2} g_{i,j}(t) F_i \rho(t) F_j^\dagger + F(t) \rho(t) + \rho(t) F(t)^\dagger + g(t) \rho(t), \quad (1.41c)$$

where we have defined

$$g_{i,j}(t) = \lim_{\delta t \rightarrow 0} \frac{C_{i,j}(t + \delta t, t)}{\delta t}, \quad (1.42a)$$

$$F(t) = \lim_{\delta t \rightarrow 0} \frac{C_{i,1}(t + \delta t, t)}{\delta t} F_i, \quad (1.42b)$$

$$g(t) = \lim_{\delta t \rightarrow 0} \frac{1}{\delta t} \left( \frac{1}{\sqrt{d}} C_{1,1}(t + \delta t, t) - 1 \right). \quad (1.42c)$$

We now separate  $F(t)$  into its Hermitian and anti-Hermitian parts as

$$F(t) = G(t) - iH(t), \quad (1.43)$$

and then define  $\tilde{G}(t) = G(t) + g(t)/2$  to absorb the term which is proportional to the identity operator. Dropping the time dependence of  $\rho(t)$  this gives

$$\frac{d}{dt}\rho = -i[H(t), \rho] + \sum_{i,j=2}^{d^2} g_{i,j}(t) F_i \rho F_j^\dagger + \{\tilde{G}(t), \rho\}. \quad (1.44)$$

Since they come from an outer-product in Eq. (1.40), the numbers  $g_{i,j}(t)$  form a positive semi-definite Hermitian matrix at all  $t$  and hence we can diagonalise

$$\sum_{i,j=2}^{d^2} g_{i,j}(t) F_i \rho F_j^\dagger = \sum_k L_k(t) \rho L_k(t)^\dagger. \quad (1.45)$$

Finally, we also impose trace preservation which implies that

$$\tilde{G}(t) = -\frac{1}{2} \sum_k L_k(t)^\dagger L_k(t). \quad (1.46)$$

This gives us the Lindblad, or Gorini-Kossakowski-Sudarshan-Lindblad, master equation [57]:

$$\boxed{\frac{d}{dt}\rho = -i[H(t), \rho] + \sum_k \left( L_k(t)\rho L_k(t)^\dagger - \frac{1}{2}\{L_k(t)^\dagger L_k(t), \rho\} \right)}, \quad (1.47)$$

which describes the most general Markovian dynamics in a quantum system. We will call the generator,

$$\mathcal{L}_t[\rho] = -i[H(t), \rho] + \sum_k \left( L_k(t)\rho L_k(t)^\dagger - \frac{1}{2}\{L_k(t)^\dagger L_k(t), \rho\} \right), \quad (1.48)$$

the quantum *Liouvillian*.

### 2.2.2 The limit of weak system-environment interactions

Although the above derivation demonstrates that the Lindblad equation is very general, it does not give us much insight into what the different parts of it physically represent. To this end, we will now present an alternative derivation that will provide us with the intuition behind how the Lindblad equation relates to open quantum systems.

Following [43] and [45] this alternative approach begins with Eq. (1.21) where we expressed the evolution of our system by partially tracing out the environment,

$$\rho^S(t) = \text{Tr}_E \left( U(t) \rho^{SE}(0) U(t)^\dagger \right). \quad (1.49)$$

We further assume for simplicity that the evolution of the joint system is time-homogeneous and described by the time-independent Hamiltonian

$$H_T = H_S \otimes \mathbb{1} + \mathbb{1} \otimes H_E + \alpha H_I, \quad U(t) = e^{-iH_T t}. \quad (1.50)$$

Here  $\alpha$  is a small parameter which controls the strength of the coupling between the system and the environment. It is also convenient to decompose the interaction Hamiltonian as

$$H_I = \sum_k S_k \otimes E_k. \quad (1.51)$$

Using perturbation theory to second order, and switching to the interaction picture (indicated by a tilde and additional time dependence) we have

$$\frac{d}{dt} \tilde{\rho}^{SE}(t) = -i\alpha [\tilde{H}_I(t), \tilde{\rho}^{SE}(0)] - \alpha^2 \int_0^t ds [\tilde{H}_I(t), [\tilde{H}_I(s), \tilde{\rho}^{SE}(t)]] + \mathcal{O}(\alpha^3). \quad (1.52)$$

We must now trace out the environment in order to obtain an evolution equation for  $\tilde{\rho}^S(t)$ . To make progress we make two further assumptions:

- i) At time  $t = 0$  the system and environment are separable, i.e  $\rho_{SE}(0) = \rho^S(0) \otimes \rho^E(0)$ .
- ii) The environment is initially in the thermal state,  $\rho^E(0) = e^{-\beta H_E} / \text{Tr} (e^{-\beta H_E})$ .

After taking the partial trace, these assumptions allow us to deduce that the first term in Eq. (1.52) can be written as

$$\text{Tr}_E[\tilde{H}_I(t), \tilde{\rho}^{SE}(0)] = \sum_k [\tilde{S}_k(t), \tilde{\rho}^S(0)] \text{Tr}_E(\tilde{E}_k(t) \tilde{\rho}^E(0)). \quad (1.53)$$

It is always possible to ensure that  $\text{Tr}_E(\tilde{E}_k(t) \tilde{\rho}^E(0)) = 0$  by adding a trivial energy shift term to the full Hamiltonian which does not affect the dynamics [45], and hence this first term vanishes. We then make a more restrictive assumption that due to the weak coupling between the system and the environment the environment is *always* in a thermal state and decoupled from the system. This leaves us with

$$\frac{d}{dt} \tilde{\rho}^S(t) = -\alpha^2 \int_0^t ds \text{Tr}_E([\tilde{H}_I(t), [\tilde{H}_I(s), \tilde{\rho}^S(t) \otimes \tilde{\rho}^E(0)]] + \mathcal{O}(\alpha^3), \quad (1.54)$$

which while now only dependent on  $\tilde{\rho}^S(t)$ , is implicitly non-Markovian. To make further progress, since we know from above that the Lindblad equation holds only for Markovian evolutions, we assume that the  $s$  dependence decays fast enough that we can freely extend the integration limits. After also changing variables we have

$$\frac{d}{dt} \tilde{\rho}^S(t) = -\alpha^2 \int_0^\infty ds \text{Tr}_E([\tilde{H}_I(t), [\tilde{H}_I(s-t), \tilde{\rho}^S(t) \otimes \tilde{\rho}^E(0)]] + \mathcal{O}(\alpha^3). \quad (1.55)$$

This is known as the Redfield equation which was first applied for studying nuclear magnetic resonances [58]. Our final assumption is to make the rotating wave approximation which after some algebra and transforming back to the Schrodinger picture gives [45]

$$\frac{d}{dt} \rho = -i[H_S + H_{Ls}, \rho] + \sum_{i,j,\omega} \gamma_{ij}(\omega) [S_i(\omega) \rho S_j(\omega)^\dagger - \frac{1}{2} \{S_j^\dagger S_i(\omega), \rho\}]. \quad (1.56)$$

Here the term  $H_{Ls}$  is the Lamb-shift Hamiltonian which renormalises the system's energy levels due to its interaction with the environment. The  $S_i(\omega)$  operators are a frequency expansion of the  $S_i$  operators from the system-environment interaction Hamiltonian which obey

$$[H_S, S_i(\omega)] = -\omega S_i(\omega). \quad (1.57)$$

The coefficients  $\gamma_{ij}(\omega)$  form a positive semi-definite Hermitian matrix and so as before we can diagonalise to obtain the Lindblad equation as in Eq. (1.47).

This derivation indicates that under the assumption of weak, Markovian system-environment interactions, the  $L_k$  operators in Eq. (1.47) can be directly related to the interaction Hamiltonian. In some cases, these can even be derived explicitly from first principles following this or similar approaches [59]. Intuitively, they represent the instantaneous interaction between the system and the environment, and are thus referred to as “jump operators”. In practice, they are often taken to be particle creation/annihilation operators to describe particle gain/loss or number operators to describe dephasing, but more exotic choices are also sometimes used.

### 2.2.3 Example: A two level system with decay

In order to understand the relevance of the Lindblad equation, we will briefly discuss the simplest example of a two level system experiencing decay. Consider a system with two energy eigenstates, the ground state  $|g\rangle$  and the excited state  $|e\rangle$ . The Hamiltonian is then expressible as

$$H = |g\rangle \langle g| + \Delta |e\rangle \langle e|, \quad (1.58)$$

where we have set the ground state energy to be unity and the energy gap to be  $\Delta - 1$ . In the absence of dissipation a generic density operator state will evolve as

$$\rho(t) = \begin{pmatrix} \rho_{00} & e^{i(\Delta-1)t} \rho_{01} \\ e^{-i(\Delta-1)t} \rho_{01}^* & 1 - \rho_{00} \end{pmatrix}, \quad (1.59)$$

where  $\rho_{00} \in \mathbb{R}$  and  $\rho_{01} \in \mathbb{C}$  describe the initial state of the system and satisfy  $|\rho_{01}|^2 \leq \rho_{00}(1 - \rho_{00})$ . Importantly we see that the probability of the system being in either the ground or excited state, which is given by the two diagonal entries respectively, does not depend on time, while the off diagonal *coherences* oscillate at a frequency  $\omega = \Delta - 1$ .

Now suppose that the system were in contact with some environment which induces decay from the excited state to the ground state at a rate  $\Gamma$ . This would be modelled by introducing a Lindblad operator

$$L = \sqrt{\Gamma} |g\rangle \langle e|. \quad (1.60)$$

The density operator describing the system will now evolve as

$$\rho(t) = \begin{pmatrix} (\rho_{00} - 1) e^{-2\Gamma t} + 1 & \rho_{01} e^{-t(\Gamma - i(\Delta-1))} \\ \rho_{01}^* e^{-t(\Gamma + i(\Delta-1))} & (1 - \rho_{00}) e^{-2\Gamma t} \end{pmatrix}. \quad (1.61)$$

Now we observe that probability of the system being in the excited state decays exponentially so that after a time period on the order of  $1/\Gamma$  the system is almost certainly in the ground state. We also notice that the off-diagonal elements decay, indicating the decoherence of the system.

### 2.2.4 Non-Markovian dynamics

Before moving on to the important matter of solving the Lindblad equation, we make some brief remarks about the description of non-Markovian dynamics.

Non-Markovian dynamics in quantum systems are usually defined in terms of *CP-divisibility* of the evolution operators  $\Lambda_t$ .

**Definition** (CP-divisibility). A one-parameter family of evolution operators,  $\Lambda_t$  is said to be CP-divisible if for all  $t \geq 0$  there exists a map  $\tilde{\Lambda}_{t,s}$  such that

$$\Lambda_t = \tilde{\Lambda}_{t,s} \circ \Lambda_s \quad (1.62)$$

with  $\tilde{\Lambda}_{t,s}$  CPTP for all  $0 \leq s \leq t$ .

A quantum evolution is then said to be Markovian if it is CP-divisible [60, 61]. Recall that when we derived the Lindblad equation as a generator of CPTP maps above, we explicitly assumed this behaviour. This definition attempts to extend the classical ideas of Markovian processes to quantum evolutions, indeed the definition of CP-divisibility is strikingly similar to the usual Chapman-Kolmogorov equations [62]. It can be shown that this definition corresponds to interactions with a memoryless environment in the context of collisional-type system-environment interactions such as [63–65]. There also exists a more rigorous, algebraic definition of Markovian evolutions in the language of  $C^*$ -algebras that implies the above definition [66]. Recent progress has been made in quantifying the ‘degree’ of non-Markovianity in an evolution by looking at the change of trace-distance between two states under the same evolution [67–69] which can be interpreted as a flow of information, although the two definitions appear to diverge under certain conditions [70] and the matter is far from settled with many other measures and witnesses being studied [61, 71].

Intuitively, non-Markovian dynamics are where the evolution retains some ‘memory’ of its previous state. This is made obvious in the most often used non-Markovian master equation, the Nakajima-Zwanzig equation [43, 72],

$$\frac{d}{dt}\rho(t) = \int_0^t ds \mathcal{K}(t-s)\rho(s), \quad (1.63)$$

where the operator  $\mathcal{K}(t-s)$  is called a memory kernel. This clearly shows that the evolution of the state at time  $t$  depends on its state at all previous times that the memory kernel is non-zero. In this form, there are no straightforward conditions on the kernel,  $\mathcal{K}(s)$ , that will generally guarantee CPTP dynamics, although some progress has been made towards this [73]. Further, there is often no easy correspondence between terms in the memory kernel and the microscopic interactions that are being described. This problem can often lead to physically motivated memory kernels which unfortunately produce ill-defined or unphysical

dynamics [74]. In spite of these difficulties much work is being done to better understand non-Markovian dynamics in quantum systems, partially as they have a number of interesting applications in quantum technologies [75–78]. While this is an interesting topic, the remainder of this thesis is concerned exclusively with Markovian dynamics. We will thus use the term “open system” to refer to a system whose dynamics are described by the Lindblad equation.

## 2.3 Solving the Lindblad equation

We have now introduced the Lindblad equation, which will be the central equation for the remainder of this thesis. Indeed, this thesis aims to provide algebraic solutions to the Lindblad equation for many-body systems which can be used to study dynamical phases of matter. It is, therefore, useful to give a discussion of the methods currently available for tackling these dynamics.

At a basic level, the Lindblad equation is simply a system of  $\frac{1}{2}(d^2 + d - 1)$  coupled first-order ordinary differential equations<sup>2</sup>. While some analytic techniques exist for solving general systems of coupled ODEs [79, 80] these are often impractical due to the often large dimension of the system. For example, even in a two-level, time-independent system sophisticated techniques and non-trivial algebra are required [81]. Occasionally perturbative techniques such as those used to study time-dependent closed systems can be applied, but these are often still restricted to relatively small systems and to situations where only short time dynamics are being studied. Therefore it is almost always necessary to resort to numerical integration of some kind. While this is feasible for systems of only a handful of particles, up to the usual challenges of numerically integrating coupled ODEs, we once again reach the curse of dimensionality and cannot cope with the exponential size of the Hilbert space for many-body systems. In these cases, many of the numerical methods outlined in Sec. 1.1 have been adapted to deal with open quantum systems. For general time-dependent Liouvillians, one straightforward method is to apply t-DMRG/t-MPS algorithms to the space of density operators using matrix-product-operators or matrix-product-states to describe the state [25, 29, 82, 83]. Alternatively, if the evolution of a pure initial state is required then the quantum trajectories method can provide a more efficient option [84, 85]. These two methods are both used to provide numerical simulations in this thesis and are outlined in the Appdx C. It should be noted that these techniques often suffer from numerical instabilities. For instance, naive extensions of the TEBD algorithm often do not preserve the trace or Hermiticity of the state due to the approximations

---

<sup>2</sup>Note this assumes we are restricting ourselves to the space of unit-trace Hermitian operators relevant for describing quantum states.

that are made to reduce dimensionality. While solutions to this problem exist [86, 87], they are often more computationally expensive or difficult to implement.

Focussing now on the case that the Liouvillian,  $\mathcal{L}$ , is time-independent, it is known that the evolution operators  $\Lambda_t$  form a semi-group,

$$\Lambda_{t+s} = \Lambda_t \circ \Lambda_s, \quad t, s \geq 0 \quad (1.64)$$

and can be formally expressed as the exponential,

$$\Lambda_t = e^{\mathcal{L}t}. \quad (1.65)$$

Evan's theorem [88, 89] also proves that there always exists at least one non-equilibrium steady state (NESS),  $\rho_\infty$  which satisfies

$$\mathcal{L}[\rho_\infty] = 0. \quad (1.66)$$

It is often physically relevant to find this NESS but such calculations present significant challenges. Numerically evolving the system until it converges is often impractical due to the numerical instabilities which prevent long time calculations. Direct diagonalisation techniques based on Arnoldi iterations and Krylov subspaces can prove useful [90] and are often better than numerical integration, but these are again restricted to relatively small systems. The most progress can often be made when the Liouvillian has particular symmetries [91]. For example, if the jump operators satisfy the condition

$$\sum_k L_k^\dagger L_k = \sum_k L_k L_k^\dagger \quad (1.67)$$

then the completely mixed state,  $\mathbb{1}/\sqrt{d}$ , is a NESS. In this case, the Liouvillian is called *unital*. Symmetries and their applications will be discussed in more detail in Sec. 3 and will be central to the approaches used in this thesis for providing analytic solutions to the Lindblad equation.

Diagonalisation, when possible, can also provide an approach to finding the dynamics of an open system. It is important to note that the superoperator  $\mathcal{L}$  need not be self-adjoint or even normal, and thus cannot always be diagonalised. When it can, there exist separate sets of left and right eigenstates,  $\{\rho_k, \sigma_k\}$  which obey

$$\mathcal{L}|\rho_k\rangle\rangle = \lambda_k |\rho_k\rangle\rangle, \quad \mathcal{L}^\dagger |\sigma_k\rangle\rangle = \lambda_k^* |\sigma_k\rangle\rangle, \quad \langle\langle \sigma_k | \rho_l \rangle\rangle = \delta_{k,l}. \quad (1.68)$$

This allows us to decompose the evolution operator as

$$\Lambda_t = \sum_k e^{\lambda_k t} |\rho_k\rangle\rangle \langle\langle \sigma_k|. \quad (1.69)$$

Note that the eigenstates,  $\{\rho_k, \sigma_k\}$ , are not necessarily density operators. We will make extensive use of this decomposition throughout this work, and by studying symmetries to understand the spectrum of the Liouvillian we will present analytic solutions to the dynamics of open quantum systems.



### 3 Symmetries in quantum systems and their generalisations

Having introduced the key ideas behind many-body and non-equilibrium quantum mechanics, let us discuss the role of symmetries in quantum theories and argue why this thesis will use techniques based on symmetries to solve the Lindblad equation analytically.

Symmetries have played a central role in physics for centuries and are generally responsible for reducing the complexity of a given system by fixing certain degrees of freedom. This idea was formalised in 1918 when Emmy Noether proved that every smooth symmetry of a system is associated with a conservation law [92]. The same idea is at the heart of quantum theory although the symmetries are generally more exotic. It is interesting to note that even though group theory had existed in mathematics since the early 1800s, it was only around the 1920s that the theory of group representations emerged, coinciding with the developments of early quantum theory [93]. Representations are the crucial link with which to connect abstract groups and symmetries in physical systems and so their introduction alongside quantum theory illustrates the importance of symmetries in quantum mechanics.

#### 3.1 Groups and representations

Before defining what we mean by a symmetry of a quantum system, let us first recall some elementary group theory to establish the nomenclature. We have two definitions:

**Definition** (Group). A group  $G = (G, \cdot)$  is defined as a set  $G$  and a closed binary operation,  $\cdot : G \times G \rightarrow G$  which satisfies

1. (Identity) There exists a unique element  $e \in G$  such that  $\forall g \in G, e \cdot g = g \cdot e = g$ .
2. (Inverse) For every  $g \in G$  there exists an inverse element  $g^{-1} \in G$  such that  $g \cdot g^{-1} = g^{-1} \cdot g = e$ .
3. (Associativity) For all  $a, b, c \in G, (a \cdot b) \cdot c = a \cdot (b \cdot c)$ .

**Definition** (Unitary Representation). A unitary representation of a group  $G$  on a Hilbert space  $\mathcal{H}$  is a homomorphism from  $G$  to the group of unitary transformations acting on  $\mathcal{H}$ .

We write the representation of  $G$  on  $\mathcal{H}$  as  $U(g)$  for each  $g \in G$ . If the group  $G$  is also a simply connected Lie group, i.e a group that is also a connected differentiable manifold with no holes, then we can associate each representation  $U$  of  $G$  with a representation,  $\pi$ , of the corresponding Lie algebra  $\mathfrak{g}$  via the exponential map

$$U(e^X) = e^{-i\pi(X)}, \quad X \in \mathfrak{g}, \quad g = e^X \in G. \quad (1.70)$$

Importantly  $\pi(X)$  is a Hermitian operator acting on  $\mathcal{H}$ . This corresponding representation of  $\mathfrak{g}$  preserves the Lie bracket in the sense that

$$\pi(X_1)\pi(X_2) - \pi(X_2)\pi(X_1) = \pi([X_1, X_2]). \quad (1.71)$$

We will often refer to the commutation relations of a representation  $\pi$ , which are in turn the commutation relations of given Lie algebra,  $\mathfrak{g}$ , as “the algebra” of  $\mathfrak{g}$ . There are of course more complicated prescriptions for non simply-connected Lie groups but these will not be important for the following discussions and further details can be found in many textbooks such as [94, 95].

## 3.2 Symmetries and conservation laws

### 3.2.1 Closed systems

Let us now return to the matter of symmetries in quantum systems. For a closed system described by the Hamiltonian,  $H$ , if there exists a group  $G$  and a unitary representation,  $U$ , of  $G$  acting on  $\mathcal{H}$  such that for all  $g \in G$

$$U(g)HU(g)^\dagger = H, \quad (1.72)$$

then we say that  $G$  is a symmetry group of the system. The individual elements  $U(g)$  are referred to as symmetries. If  $G$  is a simply connected Lie group then this is equivalent to

$$[H, \pi(X)] = 0, \quad \forall X \in \mathfrak{g}, \quad (1.73)$$

where  $\pi$  is the corresponding representation of  $\mathfrak{g}$ . Since  $\pi(X)$  is Hermitian, we can interpret it as an observable quantity and then the Schrodinger equation trivially implies that its expected value,  $\langle \pi(X) \rangle$ , is a conserved quantity and does not vary in time. This is reminiscent of Noether’s equivalence between symmetries and conserved quantities. For pure states, one can think about a symmetry of the Hamiltonian as restricting the evolution to a fixed manifold within  $\mathcal{H}$  in a similar way to how symmetries in classical systems restrict the trajectories in phase space.

It is important to consider the *locality* of symmetries and conserved charges, i.e. the region of space on which the operator has support. For instance, in the

lattice models we will be considering in this work a conserved charge is said to be *local* if it can be written as the sum

$$Q_l = \sum_x q_x^l, \quad (1.74)$$

where  $q_x^l$  is a strictly local operator which acts only on the site  $x$  and its  $l$  nearest neighbours. We also say that a conserved quantity is *extensive* if its norm scales with the size of the system. If instead the operator  $q_x^l$  were a conserved charge, we would call this a *strictly-local* conserved charge. As an example, consider the Hamiltonian for free, spinless fermions on a periodic ring,

$$H = \sum_{x=1}^L c_x^\dagger c_{x+1} + c_{x+1}^\dagger c_x, \quad (1.75)$$

where  $c_x^\dagger$  creates a fermion on site  $x$  and site  $L + 1$  is identified with site 1. Two examples of local symmetries are the total fermion number, and the total current

$$N = \sum_x c_x^\dagger c_x, \quad J = i \sum_x c_x^\dagger c_{x+1} - c_{x+1}^\dagger c_x \quad (1.76)$$

which are each comprised of sums of operators with support on only one or two sites respectively. Symmetries that are *not* local include projectors to energy eigenstates. Take, for simplicity, the one body energy eigenstates

$$|k\rangle = \sum_x e^{ikx} c_x^\dagger |\Omega\rangle, \quad (1.77)$$

where  $|\Omega\rangle$  is the vacuum. Then the operators  $P_k = |k\rangle \langle k|$  trivially commute with the Hamiltonian but when written as a sum of individual terms,

$$P_k = \sum_x \sum_y e^{ik(x-y)} c_x^\dagger |\Omega\rangle \langle \Omega| c_y, \quad (1.78)$$

we see that this includes long range terms with support at distantly separated sites, and is thus not local. We can also see that the operator norm of these projectors is independent of system size, thus they are not extensive symmetries either.

The existence of local conserved charges can have important consequences for the transport properties of a system, through the Mazur bound [96, 97]. The Mazur bound places lower bounds on the long-time averaged autocorrelation functions of observables in terms of equilibrium correlation functions of conserved charges. More recent work has generalised these ideas to quasi-local conserved quantities, which have been successfully used to explain transport properties, thermalisation behaviour and quench dynamics in integrable lattice models [98–103]. This emphasises the physical significance local symmetries when studying many-body systems.

A slight variant on this notion of symmetries are so-called *dynamical symmetries* [104–106], defined as operators that obey the closure relation

$$[H, A] = \omega A, \quad (1.79)$$

for non-zero  $\omega$ . This relation can also be viewed as a spectrum generating algebra<sup>3</sup> since it generates a series of energy eigenstates with evenly spaced energies. Similarly to conserved quantities, such operators can be trivially constructed by taking the outer product of two energy eigenstates with differing energies, i.e  $A = |E_k\rangle \langle E_l|$  with  $E_k \neq E_l$  which describe transitions between energy levels. However, in many-body systems, these operators are non-local and consequently do not influence the local physics on longer timescales. Instead, particular interest is given to dynamical symmetries which are extensive. These extensive dynamical symmetries are relevant in the thermalisation of many-body systems [106] and we will also use them to study persistent non-stationarity of non-equilibrium systems in Chs 3-5. Further, strictly local dynamical symmetries have been shown to have interesting consequences in quasi one dimensional lattice models, such as the emergence of a classical many-body attractor even in the absence of a well defined classical limit [110].

## Open systems

The classification of continuous symmetries and conserved quantities is less straightforward when we are considering dynamics defined by the Lindblad equation and to do so we must introduce some additional notation. First, the adjoint Liouvillian is given by the superoperator

$$\mathcal{L}^\dagger[\omega] = i[H, \omega] + \sum_k L_k^\dagger \omega L_k - \frac{1}{2} \{L_k^\dagger L_k, \omega\}, \quad \omega \in \mathcal{B}(\mathcal{H}), \quad (1.80)$$

and is used to describe the evolution of observables in the Heisenberg picture. Second, we introduce the adjoint representation of an operator  $U$  in the superoperator level [91, 111] as

$$\mathcal{U} : \mathcal{B}(\mathcal{H}) \rightarrow \mathcal{B}(\mathcal{H}), \quad \mathcal{U}[\omega] = U \omega U^\dagger. \quad (1.81)$$

Note that if  $U = e^{-itA}$  for some Hermitian  $A$ , then the adjoint representation of  $U$  can be written as

$$\mathcal{U} = e^{-it\mathcal{A}}, \quad \mathcal{A}[\rho] = [A, \rho]. \quad (1.82)$$

We can then make three definitions [111].

---

<sup>3</sup>Note that these terms have been previously used to describe various related but slightly different concepts [107–109].

**Definition** (Strong Symmetry). An open system has a strong symmetry if there exists a unitary operator,  $U$ , acting on  $\mathcal{H}$  which commutes with each individual element of the set  $\{H, L_k, k = 1, 2, \dots\}$ ,

$$[U, H] = 0, \quad [U, L_k] = 0, \quad k = 1, 2, \dots \quad (1.83)$$

**Definition** (Weak Symmetry). An open system has a weak symmetry if there exists a unitary operator  $U$  acting on  $\mathcal{H}$  such that for all  $\rho \in \mathcal{B}(\mathcal{H})$

$$\mathcal{L}[U\rho U^\dagger] = U(\mathcal{L}[\rho])U^\dagger. \quad (1.84)$$

**Definition** (Conserved quantity). An open system has a conserved quantity,  $A = A^\dagger$ , if

$$\mathcal{L}^\dagger[A] = 0. \quad (1.85)$$

As we have discussed, these three definitions are equivalent for closed systems but this is not the case for open systems. It is immediate that the existence of a strong symmetry implies the existence of a weak symmetry and the existence of a conserved quantity, but the converse does not hold. Also, a weak symmetry,  $U = e^{-itA}$  does not imply the existence of a conserved quantity,  $A$ , with

$$\frac{d}{dt}A = \mathcal{L}^\dagger[A] = 0. \quad (1.86)$$

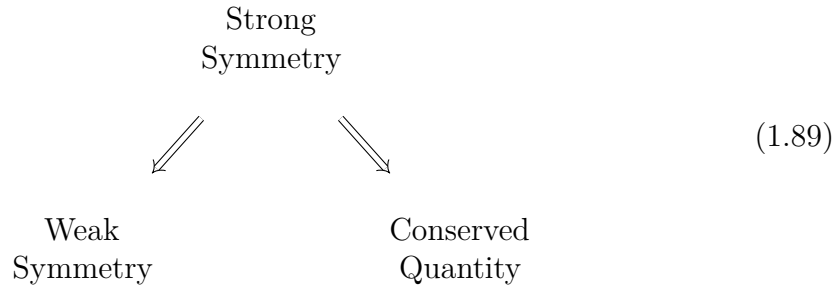
As a trivial example of this, consider a single bosonic mode,  $a$ , with Liouvillian

$$\mathcal{L}[\rho] = 2a\rho a^\dagger - a^\dagger a\rho - \rho a^\dagger a \quad (1.87)$$

where the unitary operator  $U(s) = e^{-isa^\dagger a}$  is a weak symmetry for all  $s \in \mathbb{R}$  but

$$\frac{d}{dt}a^\dagger a = (a^\dagger)^2 a^2 - (a^\dagger a)^2 \neq 0, \quad (1.88)$$

demonstrating that  $a^\dagger a$  is not conserved. Further, a conserved quantity implies neither the existence of a weak nor strong symmetry as is immediate from the trivial conservation of the identity operator. These relations can be summarised in the following diagram adapted from [91].



It should be noted that these relations hold only for *continuous* symmetries and that stronger conditions hold in the case of discrete symmetries such as reflections, discrete rotations or parity transformations [91].

### 3.3 Applications of symmetries

The existence of symmetries and conserved quantities place constraints on the evolution of open systems. Several previous results [91, 111–116] have been concerned with studying the number of stationary states of the system and deducing their properties. Weak symmetries are useful because they allow for the Liouvillian to be block diagonalised with each block corresponding to an eigenvalue of  $\mathcal{U}$ . However, this does not necessarily constrain the number of steady states. Instead, if one has a strong symmetry,  $U$ , then it is possible to bound the number of distinct steady states as being greater than or equal to the number of distinct eigenvalues of  $U$  [111]. Further, when the system has a unique steady state,  $\rho_\infty$ , weak symmetries are sufficient to construct selection rules that can be used to deduce some long-time properties of the system directly from its initial state [116].

It is also possible to consider symmetries that only preserve the steady-state subspace [91, 113]. By this we mean that if  $L_{ss} \subset \mathcal{B}(\mathcal{H})$  is the space of all steady-states then steady-state subspace symmetries are those unitary operators,  $U_{ss}$ , such that

$$U_{ss}\rho_\infty U_{ss}^\dagger \in L_{ss}, \quad \forall \rho_\infty \in L_{ss}. \quad (1.90)$$

Although all weak and strong symmetries of the system are steady-state symmetries, there can exist steady-state symmetries that are *not* symmetries of the full system. These are related to the block diagonal structure of the steady states which can be rotated within themselves and exchanged with other blocks of the same dimension. Since a steady-state symmetry,  $U_{ss}$ , needs only have support on  $L_{ss}$  it is in some cases possible to extend steady-state subspace symmetries to global symmetries of the whole system, provided Eq. (1.90) is maintained [91]. This procedure can allow one to control decoherence-free subspaces and noiseless subspaces which are used to protect qubits in quantum computers. It has further been demonstrated that the generators of these subspace symmetries can be approximated using physically realisable operations [117].

On the other hand, conserved quantities are very useful for determining the long-time properties of a system directly from their initial conditions. One can relate the existence of conserved quantities to the dimensions of the steady-state subspace through the conserved quantity – steady state correspondence [91, 112]. This states that in the absence of purely imaginary eigenvalues of the Liouvillian, if we choose an orthonormal basis  $\{M_\mu\}_{\mu=1}^D$  for  $L_{ss}$  then there exist  $D$  linearly independent conserved quantities,  $J_\mu$ , such that

$$\rho_\infty = \lim_{t \rightarrow \infty} e^{\mathcal{L}t} \rho_0 = \sum_{\mu=1}^D \text{Tr}[J_\mu^\dagger \rho_0] M_\mu. \quad (1.91)$$

This shows that in the more common case where the steady-state is unique, no information about the initial state is preserved by the evolution.

When considering dynamics, symmetries have also been demonstrated to have significant use. In particular, several of the above results contain the caveat “*assuming the absence of purely imaginary eigenvalues*”. When the Liouvillian has purely imaginary eigenvalues the resulting long-time state does not become stationary but instead continues to oscillate. Recent work studying decoherence-free subspaces [118] and strong dynamical symmetries [119, 120] have provided sufficient conditions for the existence of these purely imaginary eigenvalues. These results will be extended in Ch 3 and applied in Chs 4 & 5.

Moving away from symmetries of the Lindblad equation, another setting where symmetries have proven to be very useful is for studying integrable systems. In these systems, an extensive set of local conservation laws places sufficient constraints on the Hamiltonian that the eigenvalues and eigenstates can be expressed in terms of solutions to the Bethe equations [121–124]. Although these equations are often difficult to solve completely, even numerically, much has been learned about the thermalisation and transport properties of isolated integrable systems. More recent work has been interested in studying open integrable systems, which can in principle mean two things:

- The full Liouvillian can be mapped to an isolated non-Hermitian system that is integrable, or
- The open system in question has a Hamiltonian,  $H$ , which is integrable but the influence of the environment must now be considered.

The mapping of full Liouvillians to non-Hermitian integrable systems has been studied extensively for various models [125–128] and has uncovered several interesting properties. However, the models to which this method can be applied can sometimes be rather contrived and less experimentally relevant. The question of integrable systems in the presence of an environment, which is arguably more relevant to experiments and technological applications, has been less studied analytically and will be the topic of Ch 2.

These various applications of symmetries and the corresponding algebras demonstrate the utility of algebraic methods for studying the dynamics of quantum systems, even in the presence of an environment. These methods often have the advantage of being independent of system size and being well defined in the thermodynamic limit through  $C^*$ -algebras. It is for these reasons that this thesis will use algebraic techniques to provide solutions to the dynamics of many-body open quantum systems.

## 4 Dynamical phases of matter and their technological applications

Having introduced the main ideas behind the focus of this thesis – solving the dynamics of the Lindblad equation for many-body systems using symmetries – let us outline some of the phenomena that we will study with these solutions. In this work, we will focus on lattice systems, which are particularly relevant for quantum technologies and material science, and thus we refer to the broad class of phenomena as dynamical phases of matter. More specifically we will be interested in three main phenomena: transport properties and superconductivity, synchronisation and time crystals.

### Transport properties and superconductivity

In condensed matter and atomic physics, there has been a long-standing interest in understanding the motion of quantum charges such as energy, electric charge and spin through a system that is not in equilibrium. Historically, transport has either been classified as ballistic, where the total current is proportional to the total charge, or diffusive, where the current scales as  $1/L$  where  $L$  is the system size. These phases correspond to the charge carriers moving either with constant velocity or evolving according to the diffusion equation respectively. When studying transport in quantum systems, these phases are usually characterised by studying the Drude weight and Onsager matrix [129] or by the scaling of two point correlation functions. Recent works in this direction have been focused on classifying the dynamical phases of a quantum system into these different universality classes using a variety of theoretical techniques and experimental evidence to understand their origins [130]. It has also been found that there exists another universal transport phase, referred to as KPZ-diffusion [131–134], where higher order noise terms become relevant in the hydrodynamic description of the system, leading to a new scaling law.

Studying the transport of quantum systems in the hydrodynamic regime has led to the recent development of generalised hydrodynamics (GHD) [129, 135, 136]. GHD uses the thermodynamic Bethe ansatz for integrable quantum systems [137, 138] to describe the dynamics of these systems in the hydrodynamic limit using non-linear wave equations. We will discuss GHD further in Ch 2, focussing in particular on its application to systems experiencing dissipation.

The final transport property of quantum matter that we will be interested in is superconductivity. First discovered by Onnes in 1911 [139] and described microscopically for the first time by Bardeen, Cooper, and Schrieffer in 1957 [140], superconductivity describes a phase of matter where electrical resistance vanishes and magnetic fields are expelled. The magnetic behaviour is evidence that this phase



cannot simply be understood through extensions of classical perfect conductivity. Superconducting materials have a wide array of applications, but are primarily limited by only existing at extremely low temperatures. Many studies have been concerned with inducing and stabilising superconductivity in materials at higher temperatures and this will be the topic of Ch 6.

## **Synchronisation**

The scientific study of synchronised dynamical systems dates back to 1673 when Huygens studied the motions of two weakly coupled pendula [141]. He observed that pendula clocks hanging from the same bar had matched their frequency and phase exactly. Since Huygens in the 17th century, synchronisation has been a topic of significant interest in an ever-expanding range of scientific and technological fields [142, 143]. The synchronisation in quantum systems has also been attracting more recent attention with several systems having been studied in a case-by-case manner and various measures of quantum synchronisation having been introduced [144–156]. Unfortunately, much of this work has been focused on small systems using methods that often do not scale well for many-body problems.

However, synchronisation in quantum systems holds much technological promise. For instance, by synchronising spins one could engineer homogeneous and coherent time-dependent magnetic field sources. Such sources of homogeneous and coherent time-dependent magnetic fields have the significant potential application of improving the resolution of MRI images [157]. In an alternative direction, the role of synchronisation in the security of quantum key distribution (QKD) protocols has been recently explored [158–160]. One could envisage that by improving our understanding of quantum synchronisation we could improve security against specialist attacks that exploit the dependence of several QKD schemes on a synchronisation calibration step.

## **Time crystals**

Time crystals are states of quantum matter that are ordered in the time domain and break time translational symmetry. They were first proposed by Wilczek in [161] for undriven closed systems. This original proposal was soon claimed to be impossible by Watanabe and Oshikawa [162], but their original proof was incorrect [163] and required revision [164]. Slight variations on Wilczek’s initial proposal for a time crystal in an undriven closed system have also been studied [106, 165].

The original no-go theorem of Watanabe and Oshikawa motivated the study of more exotic criteria for time crystals in non-equilibrium and driven systems such as Floquet time crystals in periodically driven systems [166–169], dissipative time crystals where the ordered state is induced by a noisy environment [119, 170, 171]

and extensions to classical models [172–174] among many others. The reader is directed to the review of Khemani et al. [163] for an extensive discussion of the current state of the time crystal landscape.

From a theoretical viewpoint, time crystals have provided a new insight into thermalisation and relaxation to equilibrium or more interestingly the alternatives that can and do exist. Additionally, the study of Floquet time crystals has driven a number of advances in our understanding of periodically driven systems and the techniques available to study them. On the experimental front, recent experiments have been able to create several types of time crystals for the first time [175–179]. Further, there are proposals to utilise time crystals to improve the performance of quantum computers at warmer temperatures, or to improve atomic clocks [180, 181].

## 5 Summary

To summarise, in this comprehensive introductory chapter we have introduced the ideas of many-body non-equilibrium quantum systems and set the scene for the remainder of this thesis. In particular, we have derived the Lindblad equation as the most general evolution for a Markovian system that is interacting with the environment. We highlighted the challenges that arise when trying to solve the Lindblad equation for many-body systems and argued how symmetry constraints and the related algebras can provide a natural language with which to construct solutions.

The remainder of this thesis will be focused on solving the dynamics of non-equilibrium quantum systems in different settings. We will first study integrable systems, which have so many symmetries that when isolated their spectrum can be completely solved analytically. We will study the consequences of loss in such systems and construct a method to analytically find the Liouvillian spectrum. We then use this to understand the transport phenomena of an XXZ spin chain with boundary loss, although other possible examples where this method can be applied will be indicated.

We then move on to study more general systems with less strict algebraic structure. In these systems we will be able to give necessary and sufficient conditions for the system described by the Lindblad equation to be persistently non-stationary, almost akin to a perpetual motion machine. These conditions will then allow us to study the phenomena of time crystals and quantum synchronisation in experimentally realisable models.

Our final topic will be to study non-equilibrium superconductivity in driven materials. Here we will not use the Lindblad equation directly, but instead rely on even more general principles of thermalisation in an attempt to understand how recent experiments have succeeded in inducing superconductivity well above

$T_c$  using laser driving. We will propose a theory based on approximately conserved symmetries related to Yang's  $\eta$ -pairing of electrons.

We will then conclude by evaluating our results and discussing avenues for future follow-up work. Details of the numerical methods used to perform the simulations in the thesis are presented in the appendices.

# 2

## Integrable systems in the presence of dissipation

For centuries, physical systems that can be exactly solved analytically in terms of a few dependent parameters have been studied. The most canonical examples from classical physics include harmonic oscillators and motion in central forces such as gravity or electromagnetism. The reason for the sustained interest in these integrable models is two-fold: firstly, analytic solutions generally allow for more straightforward analysis of exciting features of the dynamics such as phase transitions, stationary states or bifurcations. Secondly, we can use our exact solutions to perturbatively solve similar models or to construct more complex models and theories that can also be solved exactly.

In quantum mechanics, integrable models of lattice electrons, spin chains and 1D Bose gasses, all in isolated systems, have been studied extensively over the last 90 years, both theoretically and experimentally. The first topic of this thesis will be to study the dynamics of these integrable quantum systems in the presence of dissipation, a subject that is only recently attracting attention. We will present a method that can be employed to solve for the Liouvillian eigenvalues of integrable systems in the presence of either pure loss or pure gain. This method will be applied to study the interesting dynamics of an XXZ spin chain with localised loss at one boundary.

We will then discuss the issues that arise when extending our techniques to the thermodynamic limit. This will lead naturally to a discussion of the recently developed field of generalised hydrodynamics, where the dynamics of quantum systems are studied using an approach similar to that of fluid dynamics. We will comment on how these new ideas can be used to study dissipative systems and indicate some interesting potential applications.

# 1 Introduction to integrability

Let us first give a very brief introduction to integrability to highlight the techniques that will be important in subsequent sections. Unfortunately, it will be impossible to provide a comprehensive review of the field nor details of all the related derivations and calculations as such a discussion would consume this whole thesis if not more. Instead, we will focus on highlighting the key concepts and only presenting details directly relevant to the new results presented in the following sections. For more comprehensive treatments, see [123, 182, 183] and the further references therein.

The study of integrability has its roots in classical dynamics, where integrability generally refers to the existence of sufficiently many conserved quantities, also sometimes called first integrals, such that the evolution is restricted to a submanifold of phase space with significantly fewer degrees of freedom than the dimension of phase space. One of the most famous results in this field is the Arnold-Liouville theorem [184], which completely solves a time-homogeneous Hamiltonian system with a  $2n$ -dimensional phase space in terms of action-angle variables constructed through integration over  $n$ -dimensional tori provided the system has at least  $n$  independently conserved quantities. This result explicitly solves the system's dynamics in terms of the conserved quantities and completely determines the motion in terms of the initial conditions.

Unfortunately, the Arnold-Liouville approach is only suited to Hamiltonian systems of ordinary differential equations. However, alternative methods have been developed for non-linear partial differential equations, most notably the inverse scattering method and the GLM equation [185–188]. Inspired by the discovery of solitons solutions to the KdV equation in the 1960's [189], these and similar methods rewrite the PDE using a Lax pair, which then fixes the spectral evolution and allows the dynamics to be determined from the initial conditions in a similar way to the application of Fourier analysis for linear PDEs. These Lax operators can also then be used to construct an infinite hierarchy of conserved quantities.

## 1.1 Integrability of a quantum system and the Yang-Baxter equations

The development of the inverse scattering method for PDEs subsequently inspired a unification of quantum integrability. Previously, it had been known that the eigenvalues and eigenstates of several systems could be solved for exactly in terms of Bethe equations using an ansatz<sup>1</sup> for the wavefunction, but the general underlying structure that connected these seemingly unrelated models was not very well understood. This unification is known as the algebraic Bethe ansatz, which can be

---

<sup>1</sup>See Sec 1.2 for more details.

viewed as a second quantisation of the previously used coordinate Bethe ansatz and uses the Yang-Baxter algebra to construct excitation operators that give the Hamiltonian eigenstates [123]. This formulation has allowed integrable quantum systems to be understood in terms of quantum groups and their related algebras [190]. It is also interesting to note that the algebraic Bethe ansatz provides a connection between integrable 1D quantum systems and two-dimensional integrable classical models from statistical physics, providing yet another possible angle from which to understand quantum systems [123, 191, 192].

We will now briefly outline the algebraic Bethe ansatz using the example of a closed XXX spin-1/2 chain. The XXX model is one of the earliest examples of an integrable quantum system, being first studied by Hans Bethe in 1931 [124], and is often taken as the simplest model of quantum magnetism. It can also be applied, following a Jordan-Wigner transformation<sup>2</sup>, to study spinless fermions in 1D. The XXX Hamiltonian for a chain of length  $N$  is given by

$$H = - \sum_{j=1}^N \mathbf{s}_j \cdot \mathbf{s}_{j+1}, \quad (2.1)$$

where we have assumed periodic boundary conditions so that the site  $N + 1$  is identified as the site 1. Here and throughout this thesis subscripts are used to indicate the lattice site upon which an operator acts, i.e.

$$O_j = \mathbb{1}_1 \otimes \cdots \otimes \mathbb{1}_{j-1} \otimes O \otimes \mathbb{1}_{j+1} \otimes \cdots \otimes \mathbb{1}_N. \quad (2.2)$$

Note that we can also write the Hilbert space of the system as

$$\mathcal{H} = \bigotimes_{j=1}^N h_j \quad (2.3)$$

where  $h_j \cong \mathbb{C}^2$  is the local Hilbert space of each site. We will use the  $z$  basis for each site, denoting a spin up as  $|\uparrow\rangle$  and a spin down as  $|\downarrow\rangle$ . We have also use the spin-1/2 operators, which in this basis are defined as

$$s^x = \frac{1}{\sqrt{2}} \begin{pmatrix} 0 & 1 \\ 1 & 0 \end{pmatrix}, \quad s^y = \frac{1}{\sqrt{2}} \begin{pmatrix} 0 & -i \\ i & 0 \end{pmatrix}, \quad s^z = \frac{1}{2} \begin{pmatrix} 1 & 0 \\ 0 & -1 \end{pmatrix}, \quad (2.4)$$

with the raising and lowering operators also given by

$$s^+ = \frac{1}{2} (s^x + i s^y), \quad s^- = \frac{1}{2} (s^x - i s^y). \quad (2.5)$$

To formulate the algebraic Bethe ansatz, we must now construct the Lax operators, labelled  $L_{j,a}$ . These operators act on the space  $h_j \otimes V_a$  where  $V_a$  is an

---

<sup>2</sup>See appendix A for details of the Jordan-Wigner transformation.

auxiliary space. For the examples of an XXX spin-1/2 chain, we take  $V_a \cong \mathbb{C}^2$ , but in general,  $h_j$  and  $V_a$  need not be the same. Our Lax operators are defined for some complex spectral parameter  $\lambda$  as

$$L_{j,a}(\lambda) = \lambda \mathbb{1} + i s_j \otimes \sigma_a = \begin{pmatrix} \lambda + i s_j^z & i s_j^- \\ i s_j^+ & \lambda - i s_j^z \end{pmatrix}, \quad (2.6)$$

where we have written the matrix representation in block form. These operators can be interpreted as a kind of connection along the chain in the sense that when we take the classical continuum limit the Lax operator performs parallel transport [193]. Following this interpretation it is natural to define the monodromy matrix

$$\begin{aligned} \mathcal{T}_a(\lambda) &: \mathcal{H} \otimes V_a \rightarrow \mathcal{H} \otimes V_a \\ \mathcal{T}_a(\lambda) &= L_{N,a}(\lambda) L_{N-1,a}(\lambda) \dots L_{1,a}(\lambda), \end{aligned} \quad (2.7)$$

which describes parallel transport around one complete loop of the chain. We then require that transport around two loops of the chain should be related by a similarity transform

$$\mathcal{T}_a(\lambda) \mathcal{T}_b(\mu) R_{a,b}(\mu - \lambda) = R_{a,b}(\mu - \lambda) \mathcal{T}_b(\mu) \mathcal{T}_a(\lambda), \quad (2.8)$$

where  $R_{a,b} : V_a \otimes V_b \rightarrow V_a \otimes V_b$  is known as the  $R$ -matrix. The existence of such a similarity transform follows from the  $R$ -matrix satisfying the Yang-Baxter equation

$$R_{1,2}(\lambda - \mu) R_{1,3}(\lambda - \nu) R_{2,3}(\mu - \nu) = R_{2,3}(\mu - \nu) R_{1,3}(\lambda - \nu) R_{1,2}(\lambda - \mu). \quad (2.9)$$

This equation is usually taken as the definition of integrability, and all solutions to it generate a family of integrable models by using the following construction. However, there is no known predefined method for determining the  $R$ -matrix corresponding to a given Hamiltonian if it even exists. Instead, the usual approach is to seek a solution to Eq. (2.9) for a given auxiliary space and then use the corresponding Lax operators to derive the resulting model. Reasonable guesses for such an ansatz can be made from the methods developed for 2D classical integrable models [191]. In the case of the XXX model we are considering, the  $R$ -matrix is given by

$$R_{a,b}(\lambda) = \begin{pmatrix} \lambda + i & 0 & 0 & 0 \\ 0 & \lambda & i & 0 \\ 0 & i & \lambda & 0 \\ 0 & 0 & 0 & \lambda + i \end{pmatrix}. \quad (2.10)$$

Given an  $R$ -matrix and corresponding Lax operators, the Hamiltonian is defined in terms of the transfer matrix. The transfer matrix, which acts only on the Hilbert space  $\mathcal{H}$ , is found by tracing out the auxiliary space from the monodromy matrix

$$\mathbf{T}(\lambda) = \text{Tr}_{V_a} \mathcal{T}_a(\lambda). \quad (2.11)$$

Notice from the definition of the monodromy matrix that the transfer matrix is a polynomial of order  $N$  in  $\lambda$ . Importantly, the transfer matrices with different spectral parameters all commute,

$$[\mathbf{T}(\lambda), \mathbf{T}(\mu)] = 0, \quad (2.12)$$

as a direct consequence of Eq. (2.8). Since the transfer matrices are polynomials of degree  $N$  in  $\lambda$  this construction has provided a set of  $N$  independent commuting operators on  $\mathcal{H}$ . The Hamiltonian is then defined as

$$H = -\frac{i}{2} \frac{d\mathbf{T}}{d\lambda} \cdot \mathbf{T}^{-1} \Big|_{\lambda=\frac{i}{2}} + \frac{N}{2}. \quad (2.13)$$

Note that, in general, different constants can be chosen for different models, but this combination recovers Eq. (2.1). Since we have constructed  $H$  in terms of commuting transfer matrices, we can conclude that  $\mathbf{T}(\lambda)$  is a conserved quantity for each  $\lambda$ , and thus we have found  $N$  independently conserved quantities. This connects us back to the classical definition of integrability from the Arnold-Liouville theorem.

We can now also construct the eigenstates of  $H$  in terms of the monodromy matrix. To do so we write

$$\mathcal{T}_a(\lambda) = \begin{pmatrix} A(\lambda) & B(\lambda) \\ C(\lambda) & D(\lambda) \end{pmatrix}, \quad (2.14)$$

so that when we trace over the auxillary space we have

$$\mathbf{T}(\lambda) = A(\lambda) + D(\lambda). \quad (2.15)$$

The Yang-Baxter equations give us a long list of relations between these operators, most importantly

$$[B(\lambda), B(\mu)] = 0, \quad (2.16a)$$

$$A(\lambda)B(\mu) = \frac{\lambda - \mu - i}{\lambda - \mu} B(\mu)A(\lambda) + \frac{i}{\lambda - \mu} B(\lambda)A(\mu), \quad (2.16b)$$

$$D(\lambda)B(\mu) = \frac{\lambda - \mu + i}{\lambda - \mu} B(\mu)D(\lambda) - \frac{i}{\lambda - \mu} B(\lambda)D(\mu). \quad (2.16c)$$

We then define the vacuum state as

$$|\Omega^+\rangle = |\uparrow \dots \uparrow\rangle, \quad (2.17)$$

which is an eigenstate of  $\mathbf{T}(\lambda)$  with eigenvalue

$$\Lambda(\lambda) = \left(\lambda + \frac{i}{2}\right)^N + \left(\lambda - \frac{i}{2}\right)^N. \quad (2.18)$$



We can then use the relations in Eq. (2.16) to show that for a set of values  $\{\lambda_k\}_{k=1}^M$  the so-called Bethe states

$$|\{\lambda_k\}\rangle = B(\lambda_1) \dots B(\lambda_M) |\Omega^+\rangle, \quad (2.19)$$

have eigenvalues

$$\Lambda(\lambda; \{\lambda_k\}) = \left(\lambda + \frac{i}{2}\right)^N \prod_{k=1}^M \frac{\lambda - \lambda_k - i}{\lambda - \lambda_k} + \left(\lambda - \frac{i}{2}\right)^N \prod_{k=1}^M \frac{\lambda - \lambda_k + i}{\lambda - \lambda_k}. \quad (2.20)$$

Notice however that this equation has poles at  $\lambda = \lambda_k$ . These are removed exactly when

$$\left(\frac{\lambda_k + i/2}{\lambda_k - i/2}\right)^N = \prod_{m \neq k} \frac{\lambda_k - \lambda_m + i}{\lambda_k - \lambda_m - i}, \quad k = 1, \dots, M, \quad (2.21)$$

and in this case we can conclude that these states are eigenstates of  $H$  with energies

$$E(\{\lambda_k\}) = \frac{1}{2} \sum_{k=1}^M \frac{1}{\lambda_k^2 + \frac{1}{4}}. \quad (2.22)$$

The parameters  $\{\lambda_k\}$  are known as the Bethe roots or rapidities, while Eq. (2.21) are known as the Bethe equations. We can interpret the  $B(\lambda)$  operators as creating excitations on top of the vacuum, each with a quasi-momentum  $\lambda$ . It can also be shown that a state corresponding to  $M \leq N/2$  Bethe roots is an eigenstate of the total  $S^z = \sum s_k^z$  operator with eigenvalue  $\frac{N}{2} - M$  and vanishes under the action of  $S^+ = \sum s_k^+$ . The remaining states with magnetisation less than zero can be found by applying the lowering operator,  $S^- = \sum s_k^-$ , to the Bethe states or by following a similar construction from the alternative vacuum state,  $|\Omega^-\rangle = |\downarrow \dots \downarrow\rangle$ .

## 1.2 Coordinate Bethe-ansatz

Before discussing the consequences of these results, we will also present an alternative derivation known as the coordinate Bethe ansatz. This is the original method proposed by Bethe in [124] and extended by others to many other models [194–199]. We will follow [194] and use this method to derive the Bethe equations for an open XXZ spin-1/2 model with a boundary term, as this will be relevant to our example in the next section.

Our starting point is the Hamiltonian

$$H = \alpha s_1^z + \sum_{k=1}^{N-1} s_k^x s_{k+1}^x + s_k^y s_{k+1}^y + \Delta s_k^z s_{k+1}^z. \quad (2.23)$$

We take the state

$$|\phi_m\rangle = \sum_{1 \leq x_1 < \dots < x_m \leq N} f(x_1, \dots, x_m) |x_1, \dots, x_m\rangle, \quad (2.24)$$

for a state with total magnetisation  $m - N/2$ . Note that  $|x_1, \dots, x_m\rangle$  indicates the positions of  $m$  sites with spin up while all other sites have spin down. We use the coordinate ansatz

$$f(x_1, \dots, x_m) = \sum_P \epsilon_P A(k_1, \dots, k_m) e^{i(k_1 x_1 + \dots + k_m x_m)}, \quad (2.25)$$

where the summation is over all permutations and negations of the set  $\{k_j\}$  and  $\epsilon_P$  changes sign with each such *mutation*. Directly solving the eigenvalue equation for  $H$ , after a little algebra we arrive at the Bethe equations

$$\frac{e^{2iNk_j}(\Delta - e^{ik_j})(e^{ik_j} - 2\alpha - \Delta)}{(e^{ik_j}\Delta - 1)(1 - e^{ik_j}(2\alpha + \Delta))} = \prod_{l \neq j}^m S(e^{ik_j}, e^{ik_l}). \quad (2.26)$$

Here we have written the two body scattering matrix as

$$S(a, b) = \frac{(a - 2\Delta ab + b)(1 - 2\Delta a + ab)}{(a - 2\Delta + b)(1 - 2\Delta b + ab)}, \quad (2.27)$$

and find that the coefficients  $A(k_1, \dots, k_m)$  are given by

$$A(k_1, \dots, k_m) = \prod_{j=1}^m (\Delta e^{-ik_j N} - e^{-i(N+1)k_j}) \prod_{1 \leq j < l \leq m} B(-k_j, k_l) e^{-ik_l}, \quad (2.28)$$

$$B(k, k') = (1 - 2\Delta e^{ik'} + e^{i(k+k')})(1 - 2\Delta e^{-ik} + e^{i(k'-k)}).$$

Finally, this calculation gives us the energy of the state as

$$E(\{k_j\}) = \frac{1}{4} ((N-1)\Delta - 2\alpha) + \sum_{j=1}^m (\cos k_j - \Delta). \quad (2.29)$$

We note that this same result can be obtained using the algebraic Bethe ansatz in a similar way to our explanation above. However, since the pseudo-Hamiltonian contains a boundary term, the definition of the monodromy matrix must be modified using Sklyanin's reflection algebra [200]. Additionally, adapting the algebraic Bethe ansatz to allow for  $\Delta \neq 1$  requires q-deformation [201, 202]. Thus, in this case, it is arguably more straightforward to use a sensible coordinate ansatz and solve the eigenvalue equation directly.

### 1.3 Discussion

The two preceding sections have demonstrated how Bethe ansatz techniques enable us to transfer the problem of diagonalising an exponentially growing Hamiltonian, to solving a system of Bethe equations. At the heart of both methods is the simplification that arises from the  $M$ -body scattering amplitude factorising into

products of the 2-body scattering amplitude. We can see this by rewriting the Bethe equations in (2.21) as

$$e^{ip(\lambda_k)N} = \prod_{m=1}^M S(\lambda_k - \lambda_m), \quad (2.30a)$$

$$S(\lambda) = \frac{\lambda + i}{\lambda - i}, \quad p(\lambda) = -i \log \frac{\lambda + i/2}{\lambda - i/2}. \quad (2.30b)$$

Here we have expressed the momentum of an excitation with quasi-momentum  $\lambda_k$  as  $p(\lambda_k)$  and written the two-body scattering amplitude as  $S(\lambda)$ . From this, it is clear that the Bethe equations precisely describe how the  $M$ -body scattering amplitude is expressible in terms of 2-body amplitudes. This phenomenon is, in fact, one manifestation of the integrability of a general model.

Unfortunately, the solution provided by the Bethe ansatz is not as straightforward to use in practical applications as one might hope. Firstly, for most systems, the Bethe equations are very difficult to solve, even numerically, as they are highly non-linear coupled equations. While effort has been devoted to developing methods for solving these equations [203–205], it remains a non-trivial task that must be completed to use the subsequent results. The second difficulty arises when trying to compute expectation values and overlaps. This is because the eigenstates given by the construction in Eq. (2.19) are expressed in terms of highly non-local  $B(\lambda)$  operators whose expression in the  $z$  basis is far from straightforward. There have been substantial results in this direction, with the relevant form factors for several models being calculated [206–212]. However, in general, it remains a difficult question to calculate the overlap between a Bethe state and some initial state as is required when calculating dynamics.

As a result of these difficulties, many successes in studies of integrable models have been in the thermodynamic limit. Here, the thermodynamic Bethe ansatz (TBA) [138, 213] has been developed to extend the ideas above which apply to strictly finite-dimensional systems. More recently these ideas have been extended to study dynamics through generalised hydrodynamics (GHD) [129, 136, 214]. We will give more details of both the TBA and GHD later in this chapter. Using these techniques, much has been learnt about the transport and thermalisation properties of closed integrable systems.

## 2 Dissipative Bethe Ansatz

Having given a brief outline of the basic techniques of integrability in quantum systems, we are ready to introduce the dissipative Bethe ansatz. This novel method allows us to exactly calculate the spectra of interacting, many-body Liouvillians

where the system is experiencing pure losses. The dissipative Bethe ansatz opens the possibility of analytically calculating the dynamics of a wide range of experimentally relevant models, including cold atoms subjected to one and two body losses, coupled cavity arrays with bosons escaping the cavity, and cavity quantum electrodynamics. Such analytic results have previously been inaccessible for systems of this type.

It is important to distinguish our results from two classes of similar studies. Firstly, there has been intense recent interest in studying integrable Liouvillians. In these models, the full Liouvillian can be mapped to some non-Hermitian Hamiltonian, which is integrable using the above techniques [125–128, 215–217]. In our case, it will not be necessary that the full Liouvillian be integrable in this sense. Indeed for the example that we study in detail, the Liouvillian itself does not seem to be mappable to any known integrable non-Hermitian Hamiltonian. We checked this by performing vectorisation and then attempting to solve a reflection equation that would generate the Liouvillian, but it proved impossible<sup>3</sup>. Secondly, we must emphasise that, in general, the models that this method applies to are strongly interacting. This should be contrasted with results based on 3<sup>rd</sup>-quantisation [218, 219] which reduces the dimensionality of the problem to polynomial rather than exponential. Importantly 3<sup>rd</sup>-quantisation can only be applied to models that are *quadratic* in either bosonic or fermionic operators, or weakly interacting models through perturbative analysis.

## 2.1 Spectral solutions to models with loss

The problem of interest will be to find the spectrum of some Liouvillian describing a quantum evolution through the Lindblad equation,

$$\frac{d}{dt}\rho(t) = \mathcal{L}\rho(t) := -i[H, \rho(t)] + \sum_{\mu} \left( 2L_{\mu}\rho(t)L_{\mu}^{\dagger} - \{L_{\mu}^{\dagger}L_{\mu}, \rho(t)\} \right), \quad (2.31)$$

where  $H$  is the system Hamiltonian and  $L_{\mu}$  are the Lindblad jump operators modeling the influence of the environment on the system. As we discussed in Ch 1, under the assumption that the system is diagonalisable we can decompose the evolution of operators in terms of the eigenstates and eigenvalues. Thus solving for the spectrum of the Liouvillian provides great insight into the dynamics of the system.

The general setup that we consider comprises an integrable Hamiltonian  $H$  with a conservation law  $M$  and Lindblad operators  $L_{\mu}$  that change the eigenvalue of  $M$  by well-defined amounts

$$[M, L_{\mu}] = -m_{\mu}L_{\mu}, \quad m_{\mu} > 0. \quad (2.32)$$

---

<sup>3</sup>Note that the spectral statistics cannot be used to check for integrability because the spectrum of the Liouvillian is the same as that of the integrable non-Hermitian Hamiltonian.

Such Lindblad operators can be interpreted as inducing the loss of the quantity  $M$  in the system. For instance  $M$  can be the total particle number and  $L_\mu$  particle annihilation operators. For the following discussion it will be useful to represent the Liouvillian superoperator in Fock-Liouville space with doubled degrees of freedom using vectorisation

$$|\psi\rangle\langle\phi| \rightarrow |\psi\rangle \otimes |\phi\rangle, \quad (2.33)$$

which gives

$$\mathcal{L} = -i(H \otimes \mathbb{1} - \mathbb{1} \otimes H^T) + \sum_{\mu} \left( 2L_{\mu} \otimes L_{\mu}^* - L_{\mu}^{\dagger} L_{\mu} \otimes \mathbb{1} - \mathbb{1} \otimes (L_{\mu}^{\dagger} L_{\mu})^T \right). \quad (2.34)$$

We then define the non-Hermitian pseudo-Hamiltonian [81, 220]

$$\tilde{H} \equiv -iH - \sum_{\mu} L_{\mu}^{\dagger} L_{\mu}, \quad (2.35)$$

so that the Liouvillian in Eq. (2.34) can be decomposed as

$$\mathcal{L} = \text{ad}\tilde{H} + \mathcal{D}, \quad (2.36a)$$

$$\text{ad}\tilde{H} = \tilde{H} \otimes \mathbb{1} + \mathbb{1} \otimes \tilde{H}^*, \quad (2.36b)$$

$$\mathcal{D} = 2 \sum_{\mu} L_{\mu} \otimes L_{\mu}^*. \quad (2.36c)$$

Let us now consider a basis of states that are eigenstates of the conservation law superoperator

$$\mathcal{M} = M \otimes \mathbb{1} + \mathbb{1} \otimes M, \quad (2.37)$$

and ordered by their corresponding eigenvalues. Since the action of  $L_{\mu}$  is to strictly lower the value of the conservation law, the matrix elements of  $\mathcal{D}$  in this basis will lie strictly above the diagonal. Further, since  $[\tilde{H}, M] = 0$  the matrix elements of  $\text{ad}\tilde{H}$  all lie on the diagonal in this basis. This immediately implies that the eigenvalues of  $\mathcal{L}$  coincide with those of  $\text{ad}\tilde{H}$ . Finally, since  $\text{ad}\tilde{H}$  is a sum of two operators acting on the factors in a tensor product independently, we can deduce that its eigenvalues are given by

$$\lambda_{j,k} = \tilde{E}_j + \tilde{E}_k^*, \quad (2.38)$$

where  $\tilde{E}_k^*$  are the pseudo energies of  $\tilde{H}$ . Thus, provided that the non-hermitian Hamiltonian  $\tilde{H} = -iH - \sum_{\mu} L_{\mu}^{\dagger} L_{\mu}$  is exactly solvable, we have found the full spectrum of the Liouvillian. However, the structure of Liouvillian eigenvectors corresponding to the eigenvalue  $\lambda_{i,j}$  is more complicated and includes couplings between different eigenspaces of the conservation law, as we will show later in

the example. Note that systems with Lindblad operators describing pure gain can be treated on exactly the same footing.

For general interacting, many-body systems, solving  $\tilde{H}$  is still intractable due to the exponential complexity. However, in many physically relevant situations, the dissipative contribution,  $\sum_{\mu} L_{\mu}^{\dagger} L_{\mu}$ , modifying the system's integrable Hamiltonian,  $H$ , will leave  $\tilde{H}$  integrable in the following sense. Our integrable system Hamiltonian,  $H(a_1, \dots, a_k)$ , will generally depend on some parameters,  $a_j \in \mathbb{R}$ , such as interaction strengths, potentials etc.. We are interested in the situations where the pseudo-Hamiltonian can be written as

$$\tilde{H} = H(\alpha_1, \dots, \alpha_k) \quad (2.39)$$

for some modified parameters  $\alpha_j \in \mathbb{C}$ . In these cases, we may use the Bethe Ansatz solution to  $H$  with the new parameters to determine the spectrum of  $\tilde{H}$  and hence the spectrum of our full Liouvillian. In the next section, we will demonstrate how every integrable system Hamiltonian offers at least one corresponding lossy dissipative process that renders it solvable according to our approach.

## 2.2 Examples of dissipative quantum models solvable by the dissipative Bethe ansatz

Here we detail examples of physically relevant lossy dissipative processes that allow integrable Hamiltonians to remain integrable in our procedure, and thus the corresponding Liouvillian spectrum can be found analytically.

### 2.2.1 Single body loss

The most straightforward example is to take any integrable  $U(1)$  symmetric Hamiltonian with symmetry  $N = \sum_j a_j^{\dagger} a_j$ , and corresponding loss  $L_k = \gamma a_k$ ,  $[N, a_k] = -a_k$ . We have immediately that,

$$\tilde{H} = -iH - \gamma N, \quad (2.40)$$

which is trivially integrable.

### 2.2.2 Localised loss on two sides

A direct generalisation of the loss studied in the following section is putting a loss process on both ends of a 1D chain. This could be done, for instance, by studying the 1D Hubbard model,

$$H = -t \sum_{j,\sigma} \left( c_{j,\sigma}^{\dagger} c_{j+1,\sigma} + c_{j+1,\sigma}^{\dagger} c_{j,\sigma} \right) + U \sum_i n_{i\uparrow} n_{i\downarrow} \quad (2.41)$$

and introducing four Lindblad operators

$$L_{1,\uparrow/\downarrow} = \sqrt{\gamma_1} c_{1,\downarrow/\uparrow}, \quad L_{N,\uparrow/\downarrow} = \sqrt{\gamma_N} c_{N,\downarrow/\uparrow}. \quad (2.42)$$

The Liouvillian is triangular and,

$$\tilde{H} = -iH - \sum_{\sigma \in \{\uparrow, \downarrow\}} \gamma_1 n_{1,\sigma} + \gamma_N n_{N,\sigma}, \quad (2.43)$$

which is integrable [221]. Of course, the Hubbard model is just a concrete example and any other boundary integrable model would work here, too.

### 2.2.3 Two-body loss

Consider the Lieb-Liniger model of cold bosons,

$$H = \int dx \left[ -\Psi(x)^\dagger \partial_x^2 \Psi(x) + c \Psi^\dagger(x) \Psi^\dagger(x) \Psi(x) \Psi(x) \right]. \quad (2.44)$$

An experimentally relevant loss process is two-body loss [222–224],

$$\mathcal{L}\rho = -i[H, \rho] + \gamma \int dx \left[ 2\Psi^2(x) \rho \Psi^{\dagger 2}(x) - \{\Psi^{\dagger 2}(x) \Psi^2(x), \rho\} \right]. \quad (2.45)$$

This may be understood as a continuous set of Lindblad operator  $L(x) = \sqrt{\gamma} \Psi(x)^2$  inducing pure loss. This leads to the triangular form the Liouvillian required. Furthermore,

$$\tilde{H} = -i \int dx \left[ -\Psi(x)^\dagger \partial_x^2 \Psi(x) + (c - i\gamma) \Psi^\dagger(x) \Psi^\dagger(x) \Psi(x) \Psi(x) \right], \quad (2.46)$$

which is a modification of the interaction leaving  $\tilde{H}$  integrable. Another concrete physical example of two-body loss treatable with our method is the 1D Hubbard model with two-body recombination of fermions of spin-down and spin-up [225].

### 2.2.4 Dissipative lossy nearest-neighbour hopping

A related loss process is the following. Consider an XXZ spin chain with  $L_j = \sqrt{\gamma} \sigma_j^- \sigma_{j+1}^-$  with  $j = 1, \dots, N-1$ . In that case  $\mathcal{L}$  is again triangular and,

$$\tilde{H} = -iH - \sum_{j=1}^{N-1} \frac{\gamma}{4} (\mathbb{1} + \sigma_j^z)(\mathbb{1} + \sigma_{j+1}^z), \quad (2.47)$$

which is again integrable because it corresponds to an addition of constant magnetic field and boundary field. It also renders the  $\Delta$  complex. This is interesting from the point of quantum phases because it allows for a physically motivated reason to extend the already rich quantum phase diagram of the XXZ spin chain to complex  $\Delta$ . This is similar to two-level systems coupled by dipolar interactions and subject to nonlocal dissipation, i.e. decay through optical emissions [226, 227].

### 2.2.5 Collective loss processes

Collective loss processes are quite ubiquitous from the point of view of descriptions of cavity experiments [228–232] and BECs [233, 234]. As an example we will take the Bose-Hubbard dimer [235–238],

$$H = k(N_1 - N_2)^2 - \nu(N_1 - N_2) + \mu(N_1 + N_2) - \epsilon(b_1^\dagger b_2 + b_2^\dagger b_1), \quad (2.48)$$

which has the total particle number  $U(1)$  symmetry and is exactly solvable via a Bethe ansatz [239, 240]. We now take global loss  $L = \sqrt{\gamma}(b_1 + b_2)$ , which leaves the Liouvillian triangular, and the non-Hermitian Hamiltonian is just  $iH$  with  $\mu \rightarrow \mu - i\gamma$  and  $\epsilon \rightarrow \epsilon - i\gamma$ . Other possible examples of models with collective loss may include Richardson-Gaudin models [241].

## 2.3 Application to a boundary loss XXZ model

We now study the example of an XXZ spin-1/2 chain with a single boundary spin sink. Our method allows us to find the scaling of the Liouvillian gap analytically and to understand the formation of domain walls in the easy-axis regime via a class of states which we call boundary bound states which we later describe.

### 2.3.1 DBA Solution

The Heisenberg Hamiltonian reads

$$H_{XXZ} = \sum_{j=1}^{N-1} s_j^x s_{j+1}^x + s_j^y s_{j+1}^y + \Delta s_j^z s_{j+1}^z, \quad (2.49)$$

where  $\Delta$  is the anisotropy which in the Jordan-Wigner picture corresponds to an interaction strength, and  $N$  is the number of spin sites. We study the setup of single spin loss on the first site, with an arbitrary loss rate  $\Gamma$ , as described by the Lindblad operator

$$L_1 = \sqrt{\Gamma} s_1^-, \quad s_j^- = s_j^x - i s_j^y. \quad (2.50)$$

Importantly the Hamiltonian has a  $U(1)$  symmetry,

$$M = \sum_j s_j^z, \quad (2.51)$$

with

$$[M, L_1] = -\frac{1}{2} L_1. \quad (2.52)$$

We therefore follow the procedure described above, to find the corresponding pseudo-Hamiltonian

$$i\tilde{H} = H_{XXZ} - i\Gamma s_1^z - i\frac{\Gamma}{2} \mathbb{1}, \quad (2.53)$$



which we recognise from Sec 1.2 above as corresponding to an XXZ model with a boundary field, up to the addition of an identity operator. This identity operator trivially adds a constant to all eigenvalues so has no significant effect.

Since the dissipation drives the system to a state where all the spins are down, it is natural to work from a vacuum state

$$|\Omega\rangle = |\downarrow \dots \downarrow\rangle. \quad (2.54)$$

We will now refer to states with spins pointing up as *magnons*. From above, the complex energies of  $\tilde{H}$  corresponding to  $m$  magnons read

$$E(\{k_j\}) = -\frac{1}{4}i(N-1)\Delta - i\sum_{j=1}^m(\cos(k_j) - \Delta), \quad (2.55)$$

where the momenta of the magnons,  $\{k_j\}$ , are obtained by solving the Bethe equations

$$\frac{e^{2iNk_j}(\Delta - e^{ik_j})(e^{ik_j} + 2i\Gamma - \Delta)}{(e^{ik_j}\Delta - 1)(1 + e^{ik_j}(2i\Gamma - \Delta))} = \prod_{l \neq j}^m S(e^{ik_j}, e^{ik_l}). \quad (2.56)$$

The scattering matrix of two magnons is again

$$S(a, b) = \frac{(a - 2\Delta ab + b)(1 - 2\Delta a + ab)}{(a - 2\Delta + b)(1 - 2\Delta b + ab)}. \quad (2.57)$$

This gives the final Liouvillian eigenvalues as

$$\Lambda_{\{k_i\}, \{q_j\}} = E(\{k_i\}) + E(\{q_j\})^* \quad (2.58a)$$

$$= i \left( \sum_{j=1}^{m_q} \cos q_j^* - \sum_{i=1}^{m_k} \cos k_i \right). \quad (2.58b)$$

We also solve for the Liouvillian eigenstates. Recall that the Bethe states are given by

$$|\{k_j\}_{j=1}^m\rangle = \sum_{1 \leq x_1 < \dots < x_m \leq n} f(x_1, \dots, x_m; \{k_j\}) |x_1, \dots, x_m\rangle \quad (2.59a)$$

$$f(x_1, \dots, x_m; \{k_j\}) = \sum_P \varepsilon_P A(k_1, \dots, k_m) e^{i(k_1 x_1 + \dots + k_m x_m)} \quad (2.59b)$$

$$A(k_1, \dots, k_m) = \prod_{j=1}^m (\Delta e^{-ik_j N} - e^{-i(N+1)k_j}) \prod_{1 \leq j < l \leq m} B(-k_j, k_l) e^{-ik_l} \quad (2.59c)$$

$$B(k, k') = (1 - 2\Delta e^{ik'} + e^{i(k+k')})(1 - 2\Delta e^{-ik} + e^{i(k'-k)}), \quad (2.59d)$$

where the summation is performed over all permutations and negations of  $\{k_j\}$ , and  $\varepsilon_P$  changes sign with each such *mutation*. In the following we will simplify notation and label the Bethe states as simply  $|\phi_\eta^m\rangle$  where the superscript  $m$  indicates

the magnon sector and  $\eta$  denotes that state within that sector. We then use the triangular form for the Liouvillian, i.e that

$$\mathcal{L} : \mathcal{M}^a \otimes \mathcal{M}^b \rightarrow (\mathcal{M}^a \otimes \mathcal{M}^b) \oplus (\mathcal{M}^{a-1} \otimes \mathcal{M}^{b-1}), \quad (2.60)$$

where  $\mathcal{M}^a$  is the subspace with magnetisation  $a$ , to make the ansatz that the eigenstate of  $\mathcal{L}$  with eigenvalue  $E_{\phi_\eta^a} + E_{\phi_\zeta^b}^*$  is given by

$$|\Phi_{\eta,\zeta}^{a,b}\rangle = |\phi_\eta^a\rangle \overline{|\phi_\zeta^b\rangle} + \sum_{\mu=1}^{\min\{a,b\}} \sum_{i,j} B_\mu(i,j) |\phi_i^{a-\mu}\rangle \overline{|\phi_j^{b-\mu}\rangle}. \quad (2.61)$$

Substituting this gives the recurrence relation

$$B_\mu(i,j) = \frac{8\Gamma}{E_\mu(i,j)} \sum_{p,q} B_{\mu-1}(p,q) \Sigma_{a-\mu+1}(p,i) \Sigma_{b-\mu+1}(q,j)^*, \quad B_0(i,j) = \delta_{i,\eta} \delta_{j,\zeta} \quad (2.62)$$

for  $\mu = 1, \dots, \min\{a,b\}$ , where we defined

$$E_\mu(i,j) = (E_{\phi_\eta^a} + E_{\phi_\zeta^b}^*) - (E_{\phi_i^{a-\mu}} + E_{\phi_j^{b-\mu}}^*) \quad (2.63)$$

$$\Sigma_m(p,i) = \sum_{\{x_2, \dots, x_m\}, x_2 > 1} f_{m,p}(1, x_2, \dots, x_m) f_{m-1,i}(x_2, \dots, x_m). \quad (2.64)$$

In general, this recursion relation is significantly more complex than computing the Bethe states of  $\tilde{H}$ . We have also assumed that Bethe states with different magnetisation do not have the same energies so that  $E_\mu(i,j) \neq 0$ . However this construction does provide an insight into the structure of the eigenstates. Importantly the eigenvalue of a Liouvillian eigenstate depends only on the Bethe states with highest magnetisation. For later convenience we introduce a pair of labels  $(m_L, m_R)$  referring to the eigenstates of  $\mathcal{L}$  comprised of tensor product of two Bethe states with  $m_L$  and  $m_R$  magnons as well as tensor products of Bethe states with less  $q_L < m_L$  and  $q_R < m_R$  magnons.

We will now use this solution to study physically interesting properties of the dynamics of this model.

### 2.3.2 Eigenvalue Structure and the Liouvillian gap

The first problem that we consider is the Liouvillian gap,  $R$ , of  $\mathcal{L}$ . It corresponds to the maximum real part of the eigenvalues different from 0, which is the relaxation rate of the longest-lived eigenmodes. We plot it in Fig. 2.1 for different values of the anisotropy parameter  $\Delta$ . The scaling of the gap with the system size  $N$  is one of the primary features of open quantum systems governing the late time dynamics.

We observe numerically that the gap corresponds to the eigenstates of  $\mathcal{L}$  with  $m_L + m_R = 1$ , which agrees with the physical intuition that states with greater

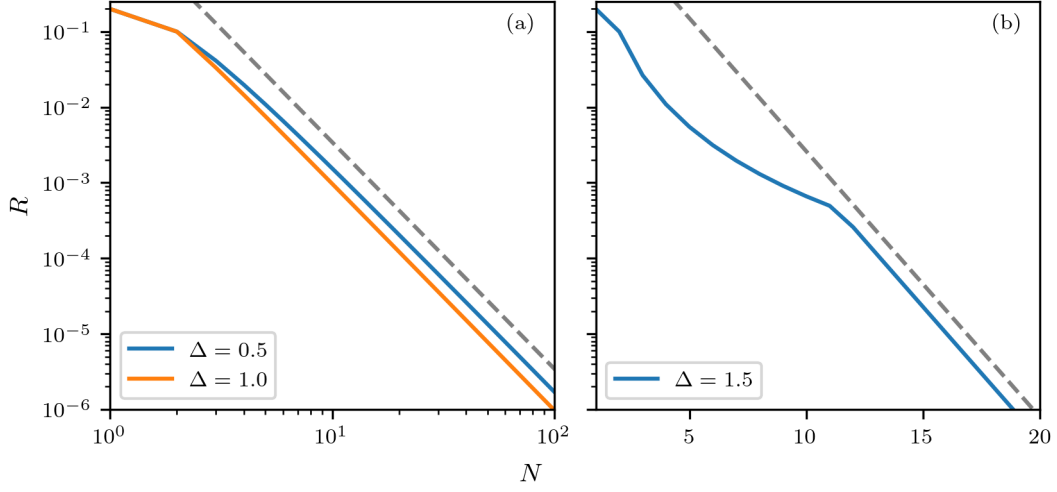


**Figure 2.1:** Scaling of the Liouvillian gap,  $R$ , with system size for  $\Gamma = 0.1$ . In each case the solid lines are numerical calculations while the dashed lines indicate the corresponding analytic scaling laws derived in the main text. (a) Power law closing of the gap for  $\Delta \leq 1$  with  $R \propto 1/N^3$  (dashed line) shown for comparison. (b) Exponential closing of the gap for  $\Delta > 1$  with  $R \propto \Delta^{-2N}$  (dashed line) shown for comparison.

magnetisation should decay quicker. These solutions can be physically understood as free magnons that live in the bulk of the system and only experience the effects of other magnons and the boundary in sub-leading order in the size of the system. By examining the single magnon,  $m = 1$ , solutions of Eq. (2.56) on top of the steady-state, we find that the gap closes at different rates depending on the value of  $\Delta$ .

**Easy plane,  $\Delta \leq 1$ , regime.** We start with the logarithmic form of the Bethe equations,

$$2ik_j = \frac{1}{N} \left( \sum_{i \neq j} \log [S(e^{ik_j}, e^{ik_i})] \right) - \frac{2i\pi I_j}{N}. \quad (2.65)$$

In the single magnon limit, where numerical evidence and physical intuition suggests the gap to be located, these equations simplify significantly to

$$2ik = \frac{\Omega(e^{ik})}{N} - \frac{2i\pi I_1}{N}, \quad (2.66)$$

where

$$\Omega(a) = \log \left( \frac{(a\Delta - 1)(-1 + a(\Delta - 2i\Gamma))}{(a - \Delta)(a + 2i\Gamma - \Delta)} \right). \quad (2.67)$$

We now expand the momenta  $k$  as the power series in  $1/N$ ,

$$k = k^{(0)} + \frac{k^{(1)}}{N} + \dots, \quad (2.68)$$

which we truncate at the order  $\mathcal{O}(1/N^3)$ . In principle the constant  $I_1$  can take any integer value between 0 and  $N$  so it is important to distinguish between the cases when  $I_1$  is close to 0 or scales with  $N$ . By checking both cases we find that the gap corresponds to  $I_1 = N - 1$ . In this case we obtain the series solution

$$k = -\pi + \frac{1}{N}\pi + \frac{1}{N^2}\pi \left( -\frac{1}{-2i\Gamma + \Delta + 1} - \frac{1}{\Delta + 1} + 1 \right) + \frac{1}{N^3} \frac{\pi (-2i\Gamma\Delta + \Delta^2 - 1)^2}{(\Delta + 1)^2 (-2i\Gamma + \Delta + 1)^2} + \mathcal{O}\left(\frac{1}{N^4}\right). \quad (2.69)$$

We finally use Eq. (2.58) with  $k$  as above and  $q = 0$ , corresponding to an off-diagonal state composed of the vacuum state and the single spin-up excitation, to obtain the Liouvillian gap

$$R = -\frac{1}{N^3} \frac{2\pi^2\Gamma}{4\Gamma^2 + (\Delta + 1)^2} + \mathcal{O}\left(\frac{1}{N^3}\right). \quad (2.70)$$

**Easy axis,  $\Delta \geq 1$ , regime.** We again consider the single magnon Bethe equation but this time we make the ansatz

$$k = i \log\left(\frac{1}{\Delta}\right) - a_1 \Delta^{-2N} + \mathcal{O}(\Delta^{-2N}), \quad (2.71)$$

and expand Eq. (2.66) to find,

$$0 = (\Delta^2 - 1)(-2i\Gamma + \Delta^2 - 1) - 2\Gamma\Delta a_1 + \mathcal{O}(\Delta^{-2N}). \quad (2.72)$$

This gives

$$k = i \log\left(\frac{1}{\Delta}\right) - \frac{(\Delta^2 - 1)(-2i\Gamma + \Delta^2 - 1)}{2\Gamma\Delta} \Delta^{-2N} + \mathcal{O}(\Delta^{-2N}), \quad (2.73)$$

which again using Eq. (2.58) with  $k$  as above and  $q = 0$  gives a Liouvillian gap

$$R = -\frac{1}{4\Gamma} \frac{(\Delta^2 - 1)^3}{\Delta^2} \Delta^{-2N} + \mathcal{O}(\Delta^{-2N}). \quad (2.74)$$

Strictly speaking, these results for both the easy axis and easy plane regime represent an upper bound on the gap. However, extensive numerical evidence shows that they are also a lower bound. This is illustrated in Fig 2.1. It may be possible to prove this rigorously by extending techniques for the isolated XXZ spin chain [242]. It is interesting to observe that for  $\Delta \leq 1$  the longest-lived excitations correspond to the solutions with  $\lim_{N \rightarrow \infty} \text{Im}(k_j) = 0$ , while for  $\Delta > 1$  they correspond to solutions with  $\lim_{N \rightarrow \infty} \text{Im}(k_j) = -\log(\Delta)$ , which illustrates that the states found for  $\Delta > 1$  cannot form except in the presence of dissipation<sup>4</sup>. The difference in

---

<sup>4</sup>Note that in the absence of dissipation all Bethe roots are real.

scaling of the Liouvillians gap between  $\Delta < 1$  and  $\Delta > 1$  is linked to the existence of boundary bound states *only* for  $\Delta > 1$ , as we will explore in the next section. These states are effectively domain walls which separate regions of up-spins from the loss site and hence effectively freeze the dynamics.

Another interesting observation regarding the Liouvillian eigenvalue structure is to consider the Ising limit where we take  $\Delta \rightarrow \infty$ . In this limit, assuming the imaginary parts of the solutions do not grow with  $\Delta$ , the Bethe equations from Eq. (2.56) reduce at zeroth order to

$$e^{2i(N-1)k_j} = \prod_{l \neq j}^m e^{2ik_l} = e^{2i(m-1)k_j}, \quad (2.75)$$

so that the Bethe roots are simply fractions of  $\pi$ . These solutions give pseudo-energies with zero real part. On the other hand, searching for solutions where the imaginary parts of the roots can grow with  $\Delta$  reveals the existence of states where exactly one of the Bethe roots is given by

$$k = i \log(\Delta - 2i\Gamma) + \mathcal{O}\left(\frac{1}{\Delta}\right). \quad (2.76)$$

States containing such a Bethe root have pseudo energies with real part  $-\Gamma + \mathcal{O}(1/\Delta)$  and are the *only* states with non-zero real part of the pseudo-energy at zeroth order. Therefore in this limit the Liouvillian eigenvalues will cluster in bands around the lines  $\text{Re}(\lambda) = 0, -\Gamma, -2\Gamma$ . This is shown in Figure 2.2 for a small system where exact diagonalisation is possible. Physically this corresponds to different subspaces of the Hilbert space decaying in separate stages, leading to a separation of time scales. Note that similar band formation occurs in the quantum Zeno [243–246] limit of taking  $\Gamma \rightarrow \infty$  for any  $\Delta$ , but that this is *not* the same phenomena we are observing here. The quantum Zeno limit will be discussed further in later chapters.

### 2.3.3 Boundary bound states, domain wall formation and dynamical phase transitions

We now study the evolution of the model from a specific initial state. We consider the case where the system is initialised in a highly excited, maximally polarised state with all spins pointing up. In this case, due to the structure of the Liouvillian eigenstates, we need only consider eigenstates with equal left and right magnetisation,  $m_L = m_R = m$ . To study the long time dynamics, we focus on the most stable eigenvalues, i.e. those with the smallest real part, in the  $m$  *top-magnon* sector. By top-magnon, we refer to a Bethe state with  $m$  spins pointing down and  $N - m$  spins pointing up. The Bethe equations for top-magnons can be obtained from Eq. (2.56) by replacing  $\Gamma \rightarrow -\Gamma$  in the sector with  $m$  magnons.

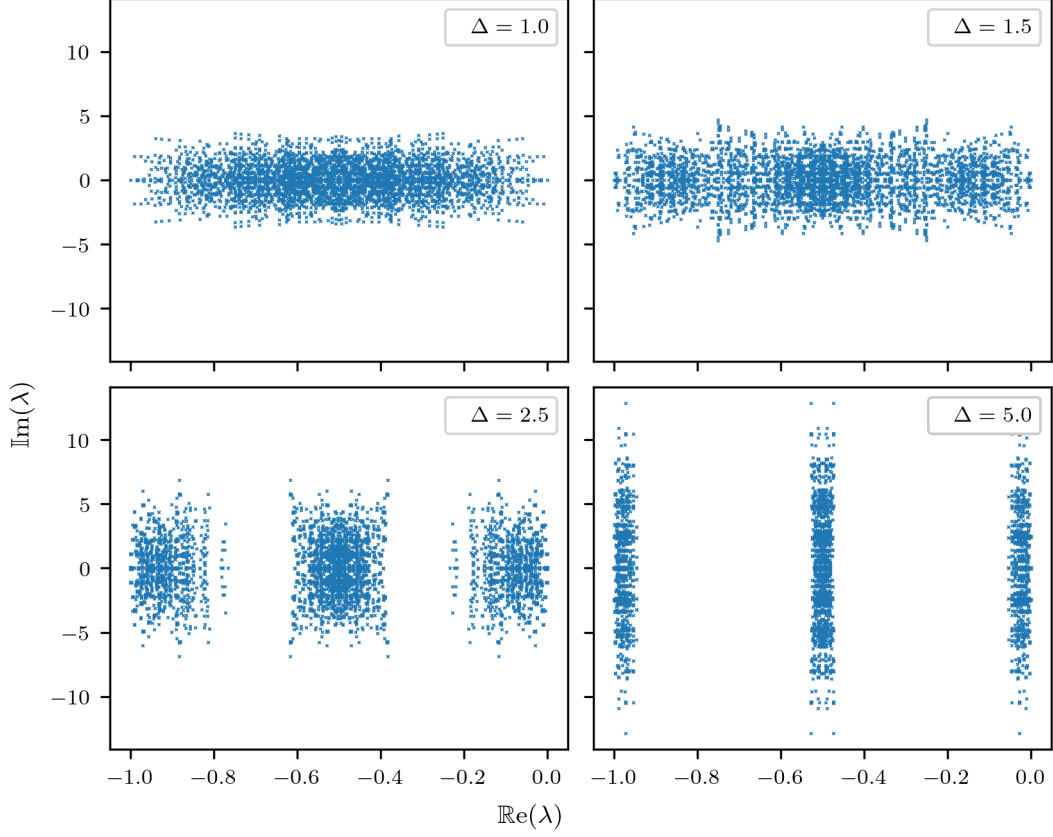


**Figure 2.2:** Full spectrum for a 6 site system with  $\Gamma = 0.5$  at various  $\Delta$ . We see the emergence of bands forming as  $\Delta$  increased at  $\text{Re}(\lambda) = 0, -\Gamma, -2\Gamma$ .

**Boundary bound states.** Focusing on the easy-axis,  $\Delta > 1$ , regime, let us consider states in the  $m$  top-magnon sector with  $\lim_{N \rightarrow \infty} \text{Im}(k_j) > 0$ . We may solve the  $m$  top-magnon Bethe equations in the  $N \rightarrow \infty$  limit by observing that  $e^{ik_j N} \rightarrow 0$  under our assumption that  $\lim_{N \rightarrow \infty} \text{Im}(k_j) > 0$ . We arrive at the following simple form of the Bethe equations in the  $N \rightarrow \infty$  limit,

$$\left(1 + e^{ik_j(-\Delta - 2i\Gamma)}\right) \prod_{i \neq j} \left(-2\Delta e^{ik_j} + e^{i(k_j - k_i)} + 1\right) \left(e^{i(k_j + k_i)} - 2\Delta e^{ik_j} + 1\right) = 0, \quad (2.77)$$

which may be recursively solved to give

$$e^{ik_j} = \frac{1}{2\Delta - e^{ik_{j-1}}}, \quad e^{ik_1} = \frac{1}{\Delta + 2i\Gamma}. \quad (2.78)$$

Importantly, since we are in the region  $\Delta > 1$ , we see inductively that we always have  $|e^{ik_j}| < 1$ . Thus we can interpret the state physically as the top-magnon with pseudo-momentum  $k_1$  being localised at the loss site with support only in the region

$$0 \leq x \lesssim \frac{1}{\Delta^2 + 4\Gamma^2}, \quad (2.79)$$

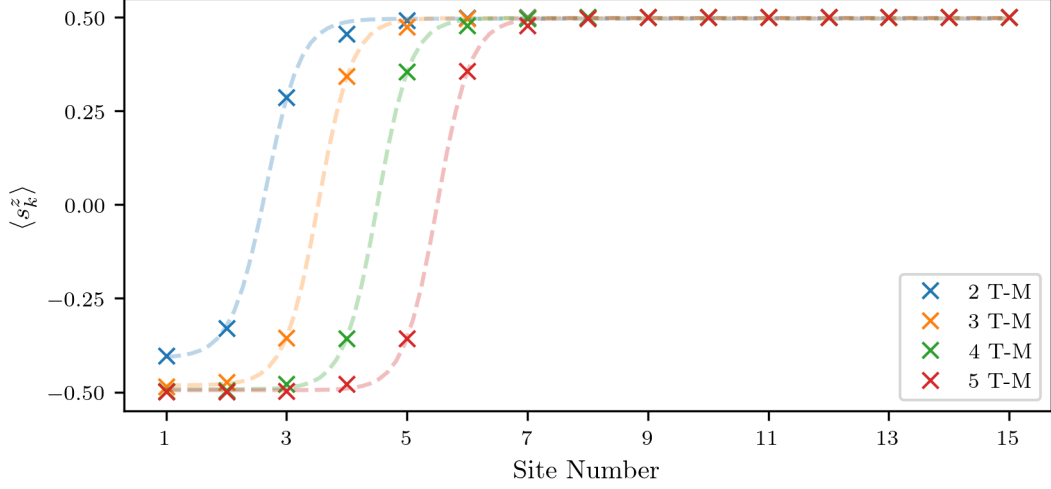


**Figure 2.3:** We plot  $\langle s_k^z \rangle$  for the lowest five top-magnon boundary bound states for  $\Delta = 1.5$ ,  $\Gamma = 0.5$ . The boundary bound states correspond to domain walls that separate the bulk positive magnetisation from the loss site which leads to the insulating behaviour for  $\Delta > 1$ . The dashed curves fit the spin profile to a typical  $\tanh(x)$  shaped domain wall to guide the eye.

and the  $j$ -th top-magnon being bound to the  $(j-1)$ -st one, which is itself recursively bound to all lower top-magnons. Since these states are recursively bound to the loss site at the boundary we call them ‘boundary bound state’. This property also characterises a domain wall state which can be seen in Fig 2.3 where we plot the spin-distribution of several boundary bound states. Note that these boundary bound states *are not* eigenstates of the full Liouvillian. The corresponding Liouvillian eigenstates involve coupling to lower magnon sectors and are far more computationally expensive to find.

To establish the lifetime of the  $m$  top-magnon boundary bound state, we first decompose the equation for its pseudo-energy as

$$E_m = -\Gamma - i \sum_{j=1}^m \left( \frac{1}{2} (e^{ik_j} + e^{-ik_j}) - \Delta \right). \quad (2.80)$$

Regrouping the terms, we simply get

$$E_m = -\frac{1}{2}i (e^{ik_m} - \Delta). \quad (2.81)$$

Therefore, in order to demonstrate stability it is sufficient to show that the imaginary part of  $e^{ik_m}$  goes to 0 in the limit of large top-magnon number,  $m \rightarrow \infty$ . Solving for the fixed points of the recurrence relation in Eq. (2.78) we find two *real* solutions

$$z_1 = \Delta - \sqrt{\Delta^2 - 1}, \quad z_2 = \Delta + \sqrt{\Delta^2 - 1}, \quad (2.82)$$

with  $z_1$  being the stable fixed point. Since we are in the region  $\Delta > 1$  we can apply the Śleszyński–Pringsheim theorem [247] to the recurrence relation in Eq. (2.78) and immediately conclude that the fixed point is converged to for any choice of  $\Delta > 1$ ,  $\Gamma > 0$ . This indicates that the boundary bound top-magnon states are exponentially stable and thus dominate the long time dynamics.

**Domain wall formation.** The existence of these boundary bound states has intriguing physical consequences as it results in domain wall formation if the system is initialised in the maximally polarised state. Naively one might think that such a state is the most unstable, however t-DMRG simulations, as shown in Fig. 2.4, in the  $\Delta > 1$  regime reveal that the total spin leaking out of the system increases only *logarithmically* with time. This can be understood as a consequence of the exponential stability of the boundary bound states. Namely, exponentially long times in  $m$  are required for the loss site to remove all the states with  $m$  down-turned spins. Moreover, in Fig. 2.6 we show that the decay rates of boundary top-magnons well describe the dynamics of magnetisation close to the spin loss site. From this, we can deduce that the system can be interpreted through the incremental decay of each top-magnon sector. On the other hand, in Figure 2.5 we see that the decay of the maximally polarised state in the  $\Delta < 1$  regime is very rapid, and the total loss of magnetisation increases linearly with time. There have recently been a number of studies addressing the dynamics of domain walls in integrable [248–251] and nonintegrable [252] systems without dissipation. While the ballistic expansion in the  $\Delta < 1$  regime is well understood, the domain wall freezing was analytically unresolved.

**Dynamical phase transition.** The existence of boundary bound states also has profound consequences on the spectral properties of the Liouvillian and results in a novel type of dynamical dissipative phase transition when the system is initialised in the maximally polarised state. To see this we study the one top-magnon sector<sup>5</sup>. The single top-magnon Bethe equations correspond to setting

$$\Omega(a) = \log \left( \frac{(a\Delta - 1)(-1 + a(\Delta + 2i\Gamma))}{(a - \Delta)(a - 2i\Gamma - \Delta)} \right) \quad (2.83)$$

in Eq. (2.66). The corresponding pseudo-energies of  $\tilde{H}$  are

$$E_p = -\Gamma - i(\cos(k_p) - \Delta), \quad (2.84)$$

while the eigenvalues of  $\mathcal{L}$  read

$$\lambda_{p,p'} = E_p + E_{p'}^*. \quad (2.85)$$

---

<sup>5</sup>States with a single spin down in a background of all spins up.



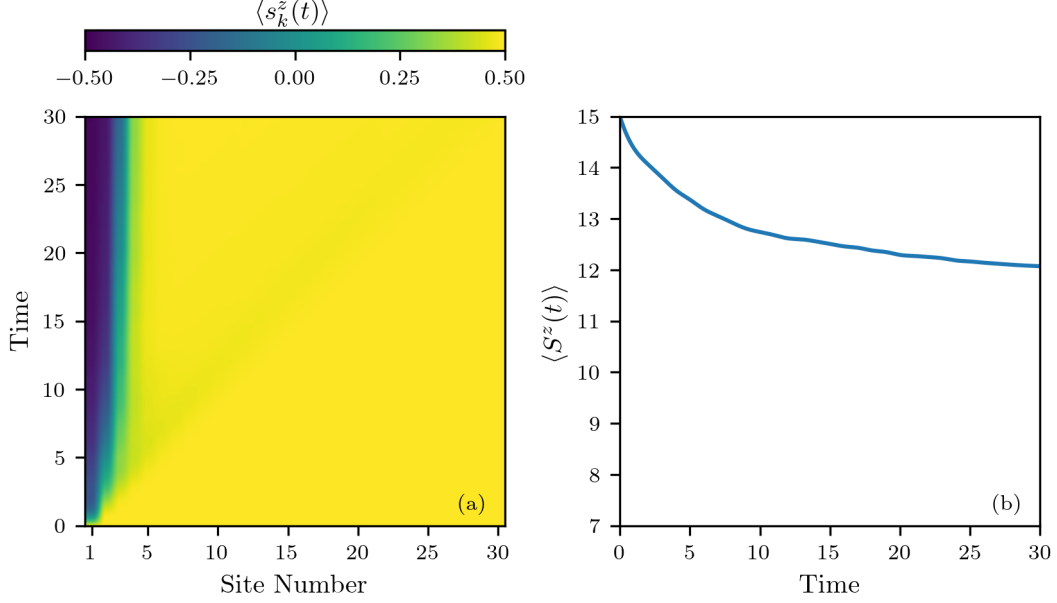


**Figure 2.4:** (a) Magnetisation along the chain as a function of time for an initially fully polarised state with  $\Gamma = 0.5$  and  $\Delta = 1.5$ . (b) The total spin in the system,  $\langle S^z(t) \rangle = \sum_x \langle s_x^z(t) \rangle$ , for the same evolutions. This is logarithmic in time as a result of the domain wall preventing spin from leaking out. Note that the axes match Fig 2.5 for direct comparison.

We follow the similar series expansion in  $N$  as before but now focus on the case when  $I_1$  is finite. Numerically we observe that this corresponds to the leading decay rates in the single top-magnon sector for  $\Delta < 1$  in the small  $\Gamma$  limit. Performing the same expansion as before, relabeling  $I_1 \rightarrow p$ , we obtain

$$k_p = -\frac{p\pi}{N} + \frac{1}{N^2} \left[ \pi p \left( -\frac{1}{-2i\Gamma + \Delta - 1} + \frac{1}{1 - \Delta} - 1 \right) \right]. \quad (2.86)$$

We take the derivative of Eq. (2.84) with respect to  $\Delta$  which gives

$$\frac{d\lambda_{p,p'}}{d\Delta} = -i \left[ -\sin(k_p) \frac{dk_p}{d\Delta} + \sin(k_{p'}^*) \frac{dk_{p'}^*}{d\Delta} \right]. \quad (2.87)$$

Using (2.86) we obtain,

$$\frac{d\lambda_{p,p'}}{d\Delta} = -i\pi^2 \left( \frac{p^2 - p'^2}{(1 - \Delta)^2} + \frac{p^2 + p'^2}{(-2i\Gamma + \Delta - 1)^2} \right) \frac{1}{N^3} + O\left(\frac{1}{N^4}\right) \quad (2.88)$$

which diverges as  $\Delta \rightarrow 1$  at leading order in  $\Gamma$ , signalling the phase transition in these highly excited states. Similar analysis can be performed in other sectors, either analytically or numerically, to obtain the same result.

In contrast to standard dissipative phase transitions [253], the stationary state remains the same. The phase transition, in our case, rather happens in all sectors

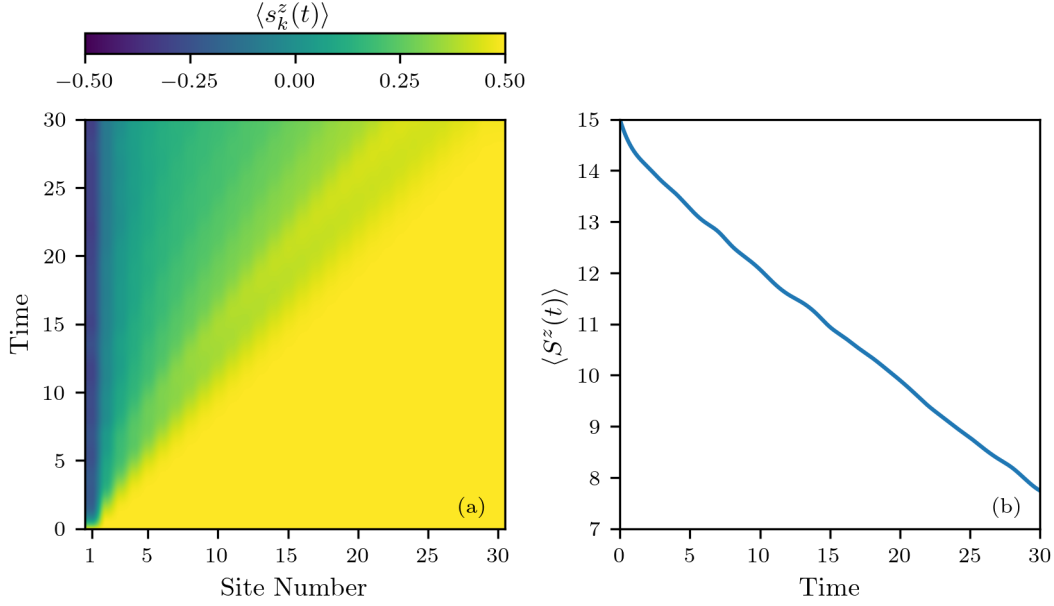


**Figure 2.5:** (a) Magnetisation along the chain as a function of time for an initially fully polarised state with  $\Gamma = 0.5$  and  $\Delta = 0.5$ . (b) The total spin in the system,  $\langle S^z(t) \rangle = \sum_x \langle s_x^z(t) \rangle$ , for the same evolutions. This is linear in time as there are no boundary bound states to create a domain wall. Note that the axes match Fig 2.4 for direct comparison.

of the relaxation spectrum. At leading order in  $\Gamma$  as  $N \rightarrow \infty$  the transition occurs at  $\Delta = 1$ . This is similar to the dynamical dissipative phase transitions studied by [254], but the discontinuous eigenvalues that are relevant for the dynamics are not only the Liouvillian gap. This is reflected in the fact that the dynamics well inside the easy-plane and easy-axis regimes are qualitatively different at short times. The discontinuity is shown in Fig. 2.7 where, by taking small  $\Gamma$ , we can see non-analyticity in eigenvalues in three different top-magnon sectors at  $\Delta = 1$ . This is characteristic of all sectors. The non-analyticity shown corresponds to the non-existence of boundary bound state solutions for  $\Delta < 1$  for all values of  $\Gamma$ .

## 2.4 Extensions to the thermodynamic limit

As mentioned briefly in Sec 1, although analytically appealing, solutions in terms of Bethe states are notoriously difficult to work with in practice. In general, solving the Bethe equations and finding the corresponding complete set of eigenstates is little easier than direct diagonalisation. Therefore finite-dimensional Bethe ansatz solutions are usually used to probe very specific properties of a system, as we have demonstrated in the example above. However, the key strength of the Bethe ansatz is its extension to the thermodynamic limit, where thermodynamic properties can be accessed directly without the need to compute eigenstates.

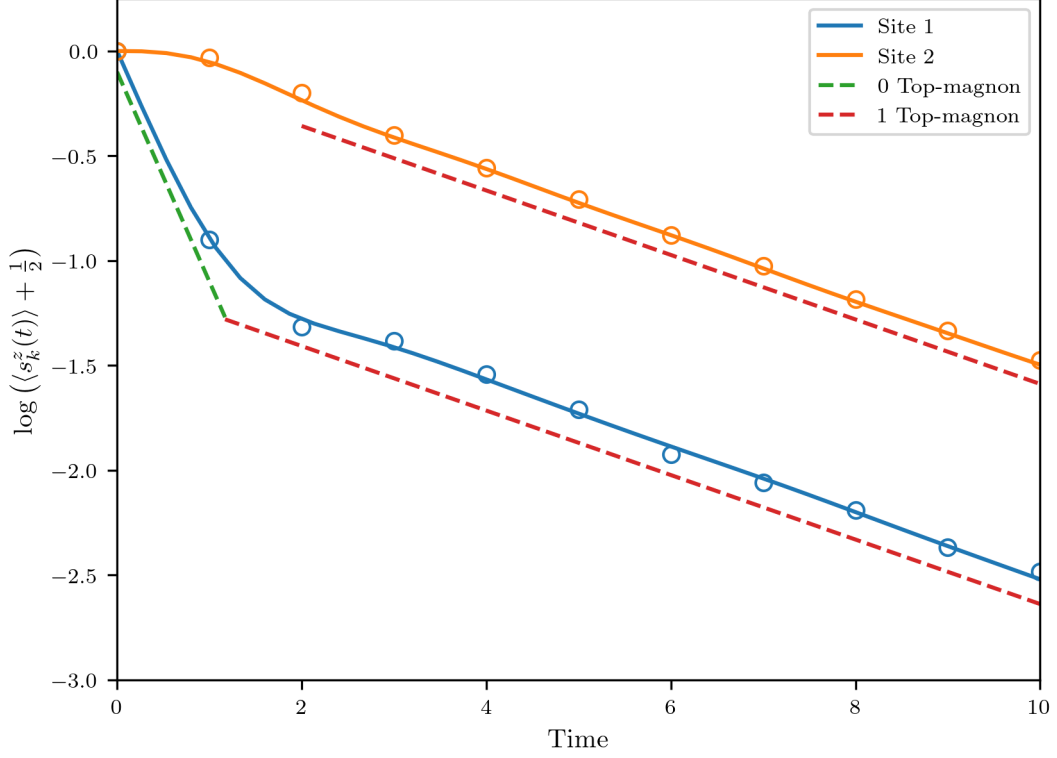


**Figure 2.6:** The spin decay on the first and second sites in 10 (solid line) and 30 (circles) site systems with  $\Delta = 1.5$ ,  $\Gamma = 0.5$ . We also plot the infinite chain 0 and 1 top-magnon decay rates in green and red respectively for comparison. Note the logarithmic axes in order to observe exponential decay.

To briefly outline the thermodynamic Bethe ansatz (TBA) [123, 138, 213], we introduce the Lieb-Liniger model, which is often used to describe one-dimensional bosonic gasses in the limit of pure contact interaction [255–257]. The Hamiltonian can be given in second quantised form as

$$H = \int_{-\infty}^{\infty} dx \partial_x \Psi^\dagger(x) \partial_x \Psi(x) + c \Psi^\dagger(x) \Psi^\dagger(x) \Psi(x) \Psi(x), \quad (2.89)$$

where  $c$  describes the interaction strength. The system has an immediate  $U(1)$  symmetry corresponding to conservation of the number operator

$$N = \int_{-\infty}^{\infty} dx \Psi^\dagger(x) \Psi(x). \quad (2.90)$$

To quantize the system we restrict the system to the box of finite length  $L$ . Then considering the sector with  $M$  total particles, the system can be solved via the Bethe ansatz leading to Bethe equations

$$e^{ik_j L} = (-1)^M \prod_{l=1}^M e^{i\theta(k_j - k_l)}, \quad j = 1, \dots, M, \quad (2.91)$$

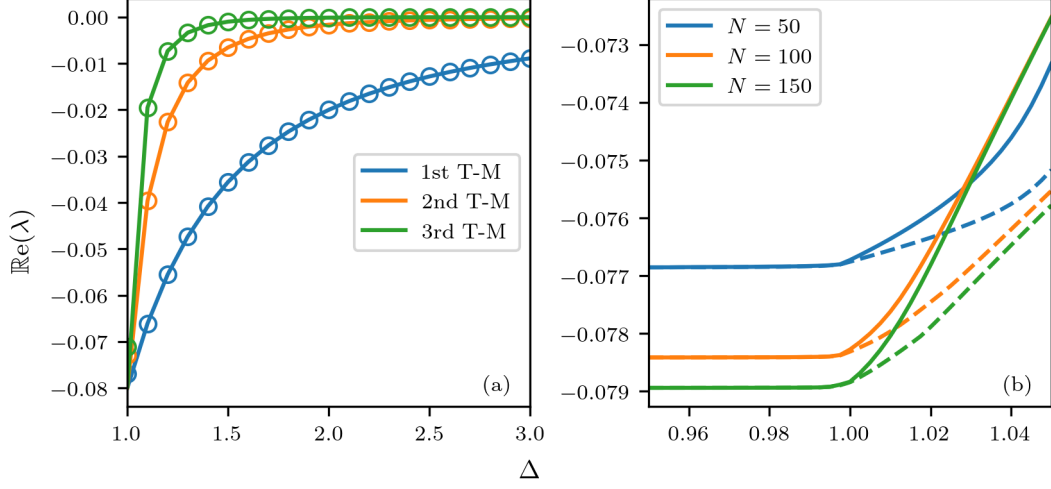


**Figure 2.7:** (a) The Liouvillian eigenvalues with maximum real part when  $N \rightarrow \infty$  (circles) for  $\Delta > 1$  compared with a 50 site system (line) for 1, 2 and 3 top-magnon sectors at  $\Gamma = 0.01$ . (b) The largest (solid line) and second largest (dashed line) real part of the eigenvalues of the Liouvillian in the one top-magnon sector for different  $N$  at  $\Gamma = 0.01$ . We see a cusp forming with increasing  $N$  close to  $\Delta = 1$  indicating the dynamical dissipative phase transition in the large  $N$  limit at leading order in  $\Gamma$ .

where  $\theta(q) = -2\arctan(q/c)$  is the two particle scattering phase. Taking the logarithm yields

$$k_j = \frac{2\pi}{L}I_j + \frac{1}{L} \sum_{l=1}^M \theta(k_j - k_l), \quad (2.92)$$

where the quantum numbers  $I_j$  uniquely characterise the state, and are always ordered,  $I_l \leq I_{l+1}$ . The corresponding energy and momentum of the Bethe state is given by

$$E = \sum_{l=1}^M k_l^2, \quad P = \sum_{l=1}^M k_l. \quad (2.93)$$

In order to move to the thermodynamic limit, we trivially rewrite Eq. (2.92) as

$$k_j - \frac{1}{L} \sum_{l=1}^M \theta(k_j - k_l) = y(k_j) \quad (2.94)$$

where  $y(k)$  is called the counting function that takes the values  $2\pi I_j/L$  at  $k = k_j$ . We then define the density of quasi-momenta as  $\rho(k) = y'(k)/2\pi$  which describes the number of excitations with quasi-momenta in the range  $[k, k + \delta k]$ . Replacing summations with integrals and taking the limit  $L, M \rightarrow \infty$  we recover the TBA integral equation, also known in this case as the Lieb-Liniger equation [255, 256]

$$\rho(k) = \frac{1}{2\pi} + \frac{1}{\pi} \int_{k_{\min}}^{k_{\max}} dk' \frac{c}{(k - k')^2 + c^2} \rho(k'). \quad (2.95)$$

This integral equation determines the density of the quasi-momenta in terms of the limits,  $k_{\min}$  and  $k_{\max}$ , which correspond to the choice of quantum numbers,  $I_j$ , before we took the thermodynamic limit. Note that these are constrained by the requirement that the total particle density is

$$\frac{M}{L} = \int_{k_{\min}}^{k_{\max}} dk' \rho(k'). \quad (2.96)$$

The usual approach is to start from the ground state, where the limits are symmetric, and then to study quasi-particle excitations above this ground state which introduce so-called ‘holes’. A careful treatment can then lead to the Yang-Yang equation, which describes the Helmholtz free energy in terms of a dressed energy per excitation [213]. From the corresponding partition function, one can calculate thermodynamic properties of the model. We also note that this procedure can be generally applied to most integrable models, such as the XXZ or Hubbard models, but the results are more complex relating to the need for the string hypothesis [258].

The immediate question is whether these well established TBA techniques can be coupled with our dissipative Bethe ansatz method for solving systems with loss. Unfortunately, as we will now demonstrate, extending our method to the thermodynamic limit using the TBA leads to obstacles that are yet to be overcome.

As one of the simplest examples, we take as our lossy model the Lieb-Liniger Hamiltonian above subject to two-body losses of strength  $\gamma$ . As we outlined in Sec 2.2 the corresponding pseudo-Hamiltonian contains a complex interaction term,  $\tilde{c} = c - i\gamma$ . In Fig. 2.8 we plot the solutions to Eq. (2.92) with the quantum numbers

$$I_j = \{-(M-1)/2, -(M-3)/2 \dots (M-3)/2\}. \quad (2.97)$$

This choice of quantum numbers is known to correspond to the ground state of the standard Lieb-Liniger Hamiltonian, although its interpretation in our case is not clear. Importantly, we see that as  $\gamma$  is varied, the Bethe roots trace out new curves in the complex plane for each  $\gamma$  which cannot be straightforwardly related to the model parameters without fully solving Eq. (2.92). Therefore unlike the usual case, where the quantum numbers determine limits of integration along the real line, here they determine a curve in the complex plane, and hence Eq. (2.95) must be adapted to

$$\rho(k) = \frac{1}{2\pi} + \frac{1}{\pi} \int_{\mathcal{C}} dk' \frac{\tilde{c}}{(k-k')^2 + \tilde{c}^2} \rho(k'), \quad (2.98)$$

where  $\mathcal{C}$  is a curve in  $\mathbb{C}$  which now characterises the state. It is unclear how to determine these curves, either analytically or numerically, such that  $\rho(k)$  remains real and positive along the curve. Further, we cannot use standard contour deformation techniques as we do not know a priori the locations of any poles of the integrand or the endpoints of the curve,  $\mathcal{C}$ .

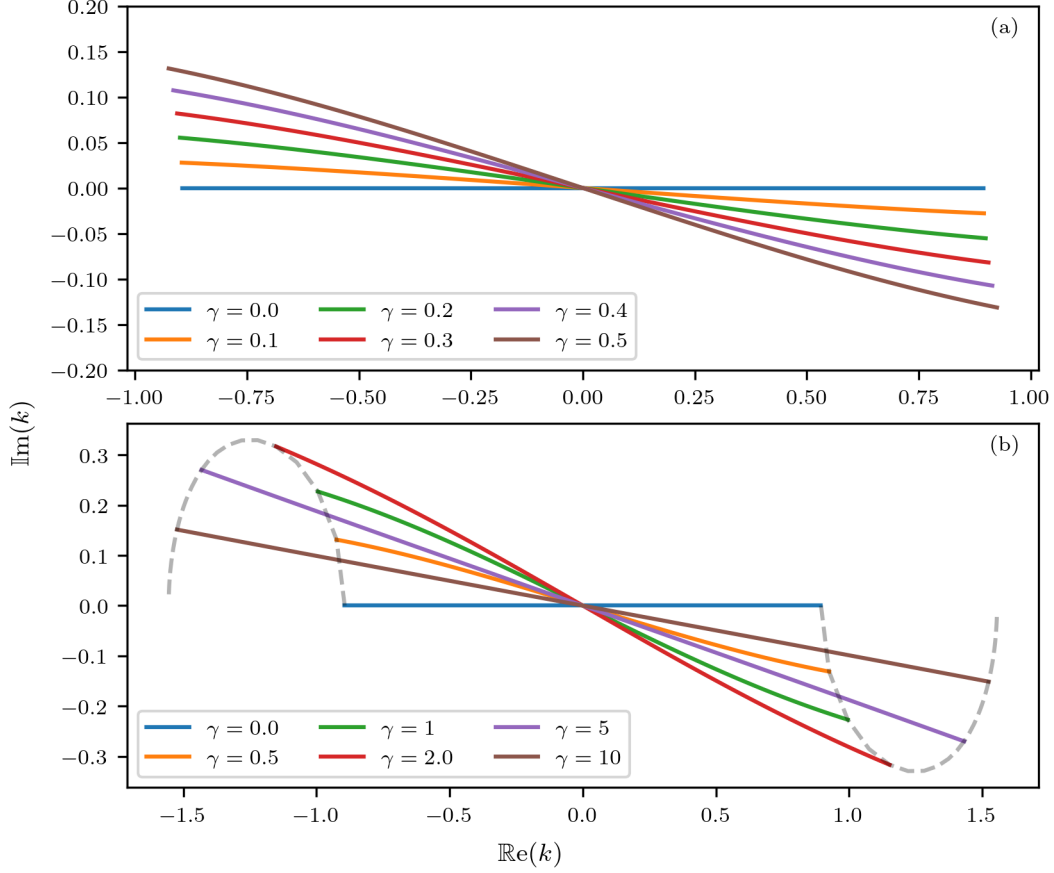


**Figure 2.8:** The Bethe roots of the Lieb-Liniger model with complex interaction  $\tilde{c} = 1 - \gamma i$  for a system with length  $L$  at half filling, found by solving Eq. (2.92). The quantum numbers were taken as  $I_j = \{-(M-1)/2, -(M-3)/2, \dots, (M-3)/2\}$  where  $M = L/2$ . In (a) we plot the roots for small  $\gamma$  while in (b) we plot them for larger  $\gamma$ . The dashed grey curve traces the end points as  $\gamma$  is varied from  $0 \rightarrow 150$ .

It is also important to consider what Eq. (2.98) means for the full Liouvillian, supposing we could solve it in some way. Given some curve  $\mathcal{C}$  describing the state and the corresponding root density,  $\rho(k)$ , we can calculate the pseudo energy and hence some Liouvillian eigenvalue. Without understanding in more detail the properties of the corresponding quantum state, particularly its relation to the vacuum, it is not clear how the eigenvalue can be used to understand the system's dynamics. Also, since the system is decaying to a known stationary state, in our case the vacuum, it is unlikely that techniques such as the Yang-Yang equation will be applicable. Unfortunately, it therefore seems that, in general, the usual TBA machinery cannot be directly used in tandem with our dissipative Bethe ansatz. We remark, however, that the work of Nakagawa et al. [225] appeared to make some progress using TBA techniques when considering the Hubbard model with two-body losses, and they were able to find both the Hubbard and Liouvillian gap, as well as a novel phase,

dubbed the ‘Zeno’ insulator. Their work relied on starting with a known set of quantum numbers and using numerical calculations to argue the location of poles and limits of integration. While successful in this limited setting, the generality of this approach is unclear, but perhaps future work in this direction could prove fruitful.

## 2.5 Discussion

So far in this chapter, we have developed a framework for diagonalising quantum Liouvillians with integrable Hamiltonians and dissipative loss. We have demonstrated the utility of our method through an example of the Heisenberg XXZ spin chain with boundary loss. The method allowed us to directly identify phase transitions in the Liouvillian spectrum and calculate the Liouvillian gap. This led us to observe two intriguing physical phenomena, namely domain wall formation and a dissipative phase transition, which we link to the existence of boundary bound top-magnons. It is expected that similar remarkable phenomena could occur in other models with localised loss, such as the 1D Hubbard model and interacting bosons in 1D [223], which are both importantly also amenable to treatment by our technique and very relevant experimentally.

Several questions remain open. The first natural extension of our results would be to directly calculate the quantum Liouvillian’s full eigenstates. It is possible that the expansion we presented in terms of Bethe states could be simplified, at least in some limit, which would allow us to study more general dynamics in at least a finite-sized system. The results in our example also suggest connections with boundary states [259, 260] and strong edge modes [261] in closed systems which should be explored further. As we have discussed, the thermodynamic Bethe ansatz does not provide a straightforward route to exploring the models in the thermodynamic limit. Still, perhaps some more advanced adaptations could prove fruitful in the future.

One alternative route to studying the dynamics of thermodynamically large integrable systems in the presence of dissipation is through the recently developing field of generalised hydrodynamics [214]. In the remainder of this chapter, we will briefly introduce this theory and discuss some possible ways it can be applied to systems with dissipation.

## 3 Generalised Hydrodynamics with dissipation

Before concluding this chapter, we will briefly discuss the recently developed field of generalised hydrodynamics and comment on some of its applications to systems with dissipation. Although no substantial new results are presented, this short section is intended to indicate the most natural extension for studying the dynamics of integrable systems in the presence of dissipation and to highlight some potential fruitful pathways for future study.

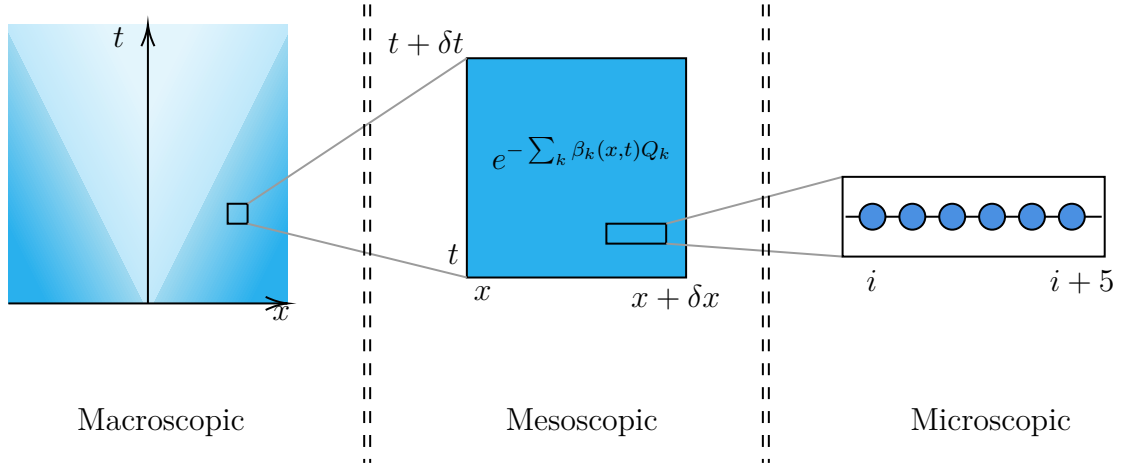


**Figure 2.9:** Separation of scales for hydrodynamics. Hydrodynamic theories are concerned with macroscopic quantities where each space-time cell can be approximated as a mesoscopic maximum entropy state. This mesoscopic state contains the details of the microscopic theory through entropy maximisation.

### 3.1 Introduction to GHD

We first give a very brief description of the fundamentals of GHD. This description will give only enough detail to motivate the key equations and sufficiently set the scene. For more details and rigorous proofs see either the lecture notes of Doyon [262, 263], or the works of [129, 135, 136, 264, 265].

In hydrodynamic theories, either classical or quantum, one is interested in studying the behaviours of local conserved charge and current densities,  $q_k(x, t)$  and  $j_k(x, t)$  respectively, which satisfy the continuity equations<sup>6</sup>

$$\partial_t q_k(x, t) + \partial_x j_k(x, t) = 0. \quad (2.99)$$

These continuity equations follow from the conservation of the total charge

$$Q_k = \int dx \, q_k(x, t), \quad \partial_t Q_k = 0. \quad (2.100)$$

The fundamental assumption of hydrodynamical theories is that to a good approximation entropy is maximised locally. This idea is related to a separation of scales from microscopic to mesoscopic to macroscopic as depicted in Fig 2.9. In particular, hydrodynamic theories consider temporal and spatial variations that are sufficiently slow that each fluid cell can equilibrate. As a result, we approximate the states at every point in space-time as being described by a local maximum entropy state.

<sup>6</sup>Throughout this section we will be considering exclusively 1D systems.



As we have mentioned earlier, integrable quantum systems possess an infinite set of quasilocal conserved charges [99], and global maximisation of entropy has been rigorously shown [103] to lead to a generalised Gibbs ensemble of the form

$$\rho \propto e^{-\sum_k \beta_k Q_k}, \quad (2.101)$$

with Lagrange multipliers  $\beta_k$ , where the charges  $Q_k$  are now quantum mechanical operators. Therefore when treating an integrable system hydrodynamically, we assume that the system at a fixed point in space-time is described by a state

$$\rho(x, t) \propto e^{-\sum_k \beta_k(x, t) q_k(x, 0)}. \quad (2.102)$$

From this, one can then derive [262] the continuity equation (2.99) for the expectation values of the charge and current densities,

$$q_k(x, t) = \langle q_k(0, 0) \rangle_{\beta(x, t)}, \quad j_k(x, t) = \langle j_k(0, 0) \rangle_{\beta(x, t)}, \quad (2.103)$$

where the  $\langle \cdot \rangle_{\beta(x, t)}$  notation indicates expectation in a local GGE state with parameters  $\beta(x, t)$ . In turn, since the fundamental quantities describing the state are the Lagrange parameters,  $\beta(x, t)$ , the continuity equation can be recast as

$$\partial_t \beta_k(x, t) + \sum_j A_{kj}(x, t) \partial_x \beta_j(x, t) = 0, \quad (2.104)$$

for a diagonalisable matrix  $A_{kj}(x, t)$  known as the *flux Jacobian*, which has a geometric interpretation [262, 264]. We then diagonalise this equation in terms of the so-called normal modes,  $\vartheta_k$ , as

$$\partial_t \vartheta_k(x, t) + v_k^{\text{eff}}(x, t) \partial_x \vartheta_k(x, t) = 0, \quad (2.105)$$

where the effective velocities,  $v_k^{\text{eff}}(x, t)$ , are interpreted as the velocity of each normal mode so that this is effectively a wave equation.

It is not evident that progress has been made since we still do not know how to relate these normal modes to physical quantities or calculate the corresponding effective velocities. These problems can be resolved when considering integrable systems where the thermodynamic Bethe ansatz can be used. To minimise notation, we will consider primarily the Lieb-Liniger model since this has only a single spectral parameter, but the general principles apply to any integrable model after suitable adaptation.

Recall that the thermodynamic Bethe ansatz describes the state by a quasi-particle density,  $\rho(k)$ . From this, it is possible to calculate the expected value of an observable from the corresponding *one particle eigenvalue*,  $h(k)$ , by

$$\langle q[h] \rangle = \int dk \rho(k) h(k). \quad (2.106)$$

In the Lieb-Liniger model, for example, the one particle eigenvalue for the energy density is  $\epsilon(k) = k^2$  while for momentum density it is  $p(k) = k$ . It has then been found that the normal modes, and corresponding velocities in Eq. (2.105) are given by

$$\vartheta(k) = \frac{2\pi\rho(k)}{[p'(k)]^{\text{dr}}}, \quad v^{\text{eff}}(k) = \frac{[\epsilon'(k)]^{\text{dr}}}{[p'(k)]^{\text{dr}}}, \quad (2.107)$$

where the dressing operation is defined by solving the integral equation

$$[f(k)]^{\text{dr}} = f(k) - \int \frac{d\kappa}{2\pi} \theta'(k - \kappa) \vartheta(\kappa) [f(\kappa)]^{\text{dr}}. \quad (2.108)$$

Here  $\theta(k)$  is the usual two-particle scattering matrix for the integrable model. The normal modes,  $\vartheta(k)$ , are now referred to as the filling function, satisfying  $0 \leq \vartheta(k) \leq 1$ . Notice also that the expression for the effective velocity is analogous to the usual group velocity, up to applying the chain rule and introducing the dressing operator. We now make the hydrodynamic approximation outlined above so that the filling function now varies in space-time, and we arrive at the final GHD equation

$$\partial_t \vartheta(x, t, k) + v^{\text{eff}}(x, t, k) \partial_x \vartheta(x, t, k) = 0. \quad (2.109)$$

This is a highly non-linear system of both integral and differential equations that is far from straightforward to solve in general. However, reducing a many-body quantum mechanical system with an exponentially growing Hilbert space to the system of numerically tractable equations is a significant achievement and has led to several interesting results. One notable example has been to calculate the exact charge and current profiles of a thermodynamically large XXZ spin chain following a quench [135]. The results obtained using the analytic solution of Eq. (2.109) are in impressive agreement with numerical simulations using matrix product state methods, indicating the accuracy of GHD for even relatively small systems. Additionally, the appealingly intuitive form of Eq. (2.109) has been extended to describe systems with fields that vary in both space and time, which correspond to forcing terms [265–267]. Such has been the interest in generalised hydrodynamics from both theoretical and experimental perspectives that an open-source numerical package has been developed specifically to solve the GHD equations for some standard models [268].

We will now briefly comment on two applications of GHD to systems experiencing dissipation that we envisage as interesting for future study.

### 3.2 Lossy systems

Our first example is related to the previous work of this chapter regarding localised losses. Consider again the XXZ spin chain with loss on the center site, where the evolution of a general observable is described by

$$\frac{d}{dt}\langle\hat{O}\rangle = -i\text{Tr}([H, \hat{\rho}]\hat{O}) + \Gamma\text{Tr}((2\sigma_0^-\hat{\rho}\sigma_0^+ - \sigma_0^+\sigma_0^-\hat{\rho} - \hat{\rho}\sigma_0^+\sigma_0^+)\hat{O}) \quad (2.110)$$

where  $\hat{\rho}(t)$  is the state of the system at time  $t$ . We now follow a similar idea to Bouchoule et al. when studying atomic losses in the Lieb-Liniger model [269] and take the thermodynamic limit so that position is now labeled by  $x \in (-\infty, \infty)$ . We make the standard hydrodynamic assumptions outlined above so that away from  $x = 0$  the system rapidly relaxes locally and it may be described by  $\hat{\rho}_{\text{GGE}}$ . Now consider the evolution of the local conserved charges  $q_{\mathbf{k}}(x)$ . Away from  $x = 0$  we have the usual GHD equation

$$\frac{d}{dt}\langle q_{\mathbf{k}}(x) \rangle_{\hat{\rho}_{\text{GGE}}} = 0 \quad \Rightarrow \quad \frac{d}{dt}\rho(x, \mathbf{k}) = 0 \quad (2.111)$$

where  $\rho(\mathbf{k})$  is the rapidity distribution. This follows from  $\langle q_{\mathbf{k}}(x) \rangle_{\hat{\rho}_{\text{GGE}}} \approx \rho(x, \mathbf{k})$ , where we have now used a vector of spectral parameters,  $\mathbf{k}$ , as required for the XXZ model in the  $\Delta > 1$  regime. However, at  $x = 0$  we instead have

$$\frac{d}{dt}\langle q_{\mathbf{k}}(0) \rangle = 2\Gamma\langle\sigma^-(0)[q_{\mathbf{k}}(0), \sigma^+(0)]\rangle_{\hat{\rho}_{\text{GGE}}}. \quad (2.112)$$

We rewrite this as

$$\frac{d}{dt}\rho(0, \mathbf{k}) = \Gamma F[\rho(0, \mathbf{k})], \quad (2.113)$$

for some functional  $F$ . These equations can then be written as

$$\partial_t \rho(x, t, \mathbf{k}) + \partial_x [v^{\text{eff}}(x, t, \mathbf{k}) \rho(x, t, \mathbf{k})] = 0 \quad (2.114a)$$

$$\partial_t \rho(0, t, \mathbf{k}) + \partial_x [v^{\text{eff}}(x, t, \mathbf{k}) \rho(x, t, \mathbf{k})]|_{x=0} = \Gamma F[\rho(0, t, \mathbf{k})] \quad (2.114b)$$

which correspond to Eq. (2.109) rewritten in terms of the quasi-particle density rather than the filling function.

The critical question is to evaluate the functional  $F[\rho]$ . In [269], it was demonstrated that this could be achieved through Monte-Carlo sampling of Bethe states, although this method was found to be incredibly expensive computationally. However, in that context, the model was taken as the Lieb-Liniger model, where the exact forms of the local conserved charges are not known [270]. It may be feasible to compute them for the XXZ model instead, perhaps at least in the Ising limit of  $\Delta \rightarrow \infty$  where the conserved charges coincide with those of the XY model [271],

and to obtain  $F[\rho]$  in this way. Alternatively, perhaps a series expansion could be obtained assuming that  $\rho(x, t, \mathbf{k})$  varies sufficiently slowly in both space and quasi-momentum,  $\mathbf{k}$ . It would also be interesting to study carefully the effects of a boundary at  $x = 0$  in order to make a connection with the results from earlier in this chapter or to consider perhaps systems with two boundaries with losses at one side and gain at the other which would be similar to previous studies of driven transport in integrable systems.

### 3.3 Dephased systems

The second example is to consider systems with localised dephasing. In particular, consider the Lieb-Liniger model from Sec 2.4 with localised particle number dephasing at  $x = 0$  described by the Lindblad operator  $L = \sqrt{\gamma}\Psi^\dagger(0)\Psi(0)$ . It is known that self adjoint Lindblad operators can be absorbed into the Hamiltonian dynamics by introducing a stochastic, time dependent term [272, 273]. In our case our Hamiltonian becomes

$$H(t) = \int_{-\infty}^{\infty} dx \partial_x \Psi^\dagger(x) \partial_x \Psi(x) + c \Psi^\dagger(x) \Psi^\dagger(x) \Psi(x) \Psi(x) + \sqrt{2\gamma} \eta(t) \delta(x) \Psi^\dagger(x) \Psi(x), \quad (2.115)$$

where  $\eta(t)$  is white noise with  $\mathbb{E}[\eta(t)\eta(t')] = \delta(t - t')$ . Following the work of [267] regarding generalised hydrodynamics with stochastic fields, we obtain GHD equations

$$\frac{\partial}{\partial t} \vartheta(k) + v^{\text{eff}}(k) \frac{\partial}{\partial x} \vartheta(k) + \sqrt{2\gamma} \eta(t) \delta'(x) \frac{\partial}{\partial k} \vartheta(k) = 0. \quad (2.116)$$

The delta function introduces a discontinuity to the filling function and effective velocities at  $x = 0$ . After careful treatment using regularisations of the delta function, we obtain the jump condition,

$$v^+(0, \lambda) \vartheta^-(0, \lambda) = \sqrt{\frac{\gamma}{2}} \eta(t) \frac{\partial^2}{\partial x \partial \lambda} \vartheta^+(0, \lambda) \quad (2.117a)$$

$$\vartheta^-(0, \lambda) = \text{const.} \quad (2.117b)$$

where we have for convenience defined

$$\vartheta^\pm(x, \lambda) = \frac{1}{2} (\vartheta(x, \lambda) \pm \vartheta(-x, \lambda)) \quad \& \quad v^\pm(x, \lambda) = \frac{1}{2} (v^{\text{eff}}(x, \lambda) \pm v^{\text{eff}}(-x, \lambda)). \quad (2.118)$$

Away from  $x = 0$  we have the ‘free’ GHD equation but importantly due to the non-linearity this cannot be recast in terms of  $\vartheta^\pm(x, \lambda)$  separately.

While the jump condition can be written neatly, the practicality of using this in numerical calculations remains unexplored. However, it has been conjectured that this and/or similar models may display a phase transition as the strength

of the dephasing noise is increased past a critical point [274]. Generalised hydrodynamics provides a very promising platform from which to study such a phase transition should it exist. However, it is unclear whether such a transition would be unobservable due to the hydrodynamic assumptions that have been made. This is certainly a question which warrants further study.

## 4 Conclusions

In this chapter, we have studied integrable systems in the presence of dissipation. This study has been complementary to, but distinct from, similar studies [126, 217] concerning integrable quantum Liouvillians. Our main result has been to develop a method, dubbed the dissipative Bethe ansatz, to analytically calculate the Liouvillian spectrum of integrable systems subject to specific loss mechanisms. We used our method to study the experimentally relevant example of an XXZ spin chain subjected to boundary losses where we were able to directly identify phase transitions in the Liouvillian spectrum and calculate the Liouvillian gap. This led us to observe two intriguing physical phenomena, namely domain wall formation and a dissipative phase transition, which we link to the existence of boundary bound top-magnons. Such remarkable phenomena could also occur in other models with localised loss, such as the 1D Hubbard model or interacting bosons in 1D, which can also be studied analytically using our method.

We then discussed the problem of extending our method to the thermodynamic limit, particularly the issue of determining which curves in the complex plane the quasi-momenta lie on. Progress on this seems to have been made by [225], but further study is required in order to examine the limits of applicability. We then finally introduced generalised hydrodynamics and discussed some directions for interesting further study.

In the remainder of this thesis, we will move away from the strict symmetry structure provided by integrable systems. It is important to do so as the vast majority of quantum models are *not* integrable. In general, this means that analytic calculations become more challenging, but as we will see, much can still be learned about long-time dynamics even when the system has a much weaker symmetry structure.

# 3

## Algebraic conditions for persistent non-stationarity in dissipative systems

Perpetual motion was long ago thought to be the holy grail of physics. While several machines claimed to produce limitless energy, our modern understanding of statistical mechanics and thermodynamics precludes the existence of such an engine. Indeed, as we discussed in Ch 1, under a generic Liouvillian, an open quantum system will reach a non-equilibrium steady state on a time scale usually comparable to the energy scale of the Hamiltonian. This equilibration is also consistent with the eigenstate thermalisation hypothesis. However, for most microscopic models, these time scales are atomic, suggesting that systems should reach stationarity incredibly quickly. Such short thermalisation times are entirely at odds with the world around us, where non-stationarity persists for extraordinarily long times, many orders of magnitude above the atomic scale. This disparity motivates studying non-stationarity in quantum systems, particularly those with dissipation, with the ultimate goal of understanding how macroscopic non-stationarity can be consistent with our microscopic models.

In this chapter, we will approach the problem of persistent non-stationarity by studying the purely imaginary eigenvalues of quantum Liouvillians, which correspond to persistent oscillations. We will extend previously studied conditions for the existence of these special eigenmodes, which are purely algebraic and can be applied to systems of arbitrary size. We will also study the behaviour of purely imaginary eigenvalues under small perturbations to understand how persistent non-stationarity can be broken.

# 1 Solutions to long time dynamics of time homogeneous open systems

Recall that under the Lindblad equation, the state,  $\rho(t)$ , of a quantum system evolves according to

$$\frac{d}{dt}\rho(t) = \mathcal{L}[\rho(t)] = -i[H, \rho(t)] + \sum_{\mu} 2L_{\mu}\rho(t)L_{\mu}^{\dagger} - \{L_{\mu}^{\dagger}L_{\mu}, \rho(t)\}. \quad (3.1)$$

Note we have restricted to the case that the evolution is time homogeneous. We will also make the restriction, as we have throughout, that the systems have an arbitrarily large, but strictly finite Hilbert space. We can formally solve this evolution in terms of the superoperator exponential as

$$\rho(t) = e^{t\mathcal{L}}[\rho(0)]. \quad (3.2)$$

Now we must note that the Liouvillian,  $\mathcal{L}$ , is not necessarily diagonalisable and so care must be taken when dealing with this superoperator exponential. Using the Jordan normal form of  $\mathcal{L}$  we can write the superoperator exponential in Fock-Liouville space as

$$e^{t\mathcal{L}} = \sum_k \sum_{n_k=0}^{N_k} \sum_{m_k=n_k}^{N_k} t^{m_k-n_k} e^{\lambda_k t} |\rho_k^{n_k}\rangle \langle \sigma_k^{m_k}|, \quad (3.3)$$

where the index  $k$  runs over the Liouvillian eigenvalues,  $\{\lambda_k\}$ , the states  $\{|\rho_k^{n_k}\rangle, |\sigma_k^{m_k}\rangle\}$  are the generalised eigenstates corresponding to the eigenvalue  $\lambda_k$  and  $N_k$  is the dimension of the respective Jordan block. The generalised eigenstates satisfy the orthogonality relation

$$\langle \langle \sigma_k^{m_k} | \rho_j^{n_j} \rangle \rangle = \delta_{k,j} \delta_{m_k, n_j}. \quad (3.4)$$

Since the Liouvillian generates a CPTP map, the eigenvalues are known to lie in the left hand side of the complex plane,  $\text{Re}(\lambda_k) \leq 0$ . Thus we can deduce that after sufficiently long times the dynamics are governed exclusively by the purely imaginary eigenvalues

$$\lim_{t \rightarrow \infty} e^{t\mathcal{L}} = \sum_{k: \lambda_k = i\omega_k} \sum_{n_k=0}^{N_k} \sum_{m_k=n_k}^{N_k} t^{m_k-n_k} e^{i\omega_k t} |\rho_k^{n_k}\rangle \langle \sigma_k^{m_k}|. \quad (3.5)$$

At this point we can use the following Lemma to reduce this expression further.

**Lemma 1.** *The purely imaginary eigenvalues of  $\mathcal{L}$  have one-dimensional Jordan blocks.*

*Proof.* Let the CPTP map generated by  $\mathcal{L}$  be  $\mathcal{T}_t = e^{t\mathcal{L}}$ . Note that the eigenspace of  $\mathcal{L}$  with eigenvalue  $i\omega$  is also an eigenspace of  $\mathcal{T}_t$  with eigenvalue  $e^{it\omega}$  which has unit modulus. Thus by proposition 6.1 of [275] the Jordan blocks corresponding to  $e^{it\omega}$  in  $\mathcal{T}_t$  are all one-dimensional. It follows that the Jordan blocks of  $\mathcal{L}$  corresponding to  $i\omega$  are also all one-dimensional.  $\square$

Consequently our expression for the long time exponential reduces to the far simpler expression,

$$\lim_{t \rightarrow \infty} e^{t\mathcal{L}} = \sum_k e^{i\omega_k t} |\rho_k\rangle\rangle \langle\langle \sigma_k|, \quad (3.6)$$

which then allows us to express the state at late times as

$$\lim_{t \rightarrow \infty} |\rho(t)\rangle\rangle = \sum_k e^{i\omega_k t} |\rho_k\rangle\rangle \langle\langle \sigma_k | \rho(0) \rangle\rangle. \quad (3.7)$$

This reduction of the long time dynamics under a time-homogeneous quantum Liouvillian motivates studying the purely imaginary eigenvalues of  $\mathcal{L}$ . In the following sections, we will completely characterise the existence of purely imaginary eigenvalues in terms of algebraic requirements and study how these eigenvalues behave when the system is perturbed.

## 2 Conditions for persistent non-stationarity in quantum systems

We first give a theorem that completely characterises the purely imaginary eigenvalue of a Liouvillian in terms of a unitary operator,  $A$ , and a proper NESS,  $\rho_\infty$ . By proper we mean that the NESS is a density operator and thus a true quantum state.

**Theorem 1.** *The following condition is necessary and sufficient for the existence of an eigenstate  $\rho$  with purely imaginary eigenvalue  $i\omega$ ,  $\mathcal{L}\rho = i\omega\rho$ ,  $\omega \in \mathbb{R}$ :*

*We have  $\rho = A\rho_\infty$ , where  $\rho_\infty$  is a proper NESS (non equilibrium steady state; c.f. Eq. (1.66)) and  $A$  is a unitary operator which together obey,*

$$[L_\mu, A]\rho_\infty = 0, \quad (3.8)$$

$$\left( -i[H, A] - \sum_\mu [L_\mu^\dagger, A]L_\mu \right) \rho_\infty = i\omega A\rho_\infty, \quad \omega \in \mathbb{R}. \quad (3.9)$$



*Proof.* Sufficiency can be checked directly by calculating  $\mathcal{L}[\rho] = \mathcal{L}[A\rho_\infty]$  as follows.

$$\mathcal{L}[A\rho_\infty] = -i[H, A\rho_\infty] + \sum_\mu 2L_\mu A\rho_\infty L_\mu^\dagger - \{L_\mu^\dagger L_\mu, A\rho_\infty\} \quad (3.10a)$$

$$= -i[H, A]\rho_\infty - iA[H, \rho_\infty] + \sum_\mu 2A(L_\mu\rho_\infty L_\mu^\dagger) + 2[L_\mu, A]\rho_\infty L_\mu^\dagger \quad (3.10b)$$

$$\begin{aligned} & - A\rho_\infty L_\mu^\dagger L_\mu - [L_\mu^\dagger L_\mu, A]\rho_\infty - AL_\mu^\dagger L_\mu\rho_\infty \\ & = -i[H, A]\rho_\infty - \sum_\mu [L_\mu^\dagger L_\mu, A]\rho_\infty \end{aligned} \quad (3.10c)$$

$$= \left( -i[H, A] - \sum_\mu [L_\mu^\dagger, A]L_\mu \right) \rho_\infty \quad (3.10d)$$

$$= i\omega A\rho_\infty. \quad (3.10e)$$

To prove necessity we first observe that  $\rho$  is also an eigenstate of the corresponding quantum channel  $\mathcal{T}_t = e^{t\mathcal{L}}$  with eigenvalue  $e^{i\omega t}$ . Since this lies on the unit circle we may apply Theorem 5 of [276] to deduce that  $\rho$  admits a polar decomposition of the form  $\rho = AR$  where  $A$  is unitary and  $R$  is positive semi-definite with  $\mathcal{T}_t R = R$ . In particular this implies  $\mathcal{L}[R] = 0$  so that  $R$  is a steady-state of  $\mathcal{L}$  which we now call  $\rho_\infty = R$ . Note that this also implies  $\rho_\infty$  is Hermitian and may be scaled to have unit trace, thus making  $\rho_\infty$  a proper NESS.

Writing the channel in Kraus form as

$$\mathcal{T}_t[x] = \sum_k M_k(t)xM_k^\dagger(t), \quad (3.11)$$

we can apply Theorem 5 of [276] again to find

$$M_k(t)A\rho_\infty = e^{i\omega t}AM_k(t)\rho_\infty. \quad (3.12)$$

Now note that the adjoint channel is given by  $\mathcal{T}_t^\dagger[x] = \sum_k M_k(t)^\dagger x M_k(t)$ , and so we can compute the adjoint Liouvillian as,

$$\mathcal{L}^\dagger[x] = \frac{d\mathcal{T}_t^\dagger}{dt}\bigg|_{t=0} \quad (3.13a)$$

$$= \sum_k \dot{M}_k^\dagger(0)xM_k(0) + M_k^\dagger(0)x\dot{M}_k(0). \quad (3.13b)$$

Using the of derivative Eq. (3.12) and the requirement that Kraus operators satisfy

$\sum_k M_k^\dagger M_k = \mathbb{1}$  we can calculate,

$$\mathcal{L}^\dagger[A]\rho_\infty = \sum_k \dot{M}_k^\dagger(0) A M_k(0) \rho_\infty \quad (3.14a)$$

$$\begin{aligned} &+ M_k^\dagger(0) A \dot{M}_k(0) \rho_\infty \\ &= \sum_k \dot{M}_k^\dagger(0) M_k(0) A \rho_\infty \\ &+ M_k^\dagger(0) \dot{M}_k(0) A \rho_\infty \end{aligned} \quad (3.14b)$$

$$\begin{aligned} &+ i\lambda M_k^\dagger(0) A M_k(0) \rho_\infty \\ &= \sum_k \frac{d}{dt} [M_k^\dagger(t) M_k(t)]_{t=0} A \rho_\infty \\ &+ i\omega \sum_k M_k^\dagger(0) M_k(0) A \rho_\infty \end{aligned} \quad (3.14c)$$

$$= i\omega A \rho_\infty. \quad (3.14d)$$

A similar calculation using the conjugate equations, noting that  $\rho_\infty$  is Hermitian, yields

$$\rho_\infty \mathcal{L}^\dagger[A^\dagger] = -i\omega \rho_\infty A^\dagger. \quad (3.15)$$

We will now also introduce the *dissipation function* [57, 112], defined for any operator  $x$  as

$$\begin{aligned} D[x] &= \mathcal{L}^\dagger[x^\dagger x] - \mathcal{L}^\dagger[x^\dagger] x - x^\dagger \mathcal{L}^\dagger[x] \\ &= \sum_\mu [L_\mu, x]^\dagger [L_\mu, x]. \end{aligned} \quad (3.16)$$

Then by unitarity of  $A$  and the above results for  $\mathcal{L}^\dagger[A]$ ,  $\mathcal{L}^\dagger[A^\dagger]$  we compute

$$0 = \rho_\infty D[A] \rho_\infty = \sum_\mu \rho_\infty [L_\mu, A]^\dagger [L_\mu, A] \rho_\infty = \sum_\mu \|[L_\mu, A] \rho_\infty\|^2. \quad (3.17)$$

Since this sum is positive definite we must have  $[L_\mu, A] \rho_\infty = 0 \ \forall \mu$ . We now compute  $\mathcal{L}[A \rho_\infty] = i\omega A \rho_\infty$  using  $\mathcal{L}[\rho_\infty] = 0$  and  $[L_\mu, A] \rho_\infty = 0$  to obtain

$$\left( -i[H, A] - \sum_\mu [L_\mu^\dagger, A] L_\mu \right) \rho_\infty = i\omega A \rho_\infty, \quad (3.18)$$

as required.  $\square$

This result allows us to see precisely when a purely imaginary eigenvalue will occur and provides us with an exact expression for the corresponding state. As promised, this condition depends only on the algebra of the Lindblad operators and the Hamiltonian. The proof also highlights two important points. Firstly, for sufficiency, the operator  $A$  need not be unitary, and the NESS need not be a density operator. Similarly, we can note that the sufficiency of these criteria

holds even in the case of infinite Hilbert spaces, such as for bosonic modes, but necessity does not. We can also rephrase the necessity conditions of Eq. (3.8) and Eq. (3.9) by making the following manipulations. First we may use the unitarity of  $A$  and  $[L_\mu, A]\rho_\infty = 0 \ \forall \mu$  to obtain

$$\rho_\infty A^\dagger [L_\mu^\dagger, A] L_\mu \rho_\infty = 0, \ \forall \mu. \quad (3.19)$$

We then left multiply Eq. (3.18) by  $\rho_\infty A^\dagger$  and use Eq. (3.19) to obtain

$$-i\rho_\infty A^\dagger [H, A] \rho_\infty = i\omega \rho_\infty^2. \quad (3.20)$$

Finally using Eq. (3.19) and the unitarity of  $A$ , (which trivially gives  $[L_\mu^\dagger, A^\dagger A] = 0$ ), we find  $\rho_\infty [L_\mu^\dagger, A^\dagger] L_\mu \rho_\infty = 0, \forall \mu$ . This immediately gives us the following corollary.

**Corollary 1.** *The Liouvillian super-operator,  $\mathcal{L}$ , admits a purely imaginary eigenvalue,  $i\omega$ , only if the polar decomposition of the corresponding eigenstate can be written as  $\rho = A\rho_\infty$  with  $\rho_\infty$  a proper NESS and  $A$  unitary satisfying*

$$-i\rho_\infty A^\dagger [H, A] \rho_\infty = i\omega \rho_\infty^2, \quad (3.21)$$

$$\rho_\infty A^\dagger [L_\mu^\dagger, A] L_\mu \rho_\infty = 0, \ \forall \mu, \quad (3.22)$$

$$\rho_\infty [L_\mu^\dagger, A^\dagger] L_\mu \rho_\infty = 0, \ \forall \mu. \quad (3.23)$$

We can also use Thm 1 to understand the nature of the stationary state, if there exists a non-zero purely imaginary eigenvalue.

**Corollary 2.** *Suppose  $\mathcal{L}$  has a non-zero purely imaginary eigenvalue,  $i\omega \neq 0$ , then at least one NESS of  $\mathcal{L}$  does not have full rank.*

*Proof.* By Thm 1 we can express the corresponding eigenmode as  $\rho = A\rho_\infty$  with  $A$  unitary. Suppose, for a contradiction, that  $\rho_\infty$  has full rank and is thus invertible. Right multiplying the conditions of Thm 1 by  $\rho_\infty^{-1}$  and  $\rho_\infty^{-1} A^\dagger$  respectively gives

$$[L_\mu, A] = 0, \quad (3.24)$$

$$-i[H, A]A^\dagger - \sum_\mu [L_\mu^\dagger, A] L_\mu A^\dagger = i\omega \mathbb{1}. \quad (3.25)$$

Using  $[L_\mu, A] = 0$  in the second line and taking the trace gives

$$i\omega \|A\|^2 = 0, \quad (3.26)$$

and since  $A \neq 0$  this must imply  $\omega = 0$ , giving us our contradiction.  $\square$

Unfortunately, while these results completely characterise the purely imaginary eigenvalues using only algebraic conditions and give some useful consequences, they are often too complicated to use in practice for many body systems. This will become clear when studying examples of quantum synchronisation later and is why we will now make a connection with previous works studying purely imaginary eigenvalues of quantum Liouvillians to obtain more applicable conditions.

In [119], it was first shown that the existence of a strong dynamical symmetry was sufficient for the existence of purely imaginary eigenvalues. A strong dynamical symmetry is the natural promotion of a dynamical symmetry of a closed system to a symmetry of the Lindblad equation in the strong sense as per the discussion in Ch 1.

**Definition** (Strong dynamical symmetry). An operator,  $A$ , is a strong dynamical symmetry if

$$[H, A] = \omega A, \quad [L_\mu, A] = [L_\mu^\dagger, A] = 0, \quad \forall \mu \quad \text{with } \omega \in \mathbb{R}. \quad (3.27)$$

Strong dynamical symmetries, and their extensions, have since been used in several places when studying the persistent dynamics of open quantum systems [119, 120, 277]. We now extend the results of [119] to show that if there exists a stationary state with full rank, then strong dynamical symmetries are, in fact, necessary for the existence of purely imaginary eigenvalues. To streamline the proof of this extension, we first prove a proposition regarding the eigenstates of the adjoint Liouvillian when there exists a full rank stationary state.

**Proposition 1.** *Suppose there exists a faithful (i.e. full-rank/invertible) stationary state,  $\tilde{\rho}_\infty$ , and let  $A$  be an eigenstate of the adjoint Liouvillian with purely imaginary eigenvalue,  $\mathcal{L}^\dagger[A] = -i\omega A$ . Then  $A$  is a strong dynamical symmetry.*

*Proof.* The asymptotic subspace of the Liouvillian,  $As(\mathcal{H})$ , is defined as a subspace of the space of  $\mathcal{B}(\mathcal{H})$  that all initial states,  $\rho(0)$ , arrive in at infinite times,  $\rho(t \rightarrow \infty) \in As(\mathcal{H})$ . The projector  $P$  to the corresponding non-decaying part of the Hilbert space is uniquely defined [112, 278] as, for all  $\rho_\infty \in As(\mathcal{H})$ ,

$$\rho_\infty = P\rho_\infty P, \quad \text{tr}(P) = \max_{\rho_\infty \in As(\mathcal{H})} \{\text{rank}(\rho_\infty)\}. \quad (3.28)$$

It follows that if there is a full rank  $\tilde{\rho}_\infty$  then  $P = \mathbb{1}$ . From the proof of Theorem 4 (Eqs. (2.39-2.40)) of [112] since  $A$  is an eigenmode of the adjoint Liouvillian with purely imaginary eigenvalue,  $\mathcal{L}^\dagger[A] = -i\omega A$ , we have,

$$\begin{aligned} [PHP, PAP] &= \omega PAP, \\ [PL_\mu P, PAP] &= [PL_\mu^\dagger P, PAP] = 0, \end{aligned} \quad (3.29)$$

which reduces to

$$\begin{aligned} [H, A] &= \omega A, \\ [L_\mu, A] &= [L_\mu^\dagger, A] = 0, \end{aligned} \quad (3.30)$$

since  $P = \mathbb{1}$ . Hence  $A$  is a strong dynamical symmetry.  $\square$

We can now prove the following theorem.

**Theorem 2.** *When there exists a faithful (i.e. full-rank/ invertible) stationary state,  $\tilde{\rho}_\infty$ ,  $\rho$  is an eigenstate with purely imaginary eigenvalue if and only if  $\rho$  can be expressed as,*

$$\rho = \rho_{nm} = A^n \rho_\infty (A^\dagger)^m, \quad (3.31)$$

where  $A$  is a strong dynamical symmetry obeying

$$\begin{aligned} [H, A] &= \omega A \\ [L_\mu, A] &= [L_\mu^\dagger, A] = 0 \quad \forall \mu, \end{aligned} \quad (3.32)$$

and  $\rho_\infty$  is some NESS, not necessarily  $\tilde{\rho}_\infty$ . Moreover the eigenvalue takes the form

$$\lambda = -i\omega(n - m). \quad (3.33)$$

Furthermore, the left eigenstates, with  $\mathcal{L}^\dagger[\sigma_{mn}] = i\omega(n - m)\sigma_{mn}$ , are given by  $\sigma_{mn} = (A')^m ((A')^\dagger)^n$  where  $A'$  is also a strong dynamical symmetry.

*Proof.* Since the sufficiency direction of the first statement was shown in [119], we need only show necessity.

Assume that  $\mathcal{L}$  has a purely imaginary eigenvalue  $i\omega$  with corresponding eigenstate  $\rho$ . This eigenstate is then also an eigenstate of the map  $\mathcal{T}_t = \exp(t\mathcal{L})$  with eigenvalue  $e^{i\omega t}$ . Since this eigenvalue lies on the unit circle, and  $\tilde{\rho}_\infty$  is strictly positive, by Lemma 3 of [276], there exists a corresponding eigenstate,  $A = \rho \tilde{\rho}_\infty^{-1}$ , of  $\mathcal{L}^\dagger$ . Hence by Proposition 1,  $A$  is a strong dynamical symmetry. Thus we have

$$\rho = A \tilde{\rho}_\infty, \quad (3.34)$$

so  $\rho$  must be of the form required by Eq. (3.31).

For the final statement regarding the purely imaginary eigenstates of the adjoint Liouvillian, necessity follows immediately from Proposition 1 while sufficiency is a direct calculation.  $\square$

Compared with Theorem 1, we see that this result is significantly simpler, provided it is obvious that a full rank stationary state exists, as it depends only on understanding the symmetries of the Hamiltonian and then checking their compatibility with the Lindblad operators. While checking the existence of a full rank stationary state is generally non-trivial, it is immediately satisfied if the Liouvillian is unital. A Liouvillian is unital if

$$\mathcal{L}[\mathbb{1}] = 0, \quad (3.35)$$

which in terms of the Lindblad operators reduces to

$$\sum_{\mu} L_{\mu}^{\dagger} L_{\mu} = \sum_{\mu} L_{\mu} L_{\mu}^{\dagger}. \quad (3.36)$$

This condition can be easily satisfied when for example the Lindblad operators are self-adjoint, such as for dephasing, or when both  $L_{\mu}$  and  $L_{\mu}^{\dagger}$  appear as separate jump operators, such as for balanced loss and gain. We will see later that unital maps are particularly relevant for quantum synchronisation. We also remark that in contrast with Thm. 1, the strong dynamical symmetries are *not* unitary if we are to have  $\omega \neq 0$ . This can be easily seen by the manipulations

$$[H, A] = \omega A \quad (3.37a)$$

$$A^{-1} H A - H = \omega \mathbb{1} \quad (\text{Assuming } A \text{ is invertible}) \quad (3.37b)$$

$$0 = \omega \text{Tr}(\mathbb{1}) \quad (\text{Taking trace}). \quad (3.37c)$$

We can also take the trace directly of Eq. (3.27) to see that strong dynamical symmetries must be traceless.

The equivalence between purely imaginary eigenvalues, persistent non-stationarity, and strong dynamical symmetries under reasonably general assumptions is incredibly powerful, as we will see in the applications to time crystals and synchronisation. These results also allow us to present a theorem that can determine the absence of persistent non-stationarity by considering only the *commutant* of the Hamiltonian and the Lindblad operators.

**Definition** (Commutant). Let  $\mathcal{M} \subset \mathcal{B}(\mathcal{H})$ . The commutant of the set  $\mathcal{M}$  is defined as the set of all elements in  $\mathcal{B}(\mathcal{H})$  which commute with all the elements of  $\mathcal{M}$ . We denote the commutant of  $\mathcal{M}$  as  $\mathcal{M}'$ . Recall from Ch 1 that  $\mathcal{B}(\mathcal{H})$  is the set of bounded linear operators on the Hilbert space  $\mathcal{H}$ .

Notice that by definition, multiples of the identity operator always belong to the commutant. If these are the only elements of the commutant, then we say the commutant is *trivial*. We can now prove the following.

**Theorem 3.** *If there is a full rank stationary state  $\tilde{\rho}_{\infty}$  (i.e. no zero eigenvalues, invertible) and the commutant of  $\{H, L_{\mu}, L_{\mu}^{\dagger}\}$  is trivial, then there are no non-zero purely imaginary eigenvalues of  $\mathcal{L}$ .*

*Proof.* Suppose that there exists a state  $\rho$  with purely imaginary eigenvalue  $i\omega$ . Since  $\tilde{\rho}_{\infty}$  has full rank, by Thm. 2 we can write  $\rho = A\rho_{\infty}$  where  $[H, A] = \omega A$ ,  $[L, A] = [L^{\dagger}, A] = 0$  and  $\mathcal{L}[\rho_{\infty}] = 0$ . We then see that  $A^{\dagger}A$  and  $AA^{\dagger}$  both belong to the commutant  $\{H, L_{\mu}, L_{\mu}^{\dagger}\}'$ , and so

$$A^{\dagger}A = c_1 \mathbb{1}, \quad AA^{\dagger} = c_2 \mathbb{1}. \quad (3.38)$$

Taking the trace trivially gives  $c_1 = c_2 = c$ . Notice that  $c \neq 0$ , since  $c = \frac{1}{d} \text{Tr}(A^\dagger A) = \frac{1}{d} \|A\|^2$ , and so  $c = 0$  would correspond to  $A = 0$ . Now we compute,

$$\text{Tr}(A^\dagger[H, A]) = \text{Tr} \omega A^\dagger A \quad (3.39a)$$

$$\text{Tr}(A^\dagger H A - A^\dagger A H) = \omega \text{Tr} A^\dagger A \quad (3.39b)$$

$$0 = \omega \text{Tr}(A^\dagger A). \quad (3.39c)$$

Hence  $\omega = 0$ . Consequently, no non-zero purely imaginary eigenvalue can exist.  $\square$

This condition is particularly useful as we know from the theorems of Evans and Frigerio [89, 279, 280] that a trivial commutant is equivalent to the full rank stationary state being the unique steady state. A trivial commutant is also directly implied<sup>1</sup> by the set  $\{H, L_k, L_k^\dagger\}$  generating  $\mathcal{B}(\mathcal{H})$ . This can, for instance, be easily shown in the case of a system of  $N$  spin-1/2 particles with arbitrary Hamiltonian and onsite Lindblad operators,  $L_k = \gamma_k s_k^+$ ,  $\tilde{L}_k = \gamma_k s_k^-$ . The map is unital since

$$\sum_k L_k^\dagger L_k + \tilde{L}_k^\dagger \tilde{L}_k = \sum_k \gamma_k^2 s_k^+ s_k^- + \gamma_k^2 s_k^- s_k^+ = \sum_k \tilde{L}_k \tilde{L}_k^\dagger + L_k L_k^\dagger \quad (3.40)$$

and the spin raising and lowering operators generate  $\mathcal{B}(\mathcal{H})$ . It is natural to wonder whether these conditions, which preclude persistent non-stationarity, can be related to thermalisation since this is by definition the approach to stationarity of the system. Unfortunately no work has yet been pursued in this direction and the relation remains an interesting open question warranting future study.

From experience with these systems we also make the following conjecture, which generalises the previous theorem.

**Conjecture.** *Suppose the Liouvillian has a unique NESS, then there cannot exist any purely imaginary eigenvalues.*

If the unique NESS has full rank, then this is true either by the above theorem or as a consequence of Cor 2. We believe that this conjecture may be related to the fact that if  $\rho = A\rho_\infty$  has a non-zero purely imaginary eigenvalue then  $\tilde{\rho} = A\rho_\infty A^\dagger$  is also a NESS<sup>2</sup>, and in some way to Cor 2 but for now a proof or counter-example remains elusive.

<sup>1</sup>If a set  $\mathcal{M} \subset \mathcal{B}(\mathcal{H})$  generates an algebra  $\mathcal{A}$ , i.e all elements in  $\mathcal{A}$  can be written as polynomials of elements in  $\mathcal{M}$ , then  $\mathcal{M}' = \mathcal{A}'$ . Also, the commutant of  $\mathcal{B}(\mathcal{H})$  is trivial.

<sup>2</sup>This follows from a simple computation using the conditions of Thm 1. However this does not preclude  $A\rho_\infty A^\dagger = \rho_\infty$ .

### 3 Perturbations to systems possessing purely imaginary eigenvalues

In the previous section, we have presented several results that characterise entirely the purely imaginary eigenvalues of quantum Liouvillians using algebraic conditions. In practice, most systems will not perfectly satisfy these conditions, so it is essential to study how purely imaginary eigenvalues behave when the system is perturbed in some way. This analysis will be especially relevant for understanding the stability of persistent dynamics in the next chapters.

In this section we will consider a Liouvillian,  $\mathcal{L}(s)$ , with some small perturbative parameter,  $s \in \mathbb{R}$ . To avoid unwanted technicalities we will assume that this Liouvillian admits a series expansion with an infinite radius of convergence,

$$\mathcal{L}(s) = \mathcal{L}_0 + s\mathcal{L}_1 + s^2\mathcal{L}_2 + \mathcal{O}(s^3). \quad (3.41)$$

This is not a particularly significant restriction as in most cases the Hamiltonian or Lindblad operators are only perturbed to some finite order. We will label the eigenvalues of  $\mathcal{L}(s)$  as  $\lambda(s)$  and assume that  $\mathcal{L}_0$  has a purely imaginary eigenvalue, i.e.  $\lambda(0) = i\omega$ . We now divide our analysis into the cases that  $\omega = 0$  and  $\omega \in \mathbb{R} \setminus \{0\}$ .

#### 3.1 Ultra-low frequency and Zeno dynamics

Considering first the case where  $\lambda(0) = 0$ , it is important to note that this eigenvalue can only be perturbed if the zero eigenstate of  $\mathcal{L}_0$  is degenerate, since there must always exist a zero eigenmode. This regime has been studied extensively by Macieszczak et al. [281] who showed that when  $\mathcal{L}(s)$  is perturbed away from  $s = 0$  the degeneracy in the 0 eigenvalue is lifted in such a way that the eigenvalues are at least twice continuously differentiable,

$$\lambda(s) = i\lambda_1 s + \lambda_2 s^2 + o(s^2), \quad (3.42)$$

where  $\lambda_1 \in \mathbb{R}$  and  $\text{Re}(\lambda_2) \leq 0$ .

This result shows that the resulting oscillations have a time period that scales as  $\sim 1/s$  and a lifetime that scales as  $\sim 1/s^2$ . For experimental purposes, this behaviour is likely difficult to detect since as we tune our system to extend the lifetime of the dynamics, the oscillations occur over more extended time periods and are thus harder to observe on experimental time scales. This case will consequently be less relevant for our later discussion of dynamically ordered phases of matter.

A more experimentally relevant regime in which to apply these results is when we can write the Liouvillian as

$$\mathcal{L}[\rho] = -i[H, \rho] + \gamma\mathcal{D}[\rho] + \mathcal{O}\left(\frac{1}{\gamma}\right), \quad (3.43)$$



for some large  $\gamma > 0$ , where the evolution is dominated by the dissipative term

$$\mathcal{D}[\rho] = \sum_{\mu} 2L_{\mu}\rho L_{\mu}^{\dagger} - \{L_{\mu}^{\dagger}L_{\mu}, \rho\}. \quad (3.44)$$

This regime is usually referred to as the *Zeno regime* [243–246]. Now rescale the full Liouvillian as

$$\tilde{\mathcal{L}} = \frac{1}{\gamma}\mathcal{L}, \quad (3.45)$$

and use  $s = 1/\gamma$  as our perturbative parameter. We denote the eigenvalues of  $\tilde{\mathcal{L}}$  as  $\tilde{\lambda}(s)$ . Assuming  $\tilde{\lambda}(0) = 0$  is degenerate we observe that by the previous results we have

$$\tilde{\lambda} = i\omega s + \lambda_2 s^2 + o(s^2) \quad (3.46a)$$

$$= i\omega \frac{1}{\gamma} + \lambda_2 \frac{1}{\gamma^2} + o(s^2), \quad (3.46b)$$

and hence

$$\lambda(\gamma) = i\omega + \lambda_2 \frac{1}{\gamma} + o\left(\frac{1}{\gamma}\right), \quad \text{Re}(\lambda_2) \leq 0. \quad (3.47)$$

Here we see that a system with a degenerate stationary state in the limit of infinite dissipation will exhibit long-lived oscillation on the characteristic time scales of the Hamiltonian when the dissipation is weakened. We will see that this effect can be observed experimentally in the example in Ch 4 Sec 3.3.3.

## 3.2 Metastable dynamics

Now let us turn to the case that  $\omega \neq 0$ . This corresponds to perturbing a system that already exhibits persistent non-stationarity and studying how stable the long-time dynamics are to such perturbations. We can apply the results of [282] to prove the following result.

**Theorem 4.** *For analytic  $\mathcal{L}(s)$  with  $\lambda(0) = i\omega$ ,  $\omega \in \mathbb{R}$  we have*

$$\lambda(s) = i\omega + i\lambda_1 s + \lambda_2 s^{1+\frac{1}{p}} + o\left(s^{1+\frac{1}{p}}\right) \quad (3.48)$$

for some integer  $p \geq 1$ . We also find that  $\lambda_1 \in \mathbb{R}$  and  $\lambda_2$  has non-positive real part.

*Proof.* We first note that if  $\lambda(0)$  is a non-degenerate eigenvalue, then it is known that  $\lambda(s)$  is analytic; thus, the above result is trivial. In fact, in this case, we also find that the eigenstate  $\rho(s)$  also depends analytically on  $s$ .

For the case where  $i\omega$  is an  $m$ -fold degenerate eigenvalue of  $\mathcal{L}_0$  we define the ‘ $\omega$ -rotating stable manifold’ ( $\omega$ -RSM) as the eigenspace spanned by the  $m$  eigenmodes corresponding to  $i\omega$ . By Lemma 1 above,  $i\omega$  is a semi-simple eigenvalue and we can directly apply Theorem 2.3 of [282] to write

$$\lambda(s) = i\omega + \lambda_1 s + \lambda_2 s^{1+\frac{1}{p}} + o\left(s^{1+\frac{1}{p}}\right) \quad (3.49)$$

for some integer  $p \geq 1$ . Finally we observe that since  $\mathcal{L}(s)$  always generates a CPTP map, we must have  $\operatorname{Re}(\lambda(s)) \leq 0$  for all  $s \in \mathbb{R}$  and thus immediately we can deduce that  $\lambda_1$  is purely imaginary and  $\lambda_2$  has non-positive real part.  $\square$

Crucially, this means that at first order in the perturbation, the eigenvalues remain purely imaginary, and their real part, which contributes to decay, is higher-order in  $s$ , and thus the decay occurs on much longer timescales. We can refine the above theorem under the additional condition that the perturbation is at leading order only in the Hamiltonian.

**Theorem 5.** *Suppose our Liouvillian  $\mathcal{L}(s)$  has Hamiltonian  $H(s)$  and jump operators  $L_\mu(s)$ . If the perturbation is such that*

$$\begin{aligned} H(s) &= H^{(0)} + sH^{(1)} + \mathcal{O}(s^2) \\ L_\mu(s) &= L_\mu^{(0)} + \mathcal{O}(s^2) \end{aligned} \quad (3.50)$$

*then we find that  $p = 1$  in the result of Theorem 4.*

*Proof.* From [282] we recall that the eigenvalues perturbed away from  $\omega$  (called the  $\omega$ -group) are not in general analytic. They are instead branches of analytic functions and the corresponding eigenstates may contain poles. However the projection onto the span of the  $\omega$ -group eigenstates is analytic and thus the restriction of  $\mathcal{L}(s)$  to this subspace is also analytic. Let us write this projection operator as  $\mathcal{P}(s)$  and thus the restricted Liouvillian is given by  $[\mathcal{L}(s)]_{\mathcal{P}(s)} = \mathcal{P}(s)\mathcal{L}(s)\mathcal{P}(s)$ . We can use the result from Section II.2 of [282] to write

$$\mathcal{P}(s) = \mathcal{P}_0 + s\mathcal{P}_1 + \mathcal{O}(s^2), \quad (3.51)$$

where

$$\mathcal{P}_1 = -\mathcal{S}\mathcal{L}_1\mathcal{P}_0 - \mathcal{P}_0\mathcal{L}_1\mathcal{S}. \quad (3.52)$$

Here  $\mathcal{P}_0$  is the zero order projector onto the  $\omega$ -RSM and  $\mathcal{S}$  is the reduced resolvent of  $\mathcal{L}(s)$  at  $i\omega$  which obeys  $\mathcal{S}\mathcal{P}_0 = \mathcal{P}_0\mathcal{S} = 0$  and  $\mathcal{S}(\mathcal{L} - i\omega \operatorname{id}) = (\mathcal{L} - i\omega \operatorname{id})\mathcal{S} = \operatorname{id} - \mathcal{P}_0$ . We also write (as on page 78 of [282])

$$[\mathcal{L}(s)]_{\mathcal{P}(s)} = i\omega\mathcal{P}_0 + s[\mathcal{L}_1]_{\mathcal{P}_0} + \mathcal{O}(s^2\|\mathcal{L}_2\|). \quad (3.53)$$

Since  $\mathcal{L}_1 = -i[H^{(1)}, \circ]$  we can see that  $\mathcal{L}_1$  generates unitary dynamics, and thus its projection to the  $\omega$ -RSM,  $[\mathcal{L}_1]_{\mathcal{P}_0}$ , also generates unitary dynamics and consequently has purely imaginary eigenvalues which are semi-simple. By the reduction arguments in Section II.3 [282], we can deduce that the eigenvalue  $\lambda(s)$  is twice differentiable,

$$\lambda(s) = i\omega + i\lambda_1 s + \lambda_2 s^2 + o(s^2), \quad (3.54)$$

corresponding to  $p = 1$  in Thm 4.  $\square$

This theorem should be contrasted with the earlier ultra-low frequency case in Eq. (3.42). Under these perturbations, we observe that there are two orders of  $s$  between the decay rate,  $-\text{Re}\lambda_2 s$ , and the oscillation frequency,  $\omega + \lambda_1 s$ , of the resulting dynamics. This demonstrates that these are more stable and thus easier to observe experimentally and more relevant for utilisation than the ultra-low frequency case where there was only one order of  $s$  difference. These results together also confirm the intuition that weakly breaking the algebraic conditions of Thms 1 & 2 should only weakly break the persistent non-stationarity. One final result we shall present shows that the first-order change in the purely imaginary eigenvalue vanishes under particular types of perturbations.

**Proposition 2.** *Let  $\mathcal{A} : \mathcal{B}(\mathcal{H}) \rightarrow \mathcal{B}(\mathcal{H})$  be a superoperator that acts trivially on the left and right eigenspaces of  $\mathcal{L}_0$  with purely imaginary eigenvalues. If the first order perturbation,  $\mathcal{L}_1$ , is anti-symmetric under  $\mathcal{A}$ , i.e.  $\mathcal{A}^\dagger \mathcal{L}_1 \mathcal{A} = -\mathcal{L}_1$ , then the frequency of long-lived oscillations is stable to next-to-leading order in  $s$ , i.e.  $\lambda_1 = 0$ .*

*Proof.* Note again that the projector,  $\mathcal{P}(s)$ , to the  $\lambda(s)$  group is differentiable to leading order [282]. We may write the eigenmode equation  $\mathcal{L}(s)\rho(s) = \lambda(s)\rho(s)$  using projection operators and Eq. (3.53) as,

$$[\mathcal{L}(s)]_{\mathcal{P}(s)} |\rho(s)\rangle\rangle = \lambda(s) \mathcal{P}(s) |\rho(s)\rangle\rangle \quad (3.55a)$$

$$\begin{aligned} (i\omega \mathcal{P}_0 + s \mathcal{P}_0 \mathcal{L}_1 \mathcal{P}_0 + \mathcal{O}(s^2)) |\rho(s)\rangle\rangle &= (i\omega + s\lambda_1 + \mathcal{O}(s^{1+1/p})) \\ &\cdot (\mathcal{P}_0 + s \mathcal{P}_1 + \mathcal{O}(s^2)) |\rho(s)\rangle\rangle \end{aligned} \quad (3.55b)$$

$$s \mathcal{P}_0 \mathcal{L}_1 \mathcal{P}_0 |\rho(s)\rangle\rangle = s (i\omega \mathcal{P}_1 + \lambda_1 \mathcal{P}_0 + \mathcal{O}(s^{1+1/p})) |\rho(s)\rangle\rangle \quad (3.55c)$$

$$\text{Using } |\rho(s)\rangle\rangle = |\rho(0)\rangle\rangle + o(s)$$

$$\mathcal{P}_0 \mathcal{L}_1 \mathcal{P}_0 |\rho(0)\rangle\rangle = (i\omega \mathcal{P}_1 + \lambda_1 \mathcal{P}_0) |\rho(0)\rangle\rangle + o(s) \quad (3.55d)$$

$$\text{Left multiplying by } \langle\langle \sigma(0) | \text{ the left eigenstate which is orthonormal to } |\rho(0)\rangle\rangle$$

$$\langle\langle \sigma(0) | \mathcal{L}_1 |\rho(0)\rangle\rangle = \lambda_1 + i\omega \langle\langle \sigma(0) | \mathcal{P}_1 |\rho(0)\rangle\rangle. \quad (3.55e)$$

Now we recall the equation for  $\mathcal{P}_1$  from above

$$\mathcal{P}_1 = -\mathcal{S} \mathcal{L}_1 \mathcal{P}_0 - \mathcal{P}_0 \mathcal{L}_1 \mathcal{S}, \quad (3.56)$$

where  $\mathcal{S}\mathcal{P}_0 = \mathcal{P}_0\mathcal{S} = 0$ . This implies  $\langle\langle\sigma(0)|\mathcal{P}_1|\rho(0)\rangle\rangle = 0$ , so that we are left with the familiar expression

$$\lambda_1 = \langle\langle\sigma(0)|\mathcal{L}_1|\rho(0)\rangle\rangle. \quad (3.57)$$

Now we use the hypothesis that  $\mathcal{L}_1$  is anti-symmetric under  $\mathcal{A}$ , to obtain

$$\lambda_1 = -\langle\langle\sigma(0)|\mathcal{A}^\dagger\mathcal{L}_1\mathcal{A}|\rho(0)\rangle\rangle. \quad (3.58)$$

But also by assumption  $\mathcal{A}|\rho(0)\rangle\rangle = |\rho(0)\rangle\rangle$  and  $\mathcal{A}|\sigma(0)\rangle\rangle = |\sigma(0)\rangle\rangle$  which gives  $\lambda_1 = -\lambda_1$  hence  $\lambda_1 = 0$ .  $\square$

This result is somewhat unintuitive as it implies that the system is most robust to perturbations which explicitly breaks some symmetry of the purely imaginary eigenmodes. We will see that this result is particularly relevant to quantum synchronisation, where a translationally invariant synchronised quantum system is most robust to perturbations that anti-symmetrically break this translational symmetry.

## 4 Summary

To summarise this chapter, we have presented several results on the existence and perturbative behaviour of purely imaginary eigenvalues of quantum Liouvillians. We first wholly characterised purely imaginary eigenmodes in terms of what we will refer to as “ $\mathcal{A}$ -operators” and their algebraic relations with the Hamiltonian and Lindblad operators. If the system has a full rank stationary state, we were able to refine this result and show that the existence of purely imaginary eigenmodes was equivalent to the existence of strong dynamical symmetries. This result is particularly useful in the case of unital maps where a full rank stationary state exists by definition. We also showed that if a system has a unique stationary state that further has full rank, this precludes any persistent non-stationarity.

We then studied the behaviour of purely imaginary eigenvalues under perturbations. We showed that they are always once continuously differentiable and that under the additional assumption that the perturbation to the Lindblad operators is at least quadratic the purely imaginary eigenvalues are twice differentiable. These results help us understand the time scales on which the resulting long-time oscillations will decay. We also showed that if a first-order perturbation explicitly breaks some symmetry of the purely imaginary eigenstates, then the perturbed eigenvalues do not change at first order.

In the following two chapters, we will use these results to study what we will refer to collectively as persistently ordered dynamical phases of matter that remain both dynamic and ordered forever in the absence of perturbations. The first will be dissipative time crystals, where we find that environmental noise can stabilise the

dynamics of a system so that it displays clean periodic oscillations. This chapter, and in particular the discussions in Sec. 2, will help to elucidate more concretely the various definitions we have introduced here. The second dynamical phase of matter will be spontaneously synchronised quantum systems that arrive in a non-stationary synchronised state after some transient time period.

# 4

## Dissipative time crystals

Crystalline structures can be found everywhere in the world around us. Characterised by a fixed unit cell that is repetitively translated along its principal axes, crystals in one, two or three-dimensional space come in a vast array of different geometries and are at the heart of many studies in physics, material science, engineering and chemistry. Crucially, in all crystals, the repeated translation breaks the continuous translational symmetry of space into a discrete translational symmetry by fixed unit vectors.

Time crystals are a proposed phase of matter that similarly break continuous-time translational symmetry into a discrete symmetry with a fixed time-step. While trivial examples of a time crystal behaviour can be found in single body systems, such as a spin- $1/2$  particle undergoing Larmor precession around a magnetic field which continues to oscillate forever at a fixed frequency, to be a genuine time crystal, it is generally agreed that the system must be many-bodied, strongly interacting and have some degree of stability to perturbation.

In this chapter, we will define and study dissipative time crystals, where the time crystallinity occurs *only* in the presence of dissipation. This phenomenon will be studied using the techniques developed in the previous chapter for studying persistent non-stationarity in dissipative many-body quantum systems. Importantly we will provide an experimentally verifiable model of our novel phenomenon. We will also extend the concept of a dissipative time crystal to the regime of periodically driven Floquet time crystals, where the time translational symmetry imposed by periodic driving is broken by the system exhibiting a sub-harmonic response.

# 1 The origins of time crystals

We will first recap and expand upon our introduction to the field of time crystals from Chapter 1. In [161], Wilczek proposed that a quantum time crystal would be a state of matter that spontaneously broke time-translational symmetry in the same way that a normal crystal breaks space translational symmetry. This would require the system to oscillate periodically forever. Watanabe and Oshikawa [162] formalised this idea by defining a time crystal to be an undriven closed system with an extensive observable,  $O$ , which persistently oscillates at a single frequency,  $\omega$ . This required that the equilibrium autocorrelation function,

$$f(t) = \frac{\langle O(t)O(0) \rangle_{\text{eq}}}{V^2}, \quad (4.1)$$

where  $V$  is the volume of the system, should at late times be expressed as

$$f(t) \underset{t \rightarrow \infty}{=} C \cos(\omega t + \theta) + D, \quad (4.2)$$

with  $C$ ,  $D$  and  $\theta$  finite constants. This definition is akin to how one uses response functions at equilibrium to define space-translational symmetry breaking. In the same work, they then claimed to show that if the Hamiltonian is sufficiently local, then  $C$  must vanish and hence that time crystals in this sense cannot exist. Their original proof was later shown to be incorrect and they have since revised their arguments [164]. However, it is interesting to notice that the equal time correlations vanish for a wide range of equilibrium states in the thermodynamic limit at finite temperatures. In one dimension, this is a consequence of the Mermin-Wagner theorem [283, 284] and hence one could instead interpret Watanabe and Oshikawa's conditions as probing the absence of long-range spatial order rather than the presence of temporal order.

Two possible relaxations of these original conditions have been proposed for undriven, closed quantum systems. The first, proposed in [106], is to instead measure the correlation function

$$\frac{\langle O(t)O(0) \rangle_{\text{eq}}}{\langle O(0)^2 \rangle_{\text{eq}}} \underset{t \rightarrow \infty}{=} C \cos(\omega t + \theta) + D. \quad (4.3)$$

It was shown that a non-zero  $C$  can be implied by the existence of an extensive dynamical symmetry,  $A$ , provided  $\text{Tr}(A^\dagger O(0)) \neq 0$ . This is because in the presence of a dynamical symmetry, the system can be locally described<sup>1</sup> by a time-dependent generalised Gibbs ensemble (tGGE),

$$\rho(t) \underset{t \rightarrow \infty}{=} Z^{-1} \exp(-\beta H + \sum_j \mu_j^Q Q_j - \mu_j^A e^{i\omega_j t} A_j - (\mu_j^A)^* e^{-i\omega_j t} A_j^\dagger), \quad (4.4)$$

---

<sup>1</sup>In the sense that  $\rho_{\text{tGGE}}$  should only be used to evaluate expectation values of local observables.

where  $\beta$  is the temperature,  $Z$  is a partition function,  $Q_j$  are conserved charges with  $[H, Q_j] = 0$  and the  $A_j$  are orthogonal<sup>2</sup> dynamical symmetries with frequencies  $\omega_j$ . The generalised chemical potentials  $\mu_j^A$  and  $\mu_j^Q$  are determined from the initial state. This is the natural extension of the well-established generalised Gibbs ensemble (GGE) state that generically follows a quantum quench as a result of entropy maximisation [285]. If there are many incommensurate  $\omega_j$  which become dense in the thermodynamic limit, this can result in noisy dynamics or even dephasing to stationarity for sufficiently large systems. This can be particularly important for free or many-body localised models [163, 286] which are generically likely to have many dynamical symmetries.

The second extension [165] is to consider the generalised out-of-time ordered correlation function

$$C_{W_x, V_y}(t_1, t_2) = -\langle [W_x(t_1), V_y(0)][W_x(t_2), V_y(0)] \rangle_\beta, \quad (4.5)$$

where  $W_x, V_y$  are strictly local operators at sites  $x$  &  $y$  and the expectation is taken in a thermal state at inverse temperature  $\beta$ . This function quantifies the propagation of the observable  $W$  at location  $x$  to the observable  $V$  at point  $y$  during the time interval  $t : t_1 \rightarrow t_2$ . An out-of-time ordered crystal (OTO crystal) is then defined as a system which has stable persistent oscillations with frequencies  $\omega_1, \omega_2$  in both temporal arguments of  $C_{W_x, V_y}(t_1, t_2)$ . Moreover, the number of frequencies at which persistent oscillations exist should grow with the separation between  $x$  and  $y$  to ensure this is a many-body interacting effect. It was argued in [165] that dynamical symmetries alone are not sufficient to generate an OTO crystal, and the phenomenon is instead related to a novel type of local Hilbert space fragmentation [287–289].

Following Watanabe and Oshikawa’s original no-go theorem for time crystals, the focus shifted to studying discrete time translational symmetry breaking in Floquet systems with periodic driving. The resulting Floquet time crystal is defined as a periodically driven system, with period  $T$ , which presents a subharmonic response for some observable  $O$ , i.e after evolution from some generic state we have

$$\langle O(t + nT) \rangle = \langle O(t) \rangle \text{ **only** for } n \geq 1. \quad (4.6)$$

Floquet time crystals have been studied in both closed [166–168, 290–293] and open [169, 294–296] quantum systems. The time crystal concept has also been extended to classical models [172–174, 297], introducing non-local Hamiltonians [298], time quasi-crystals [299, 300] and time glass [163]. Recent experimental results [175, 176, 178, 179, 301] have also demonstrated the existence of this bizzare phase of matter, motivating its study further.

---

<sup>2</sup>Orthogonal with respect to the Hilbert-Schmidt inner product,  $\langle A, B \rangle = \langle \langle A|B \rangle \rangle = \text{Tr}(A^\dagger B)$ .



## 2 Definition of dissipative time crystals and their spectral requirements

We will now define what we mean by a dissipative time crystal and discuss the conditions under which they arise. This discussion will be closely related to the results of Ch 3, but we will see that additional considerations will need to be made, especially regarding the commensurability of eigenvalues. We will then demonstrate this discussion by example in the following section.

### 2.1 Definition

We define a dissipative time crystal as a time-homogeneous quantum system coupled to a noise inducing environment that exhibits periodic motion in some observable at late times for generic initial conditions. Importantly, we will require that after some finite transient period, during which some parts of the state decay, the observable in question must display persistent and clearly measurable oscillations which do not decay any further. This definition can be understood as the most natural extension of the quench based notion of a time crystal as a closed system that continuously oscillates periodically in time to the setting where the system is interacting with some noisy environment. Importantly, we will only consider strongly interacting, many-body systems to exclude single-body or collective models that trivially oscillate, as is standard for studies of time crystals.

This definition should be contrasted with previous works which deal with time crystals. Here we take a system in the presence of noise and the absence of any time-dependent driving. In physics, one usually associates external noise with decoherence and as a mechanism for destroying quantum behaviour. However, here we will be studying the remarkable and unintuitive case that the external noise is, in fact, responsible for the periodic motion within the system. This behaviour is of particular interest for uncovering experimentally realisable time crystals since, in all practical settings, the quantum systems we investigate are subject to some level of external noise from an environment that we cannot eliminate completely.

We also note that this definition is presented with experimental application in mind. We envisage a setup where the system can be initialised in a random pure state that can be reliably created repeatedly to measure ensemble averages of the relevant observables over different histories of interactions with the environment. As an example, this is achievable in ultracold atom setups by using a speckle pattern of pseudo-random on-site fields for each run of the experiment [302]. It is also crucial that the resulting oscillations be clearly measurable on experimental time scales. We will see that this condition is easily satisfied when the system is engineered to have a non-trivial, i.e. extensive, strong dynamical symmetry.

## 2.2 Spectral requirements

As we have done throughout this thesis, we will assume that the dynamics of the system may be well described by the Lindblad equation,

$$\frac{d}{dt}\rho(t) = -i[H, \rho] + \sum_{\mu} 2L_{\mu}\rho L_{\mu}^{\dagger} - \{L_{\mu}^{\dagger}L_{\mu}, \rho\}. \quad (4.7)$$

Following our discussions in Ch 3, in order to observe persistent oscillations, the Liouvillian must contain purely imaginary eigenvalues,  $i\omega_k$ . However, in order for the resulting non-stationary dynamics to be periodic, these purely imaginary eigenvalues must be commensurable, that is

$$\frac{\omega_k}{\omega_l} \in \mathbb{Q}, \quad \text{for all } k, l. \quad (4.8)$$

We remark that the existence of commensurable purely imaginary eigenvalues is highly non-trivial for general quantum Liouvillians that describe strongly interacting many-body systems.

Further, the transient time which we must wait before such time crystalline behaviour is visible is determined by the Liouvillian gap,  $R$ , defined as

$$R = \min\{\|\operatorname{Re}(\lambda_k)\| : \operatorname{Re}(\lambda_k) < 0\}. \quad (4.9)$$

This value characterises the time scales of the slowest decaying parts of the system and is well defined, provided the system in question is strictly finite. Determining when the Liouvillian gap closes, in general, is an open question, although since we always consider finitely sized systems, this is not an issue for us. We will make some brief remarks in the next subsection regarding the thermodynamic limit and the connection between our work and *boundary time crystals*.

### Strong dynamical symmetries and dark states

In Ch 3 we proved that eigenstates with purely imaginary eigenvalues are completely characterised by so-called ‘ $A$ -operators’ or, in the case of unital maps, as strong dynamical symmetries. A subclass of these purely imaginary eigenstates that will be relevant in our later examples are *dark state coherences*. Dark states [118, 303] are defined as eigenstates of the Hamiltonian which are annihilated by all the Lindblad operators,

$$H|\psi_n\rangle = E_n|\psi_n\rangle, \quad L_{\mu}|\psi_n\rangle = L_{\mu}^{\dagger}|\psi_n\rangle = 0, \quad \forall \mu, \quad (4.10)$$

and are thus invisible to the dissipation. They span the decoherence free subspace of  $\mathcal{H}$  which is completely unaffected by the external noise. We then see that dark state coherences,

$$\rho_{n,m} = |\psi_n\rangle\langle\psi_m|, \quad (4.11)$$

are trivially Liouvillian eigenstates with purely imaginary eigenvalues  $\lambda_{n,m} = -i(E_n - E_m)$ . Notice that they can either be cast in  $A$ -operator form as

$$\begin{aligned}\rho_{n,m} &= A_{n,m}\rho_\infty, \quad \rho_\infty = |\psi_m\rangle\langle\psi_m|, \\ A &= \mathbb{1} + |\psi_n\rangle\langle\psi_m| + |\psi_m\rangle\langle\psi_n| - |\psi_m\rangle\langle\psi_m| - |\psi_n\rangle\langle\psi_n|,\end{aligned}\tag{4.12}$$

where  $A$  is unitary and satisfies the conditions of Eq. (3.8) & (3.9) by construction, or be interpreted as strong dynamical symmetries with

$$\rho_{n,m} = A\rho_\infty, \quad \rho_\infty = |\psi_m\rangle\langle\psi_m|, \quad A = |\psi_n\rangle\langle\psi_m|,\tag{4.13}$$

where  $[H, A] = (E_n - E_m)$  and  $[L_\mu, A] = [L_\mu^\dagger, A] = 0$ .

There is generally no way to determine the eigenvalues associated with dark state coherences in many-body systems when diagonalisation methods become impossible. Further, it is rarely the case that the resulting Liouvillian eigenvalues are commensurable, as we will show in our second example of the next section. Even when the eigenvalues can be engineered to be commensurable, it is very unlikely this commensurability will be stable to perturbations. This means that when engineering dissipative time crystals, dark states should be avoided.

Instead, we should focus our attention on strong dynamical symmetries. We know that if a strong dynamical symmetry exists, then this generates a series of purely imaginary Liouvillian eigenvalues at integer multiples of the base ‘symmetry frequency’. As we will show in our third example of the next section, this is ideal for dissipative time crystals as it can guarantee commensurability and hence period motion. We can also use our perturbative results from Ch 3 to understand the stability of this periodicity. However, we should note that if there exist multiple strong dynamical symmetries with distinct frequencies, then we find ‘strings’ of imaginary eigenvalues,  $\lambda_{n,m}^j = i(n - m)\omega_j$ , which are integer multiples of the different  $\omega_j$ . If these  $\omega_j$  are not commensurable, then again, the time crystalline behaviour will be precluded.

### 2.3 Relation to boundary time crystals

It is important to briefly highlight a related phenomenon referred to as a *boundary time crystal*. First presented in [304], these are defined as systems where time translational symmetry breaking occurs only in the thermodynamic limit and only in an infinitesimal fraction of the system. More specifically they consider a closed composite system  $\mathcal{H} = \mathcal{H}_B \otimes \mathcal{H}_b$  where  $\mathcal{H}_B$  represents the bulk while  $\mathcal{H}_b$  represents the boundary, and then consider a Hamiltonian

$$H = H_B + H_b + V,\tag{4.14}$$

where  $V$  is the interaction between the bulk and the boundary. Importantly the time translational symmetry breaking is only studied in the reduced density operator for the boundary,  $\rho_b = \text{Tr}_B(|\psi(t)\rangle\langle\psi(t)|)$ , and occurs only in the thermodynamic limit where

$$N_b, N_B \rightarrow \infty, \quad \frac{N_b}{N_B} \rightarrow 0, \quad (4.15)$$

where  $N_\alpha = \dim(\mathcal{H}_\alpha)$ . In this way, they attempt to be as close as possible to the original definition of time crystals as a thermodynamic phenomenon. However, the systems usually studied are many-body collective models that would exhibit Rabi oscillations if the dissipation were removed and can thus be described as effectively single-body systems with no interactions that exhibit persistent oscillations despite dissipation [305, 306]. Further, in the models they study that do have interactions between sites, these are described by quadratic collective operators, such as  $(S^z)^2 = (\sum_k s_k^z)^2$ , which are ‘all-to-all’ and highly non-local. Such non-local interactions raise questions regarding the physicality of such models. Additionally, since these systems are effectively treated in a mean-field limit, questions should be raised regarding the quantum nature of these phenomena.

In contrast, the example we provide below is a genuinely many-body system with strong, local interactions and no semi-classical limits. Further, it is straightforward to modify a finite-sized dissipative time crystal caused by strong dynamical symmetries, such as the model below, so that the purely imaginary eigenvalues appear only in the thermodynamic limit. By adding an ultra-local term that breaks the strong dynamical symmetries, the purely imaginary eigenvalues for any finite system size acquire a negative real part, and thus the system eventually decays. However, as a consequence of the Lieb-Robinson theorem [307] which requires a finite velocity of propagation, the effect of the ultra-local term becomes irrelevant in the bulk of the thermodynamically large system. Therefore, only the thermodynamically large system has purely imaginary eigenvalues.

More work is clearly required to understand better the link between dissipative time crystals, which we study exclusively in finite systems, and boundary time crystals that are manifestly thermodynamic phenomena. It is conceivable that this work could require reformulating dissipative time crystals using  $C^*$ -algebras so that they can be well defined and studied adequately in the thermodynamic limit. However, challenges will likely arise from the appearance of ‘unwanted’ purely imaginary eigenvalues as the Liouvillian gap closes, which will generically break the periodic nature of oscillations.

### 3 Dissipative time crystals in a heated Hubbard model

We now demonstrate the emergence of dissipative time crystals from the 1D Hubbard model by coupling it to an environment with two body loss and gain processes. The Hubbard model is the paradigmatic approximation of lattice electrons with short-range repulsions. These models are naturally realisable in cold atom settings [224]. We find that, due to the exponentially large number of eigenfrequencies, we can illustrate the basic principles while looking at only very small systems. After first outlining our methods and studying the evolution of the closed system, we will progressively add more dissipation to demonstrate pedagogically the spectral requirements discussed above. We will then introduce perturbations and study the stability of the dissipative time crystal phase.

#### 3.1 Measures of time crystalinity

To recap our setup, recall that we define a dissipative time crystal as a system that exhibits periodic motion in some observable at late times for generic initial conditions. Thus, in our simulations, we will initialise the system in some random pure state and then calculate the evolution of the expectation values of two observables. This setup could, in principle, be realised in ultra-cold atoms by fixing once a choice of some very strong pseudo-random on-site fields, in addition to those already present in the model being studied, and then cooling the system so that it is at least very nearly in the ground state. This pure ground state becomes our random initial state when we remove the additional fields and quench the system. Further, when considering a system coupled weakly to the environment, by using the same choice of pseudo-random on-site fields, we can repeatedly construct the same initial state in order to experimentally obtain ensemble averages.

We will measure the transverse fermion spin on each site and the Loschmidt echo of the initial state to witness non-stationarity. Our definition requires that at least one of these probes must oscillate persistently at late times with clearly observable periodicity.

**Loschmidt echo.** The Loschmidt echo, or return probability, is defined as

$$\mathcal{E}_I(t) = \text{Tr}(\rho(0)^\dagger \rho(t)), \quad (4.16)$$

and has seen widespread previous use in many fields such as quantum chaos [308] and more recently dynamical phase transitions [309]. It can be interpreted as the probability that the system returns to its initial state, and for a pure initial

state, it is exactly the fidelity between the state at time  $t$  and the initial state. Its periodicity is an incredibly stringent probe of time crystal-like behaviour in a setup such as ours since its evolutions will generally contain contributions from all the eigenvalues of  $\mathcal{L}$ . Since there are often many eigenvalues even in small many-body systems, the Poincare recurrence time, and thus the period of the Loschmidt echo, can be effectively infinite for experimental purposes. Unfortunately, however, the Loschmidt echo becomes impractical for studying larger systems since the amplitude of its late time oscillations is inversely related to the dimension of  $\mathcal{H}$  and thus decays exponentially with system size. It can also be less practical to measure experimentally, especially if the initial state is not precisely known. Nonetheless, for our purposes in the following examples, it perfectly demonstrates our previous discussions about the spectral requirements for dissipative time crystals.

**Transverse spin.** The model we consider will have a spin direction determined by a uniform magnetic field along the  $z$ -axis. Therefore, we will refer to the spin components in the  $x$  and  $y$  directions as the transverse spin. Since the models will all conserve both total spin,  $\mathbf{S}^2$ , and spin along the  $z$  axis,  $S^z$ , separately, we see that the total transverse spin,  $\mathbf{S}_\perp^2 = (S^x)^2 + (S^y)^2$ , is also trivially conserved. Further, since the dissipative time crystal phase will, in our case, be translationally invariant, we can conclude that the magnitude of any oscillations in the transverse spin will be proportional to the initial transverse spin but inversely proportional to the size of the system. However, for larger systems, we could envisage measuring the transverse spin over some finite fraction of the total system so that the oscillation is easier to observe.

In order to detect oscillatory behaviour in these observables, we will use the natural tool of discrete Fourier transforms (DFT), denoted  $F[f(t)]$ . Importantly, we will only calculate the DFT at late times after transient contributions have vanished. Additionally, we use Blackman windowing to reduce the effects of spectral leakage from calculating the DFT from a finite sample [310] and use a logarithmic  $y$  scale for all spectra, as is standard practice.

### 3.2 Closed Hubbard model

We begin by introducing the Hubbard model and demonstrating that the dissipative time crystal behaviour is not a trivial consequence of the dynamical properties of the closed system. For a system of spin-1/2 fermions with  $L$  lattice sites in 1D, the system is described by the Hamiltonian

$$H = - \sum_{i=1}^{L-1} \sum_{s \in \{\uparrow, \downarrow\}} (c_{i,s}^\dagger c_{i+1,s} + \text{h.c.}) + \sum_{j=1}^L U_j n_{j,\uparrow} n_{j,\downarrow} + \epsilon_j n_j + B s_j^z \quad (4.17)$$

where  $c_{j,s}$  annihilates a fermion of spin  $s$  on site  $j$  and obeys the canonical fermionic anti-commutation relations. The on-site number operators are given by

$$n_{j,s} = c_{j,s}^\dagger c_{j,s}, \quad n_j = n_{j,\uparrow} + n_{j,\downarrow}, \quad (4.18)$$

and the on-site spin operators are given by

$$s_j^z = \frac{1}{2} (n_{j,\uparrow} - n_{j,\downarrow}), \quad s_j^+ = c_{j,\uparrow}^\dagger c_{j,\downarrow}, \quad s_j^- = c_{j,\downarrow}^\dagger c_{j,\uparrow}. \quad (4.19)$$

We have included nearest neighbour hopping with unit strength, inhomogeneous onsite interactions  $U_j$ , an inhomogeneous spin independent potential  $\epsilon_j$  and a uniform magnetic field  $B$  aligned with the  $z$ -direction of the fermion spins. The inhomogeneities demonstrate the stability of the dissipative time crystal phase to almost any onsite interaction and potential. In all our numerics we chose the  $U_j, \epsilon_j \in [0, 3]$  to be a fixed realisation of independent, identically distributed (i.i.d) uniform random variables. The inhomogeneous interaction and potential break the usual  $SU(2)$   $\eta$ -symmetry of the system [311] so that we are left with only the spin  $SU(2)$  symmetry,

$$[H, S^z] = 0, \quad [H, S^\pm] = \pm B S^\pm, \quad (4.20)$$

where

$$S^z = \sum_j s_j^z, \quad S^+ = \sum_j s_j^+, \quad S^- = \sum_j s_j^-. \quad (4.21)$$

The transverse fermion spin is then given by,

$$s_j^x = \frac{1}{2} (c_{j,\uparrow}^\dagger c_{j,\downarrow} + c_{j,\downarrow}^\dagger c_{j,\uparrow}). \quad (4.22)$$

While the spectrum of  $H$  and hence  $\mathcal{L} = -i[H, \bullet]$  can be found analytically for constant  $U_j, \epsilon_j$  by solving the Bethe equations [311], here we must instead use numerical calculations. We plot the spectrum of  $\mathcal{L}$  in Figure 4.1 for a 3 site system. This system size is chosen so that the spectra may be directly compared across the different examples, and in the open cases, any larger systems are computationally too expensive<sup>3</sup>. However, the spectra of larger systems are expected to be qualitatively the same. Importantly for the discussion of periodicity, we find that the purely imaginary eigenvalues are *effectively* incommensurable. By this, we mean that while the numerically calculated eigenvalues are commensurable, as a result of finite precision computation, the time period over which any oscillations would occur is far longer than any reasonable time scale of an experiment. The immediate consequence is that unless we carefully choose our initial state and observable such that the dynamics contain only a commensurable subset of frequencies, the signal will never be periodic on experimental timescales. In general, without such specific choices, the

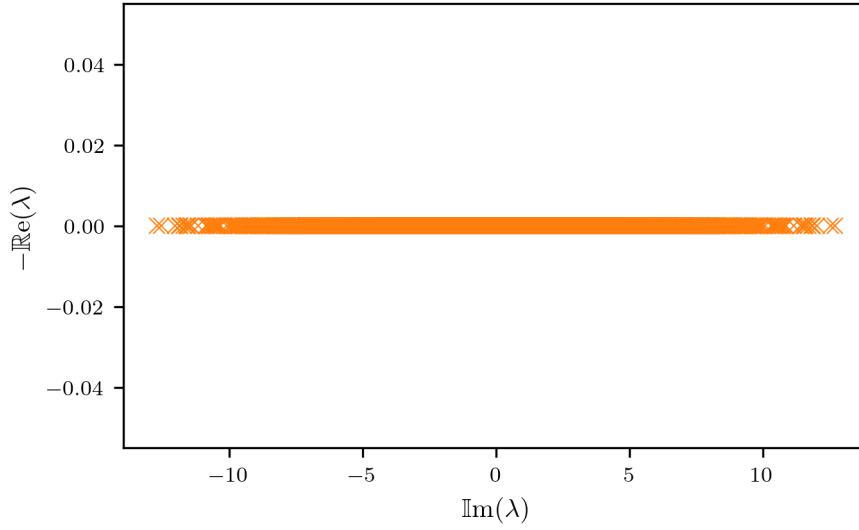


**Figure 4.1:** The spectrum of a 3 site closed system, characteristic of larger systems. Note that we plot the imaginary part on the horizontal axis. All eigenvalues are purely imaginary eigenvalues have plotted in orange to match later plots for open systems.

many incommensurate frequencies will interfere, producing either noise in smaller systems or decay to stationarity by eigenstate dephasing [312] in larger ones.

We can see the manifestation of this by looking at plots of the transverse spin and Loschmidt echo in Figure 4.2 where a four-site system has been evolved from one instance of a random initial state  $|\phi\rangle \propto \sum_n u_n |\phi_n\rangle$ . The  $u_n$  are i.i.d uniform random numbers on  $[0, 1]$  and  $|\phi_n\rangle$  are the eigenstates of  $H$ . The calculations were repeated for many different random initial states to check that indeed the resulting behaviour is generic and not a consequence of some particular initial conditions. For both probes, the signal is very noisy and far from periodic. The noise is suppressed slightly in the transverse spin signal since some eigenstates have no overlap with  $s_k^x$ , thus removing the corresponding frequencies. In addition, these observations are corroborated by the DFT spectra for the signal from both probes, which are roughly flat for the majority of the frequencies, characteristic of noise [313].

We can thus conclude that in the absence of interactions with an environment, the 1D Hubbard model does not display periodic behaviour for generic initial conditions on experimental timescales, even for very small systems. This can be understood by eigenstate dephasing and demonstrates that the dissipative time crystal behaviour we find in the open models is not a trivial consequence of the closed system's dynamics.

<sup>3</sup>The Liouvillian for the 3-site open system has rank 4096, while for a 4-site system is has rank 65536.



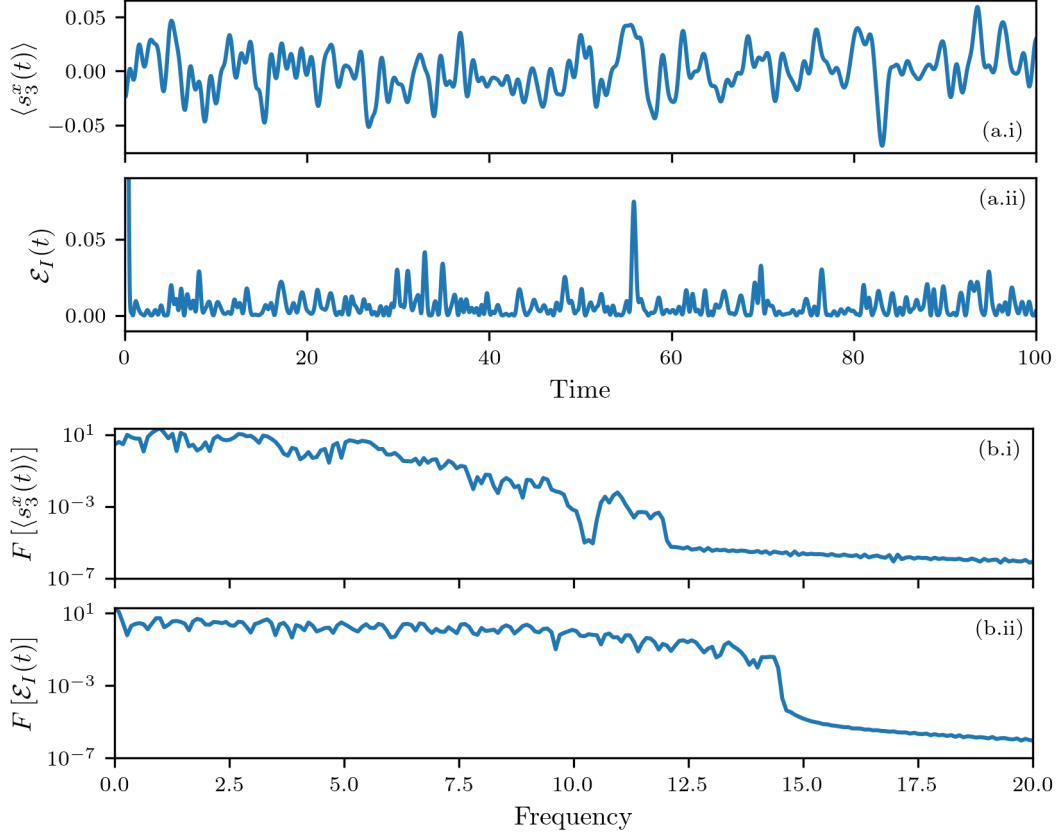


**Figure 4.2:** The evolution (a) and DFT (b) of the transverse spin on the third site and Loschmidt echo respectively for a 4 site closed system which is initialised in a random pure state.

### 3.3 Two-body loss

The first dissipative case we consider is when the system leaks eta-pairs, each composed of a spin-up and a spin-down fermion, to the environment from every site at a possibly inhomogeneous but strictly positive rate,  $\gamma_j > 0$ . This is described by introducing the set of jump operators  $L_j = \sqrt{\gamma_j} c_{j,\downarrow} c_{j,\uparrow}$  while keeping the same Hamiltonian as in Eq. (4.17).

In this system, we find numerically that the only purely imaginary eigenvalues correspond to coherences between dark states, which are left unaffected by the loss. These dark states have no overlap with any eta pairs. We expect that one could prove the non-existence of other purely imaginary eigenvalues as a consequence of Sup. Thm. 2 of [119]. There exists a strong dynamical symmetry, generated by  $S^+$  with  $[H, S^\pm] = \pm BS^\pm$ . However, we do not find any mixed coherences here as all NESSs are pure dark states, and so the states of the form  $(S^+)^n \rho_\infty (S^-)^m$  are coherences between dark states. All states with purely imaginary eigenvalues

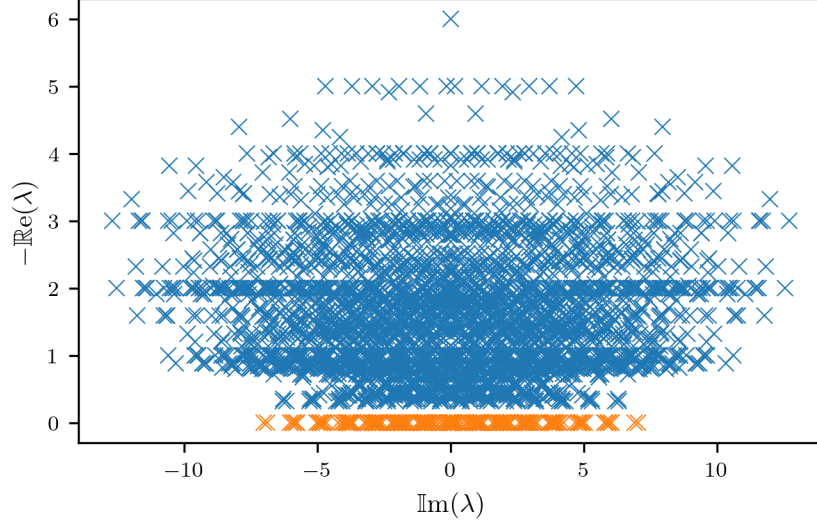


**Figure 4.3:** The spectrum of a 3 site system with pure loss, characteristic of larger systems which are computationally out of reach. Note that we plot the imaginary part on the horizontal axis. The purely imaginary eigenvalues have been highlighted.

are independent of the  $\gamma_j$ , so the only relevance of these coupling strengths for our discussion is to determine the time period of the transient dynamics.

In Figure 4.3 we plot the spectrum for a three-site system, but again this is expected to be representative of larger systems. Compared with the spectrum of the closed system, we see that there are significantly fewer imaginary eigenvalues. Again, however, we find that the remaining imaginary eigenvalues are effectively incommensurate.

We examine the time dynamics of our two stationarity probes in Figure 4.4 for a four-site system in a random initial state. Starting with the echo, we see that the signal is extremely noisy, an observation which is corroborated by the DFT being roughly flat for much of the spectrum.

Looking next at the transverse spin, we see that, while not periodic, the signal is noticeably less noisy than for the closed system. As before, this is a result of many coherences between dark states not having any overlap with  $s_k^x$  and thus the series expansion of the long time dynamics having significantly fewer terms. This is clear from the DFT spectrum, where we can now see the emergence of roughly 8-10 pronounced peaks at effectively incommensurable frequencies. While this is not strictly time crystalline behaviour, it can reasonably be called quasi-time crystalline behaviour, in analogy to quasi-periodicity created by a small number of incommensurable frequencies [299, 300].

By exploring this example, we have demonstrated that in the presence of only two body losses, our 1D Hubbard model does not exhibit experimentally observable

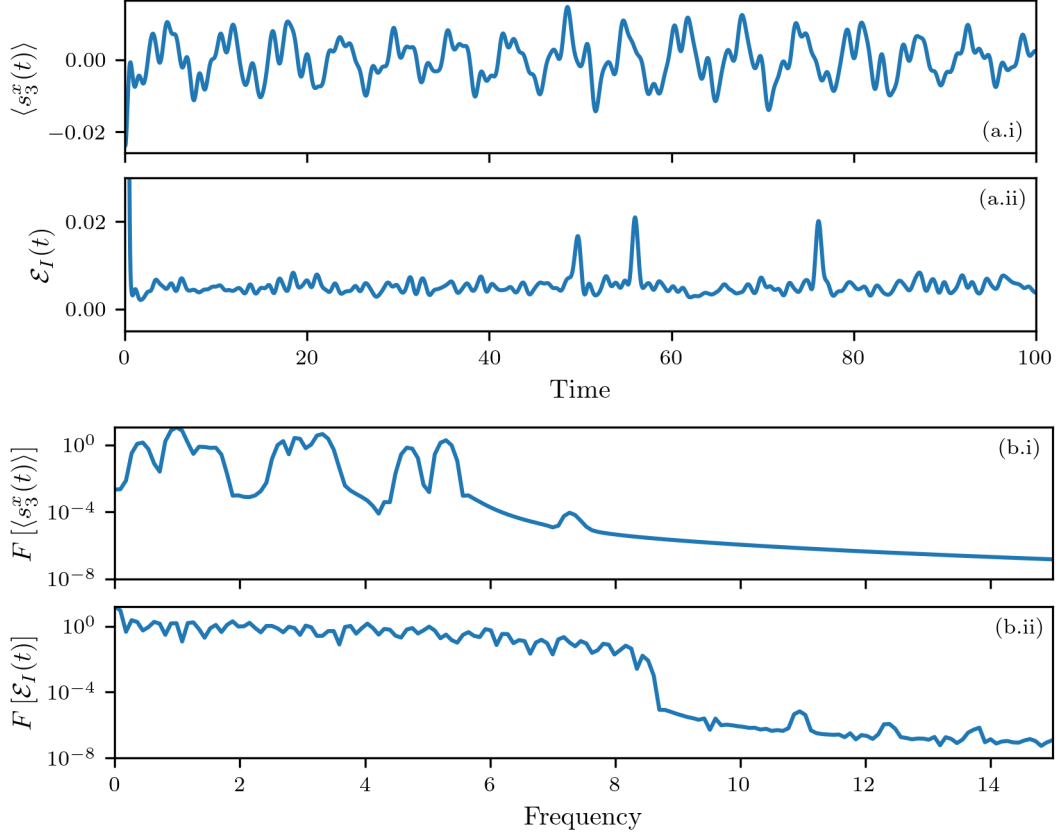


**Figure 4.4:** The evolution (a) and DFT (b) of the transverse spin on the third site and Loschmidt echo respectively for a 4 site system with pure loss which is initialised in a random pure state.

dissipative time crystalline behaviour owing again to the effectively incommensurable eigenfrequencies. This shows how the existence of a strong dynamical symmetry is not sufficient for such behaviour as this does not guarantee commensurable purely imaginary eigenvalues. We have, however, found evidence of quasi-time crystalline behaviour, at least with respect to the transverse spin,  $s_k^x$ . This weaker condition requires only that there are few frequencies present in the evolution, not that they are commensurable. We do not explore quasi-time crystal behaviour any further here; however, we envisage this to be an exciting area for further study.

### 3.4 Two-body loss and gain

To finally uncover truly dissipative time crystalline behaviour, we now additionally introduce two body gain terms into the Liouvillian as

$$L_j = \sqrt{\Gamma_j} c_{j,\uparrow}^\dagger c_{j,\downarrow}^\dagger, \quad (4.23)$$

again for  $\Gamma_j > 0$ . This now represents a system where eta-pairs are both gained and lost on each site at various rates. Importantly these additional jump operators do not break the strong dynamical  $S^+$  symmetry.

In the case that  $\Gamma_i = \gamma_i$  for each  $i$ , the Liouvillian is unital and we can apply Thm 2 to deduce that all purely imaginary eigenstates can be written in the form

$$\rho_{n,m} = (S^+)^n \rho_\infty (S^-)^m. \quad (4.24)$$

Further, when  $\Gamma_i \neq \gamma_i$  it was found numerically that a full rank stationary state still persists, and hence the purely imaginary eigenstates continue to all be of the above form.

Although the persistence of a full rank stationary state has not been proven, it can be shown that all dark state coherences are of the form in Eq. (4.24). In fact we argue that all dark states are of the form

$$|\phi_n\rangle = (S^+)^n |\downarrow \dots \downarrow\rangle. \quad (4.25)$$

To see this, note that a dark state,  $|\phi_n\rangle$ , must be annihilated by all  $L_\mu$ , and hence can only contain contributions from states where every site is singly occupied. Since  $|\phi_n\rangle$  is also an energy eigenstate,  $H|\phi_n\rangle$  cannot contain contributions from empty or doubly occupied sites. Now note that the hopping term,

$$H_{\text{Hop}} = - \sum_{x,s} \left( c_{x,s}^\dagger c_{x+1,s} + \text{c.c.} \right), \quad (4.26)$$

creates a doublon whenever there are two adjacent electrons with opposite spin. In order to cancel this,  $|\phi_n\rangle$  must contain a contribution from an otherwise identical state with these two electrons swapped. Applying this to all possible up-down pairings, we see that the only possibility is for  $|\phi_n\rangle$  to be a uniform superposition of all the states with  $n$  up spins and  $L - n$  down spins. It is easy to see that this can be written as  $|\phi_n\rangle = (S^+)^n |\downarrow \dots \downarrow\rangle$ .

As a consequence of the strong dynamical  $S^+$  symmetry generating all the purely imaginary eigenvalues, they are all integer multiples of  $B$  and thus are commensurable. We show this in Figure 4.5. This is an example of the eigenvalue structure that we require for time crystalline behaviour.

Indeed when we now look at the evolution of our probes (Figure 4.6), we see that both the transverse spin and Loschmidt echo rapidly decay into persistent oscillations. For the echo, the DTF spectrum shows that all purely imaginary eigenvalues are present, whereas, for the transverse spin, only the eigenstates with imaginary eigenvalue  $\pm iB$  contribute.

Here we have found the emergence of a dissipative time crystal. Critically the purely imaginary eigenvalues have the necessary structure of commensurability

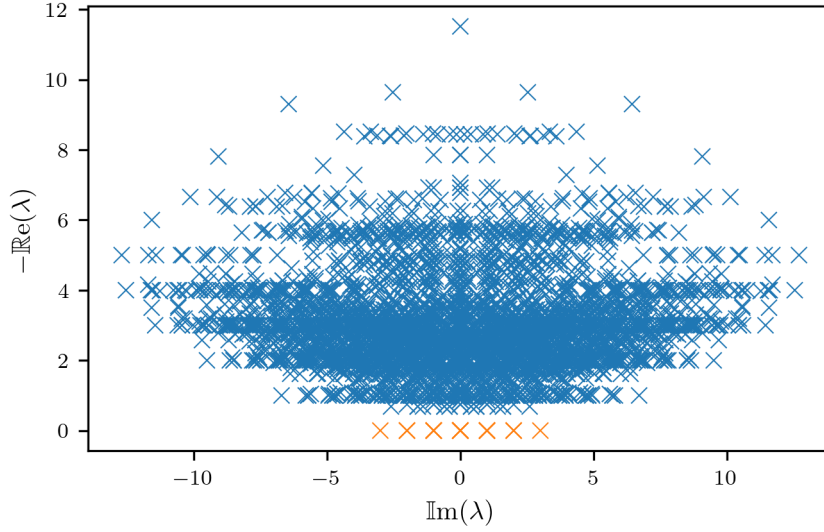


**Figure 4.5:** The spectrum of a 3 site system with two body loss and gain, characteristic of larger systems which are computationally out of reach. Note that we plot the imaginary part on the horizontal axis. The purely imaginary eigenvalues have been highlighted.

that is required for periodic behaviour. We have further seen that this structure has been provided by the strong dynamical symmetry generating *all* non-decaying eigenstates. Significantly from an experimental point of view, we have seen that this model's dissipative time crystal phase is stable to any values of the on-site repulsion and potential and the strengths of the two-body loss and gain as these do not disturb the strong dynamical symmetry.

We also note that, counterintuitively, as we can see in Figure 4.7, each individual quantum trajectory [84] for the same initial state, obtained through the stochastic unravelling of the master equations, is different, even at very late times after transient behaviour has vanished. This essentially embodies the stochastic nature of the quantum bath that acts on the system (cf. with [169]). This may also be understood as a non-stationary quantum stochastic process [314].

### 3.5 Perturbations

We now introduce a perturbation to our dissipative time crystal to illustrate how the previous results of Thm 5 and Prop 2 can be used to understand its stability. We will, in this case, set the on-site interaction, potentials, and dissipation to be uniform, and modify the magnetic term to

$$H_B = \sum_k (B + \delta_k) s_k^z. \quad (4.27)$$

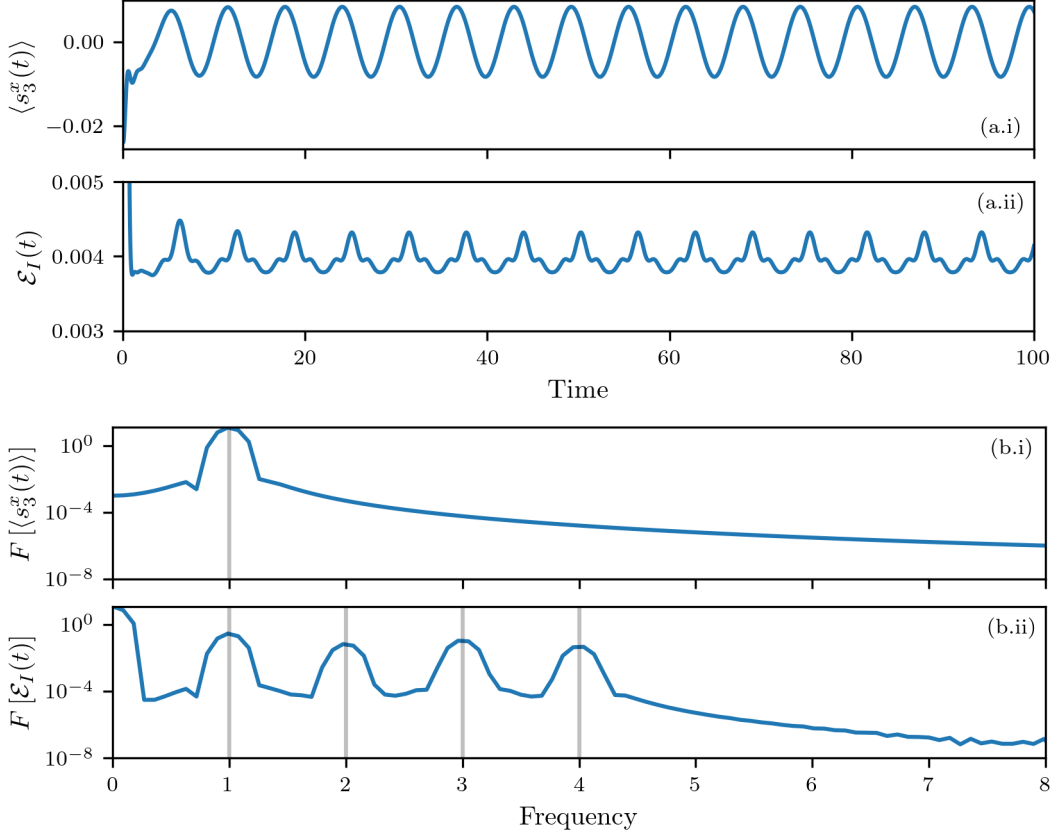


**Figure 4.6:** The evolution (a) and DFT (b) of the transverse spin on the third site and Loschmidt echo respectively for a 4 site system loss and gain which is initialised in a random pure state. We highlight the non-zero imaginary eigenvalues by dashed vertical lines on the spectra.

We define

$$\Delta = \sqrt{\sum_k \delta_k^2}, \quad (4.28)$$

as the magnitude of the perturbation. For  $\delta_k$  not all equal, this breaks the strong dynamical  $S^+$  symmetry in addition to the structure of the dark states. As a result, the two remaining dark states are the all-spin-up and all-spin-down states. Further, we find that coherences between these two states are the only eigenstates of  $\mathcal{L}$  with non-zero, purely imaginary eigenvalues, given by  $\pm i(LB + \sum_k \delta_k)$ . At late times the system therefore can only oscillate at a single frequency. In Figure 4.8 we also see that there are several eigenvalues with very small real parts, corresponding to states which would have purely imaginary eigenvalues if the disorder in  $B_j$  were removed, resulting in a very small Liouvillian gap.

The consequence of the very small Liouvillian gap is immediately seen in the signals of our two probes. It is easy to see that the coherences between all-spin-up and all-spin-down states have no overlap with  $s_k^x$  for any  $k$  and so after the

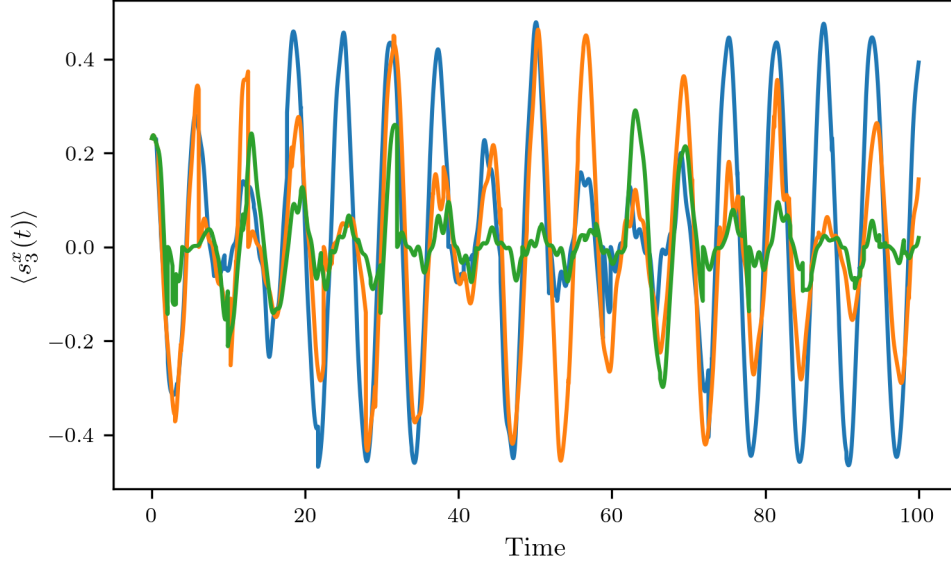


**Figure 4.7:** Three quantum trajectories of the same initial pure state for the system in Sec 3.4 with both two-body loss and gain. We plot the transverse spin on the third site over time to demonstrate that, counterintuitively, each individual quantum trajectory for the same initial state is different.

transient period, we have  $s_k^x = \text{const.}$  Thus comparing Figure 4.9 with the previous systems we find that here it takes at least an order of magnitude longer for the transient behaviour to die away. We observe the same behaviour in the echo, and the inset demonstrates that at sufficiently late times, once the transient modes have become almost insignificant, the system reaches persistent oscillations at the single frequency we expect.

After the transient period, the dynamics of the system on top of the steady states is described by the effective, non-local Hamiltonian,

$$H_{\text{eff}} = \frac{\mathcal{B}}{2} \left( |\uparrow \dots \uparrow\rangle \langle \uparrow \dots \uparrow| - |\downarrow \dots \downarrow\rangle \langle \downarrow \dots \downarrow| \right), \quad (4.29)$$

where  $\mathcal{B} = LB + \sum_k \delta_k$ . This drives coherent oscillations between two GHZ states,

$$|\text{GHZ}\rangle_{\pm} = \frac{|\uparrow \dots \uparrow\rangle \pm |\downarrow \dots \downarrow\rangle}{\sqrt{2}}. \quad (4.30)$$

Note that here we have engineered an effective non-local dark Hamiltonian [119] through a local and physical Hamiltonian in the presence of noisy dissipation, rather than assuming a closed non-local Hamiltonian with unclear stability properties [298, 315, 316]. However, the amplitude of the resulting dynamics depends on the overlap between the initial states and the GHZ states, which for arbitrary initial states will generically decrease exponentially with system size.

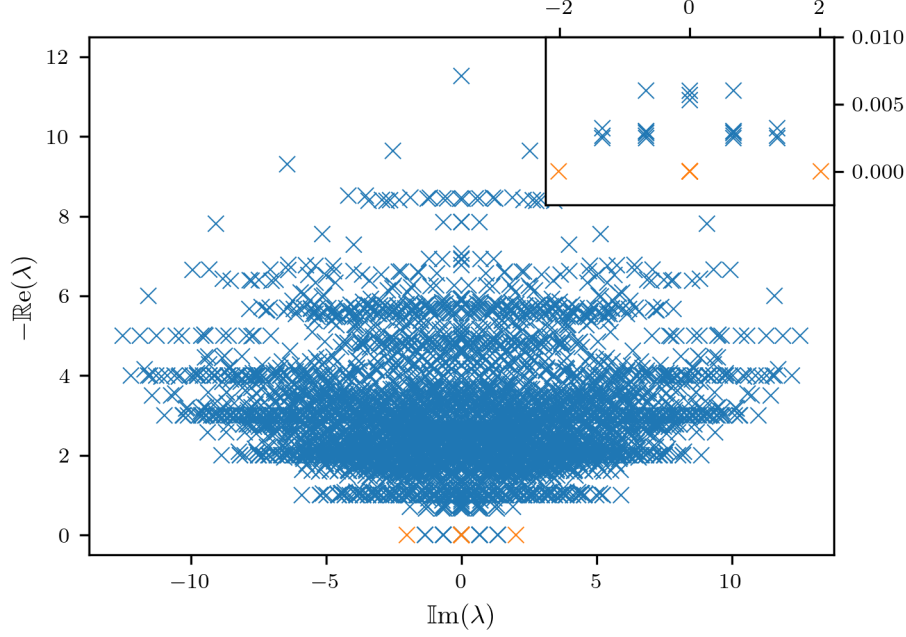


**Figure 4.8:** The spectrum of a three-site system with two body loss and gain but an inhomogeneous magnetic field, characteristic of larger systems that are computationally out of reach. Note that we plot the imaginary part on the horizontal axis. The purely imaginary eigenvalues are highlighted, and the inset focuses on those eigenvalues with very small real parts caused by the inhomogeneities of the magnetic field.

We can thus conclude that the system remains a dissipative time crystal with respect to the Loschmidt echo, at least for small systems, but not with respect to the transverse spin. It is therefore instructive to observe how the time crystalline structure with respect to the transverse spin is destroyed by the perturbation, and how this phase can be protected, at least in some sense. To this end, recall from Prop 2 that the oscillation frequency should be stable to second order in  $\Delta$  for perturbations which satisfy a certain symmetry. One class of perturbations that satisfy the conditions of Prop 2 are *detunings*, where for fixed  $i$  and  $j$  we have

$$\delta_i = -\delta_j \quad (4.31)$$

with all other  $\delta_k = 0$ . These perturbations are anti-symmetric under exchanging sites  $i$  and  $j$  while the purely imaginary eigenmodes of the unperturbed Liouvillian are unaffected by such an exchange, and hence detunings satisfy the conditions of Prop 2. This behaviour is demonstrated in Fig. 4.10 where a three site system is



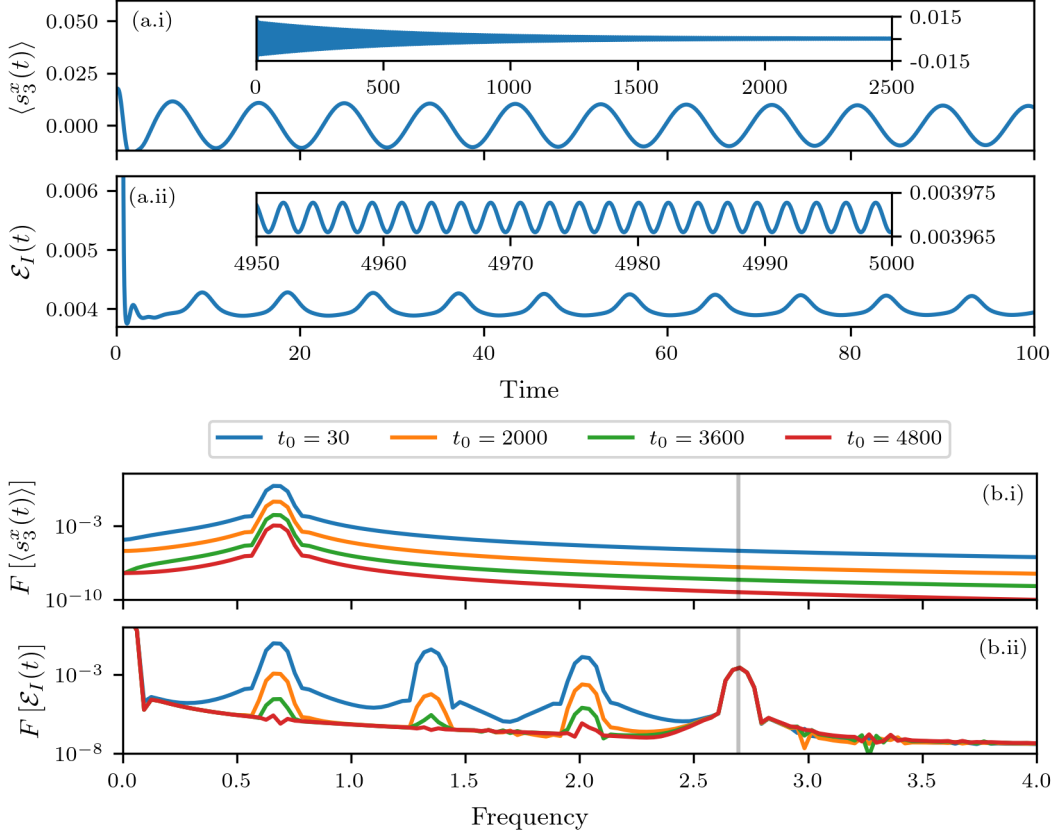


**Figure 4.9:** The evolution (a) and DFT (b) of the transverse spin on the third site and Loschmidt echo respectively for a four-site system loss, gain and an inhomogeneous magnetic field which is initialised in a random pure state. We highlight the non-zero imaginary eigenvalue,  $\mathcal{B}$ , by dashed vertical lines on the spectra. The inset in (a.i) shows the long time decay of the spin observable, while the inset in (a.ii) shows that the Loschmidt echo oscillates periodically with a fixed frequency at extremely late times. The DFT spectra are calculated over the periods  $t_0 \leq t \leq t_0 + 200$  with  $t_0$  indicated in the legend. We see the decay of all frequencies except  $\mathcal{B}$ .

studied with two separate perturbations which as an example we take as

$$\boldsymbol{\delta}^{(1)} = \Delta \left( \frac{1}{\sqrt{2}}, -\frac{1}{\sqrt{2}}, 0 \right) \quad (4.32a)$$

$$\boldsymbol{\delta}^{(2)} = \Delta \left( \frac{\sqrt{30}}{18}, \frac{7\sqrt{30}}{90}, -\frac{7\sqrt{30}}{45} \right). \quad (4.32b)$$

Note that for each of these perturbations  $\sum \delta_k = 0$  so they do not introduce a trivial shift in the mean magnetic field strength. In each case, the system evolves, and the second site's transverse spin is measured. We then extract the dominant oscillation frequency and decay rate of the slowly decaying dynamics. We see, in agreement with Prop 2, that under perturbation  $\boldsymbol{\delta}^{(1)}$  the frequencies barely change with  $\Delta$  while under  $\boldsymbol{\delta}^{(2)}$  they vary linearly. We also observe that

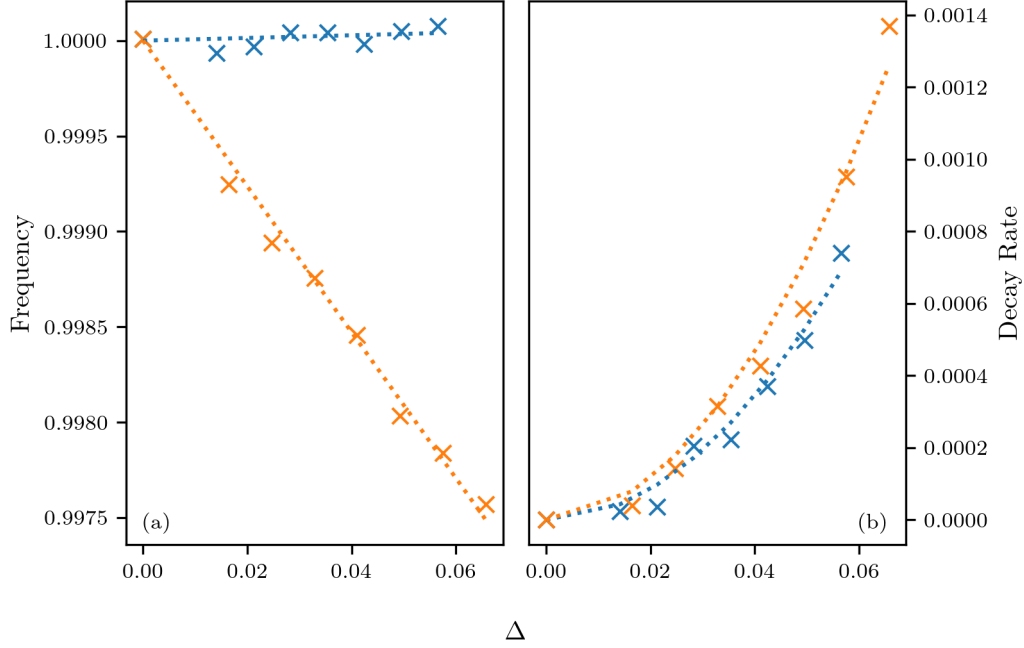


**Figure 4.10:** The crosses show the dominant oscillation frequency (a) and decay rate (b) of the slowly decaying dynamics for a system with inhomogeneous magnetic fields described by Eq. (4.32a) (blue) and Eq. (4.32b) (orange). The dashed lines indicate the linear and quadratic scaling expected from Thm 5. Since the perturbation  $\delta^{(1)}$  is anti-symmetric under exchanging sites 1 and 2, we see that by Prop 2 the frequency does not change at first order. Note that the discrepancy between the scaling and the data is a result of numerical analysis of simulated evolutions being used instead of exact diagonalisation (which is unfeasible computationally).

the decay rates vary in similar ways under both perturbations. From Sec 3.4 we know that for the transverse spin in the unperturbed case, there is only one frequency,  $\omega = \pm B$ , present at late times, and so varying this frequency does not affect the periodicity of the dynamics. However, if several commensurate frequencies were present in the unperturbed system, perturbing them linearly with  $\Delta$  would generically break this commensurability and thus periodicity. Therefore perturbations that do not affect the oscillation frequencies at first order will allow the time crystal behaviour to survive for longer. This emphasises the importance of Prop 2 for protecting dissipative time crystals.

### 3.6 Discussion

These examples demonstrate how dissipative time crystal behaviour can be induced in a finite-sized system, starting from the 1D Hubbard model through noisy contact with an external environment. They also show how purely imaginary eigenvalues

of  $\mathcal{L}$  alone are not sufficient for such behaviour to emerge. Instead, we see that these eigenvalues must at least be commensurable.

Commensurability alone is not a sufficient spectral structure in general. For a robust dissipative time crystal in a practical setting, we desire persistent oscillations that are *clearly* measurable. We discussed in Sec 3.2 that as a result of finite precision, all frequencies in both numerical calculations and experimental measurements will be commensurable. However, we may find that the corresponding time periods are significantly longer than any experimental time scales, so the motion is effectively aperiodic. We thus introduce the notion of *effective* incommensurability as commensurable frequencies with a resultant time period longer than the experimental time scale. Another way that commensurable frequencies can become effectively incommensurable is if they are too dense with respect to the inverse of the experimental timescale since the time period can grow exponentially in the number of frequencies. In such a case, the spectral peaks of the signal's DFT could also become merged and indistinguishable, rendering the commensurability of the frequencies and hence the presence of persistent periodic motion possibly undetectable. While the examples studied numerically here do not exhibit such behaviour, since quantum many-body systems have exponentially many eigenvalues, it is in principle feasible for this to occur and thus should be considered in future works.

The condition of nowhere-dense, commensurable, purely imaginary eigenvalues, which are not effectively incommensurable, is in general highly non-trivial for Liouvillians of many-body systems. Nevertheless, it can be guaranteed by the existence of a single strong dynamical symmetry that generates all continuously oscillating modes. Further, we can easily see that the imaginary eigenvalues will not be closely spaced provided the symmetry-frequency is not too small with respect to the inverse of the experimental timescale. This should be avoidable in experiments as the symmetry frequency can generally be tuned by experimental parameters, but it remains an important consideration. Suppose instead there are purely imaginary eigenvalues beyond those guaranteed by the non-trivial strong dynamical symmetry<sup>4</sup>, e.g. coming from dark states. In that case, we see that having a non-trivial strong dynamical symmetry is not sufficient for time crystalline behaviour. This is illustrated by the example having two-body loss in Sec. 3.3. We can further envisage the existence of two distinct strong dynamical symmetries with effectively incommensurate frequencies and easily see that again, such a system would not be periodic for generic initial conditions and observables on experimental timescales. In contrast, the example in Sec. 3.5 with an inhomogeneous magnetic field demonstrates that extensive strong dynamical symmetries are not necessary for dissipative time crystals.

---

<sup>4</sup>By non-trivial we mean that the dynamical symmetry is not a trivial coherence between dark states.

## 4 Dissipative Floquet time crystals in a heated Hubbard model

As we mentioned in Sec 1, a substantial portion of the efforts to study time crystals over the last decade have focused on Floquet time crystals [163, 166, 290]. These are periodically driven systems that exhibit a sub-harmonic response. More specifically, if a closed system is driven with a periodic Hamiltonian,  $H(t)$ , such that

$$H(t) = H(t + T) \quad \forall t, \quad (4.33)$$

then the system is a Floquet, or discrete, time crystal if some observable is periodic with period  $nT$  for  $n \in \{2, 3, \dots\}$ . Originally, this phenomenon is usually studied in closed systems with ‘pulsed’ Hamiltonians,

$$H(t) = \begin{cases} H_1 & 0 \leq t < \tau \\ H_2 & \tau \leq t < T \end{cases} \quad (4.34)$$

where  $\tau \in (0, T)$ . A notable example of such a Floquet time crystal is the  $\pi$ -spin glass model [317] in which the time crystallinity can be understood through many-body localisation (MBL) [318, 319] and has since been observed experimentally [177]. More recent studies have begun to explore Floquet time crystals in dissipative systems [169, 294, 320, 321]. We now give a brief discussion of how the dissipative time crystal model we have studied above can be adapted so that it becomes a Floquet dissipative time crystal.

### 4.1 Periodically driven heated Hubbard model

When studying Floquet time crystals, the central operator of interest is the discrete evolution operator

$$\mathcal{U}_T = \text{Texp} \int_0^T dt \mathcal{L}(t) \quad (4.35)$$

which evolves the system by  $T$  units of time. In general, time ordered exponentials such as this are incredibly difficult to study except in particular cases such as pulsed systems where they simplify considerably. For a Floquet time crystal, it is necessary that there exists stationary states of  $(\mathcal{U}_T)^n$  for  $n > 1$  that are *not* stationary states of  $\mathcal{U}_T$ . Equivalently,  $\mathcal{U}_T$  must have eigenvalues

$$\lambda = \frac{2\pi i}{n}. \quad (4.36)$$

One trivial way in which such eigenvalues can arise, is when there exists a fixed state,  $\rho$ , which is an eigenstate of  $\mathcal{L}(t)$  at every time  $t$  with a purely imaginary eigenvalue

$$\mathcal{L}(t)[\rho] = i\omega(t)\rho. \quad (4.37)$$

In this case,  $\rho$  will also be an eigenstate of  $\mathcal{U}_T$  with eigenvalue

$$\lambda = i \int_0^T \omega(t) dt. \quad (4.38)$$

This situation can be easily engineered in our heated Hubbard model example. For simplicity, take the homogeneous Hamiltonian

$$H(t) = - \sum_{i=1}^{L-1} \sum_{s \in \{\uparrow, \downarrow\}} (c_{i,s}^\dagger c_{i+1,s} + \text{h.c.}) + U \sum_{j=1}^L n_{j,\uparrow} n_{j,\downarrow} + B(t) \sum_{j=1}^L s_j^z, \quad (4.39)$$

with time-independent Lindblad operators

$$L_{j,+} = c_{j,\uparrow}^\dagger c_{j,\downarrow}^\dagger, \quad L_{j,-} = c_{j,\uparrow} c_{j,\downarrow}. \quad (4.40)$$

From our previous discussions we know that the only eigenstates of  $\mathcal{L}(t)$  with purely imaginary eigenvalues are

$$\rho_{n,m} = (S^+)^n (S^-)^m, \quad \omega(t) = (n - m)B(t). \quad (4.41)$$

Thus by tuning the integral of our time varying magnetic field,  $B(t)$ , we can engineer a dissipative Floquet time crystal. This time crystal will also inherit all the stability properties of the example in Sec 3.4, i.e. it will be unaffected by inhomogeneities in the strength of the on-site repulsion, interaction and dissipation. We demonstrate this in Figure 4.11 for several different periodic driving functions which are only restricted by

$$\int_0^T B(t) dt = \frac{2\pi}{n}. \quad (4.42)$$

This model of a Floquet time crystal is particularly novel because, as we see, the exact waveform of the subharmonic response can be dramatically different depending on the driving chosen. Additionally, as with the time-independent case studied above, this phenomena *only* occurs in the presence of the symmetry selective noise we have chosen. This construction is similar to the independent work of [277] but note that here we are not restricted to sinusoidal driving in order to define a rotating frame.

## 4.2 Stability to Gaussian noise

The immediate question to understand is the stability of these time crystals to perturbations. As we mentioned above, this model inherits the stability against spatial inhomogeneities in the strength of the on-site repulsion, interaction and dissipation from the time-independent case. It is also expected that the model is stable against temporal inhomogeneities in these parameters, although it is unclear

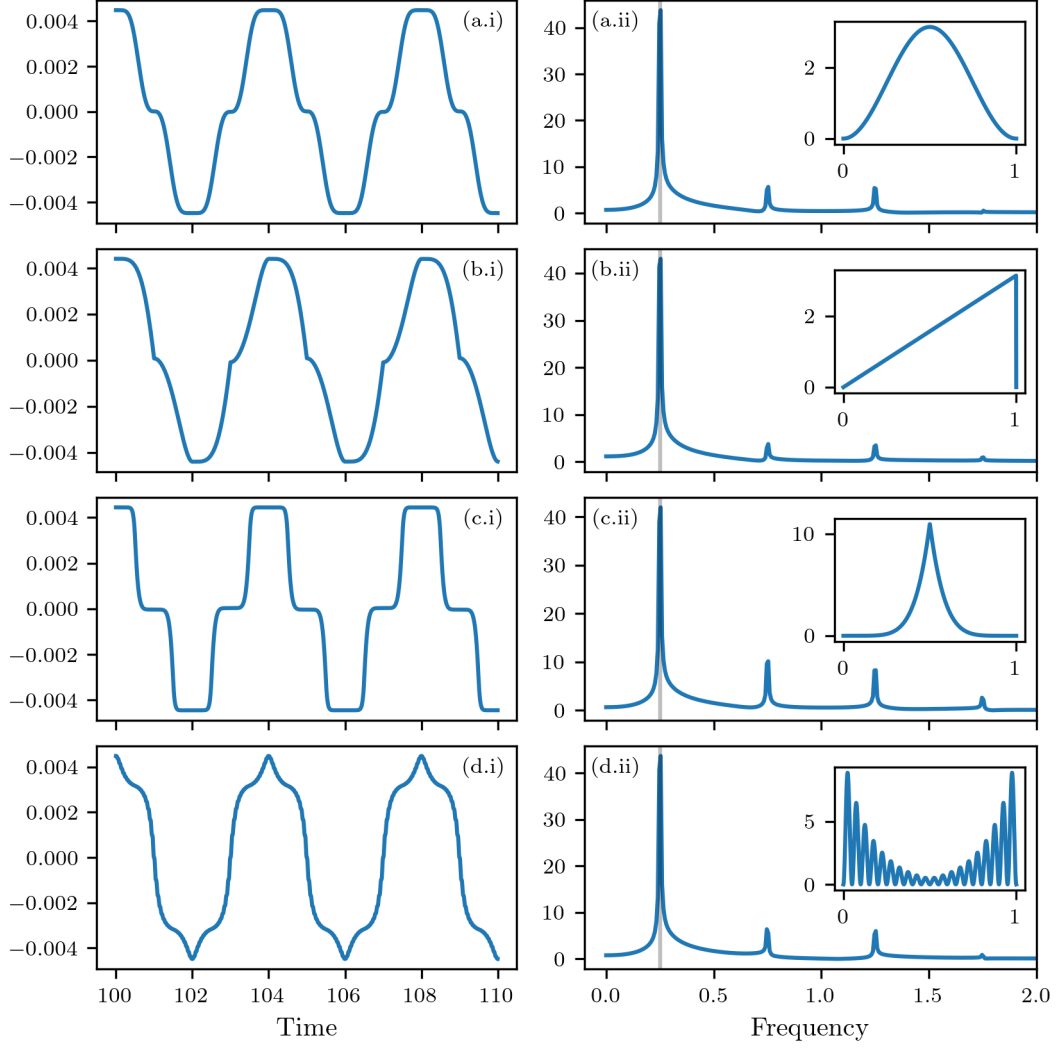


**Figure 4.11:** We evolve the heated Hubbard model with a periodic magnetic field from a random initial state and measure the response in the transverse spin. The left column plots the response,  $\langle s_2^x(t) \rangle$ , while the right shows the Fourier transform. These are plotted at late times after transient dynamics have decayed. The inset indicates the period driving waveform used in each case. Every driving function had a period  $T = 1$  and was tuned to give a 4<sup>th</sup>-order sub-harmonic response, as indicated by a spectral peak at  $k = \frac{1}{4}$ .

whether very specific driving of, say, the on-site interaction could disrupt the discrete time order. This caveat is explained further in the discussion section below.

We consider the effect of temporal noise in the magnetic field. Firstly we consider additive Gaussian noise of the form

$$B(t) \rightarrow \tilde{B}(t) = B(t) + n(t), \quad (4.43)$$

where at each time  $n(t)$  is a mean zero Gaussian random variable with variance  $\sigma^2$ . We can choose  $\sigma^2$  to vary the corresponding signal to noise ratio of the

magnetic field, which characterises the strength of the noise. We see in Figure 4.12 that our dissipative Floquet time crystal is remarkably stable to additive noise. Although the response is not strictly periodic, there is nonetheless a very evident and experimentally observable, approximate sub-harmonic response. This is easy to understand as the eigenvalues of the discrete time evolution operator,  $\mathcal{U}_T$ , depend on the integral of  $\tilde{B}(t)$ . However, the integral of  $n(t)$  vanishes almost surely, and so the integral of  $\tilde{B}(t)$  is almost surely just the integral of  $B(t)$ , which gives rise to the desired sub-harmonic response. We can also consider multiplicative noise,

$$B(t) \rightarrow \tilde{B}(t) = (1 + n(t))B(t). \quad (4.44)$$

In Fig 4.13 we once again see an impressive stability to the temporal noise. This stability suggests that this model is a good candidate for experimental study.

### 4.3 Discussion

This example indicates how strong dynamical symmetries can help construct time-dependent open quantum systems which exhibit specific properties, here Floquet time crystallinity. Recent studies [277] have developed a similar idea further and studied strong dynamical symmetries in a rotating frame, although this method is limited to sinusoidal driving terms. It would be particularly desirable to find general relationships between the purely imaginary eigenvalues of a time periodic Liouvillian,  $\mathcal{L}(t)$ , and the eigenvalues of the discrete time evolution operator,  $\mathcal{U}_T$ , that lie on the unit circle since the eigenvalues of  $\mathcal{U}_T$  on the unit circle are the ones which correspond to long time persistent non-stationarity. If one could find such a relationship, then it would be foreseeable that the necessary and sufficient conditions from Ch 3 would then be applicable to periodic systems. This would allow us to study dissipative Floquet time crystals in more detail and prove certain properties that so far are inaccessible. One example of such a property is the stability of our example above to temporal inhomogeneities in the other model parameters. Note that the example relies on the *only* eigenvalues of  $\mathcal{U}_T$  lying on the unit circle, which are not equal to one, being those that come from the persistent strong dynamical symmetry of the model. However, it is possible that some particular temporal driving of, say, the on-site field,  $\epsilon_j(t)$ , could introduce additional non-decaying dynamical modes.

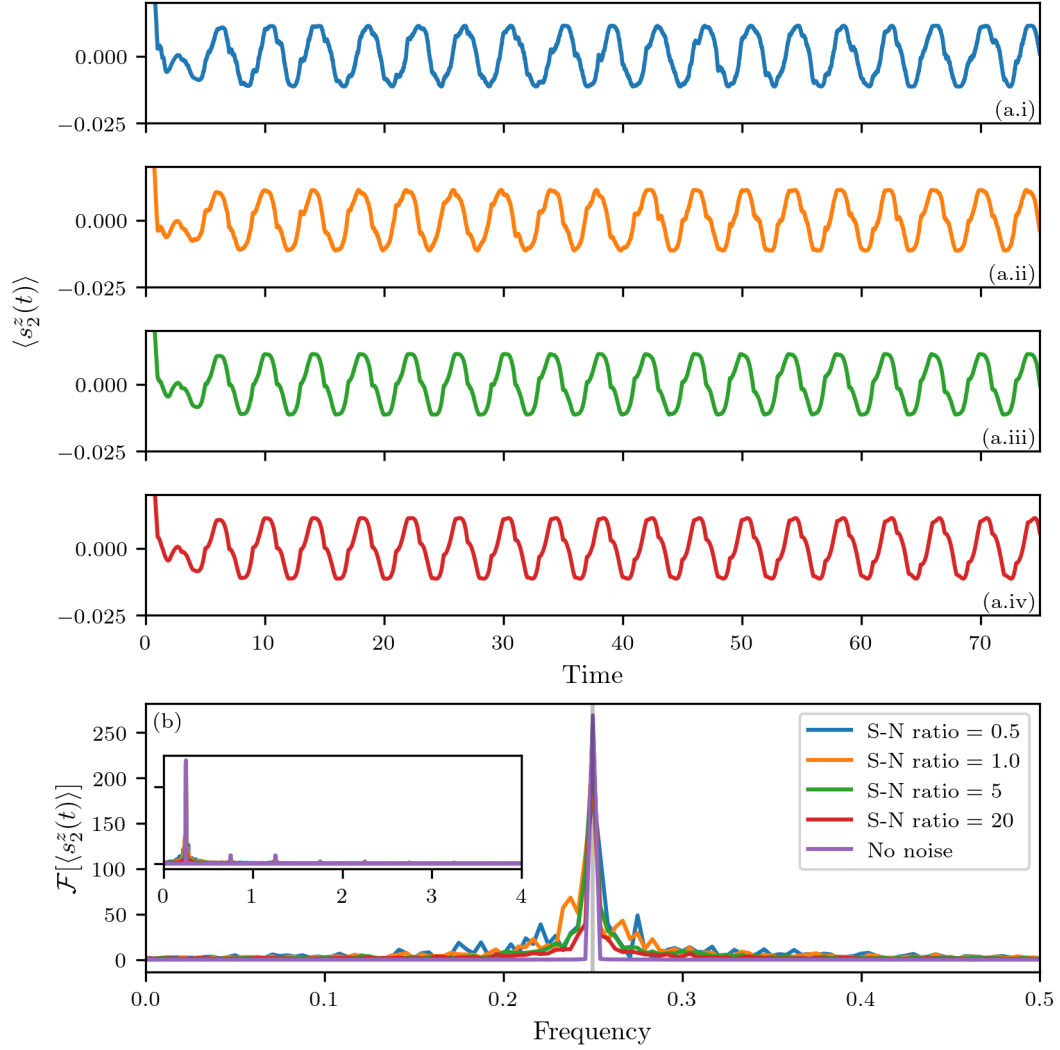


**Figure 4.12:** We evolve the heated Hubbard model with a saw tooth magnetic field as in Fig 4.11 (b) including additive Gaussian noise with varying strength. The strength is measured by the signal to noise ratio (S-N). In (a.i)-(a.iv) we plot the response of the transverse spin, while in (b) we show the Fourier spectrum, calculated after transient dynamics have decayed. Despite not being perfectly periodic, even with significant noise, there is a very recognisable quasi-periodic response which is dominated by a 4<sup>th</sup>-order sub-harmonic response, as indicated by a spectral peak at  $k = \frac{1}{4}$ . We include the Fourier spectrum of the noiseless model for comparison.



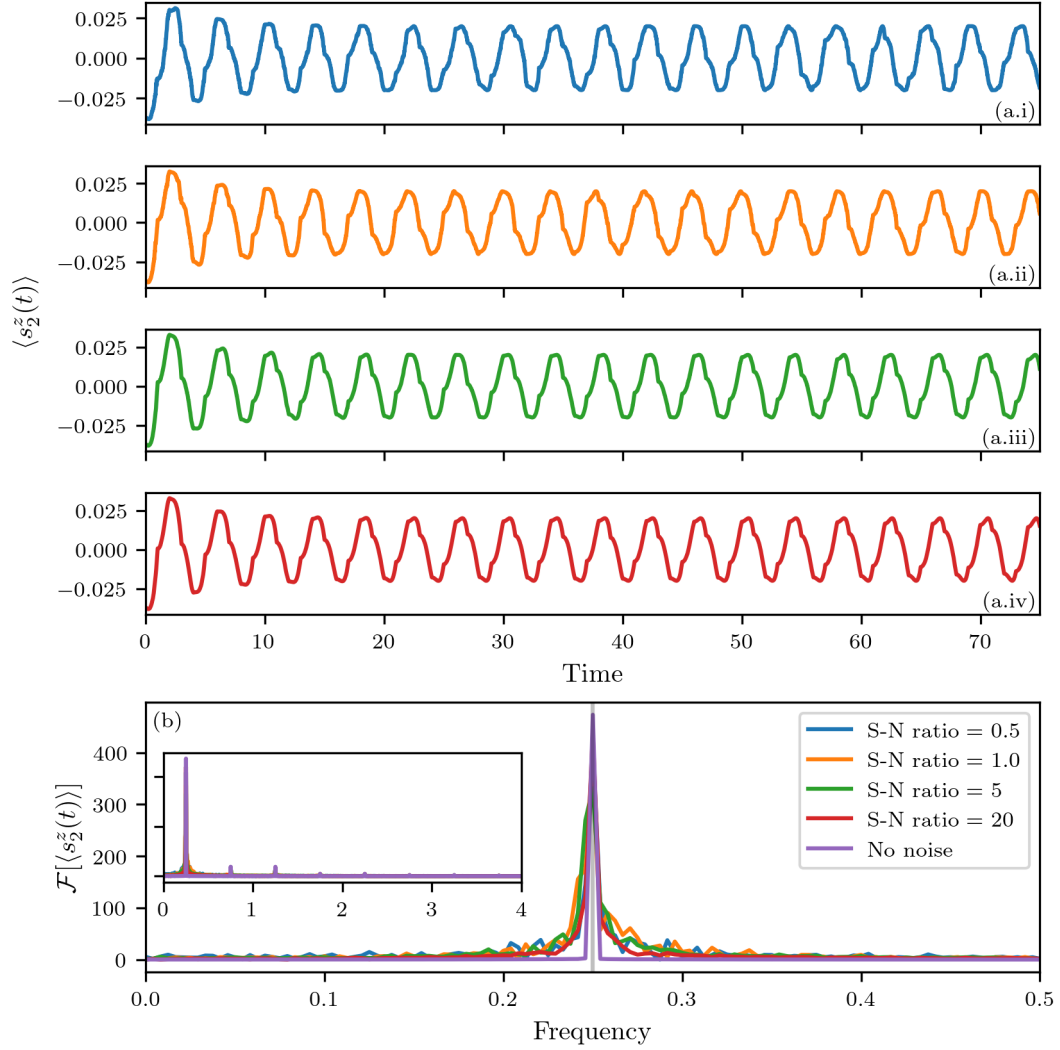


**Figure 4.13:** We evolve the heated Hubbard model with a saw tooth magnetic field as in Fig 4.11 (b) including multiplicative Gaussian noise with varying strength. The strength is measured by the signal to noise ratio (S-N). In (a.i)-(a.iv) we plot the response of the transverse spin, while in (b) we show the Fourier spectrum, calculated after transient dynamics have decayed. Despite not being perfectly periodic, even with significant noise, there is a very recognisable quasi-periodic response which is dominated by a 4<sup>th</sup>-order sub-harmonic response, as indicated by a spectral peak at  $k = \frac{1}{4}$ . We include the Fourier spectrum of the noiseless model for comparison.

It is unlikely that easily applicable conditions will exist for general periodically driven Liouvillians, although it is possible that something similar to the following conjecture holds for unital Liouvillians.

**Conjecture.** *Let  $\mathcal{L}(t)$  be a periodic Liouvillian that is unital at all times. The corresponding discrete time evolution operator  $\mathcal{U}_T$  has a non-trivial eigenvalue of unit modulus if and only if  $\mathcal{L}(t)$  has a purely imaginary eigenvalue for all  $t$ .*

Note that by non-trivial we mean that the eigenvalue is not 1. This conjecture is made because under the evolution of unital Liouvillians the  $l^2$ -norm of any state cannot increase, as we can see from the following calculation.

$$\frac{1}{2} \frac{d}{dt} \|\rho\|^2 = \text{Tr} (\rho^\dagger \dot{\rho} + \dot{\rho}^\dagger \rho) \quad (4.45a)$$

$$\begin{aligned} &= -i \text{Tr} (\rho^\dagger [H, \rho] + [H, \rho^\dagger] \rho) \\ &\quad + \sum_k \text{Tr} \left( L_k \rho^\dagger L_k^\dagger \rho + \rho^\dagger L_k \rho L_k^\dagger - \frac{1}{2} \rho^\dagger \{L_k^\dagger L_k, \rho\} - \frac{1}{2} \{L_k^\dagger L_k, \rho^\dagger\} \rho \right) \end{aligned} \quad (4.45b)$$

By cyclicity

$$= \sum_k \text{Tr} (L_k \rho^\dagger L_k^\dagger \rho + \rho^\dagger L_k \rho L_k^\dagger - \rho^\dagger \rho L_k^\dagger L_k - L_k^\dagger L_k \rho \rho^\dagger) \quad (4.45c)$$

Unitality implies  $\sum_k L_k^\dagger L_k = \sum_k L_k L_k^\dagger$  which we apply to the last term

$$= \sum_k \text{Tr} (L_k \rho^\dagger L_k^\dagger \rho + \rho^\dagger L_k \rho L_k^\dagger - \rho^\dagger \rho L_k^\dagger L_k - L_k L_k^\dagger \rho \rho^\dagger) \quad (4.45d)$$

Rewriting using H.S inner product

$$= \sum_k 2\text{Re} \langle \rho L_k^\dagger | L_k^\dagger \rho \rangle - \sum_k \|\rho L_k^\dagger\|^2 - \sum_k \|L_k^\dagger \rho\|^2 \quad (4.45e)$$

Cauchy-Schwarz

$$\leq \sum_k 2\|\rho L_k^\dagger\| \|L_k^\dagger \rho\| - \sum_k \|\rho L_k^\dagger\|^2 - \sum_k \|L_k^\dagger \rho\|^2 \quad (4.45f)$$

$$\leq - \sum_k (\|\rho L_k^\dagger\| - \|L_k^\dagger \rho\|)^2 \quad (4.45g)$$

$$\leq 0. \quad (4.45h)$$

Thus in order for a state,  $\rho$ , to be an eigenvalue of  $\mathcal{U}_T$  with a unit modulus eigenvalue its norm cannot decrease at any time during the evolution. Intuitively states whose norms do not decay are associated with purely imaginary eigenvalues of  $\mathcal{L}(t)$ , although so far subtleties relating to differing left and right eigenstates have prevented a simple proof along these lines from being found. However, as the example above and the work of [277] demonstrate, this is a line of enquiry that deserves future effort as it has the potential to allow for much easier understanding of the dynamics of certain time dependent open quantum systems in terms of algebraic structure.

## 5 Conclusions

In this chapter, we have extended the concept of a time crystal and defined the dissipative time crystal in open quantum systems. Such systems are interesting as they exhibit persistent oscillations due to being in contact with a noisy environment. This is of particular interest for realisable time crystals where the system will never be completely isolated from noisy interactions with its surroundings.

We have demonstrated the importance of structure within the purely imaginary eigenvalues of  $\mathcal{L}$  when observing the breaking of time symmetry in open, many-body quantum systems. In particular, the purely imaginary eigenvalues must form a nowhere-dense commensurable set, which must not be effectively incommensurable for robustness. This is a highly non-trivial condition for general many-body Liouvillians, which have exponentially many eigenvalues. We therefore applied the results of the previous chapter to understand when purely imaginary eigenvalues arise in the example of a heated Fermi-Hubbard model.

By first considering the isolated system, we showed that the existence of purely imaginary eigenvalues of  $\mathcal{L}$  is not sufficient for persistent oscillations for generic initial conditions and observables. However, further examples illustrated that such behaviour can emerge provided the purely imaginary eigenvalues of the Liouvillian are at least commensurable. The example with both two-body loss and gain demonstrated that the condition of commensurability is guaranteed by the existence of a single strong dynamical symmetry provided it generates *all* the continuously oscillating modes. In general, however, the existence of a strong dynamical symmetry is not sufficient for time crystalline behaviour, as illustrated by the example with only two-body loss. This example also allowed us to define a dissipative quasi-time crystal. Finally, the example with an inhomogeneous magnetic field provided an example of a dissipative time crystal without any dynamical symmetries. This model also intriguingly realises an effective non-local *dark Hamiltonian* at late times, giving coherent dynamics between two GHZ states. Remarkably, such dynamics are here achieved with a purely local physical Hamiltonian, and realistic dissipation. Further the models are robust to variations in many of the model parameters.

Open questions still remain regarding a more general theory of time crystalline behaviour in open systems. In particular in exploring whether realistic Liouvillians of this type, describing many-body systems, can have additional non-zero, purely imaginary eigenvalues which are not described by dark states or strong symmetries. Additionally, the example in Sec. 3.3 suggests the study of dissipative *quasi*-time crystals, where one can have only a few incommensurate frequencies in analogy with discrete time quasi-crystals [299, 300]. There are also clear connections that can be drawn between our dissipative time crystals and boundary time crystals,

although more work is needed to understand this relationship entirely. Such a study is likely to require a better understanding of how the Liouvillian gap closes in the thermodynamic limit, similar to the results in Ch 2 but now for more generic systems.

Finally, we presented an extension of our dissipative time crystal model which satisfied the conditions for a dissipative Floquet time crystal. This model showed impressive stability properties, suggesting it could be a suitable candidate for experimental study, for example using cold atoms. We also briefly highlighted how we believe the ideas of Ch 3 could be extended so that Floquet time crystallinity could be studied more generally in open quantum systems. Such developments would also have direct application to study driven synchronisation, as we will briefly discuss in the following chapter.

# 5

## Quantum synchronisation

Synchronisation is a ubiquitous phenomenon displayed in all manner of systems, from mechanical vibrations to the flocking of starlings and even to the spreading of epidemics and disease. Intuitively understood as the process in which individual bodies in a many-body system adjust their dynamics or configurations to match that of the collective, various notions of synchronisation have been studied for nearly 350 years and have been a cornerstone of the field of classical dynamical and chaotic system analysis. This rigorous understanding of how systems synchronise has played a crucial role in developing numerous technologies, including digital communications, nationwide electrical power supply, and automotive transmissions.

In the current age of developing quantum technologies, it is now essential to understand how synchronisation in many-body quantum systems can be engineered and controlled. In this chapter, we will use the results of Ch 3 to present an algebraic theory of spontaneous synchronisation in many-body quantum systems, which will provide several illuminating insights and general principles for engineering synchronised quantum systems. As in the previous chapter, we will first recap and extend our introductory discussion from Ch 1 before presenting our results and using them to study several pedagogical and experimentally relevant examples.

# 1 Introduction to synchronisation

Before discussing our theory of quantum synchronisation, it is instructive to discuss synchronisation in general, with some historical background, to demonstrate the subtleties surrounding the concept. We will then discuss the previous studies of synchronisation in quantum systems before giving the formal definitions that we will be using.

## 1.1 General synchronisation

The term synchronisation, or more specifically synchronous, stems from the ancient Greek words ‘syn-’ meaning “together with” and ‘kronous’ meaning “time”. Thus events are said to be synchronous if they occur at the same time. The scientific study of synchronous (or synchronised) dynamical systems dates back to 1673 when Huygens studied the motions of two weakly coupled pendula [141]. He observed that pendula clocks hanging from the same bar had matched their frequency and phase exactly. Following this observation, he explored both synchronisation and anti-synchronisation where the pendula with approximately equal (or opposite for anti-synchronisation) initial conditions would, over time, synchronise so that their motions were identical (resp. opposite). Since Huygens, synchronisation has been a topic of significant interest in an ever-expanding range of scientific and technological fields. From a theoretical point of view, synchronisation is a central issue in the study of classical dynamical and chaotic systems and is currently an area of very active research.

Classical synchronisation is broadly split into two main classes: driven and spontaneous. Studies into driven synchronisation are usually interested in when the dynamics of the system in question synchronise with a driving force. Driven synchronisation will not be relevant for our work as we will be exclusively interested in spontaneous synchronisation within quantum systems, and so we will not discuss this any further, other than to direct the reader to [322–324] for more details regarding synchronisation in driven systems, especially the most commonly studied master-slave systems. For completeness, we should also mention the related topic of Synergistics, first introduced by Haken to initially study lasers and fluid instabilities [325–327]. Synergetics studies how circular causality between microscopic systems and macroscopic order parameters can lead to self-organisation within open systems that have been driven far from equilibrium [328, 329]. In the years since its inception, the theory has been applied to a wide range of disciplines such as studying human ECG activity and machine learning [330].

Spontaneous synchronisation describes the phenomenon where individual sub-systems within a many-body system adjust their motion and rhythms to match

by mutual interactions - in the same way as Huygens' pendula. For the rest of this chapter, all synchronisation will be spontaneous, and hence we will no longer need to specify. This behaviour can be further subdivided into two main classes based on how the synchronised subsystems are related.

(i) Identical/Complete synchronisation

*For a system comprising of identical coupled subsystems. Corresponding variables in each of the subsystems become equal as the subsystems evolve in time.*

(ii) Phase synchronisation

*For a system comprising of non-identical coupled subsystems. The phase differences between given variables in the different subsystems lock while the amplitudes remain uncorrelated.*

One important additional constraint applies to both classes: synchronisation must be robust to small perturbations in the initial conditions. This is important to exclude many cases of trivially synchronised systems that arise simply through the fine-tuning of initial conditions, in particular the case of non-interacting systems. In order to make this clear throughout, we will use the term synchronised to refer to any pair of time dependant signals which are equal or sufficiently similar, usually after some transient time and the term synchronisation to refer to the non-trivial process of two subsystems becoming synchronised, in a way that is stable to perturbations in the initial conditions.

Identical synchronisation is in many ways the most fundamental and is what Huygens originally studied with his coupled pendula. It has been extensively studied in the past, both theoretically [331–336], and for its applications [337–340]. Much of this progress, which has been primarily focused on controlling synchronisation within chaotic systems, has built upon the seminal work of Pecora and Carroll [331] who formulated criteria based on the signs of Lyapunov exponents. We also note that identical synchronisation can be extended to non-identical subsystems by choosing appropriate, often de-dimensionalised, variables or coordinates for the different subsystems.

In order to detect identical synchronisation or anti-synchronisation it is useful to use the Pearson indicator [341] defined for two time-dependent signals,  $f(t)$  &  $g(t)$ , as

$$C_{f,g}(t, \Delta t) = \frac{\overline{\delta f \delta g}}{\sqrt{\overline{\delta f^2} \overline{\delta g^2}}}, \quad (5.1)$$

where  $\Delta t$  is some fixed parameter, usually taken to be the time period of any oscillations, and

$$\overline{X} = \frac{1}{\Delta t} \int_t^{t+\Delta t} X(t) dt, \quad \delta X = X - \overline{X}. \quad (5.2)$$

This measures the correlation between the two variables in the most intuitive way and has been widely applied to classical [142, 342] and in some cases quantum [120, 149, 343, 344] synchronisation. We can see that  $C_{f,g}$  takes the value  $+1$  for ‘perfect’ synchronisation and  $-1$  for ‘perfect’ anti-synchronisation, and in these cases is independent of  $\Delta t$ . Significantly the Pearson indicator is effective when the signals  $f$  and  $g$  are not periodic. This is important because while synchronisation is often understood through periodic systems, such as pendula, this is not strictly necessary for identical synchronisation. The notion of two variables that become equal over the period of evolution could just as well apply to two particles following unbound trajectories as to two particles that remain within some finite region. We can also easily present examples of quasi-periodic behaviour, that is a superposition of Fourier modes with non-commensurate frequencies. This makes the Pearson indicator an excellent order parameter for identifying identical synchronisation.

On the other hand, phase synchronisation requires periodic motion to meaningfully define a relative phase difference between the two subsystems, although extensions can be considered with simply a time delay rather than a true phase difference. This is strictly weaker than identical synchronisation, even when we consider the extension to non-identical subsystems, as it requires no direct correlation between the variables describing the subsystems. Following work on cryptography using chaotic maps [345, 346], phase synchronisation was applied as a method for secure communication [347–349]. Phase synchronisation has also been studied in the quantum setting, usually through the use of Arnold tongues and Hussimi-Q functions [144, 341]. However, these methods are usually aimed at probing the system’s response to driving rather than mutual spontaneous synchronisation between subsystems. We should also mention the interesting related case of amplitude-envelope synchronisation in chaotic systems [350] where there is no correlation between the amplitude and phases of the motion within the two systems, but instead, they both develop periodic envelopes at a matched frequency. In the remainder of our work, we will focus on studying identical synchronisation between subsystems of an extended quantum system, although many of the results are either directly applicable or can be adapted to the case of phase synchronisation.



## 1.2 Quantum synchronisation

Synchronisation is usually studied in open quantum systems since in closed systems a generic initial state will excite a large number of eigenfrequencies with random phase differences leading to noise in small systems, as in Ch 4 Sec 3.2, or to thermalisation via the ETH [35]. As a result, previous studies have focused on the open quantum system regime, where interactions with the environment cause decoherence and decay within the density operator describing the state, leaving only a handful of long-lived oscillating modes as we have seen in the previous chapters. Synchronisation in these systems has previously been studied on a case-by-case basis with various measures of quantum synchronisation having been introduced. These measures have been based primarily on phase-locking of correlations, or Husimi Q-functions [120, 144] which are often unscalable to many-body problems.

As we noted in Ch 1, quantum synchronisation holds promise for technical applications. For instance, synchronising spins in a quantum magnet would allow for homogeneous and coherent time-dependent magnetic field sources. Developing sources of homogeneous and coherent time-dependent magnetic fields has the significant potential to improve the resolution of MRI images [157]. Additionally, recent studies have explored the role of synchronisation in the security of quantum key distribution (QKD) protocols [158–160]. It is foreseeable that a better understanding of quantum synchronisation could help improve security against specialist attacks that exploit the dependence of several QKD schemes on synchronised calibration. Synchronisation has also been proposed as a method to improve atomic clocks and to store time in a quantum memory [351]. Despite the intense recent study and the promise it holds, a general theory of quantum synchronisation has been lacking until now.

In the remainder of this chapter, we will build upon the results of Ch 3, which provided necessary and sufficient conditions for persistent dynamics in many-body open quantum systems to understand in detail when the resulting dynamics will be synchronised. The generic setup we will consider is an extended system made up of arbitrarily, but finitely, many individual sites that can interact with each other and with an external environment via the Lindblad equation. This scenario is depicted in Fig 5.1. The restriction of having only finitely many sites can be reasonably justified since two infinitely separated subsystems are prevented by locality from ever being causally connected, thus rendering synchronisation impossible. Alternatively, sites infinitely far apart could be redefined as belonging to the environment and thus taken into account in that manner. As has been the case throughout this thesis, these individual sites will have finite-dimensional Hilbert spaces and thus have no well defined semi-classical limit. We will then consider synchronising the signals of observables measured on different sites or groups of sites of the system. Following

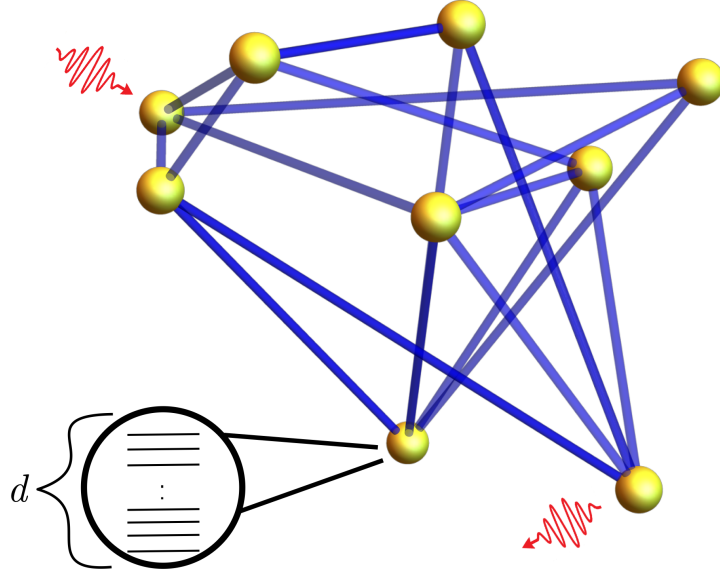


**Figure 5.1:** An arbitrary interacting quantum many-body system of  $N$  sites (illustrated as yellow spheres) which may interact with each other along the blue bonds. The sites also interact with the background environment, illustrated by the red arrows. The sites each have a finite local Hilbert space, illustrated as dimension  $d$  on one of the sites (i.e. each site has  $d$  levels). This is the general system of interest we will be focusing on. The goal will be to synchronise observables between different sites in the system. Crucially, the sites that are to be synchronised do not have  $\hbar \rightarrow 0$  or equivalent large parameter (semi-classical) limits. Rather we make no assumptions on the size of the local Hilbert space.

our discussion above regarding synchronisation in general, we will classify whether the sites are synchronised based on the behaviour of expectation values of these observables on each site over time. In this way, we have captured the fundamental essence of synchronisation intuitively within the quantum regime.

### 1.3 Definitions

To summarise our discussion from above, for two systems to be identically synchronised, we require that their matching motion be nonstationary and long-lasting. For the extended quantum systems that we are interested in, we will interpret ‘motion’ via the behaviour of some local observable,  $O_j$ , which is measured in the same basis on every site. For simplicity, we will also consider only the strictest notion of identically synchronised signals whereby after synchronisation has occurred, the two synchronised signals,  $\langle O_j(t) \rangle$  &  $\langle O_k(t) \rangle$ , are identical and do not differ by an overall phase, scale factor, or constant. This is stricter than the definition provided by considering the Pearson indicator from Eq. (5.1) but this is not so restrictive as the results we present can be suitably adapted to consider these alternative cases, as outlined later. However, as the technical discussions do not

provide significant additional insight or understanding, we will work largely with these very strict definitions given below.

In line with previous works, we consider separately stable and metastable synchronisation to be where the signals remain synchronised and nonstationary for infinitely-long, or finitely-long periods, respectively. In the case of metastable synchronisation, we require some perturbative parameter within the system that controls the lifetime of the synchronised behaviour. Finally, we must allow some initial transient time period during which synchronisation can occur. These considerations lead naturally to the following definitions.

**Definition** (Stably synchronised). We say that the subsystems  $j$  and  $k$  are *stably synchronised* in the observable  $O$  if for some initial state and after some transient time period  $\tau$  we have  $\langle O_j(t) \rangle = \langle O_k(t) \rangle$  for all  $t \geq \tau$ . Further we require that  $\langle O_j(t) \rangle$  does not become constant, i.e  $\partial_t \langle O_j(t) \rangle \neq 0$ .

**Definition** (Metastably synchronised). We say that the subsystems  $j$  and  $k$  are *metastably synchronised* in the observable  $O$  if for some initial state during the interval  $t \in [\tau, T]$  where  $T \gg \tau$  we have  $\langle O_j(t) \rangle = \langle O_k(t) \rangle$  and again  $\partial_t \langle O_j(t) \rangle \neq 0$ . Further, the cut-off time  $T$  must be controllable by some perturbative parameter,  $s$ , in the system.

Note that equality in these definitions, and as in the rest of this work, is understood as equality up to terms which are exponentially small in time and for brevity, we do not continuously write “ $+\mathcal{O}(e^{-\gamma t})$ ”. These terms will always be present for finite-dimensional systems as per Eq. (3.3) but are negligible on the longer time scales we will be concerned with. We also remark that metastable synchronisation of this form has also been previously referred to as transient synchronisation in [151, 352]. Metastable synchronisation is also sometimes weakened to allow the two signals to differ by some finite amount provided this is also controlled by the system’s perturbative parameter, for example

$$|\langle O_j(t) \rangle - \langle O_k(t) \rangle| \leq \epsilon(s). \quad (5.3)$$

It is important to observe that these definitions do not require that the system has an internal mechanism that synchronises the two sites. Since we only require the existence of some initial state for which the observables are synchronised, this initial state can be finely tuned so that the observables on the two subsystems are initially equal and their evolutions are identical. To characterise synchronisation which is robust to variation in initial conditions, we make the further definition.

**Definition** (Robustly synchronised). If the subsystems  $j$  and  $k$  are stably or metastably synchronised in the observable  $O$ , this synchronisation is *robust* if  $O_j(t) = P_{j,k}O_k(t)P_{j,k}$  and  $\partial_t O_j(t) \not\equiv 0$  on the operator level (i.e. in the Heisenberg picture). Here  $P_{j,k}$  is a permutation operator exchanging subsystems  $j$  and  $k$ . As with the definitions of stable and meta-stable synchronisation, these requirements must hold for the same respective time periods.

This definition ensures that after the transient dynamics have decayed, regardless of the system's initial state, the observable on subsystems  $j$  and  $k$  will be equal and for a large class of initial states will be nonstationary. Robustly synchronised systems are the ones where some internal mechanism causes the synchronisation process. However, as we will demonstrate later, several previously studied examples of quantum synchronisation are, in fact, not robust and require fine-tuning of the initial state. This highlights the importance of making these considerations and definitions when studying quantum synchronisation.

Notice that, as with dissipative time crystals in the previous chapter, we have defined synchronisation with respect to some observable. For most applications of synchronisation, it is sufficient for just one observable to be synchronised. We can, however, say that the two subsystems are *completely* synchronised if they are robustly synchronised, whether stably or metastably, for *all* nonstationary observables [353].

These definitions are visualised in Fig. 5.2 and characterise the possible cases of identical synchronisation within a quantum system. As earlier remarked, the results we present can be straightforwardly adapted to consider phase synchronisation provided the long-lived oscillations are periodic. Moreover, we can easily extend our analysis to other measures of synchronisation [354]. We may, for instance, define limit cycle dynamics over a phase space composed of  $\langle O_k(t) \rangle$  and another observable  $\langle Q_k(t) \rangle$  provided they do not commute,  $[Q_k, O_k] \neq 0$ .

Having made explicit what we mean when referring to quantum synchronisation and introduced some of the notation, we can study these systems in more detail.

## 2 Algebraic conditions for quantum synchronisation

### 2.1 Stable synchronisation

It is immediate from our definitions above that purely imaginary Liouvillian eigenvalues are necessary for stable synchronisation since the sites in a system cannot lock persistently into phase, frequency and amplitude if the frequency is trivially 0. We can therefore deduce that there must exist some ‘ $A$ -operators’ from Thm 1 or strong dynamical symmetries as in Thm 2. Using their existence, we can

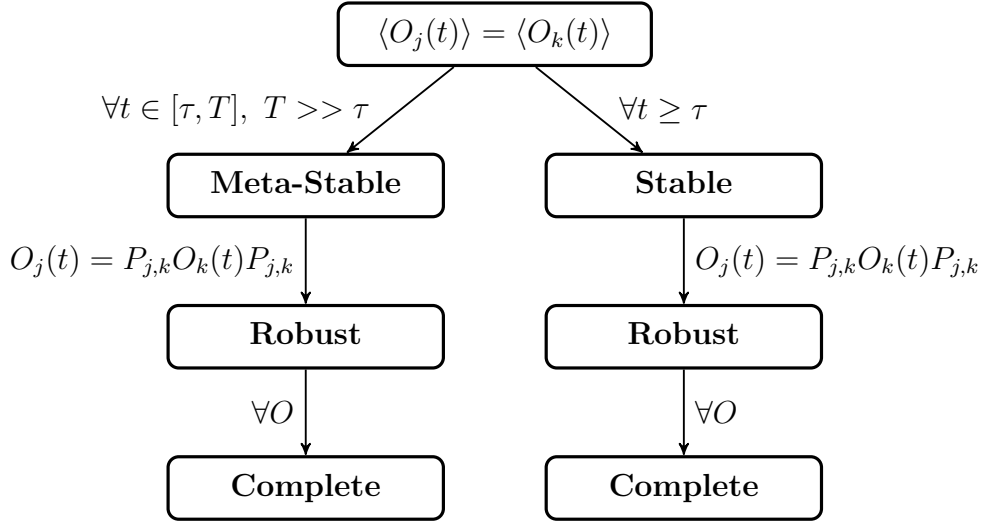


**Figure 5.2:** Visualisation of the different definitions of synchronisation. If we have equality in the expectation value of some nonstationary observable on different sites for some initial state, then we classify the signals as either stably or metastably synchronised. If we have equality on the operator level, then they are robustly synchronised. Finally, if this holds for all nonstationary observables, then we say the subsystems are completely synchronised.

formulate sufficient conditions that these  $A$ -operators must obey for two subsystems to be stably synchronised in a many-body quantum system. Recall that we denote by  $P_{j,k}$  the operator exchanging subsystems  $j$  and  $k$  and thus define  $\mathcal{P}_{j,k}(x) := P_{j,k} x P_{j,k}$  as the corresponding superoperator acting on  $\mathcal{B}(\mathcal{H})$ . We now prove the following.

**Theorem 6.** *Fulfilling all the following conditions is sufficient for robust and stable synchronisation between subsystems  $j$  and  $k$  with respect to the local operator  $O$ :*

- The operator  $P_{j,k}$  exchanging  $j$  and  $k$  is a weak symmetry [111] of the quantum Liouvillian  $\mathcal{L}$  (i.e.  $[\mathcal{L}, \mathcal{P}_{j,k}] = 0$ ).
- There exists at least one  $A$  fulfilling the conditions of Thm 1 with  $\omega \neq 0$ .
- For at least one operator  $A$  fulfilling the conditions of Thm 1 and the corresponding  $\rho_\infty$  we have  $\text{tr}[O_j A \rho_\infty] \neq 0$ .
- All  $A$  fulfilling the conditions of Thm 1 also satisfy  $[P_{j,k}, A] = 0$ .

*Proof.* In the long-time limit we have,

$$\lim_{t \rightarrow \infty} \langle O_j(t) \rangle = \text{tr} \left[ O_j \sum_n c_n A_n \rho_{\infty, n} e^{i\omega_n t} \right], \quad (5.4)$$

where  $c_n = \langle \langle \sigma_n | \rho(0) \rangle \rangle$  for an initial state  $\rho(0)$  which we assume to be arbitrary. The  $A_n$  are all operators satisfying the conditions of Thm 1 and  $\mathcal{L}[\rho_{\infty,n}] = 0$ . Since  $P_{j,k}^2 = \mathbb{1}$  we can write

$$\lim_{t \rightarrow \infty} \langle O_j(t) \rangle = \text{tr} \left[ O_j P_{j,k}^2 \sum_n c_n A_n \rho_{\infty,n} e^{i\omega_n t} \right], \quad (5.5)$$

and hence we aim to commute the  $P_{j,k}$  to the left to use the relation  $O_k = P_{j,k} O_j P_{j,k}$  which results in  $\lim_{t \rightarrow \infty} \langle O_j(t) \rangle = \lim_{t \rightarrow \infty} \langle O_k(t) \rangle$  for any initial state. By assumption,  $[A_n, P_{j,k}] = 0, \forall n$ . Hence we must show that  $[\rho_{\infty,n}, P_{j,k}] = 0, \forall n$ .

To do so we use the fact that  $P_{j,k}$  is a weak symmetry of the Liouvillian  $[\mathcal{P}_{j,k}, \mathcal{L}] = 0$ . This implies that the Liouvillian is block reduced to the eigenspaces  $\mathcal{B}_+$  and  $\mathcal{B}_-$  corresponding to the +1 and -1 eigenvalues of  $P_{j,k}$ , respectively [111]. Since the Liouvillian has been block reduced, we can conclude that the  $\rho_{n,\infty}$  must belong to either  $\mathcal{B}_-$  or  $\mathcal{B}_+$ . For all  $\rho_{\infty,n} \in \mathcal{B}_+$  we trivially have  $[\rho_{\infty,n}, P_{j,k}] = 0$ . Hence suppose that some  $\rho_{n,\infty} \in \mathcal{B}_-$ . We can then write

$$\rho_{n,\infty} = P_+ \rho_{n,\infty} P_- + P_- \rho_{n,\infty} P_+, \quad (5.6)$$

where

$$P_{\pm} = \frac{1}{2} (\mathbb{1} \pm P_{j,k}), \quad (5.7)$$

are the corresponding orthogonal projectors onto the eigenspaces of  $P_{j,k}$ . We can now choose a basis,  $\{|\psi_{\alpha}\rangle\}$ , for  $\mathcal{H}$  such that either  $P_+ |\psi_{\alpha}\rangle = |\psi_{\alpha}\rangle$ ,  $P_- |\psi_{\alpha}\rangle = 0$  or the reverse. In this basis we see that  $\rho_{n,\infty}$  contains only off diagonal elements. In the language of Baumgartner and Narnhofer [113], all  $\rho_{n,\infty} \in \mathcal{B}_-$  are *stationary phase relations*. We then use Proposition 16 of [113] which states the existence of a stationary phase relation implies the existence of a unitary  $U$  such that  $[H, U] = [L_{\mu}, U] = 0, \forall \mu$ . However, such a  $U$  must intertwine between the subspaces +1 and -1 of  $P_{j,k}$ , with projectors  $P_+$  and  $P_-$ , respectively, i.e.  $UP_+ = P_-U$  and therefore  $[U, P_{j,k}] \neq 0$ . However,  $U$  satisfies all the conditions for an  $A$  operator from Thm 1, and by assumption does not exist. Thus there are no non-zero  $\rho_{\infty,n} \in \mathcal{B}_-$  and so all  $\rho_{\infty,n}$  commute with  $P_{j,k}$ .  $\square$

The most straightforward example of a weak symmetry is when  $[H, P_{j,k}] = 0$  and  $\mathcal{P}_{j,k}$  maps the set of all the Lindblad operators  $\{L_{\mu}\}$  into itself, though more exotic cases are possible [217, 355, 356]. Thus systems satisfying the conditions of Thm 6 include, for instance, those for which  $P_{j,k}$  is a reflection operator, the Lindblad operators act on each subsystem individually and the system Hamiltonian is invariant under reflections.

We can further relax these requirements in quite general cases and achieve total synchronisation across the system, i.e. synchronisation between all pairs of subsystems. In particular, we can replace the requirement that  $\mathcal{P}_{j,k}$  be a weak symmetry with the condition that the Liouvillian be unital as follows.

**Theorem 7.** *The following conditions are sufficient for robust and stable synchronisation between subsystems  $j$  and  $k$  with respect to the local operator  $O$ :*

- *The Liouvillian,  $\mathcal{L}$  is unital ( $\mathcal{L}(\mathbb{1}) = 0$ ).*
- *There exists at least one operator  $A$  fulfilling the conditions of Thm 1.*
- *For at least one  $A$  fulfilling the conditions of Thm 1 and the corresponding  $\rho_\infty$  we have  $\text{tr}[O_j A \rho_\infty] \neq 0$ .*
- *All such  $A$  fulfilling the conditions of Thm 1 also satisfy  $[P_{j,k}, A] = 0$ .*

*Furthermore, if all  $A$  are translationally invariant,  $[A, P_{j,j+1}] = 0, \forall j$ , then every subsystem is robustly and stably synchronised with every other subsystem.*

*Proof.* We return to Eq. (5.5) in the previous proof and wish to show that  $[\rho_{\infty,n}, P_{j,k}] = 0$  but without the assumption of weak symmetry. If  $\mathcal{L}$  is unital, then all  $A_n$  satisfy conditions of Thm 2 and therefore it straightforwardly follows that  $A_n A_n^\dagger$  is a strong symmetry [111, 357] of the Liouvillian and that the projectors to the eigenspaces of  $A_n A_n^\dagger$ ,  $P_{n,a}$ , are stationary states  $\mathcal{L}[P_{n,a}] = 0$ . By assumption  $[P_{j,j+1}, A_n A_n^\dagger] = [P_{n,a}, P_{j,j+1}] = 0$ . By Theorem 3 of [113],  $P_{n,a}$  are projectors to enclosures. The existence of more minimal enclosures that do not satisfy the symmetry requirement would imply that there are more operators  $A$  (as projectors to enclosures satisfy the conditions of Thm 1 trivially), and this cannot happen by our current assumptions. Therefore,  $P_{n,a}$  are projectors to minimal enclosures. By Theorem 18 of [113] all the minimal diagonal blocks  $P_{n,a} \rho P_{n,a}$  contain a unique stationary state, which must be  $P_{n,a}$  up to a constant. The lack of stationary phase relations and oscillating coherences that do not commute with  $P_{j,k}$  follows from the fact that by Theorem 18 of [113] the unique stationary state in each off-diagonal block is of the form of  $U P_{n,a}$ . This intertwiner, like in the proof of Thm 6, satisfies the conditions for an  $A$ -operator and therefore must commute with  $P_{j,k}$  by assumption.  $\square$

This result further illustrates the power and utility of unital maps in achieving total synchronisation. Examples are 1D models that are reflection symmetric, have only one  $A$  operator, and experience dephasing. This includes the cases discussed before in [119, 120].

### Multiple frequencies and commensurability

It is important to make some brief remarks about the issues of multiple frequencies and commensurability, which is closely related to the ideas presented in Ch 4. Firstly, by allowing for multiple  $A$  operators, each of which need not correspond to the same imaginary eigenvalue, the theorems above explicitly include the case of multiple system frequencies. In general, if the multiple purely imaginary eigenvalues of a system are not commensurate then the resulting oscillations will not be periodic. This alone does not preclude quantum synchronisation, since unlike for dissipative time crystals we have not required that the long-lived dynamics be periodic.

However, if there are too many incommensurable purely imaginary eigenvalues, then they will generically dephase, leading to observables that are effectively stationary, or alternatively, the system may display noisy dynamics. This means that in systems obeying the conditions for synchronisation but with many incommensurable purely imaginary eigenvalues, additional analysis must be carried out to determine if the synchronisation survives the dephasing process and if the dynamics become chaotic. However, if all the strong dynamical symmetries are suitably permutation invariant, the subsystems will always display the same dynamics even if it is chaotic or relaxes to stationarity. For a more detailed discussion of such spectral problems from a mathematical perspective, see [312].

It should also be noted that the situation is more straightforward in unital evolutions, where each purely imaginary eigenvalue can be related to a strong dynamical symmetry,  $A$ , and thus by Thm 2 is an integer multiple of some fixed frequency corresponding to  $A$ . Generically in open quantum systems with sufficiently many Lindblad jump operators, there are very few, if any, dynamical symmetries, and thus any purely imaginary eigenvalues will be integer multiples of a few fixed values.

### Extensions to weaker definitions of synchronisation

As we have emphasised throughout, our definitions pertain only to the strictest notion of synchronisation, where the two signals must be identical. However, if we were to use the Pearson indicator from Eqn. (5.1), this would instead allow for two signals which differ by an overall additive constant or multiplicative factor. From the proof of Thm 6 we can see how the conditions should be adapted to give sufficient conditions for this relaxed notion of synchronisation. Firstly we no longer need exchange superoperator  $\mathcal{P}_{j,k}$  to be a weak symmetry and we do not need all  $A$ -operators to satisfy  $[P_{j,k}, A] = 0$ . Instead we require that if  $\rho_n = A_n \rho_{\infty, n}$  has a non-zero, purely imaginary eigenvalue, then  $P_{j,k} \rho_n = \alpha \rho_n P_{j,k}$  for some  $\alpha$  which corresponds to the constant multiplicative factor between the two signals. Note also that inhomogeneity of the NESSs under exchange,  $P_{j,k} \rho_{\infty, n} P_{j,k} \neq \rho_{\infty, n}$  leads to an additive constant between the two signals.



As an extension to this we can also see how alternate modes of synchronisation can occur. For instance if there were only a single  $A$  operator and the condition  $[P_{j,k}, A] = 0$  were replaced by  $P_{j,k}A - e^{i\theta}AP_{j,k} = 0$  then we would have

$$\lim_{t \rightarrow \infty} \langle O_j(t) \rangle = \lim_{t \rightarrow \infty} \langle O_k(t + \theta/\lambda) \rangle, \quad (5.8)$$

corresponding to phase synchronisation.

## 2.2 Metastable synchronisation

From the definitions in Sec 1.3, metastable synchronisation requires dynamics which correspond to Liouvillian eigenvalues with vanishingly small real part. We therefore refer back to the results of Ch 3 Sec 3 which classified the possible cases of Liouvillian eigenvalues with vanishingly small real part. To recall that discussion we concluded that under a perturbation of the form

$$\mathcal{L}(s) = \mathcal{L}_0 + s\mathcal{L}_1 + s^2\mathcal{L}_2 + \dots, \quad (5.9)$$

there are three important regimes:

- **Ultra-low frequency regime.** When the eigenvalue is of the form  $\lambda(s) = \lambda_1 s + \lambda_2 s^2 + \dots$  so that the perturbed dynamics occur over very long time periods. As before, we remark that in many ways this is rather unsatisfactory for the purposes of synchronisation in an applicable sense since as we extend the lifetime of our synchronisation, the periodic behaviour becomes harder to observe as a consequence of the extended time period.
- **Quantum Zeno regime.** In this related case we have a Liouvillian of the form

$$\mathcal{L}(\gamma) = -i[H, \rho] + \gamma \sum_{\mu} 2L_{\mu}\rho L_{\mu}^{\dagger} - \{L_{\mu}^{\dagger}L_{\mu}, \rho\} + \mathcal{O}(1/\gamma), \quad (5.10)$$

where  $\gamma$  is a large parameter. In this case we have Liouvillian eigenvalues of the form

$$\lambda(\gamma) = i\omega + \lambda_2 \frac{1}{\gamma} + o\left(\frac{1}{\gamma}\right), \quad (5.11)$$

leading to oscillations that occur on the relevant Hamiltonian time-scales for all  $\gamma$ .

- **Dynamical regime.** From Thms 4 & 5 if we perturb a system which has non-zero purely imaginary eigenvalues when  $s = 0$ , these eigenvalues vary as

$$\lambda(s) = i\omega + i\omega_1 s + \lambda_2 s^{1+\frac{1}{p}} + o\left(s^{1+\frac{1}{p}}\right), \quad (5.12)$$

where  $\omega_1 \in \mathbb{R}$  and  $p$  is some positive integer. We also saw that if the perturbation is purely in the Hamiltonian then  $p = 1$ .

Since they are the most relevant for experimental applications, we restrict ourselves to the Zeno and Dynamical regime, where the resulting dynamics occur on the relevant Hamiltonian time scales. To understand how synchronisation is affected by the perturbation, we observe that provided the perturbation is small enough that the Liouvillian gap does not close, the dynamics of the system are controlled exclusively by  $\mathcal{L}_0$  up to negligible contributions from  $\mathcal{L}_1$  on timescales  $t < \mathcal{O}(1/s)$ . Since we also know that  $\mathcal{L}_0$  has purely imaginary eigenvalues we can apply the Thms 6 & 7 to  $\mathcal{L}_0$  to determine whether meta-stable synchronisation occurs for some finite period before the effects of  $\mathcal{L}_1$  become relevant.

We can also apply the result from Prop 2 to determine when the frequency of synchronised oscillations is stable. In particular, as we exploited in Ch 4 Sec 3.5, if the perturbation is *anti-symmetric* under the exchange of the two synchronised subsystems, then the frequency of synchronisation is stable to next-to-leading order.

After making some brief comments on the relation between classical and quantum synchronisation, we will apply these results to study several systems that both do and do not exhibit robust quantum synchronisation.

### 2.3 Comparison between quantum and classical synchronisation

We pause to comment on the relationship between quantum synchronisation in our sense and classical synchronisation and the insights that our results provide. Even though we are deliberately studying systems with no well-defined classical limit, certain analogies can be drawn.

Firstly, by definition classical synchronisation requires stable limit cycles [143]. More specifically, suppose that a small perturbation in the neighborhood of a limit cycle  $\langle O(t) \rangle$  leads to a new trajectory  $\langle \tilde{O}(t) \rangle$ . The limit cycle is exponentially stable if there exists a finite  $a > 0$  such that  $|\langle \tilde{O}(t) \rangle - \langle O(t) \rangle| \lesssim e^{-at}$ . In our case, provided the conditions of Thm 2 hold, any perturbation of the initial state,  $\tilde{\rho}(0) = \rho(0) + \delta\rho$ , that does not change the value of the strong dynamical symmetry, i.e.  $\text{Tr}(\delta\rho A) = 0$ , renders the limit cycle of  $\langle O(t) \rangle$  exponentially stable. This follows directly by linearity from Eqs.(3.3), (3.7), Thm 2 and by noting that any finite sum of terms of the form  $x^n e^{-\alpha x}$  can always be bounded by  $e^{-\beta x}$  for some positive  $\beta$ . This fact is closely related to the guarantee that synchronisation occurs for generic initial conditions. Perturbations for which  $\text{Tr}(\delta\rho A) \neq 0$  generically change the amplitude and phase of the limit cycle due to the finite-dimensionality of the Hilbert space and linearity. This is an unavoidable implication of our results and constitutes an important fundamental difference between the time evolution of a quantum observable and a classical observable.

Secondly, stability to noise for classical synchronisation follows directly from exponential stability since classical noise may be understood as a random series of perturbations. Quantum mechanically, the influence of noise is fundamentally different as it generically induces decoherence and relaxation to stationarity. We have seen, by Thm 4 and the previous discussion of metastable synchronisation, that quantum synchronisation is stable to random noise/dissipation at least to the first order in perturbation strength. Moreover, in the quantum case, symmetry-selective noise is essential to induce synchronisation that is robust to the initial conditions. This is because, as we have seen, robust synchronisation occurs when the Lindblad operators, which represent the noise, sufficiently reduce the space of purely imaginary Liouvillian eigenstates to only those with the necessary symmetry.

Finally, in classical synchronisation, a perturbation can change the frequency of oscillations, but in a way that neither grows nor decays in time [143]. In our case, Thm 4 guarantees precisely this, and Prop 2 shows that when a perturbation anti-symmetrically breaks the synchronisation, the frequency is, counter-intuitively, one order more stable. This elucidates quantum synchronisation as a cooperative dynamical stabilisation phenomenon analogous to classical synchronisation.

### 3 Examples

We now analyse several examples, both new and from existing seminal literature of quantum synchronisation using our algebraic perspective and discuss the relevance of the results above. The first is a straightforward demonstration of how to anti-synchronise two qubits using a third ancilla qubit. While being an interesting result in its own right, since it has previously been implied that two qubits cannot synchronise in the sense of [145], this example should provide a pedagogical explanation of how our theory works. We will then explore the previously studied example of a driven-dissipative spin-1 pair which has previously been argued to display quantum synchronisation [144]. We will, in fact, show that the synchronisation is only metastable and not always robust to perturbations in the initial state. Finally, we will discuss the heated Fermi-Hubbard model, similar to that of Ch 4, and use this as a starting point to construct more general models which exhibit quantum synchronisation. This will also lead us to an experiment where our results can be directly applied and agree with the data.

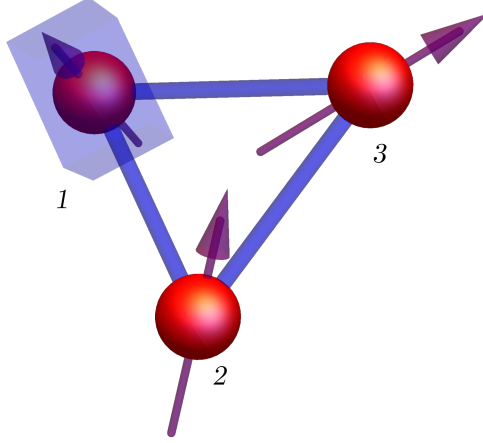


**Figure 5.3:** Anti-synchronising two spin-1/2 (sites 2, 3) via an effective non-Markovian bath. The ‘bath’ is the site 1 spin and the  $L = \gamma\sigma_1^-$  loss term (the blue box).

### 3.1 Anti-synchronising two spin-1/2s

In [145] it was argued that the smallest possible system that can be synchronised is a single spin-1 particle, although this result took a different notion of synchronisation and was later refuted by [358]. Here, using our theory, we show how it is possible to *anti-synchronise* two spin-1/2s through an effective non-Markovian bath.

Let  $\sigma_j^\alpha$ ,  $\alpha = +, -, z$ , be the standard Pauli matrices on the site  $j$ . Take any 3-site Hamiltonian which non-trivially couples the three sites, is symmetric under exchanging sites 2 and 3,

$$P_{2,3}HP_{2,3} = H, \quad (5.13)$$

and also conserves total magnetisation,

$$S^z = \frac{1}{2} \sum_j \sigma_j^z, \quad [H, S^z] = 0. \quad (5.14)$$

The Hamiltonian can then be decomposed into blocks of conserved total magnetisation. We consider the block with  $S^z = -\frac{1}{2}$  and consider the most general ansatz for an eigenstate in this block,

$$|\psi\rangle = \sum_j a_j |j\rangle, \quad (5.15)$$

where  $|j\rangle$  means there is a spin-up on site  $j$  and all other spins are down. Then to be an eigenstate with  $H|\psi\rangle = E|\psi\rangle$  we see,

$$H(P_{2,3}|\psi\rangle) = P_{2,3}HP_{2,3}P_{2,3}|\psi\rangle = P_{2,3}H|\psi\rangle = EP_{2,3}|\psi\rangle = E(P_{2,3}|\psi\rangle). \quad (5.16)$$

Thus

$$|\phi\rangle = |\psi\rangle - P_{2,3}|\psi\rangle = (a_2 - a_3)|2\rangle + (a_3 - a_2)|3\rangle, \quad (5.17)$$

is also an eigenstate of  $H$  with energy  $E$  and it has a node on site 1. Provided the Hamiltonian non-trivially couples the three sites, this state will be the unique eigenstate in the  $S^z = -1/2$  sector with a node on site 1. We may exploit this by introducing a pure loss Lindblad  $L = \gamma\sigma_1^-$  on site 1 as illustrated in Fig. 5.3. In this case we have two pure stationary states,

$$\rho_{1,\infty} = |0, 0, 0\rangle \langle 0, 0, 0|, \quad (5.18a)$$

$$\rho_{2,\infty} = \frac{1}{2}(|0, 0, 1\rangle - |0, 1, 0\rangle)(\langle 0, 0, 1| - \langle 0, 1, 0|), \quad (5.18b)$$

where as usual a 1 indicates a spin up while a 0 indicates a spin down. The  $A$  operator satisfying Thm 1 and giving rise to purely imaginary eigenvalues is the dark state coherence,

$$A = (|0, 0, 1\rangle - |0, 1, 0\rangle) \langle 0, 0, 0|, \quad (5.19)$$

and the corresponding frequency  $\omega$  will depend on the specific choice of the Hamiltonian.

Taking for example the XXZ spin chain,

$$H = \sum_{j=1}^3 \sigma_j^+ \sigma_{j+1}^- + \sigma_j^- \sigma_{j+1}^+ + \Delta \sigma_j^z \sigma_{j+1}^z + B \sigma_j^z, \quad (5.20)$$

with implied periodic boundary conditions, we have  $\omega = -1 + 2B - 4\Delta$ . Observe that there are persistent oscillations even in the absence of an external magnetic field caused by the interaction term,  $\Delta \sigma_j^z \sigma_{j+1}^z$ , which corresponds in the Wigner-Jordan picture<sup>1</sup> to a quartic term, picking out a natural synchronisation frequency. Since  $A$  is antisymmetric under exchanging sites 2 and 3, the oscillating coherences will also be antisymmetric. The symmetric stationary state  $\rho_{1,\infty}$  spoils perfect anti-synchronisation between site 2 and 3 by offsetting the equilibrium value. However, an observable that is zero in this state  $\text{Tr}(O_k \rho_{1,\infty}) = 0$ ,  $k = 2, 3$ , will be robustly and stably anti-synchronised  $\lim_{t \rightarrow \infty} \langle O_2(t) \rangle = -\lim_{t \rightarrow \infty} \langle O_3(t) \rangle$  with frequency  $\omega$ . A possible choice is the transverse spin  $O_k = \sigma_k^x$ ,  $k = 2, 3$ . This is demonstrated in Figure 5.4 where we measure both the  $\sigma_k^x$  observable and a randomly chosen Hermitian observable. This is yet another example where our definitions of synchronisation could be relaxed to allow for a fixed offset, and indeed we also show in Fig. 5.4 that the Pearson indicator classifies both observables as anti-synchronised.

Using this example, we can further link to previous studies of quantum synchronisation, which focused on limit cycles in phase space. In Figure 5.5 we plot the limit cycles of the second and third spins in the phase space defined by the usual Bloch sphere representation of a qubit. We see that the two limit cycles are perfectly out of phase, as expected for anti-synchronisation. We can also see clearly that the first site is not synchronised to either the first or second site since its phase space trajectory quickly decays to a fixed point rather than the common limit cycle of sites 1 and 2.

<sup>1</sup>See Appdx A for a description of the Jordan-Wigner mapping between fermions and spins.

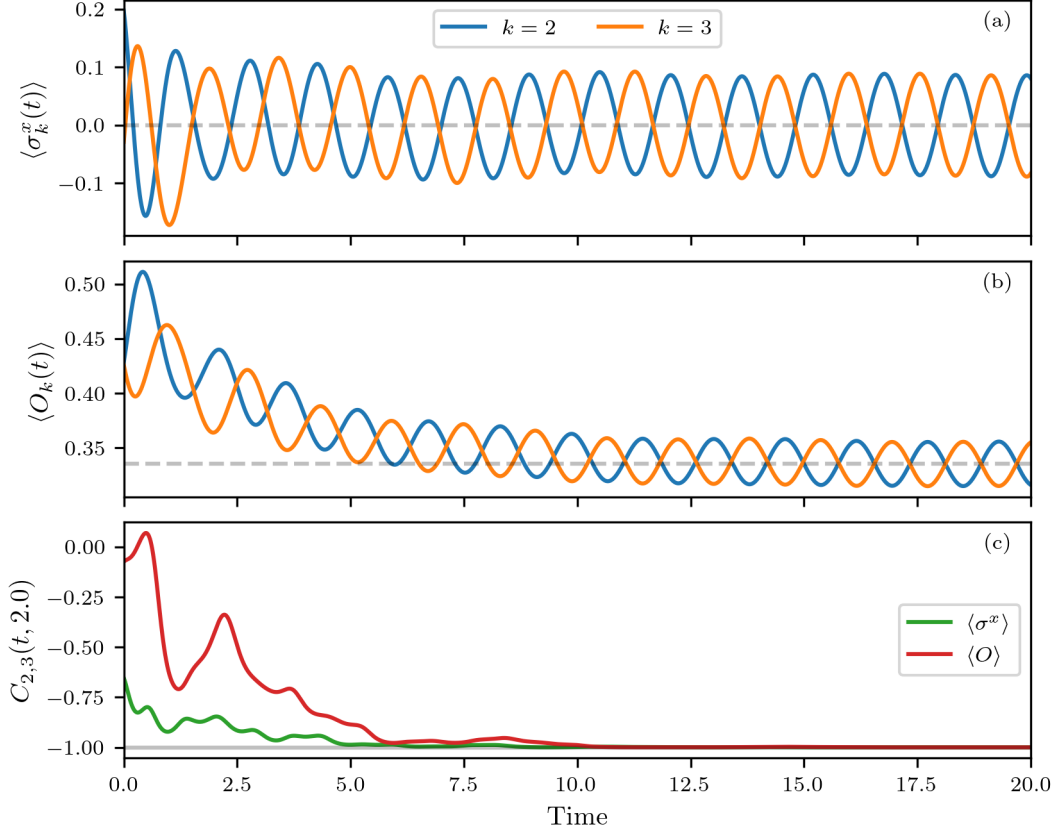


**Figure 5.4:** Evolution of the model described in Sec. 3.1 with parameters  $\Delta = 1$ ,  $B = 0.5$  and  $\gamma = 0.5$ . The system is initially described by a randomly chosen density matrix. In (a) we now compare the  $\sigma^x$  observable on each site and see perfect anti-synchronisation since  $\langle \sigma_1^z \rangle \rightarrow 0$  as  $t \rightarrow \infty$ . In plot (b) we compare a randomly generated Hermitian observable,  $O_k$  on sites 2 and 3. While they oscillate out of phase they have an offset equilibrium value which disrupts the perfect anti-synchronisation. In (c) we plot the Pearson indicator, defined in Eq. (5.1), for both the observable  $O_k$  and  $\sigma_k$  between sites 2 and 3. In both cases we see that after a transient period  $C \rightarrow -1$  indicating anti-synchronisation in this weaker notion.

### 3.2 Driven-dissipative spin-1 pair

We now explore the model of two weakly coupled, driven-dissipative spin-1 systems as previously studied in a synchronisation context by [144]. In the absence of environmental noise, two coupled spins, labelled  $A$  and  $B$ , evolve according to the Hamiltonian

$$H = \omega_A S_A^z + \omega_B S_B^z + \frac{i\epsilon}{2} (S_A^+ S_B^- - S_B^+ S_A^-), \quad (5.21)$$

where for convenience we define the detuning  $\Delta = \omega_A - \omega_B$ . We then consider the independent interactions of each spin with some external bath which, in the absence of spin-spin interactions, drives the spins towards their own non-equilibrium steady

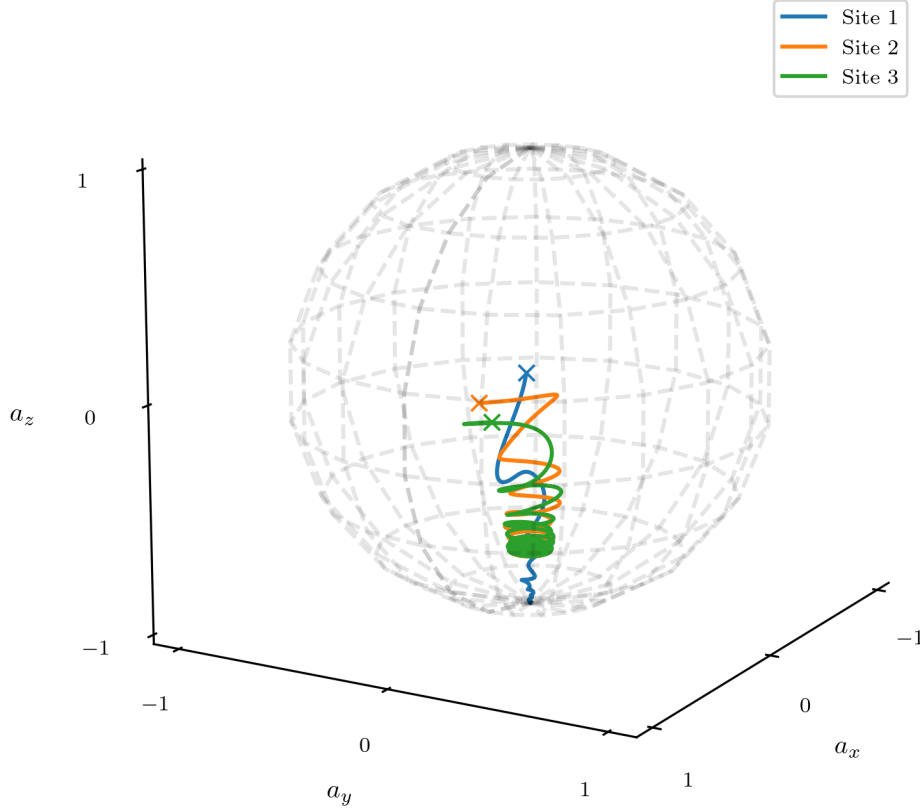


**Figure 5.5:** Bloch sphere representation of the evolution of the model described in Sec. 3.1 with parameters  $\Delta = 1$ ,  $B = 0.5$  and  $\gamma = 0.5$  and a randomly chosen initial state. We define the reduced density matrix for each site by taking the partial trace over the other sites,  $\rho_k = \text{Tr}_{A, B \neq k}(\rho)$ . We then find and plot the corresponding Bloch sphere representation,  $\mathbf{a}^{(k)}$  for the reduced states as  $\rho_k = \frac{1}{2}(\mathbb{1} + \mathbf{a}^{(k)} \cdot \boldsymbol{\sigma})$  where  $\boldsymbol{\sigma}$  are the usual Pauli matrices. The initial point of each trajectory is marked with a cross. We see the second and third sites reach a limit cycle which they orbit perfectly out of phase, while the first site rapidly decays to the  $\mathbf{a} = (0, 0, 1)$  point on the Bloch sphere. This demonstrates the anti-synchronisation between only sites 2 and 3. Note that since the reduced states are not pure, the trajectories live within the sphere not on the surface.

states. These system-bath interactions are modelled by the Lindblad operators

$$L_{u,j} = \gamma_j^u S_j^+ S_j^z, \quad L_{d,j} = \gamma_j^d S_j^- S_j^z, \quad j = A, B. \quad (5.22)$$

Using the theory we have developed, we will analyse three examples that were claimed by [144] to exhibit quantum synchronisation. The first example considers driving the two spins in opposite directions without any detuning, the second example introduces detuning but also takes the *quantum Zeno* limit of large driving, and the third considers driving two detuned spins in opposite directions.

### 3.2.1 Inverted limit cycle: metastable ultra-low frequency anti-synchronisation

We first analyse the so called inverted limit cycle. We take  $\Delta = 0$  and invert the driving on the two spins so that

$$\gamma_A^u = \gamma_B^d = \gamma, \quad \gamma_A^d = \gamma_B^u = \mu, \quad (5.23)$$

and consider the limiting case  $\mu \rightarrow 0$ . As in [144] the system is initialised in the state  $\rho(0) = \rho_A^{(0)} \otimes \rho_B^{(0)}$  where  $\rho_j^{(0)}$  is the NESS of spin  $j$  in the absence of spin-spin couplings. Thus we can consider this as a quench of the system where the weak spin-spin interactions are instantaneously turned on. We find that in the absence of spin-spin interactions, i.e  $\epsilon = 0$ , and with  $\mu = 0$ , the independent spins have degenerate stationary states

$$\begin{aligned} \rho_A^{(0)} &= p_A |0\rangle_A \langle 0|_A + (1 - p_A) |1\rangle_A \langle 1|_A, \\ \rho_B^{(0)} &= p_B |0\rangle_B \langle 0|_B + (1 - p_B) |-1\rangle_B \langle -1|_B, \end{aligned} \quad (5.24)$$

for  $p_j \in [0, 1]$ . This degeneracy is lifted as soon as  $\mu$  becomes strictly positive and we find  $p_A = p_B = 1$  in Eq. (5.24). Thus, to avoid this degeneracy and simplify discussions, in the following we consider  $\mu$  infinitesimally small but still strictly positive. Consequently we consider both  $\mu$  and  $\epsilon$  as perturbative parameters while  $\omega$ ,  $\gamma$  remain  $\mathcal{O}(1)$ .

To understand the evolution of the system it is sufficient to consider those eigenstates of  $\mathcal{L}$  which are excited by  $\rho(0)$ , and in particular which of these have eigenvalues with small real part compared to  $\omega$  and  $\gamma$ . We find that only 4 such eigenmodes are excited, with corresponding eigenvalues

$$\begin{aligned} \lambda &= 0, \quad -2\mu + \mathcal{O}(\mu^2, \epsilon^2, \epsilon\mu), \\ &\quad -\mu \pm 2i\epsilon + \mathcal{O}(\mu^2, \epsilon^2, \epsilon\mu). \end{aligned} \quad (5.25)$$

Of these, the relevant eigenvalues for synchronised oscillations are  $\lambda_{\pm} = -\mu \pm 2i\epsilon + \mathcal{O}(\mu^2, \epsilon^2, \epsilon\mu)$  since they are the only ones with a non-zero imaginary part at leading order. We conclude that this is an example of ultra-low frequency synchronisation since both the real and imaginary parts of  $\lambda_{\pm}$  are  $\mathcal{O}(\epsilon, \mu)$ . The consequences of this are shown in Figure 5.6a where we consider the  $S_j^Z$  observables. We see that the observable appears almost stationary on short time scales,  $t \sim \mathcal{O}(1)$ . When, in Figure 5.6b, we consider significantly longer timescales, however, we see the behaviour which we consider metastable synchronisation. We further find that the decay rate is inversely proportional to  $\epsilon^2$  at the next lowest order, as indicated in Prop 2. Consequently, there is only one power of  $\epsilon$  between the decay rate and the frequency of the signal unless  $\epsilon$  is sufficiently small that  $\mu > \epsilon^2$  in which case the decay rate is proportional to  $\mu$ . This example demonstrates why we generally discount ultra-low frequency dynamics since they are more difficult to observe experimentally.



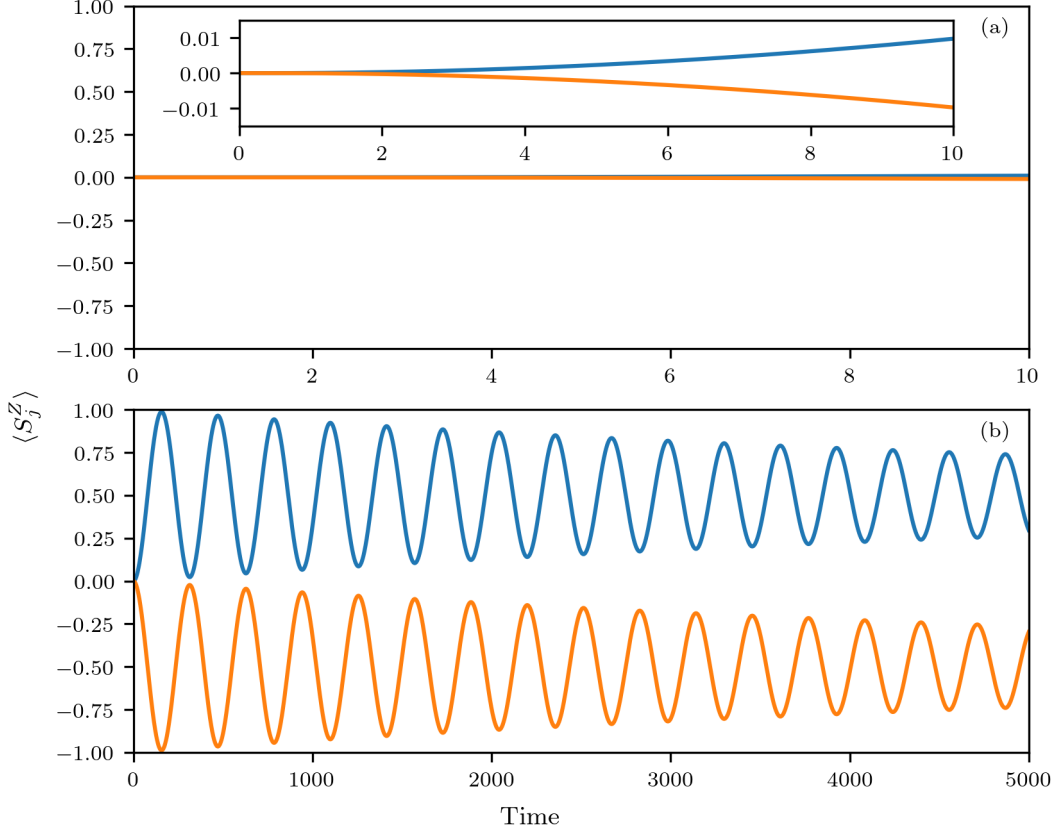


**Figure 5.6:** Evolution of  $S_j^z$  observable on sites  $A$  (blue) and  $B$  (orange) for the Spin-1 inverted limit cycle model with  $\omega = \gamma = 1$ ,  $\mu = 0.0001$ ,  $\epsilon = 0.01$ . In (a) we see over short time periods the observables are effectively stationary, as shown by the scale of the inset, while in (b) we see that over much longer time scales decaying oscillations can be measured. As per (5.25) the frequency of these oscillations is  $2\epsilon$ .

### 3.2.2 Inverted limit cycle: anti-synchronisation in the quantum Zeno limit

We again consider the same system as above, but now detuned,  $\omega_A \neq \omega_B$ , and with strong dissipation,  $\gamma_A^u = \gamma_B^d = \gamma \gg \omega_j, \epsilon$ . We find that the dissipation operator

$$\begin{aligned} \mathcal{D}[\rho] = & 2S_A^+ S_A^z \rho S_A^z S_A^- + 2S_B^- S_B^z \rho S_B^z S_B^+ \\ & - \{S_A^z S_A^- S_A^+ S_A^z, \rho\} - \{S_B^z S_B^+ S_B^- S_B^z, \rho\} \end{aligned} \quad (5.26)$$

has a stationary subspace with 16-fold degeneracy. Thus, when we lift the degeneracy of this subspace by introducing comparatively weak unitary dynamics, we introduce several eigenvalues with  $\mathcal{O}(1)$  imaginary parts and  $\mathcal{O}(1/\gamma)$  real parts as per the discussion in Ch 3 Sec 3. This leads to metastable dynamics on timescales relevant to the Hamiltonian.

Unlike the previous example, we find meta-stable anti-synchronisation of the  $S_j^z$  observables that is robust to initialising the system in arbitrary states. This

can be seen by noting that the eigenstates of the dissipation operator,  $\mathcal{D}$ , are coherences between the states

$$|0, 0\rangle, |1, -1\rangle, |0, -1\rangle, |1, 0\rangle. \quad (5.27)$$

Under strong dissipation, the system rapidly decays onto the space spanned by these eigenstates before the slower dynamics take over. Since this space spanned by coherences of the above eigenstates is invariant under the transformation

$$S_A^z \longleftrightarrow -S_B^z, \quad (5.28)$$

all dynamics within this space will satisfy  $\langle S_A^z(t) \rangle = -\langle S_B^z(t) \rangle$  regardless of the initial state and for any  $\omega_A, \omega_B, \epsilon \ll \gamma$ . However, we can easily see that the system is not completely anti-synchronised because if we measure the observable  $O_j = |-1\rangle\langle -1|_j$  we see in Figure 5.7b that  $\langle O_A(t) \rangle$  oscillates, while  $\langle O_B(t) \rangle$  rapidly becomes stationary.

### 3.2.3 Pure gain: stable limit cycles, but no robust, stable synchronisation

We now set  $\gamma_j^d = 0$ ,  $\gamma_A^u \neq \gamma_B^u \neq 0$ , although clearly the results are analogous if we instead choose to have pure loss. In that case we find three proper (density operator) stationary states,

$$\begin{aligned} \rho_{1,\infty} &= |-1, 0\rangle\langle -1, 0| \\ &\quad + \frac{i\epsilon}{\omega_A - \omega_B} (|-1, 0\rangle\langle 0, -1| - |0, -1\rangle\langle -1, 0|), \end{aligned} \quad (5.29a)$$

$$\rho_{2,\infty} = |-1, -1\rangle\langle -1, -1|, \quad (5.29b)$$

$$\rho_{3,\infty} = \frac{1}{2} (|0, -1\rangle\langle 0, -1| + |-1, 0\rangle\langle -1, 0|). \quad (5.29c)$$

Solving for the conditions of Thm 1 we find  $A$ -operators given by,

$$\begin{aligned} A_1 &= a_1 |-1, -1\rangle\langle -1, 0| \\ &\quad + i(a_2 - a_3) |-1, -1\rangle\langle 0, -1|, \end{aligned} \quad (5.30a)$$

$$A_2 = A_1^T, \quad (5.30b)$$

$$\begin{aligned} A_3 &= -i(a_2 + a_3) |-1, 0\rangle\langle -1, 0| \\ &\quad + a_1 |-1, 0\rangle\langle 0, -1| \\ &\quad - a_1 \frac{a_2 + a_3}{a_3 - a_2} |0, -1\rangle\langle -1, 0| \\ &\quad + i(a_2 - a_3) |0, -1\rangle\langle 0, -1|, \end{aligned} \quad (5.30c)$$

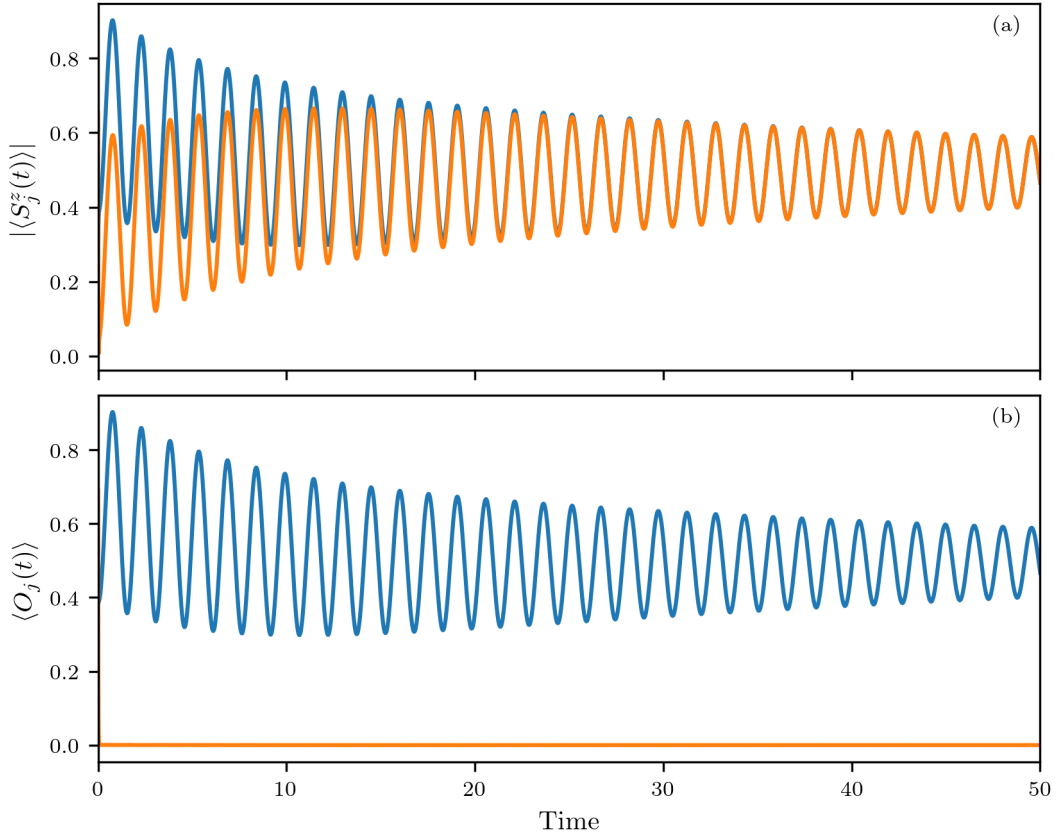


**Figure 5.7:** (a) Metastable anti-synchronisation of  $\langle S_j^Z(t) \rangle$  (note we plot the absolute values) in the inverted limit cycle model in the quantum Zeno limit with  $\gamma = 100$ ,  $\mu = 0$ ,  $\omega_A = 0.5$ ,  $\omega_B = 1.5$  and  $\epsilon = 2$  where the system has been initialised in a random initial state. The blue line indicates site  $A$  and the orange site  $B$ . (b) The dynamics of the observables  $O_j = |-1\rangle\langle -1|_j$  which do not synchronise. The metastable dynamics can be understood as a consequence of the unitary dynamics lifting the degeneracy in the stationary subspace of the dissipation. Comparison with Fig. 5.6 shows that in the Zeno limit the oscillations are now on timescales relevant to the Hamiltonian.

where  $a_1 = 2\epsilon$  and  $a_2 = (\omega_A - \omega_B)$ ,  $a_3 = \sqrt{4\epsilon^2 + (\omega_A - \omega_B)^2}$ . The corresponding frequencies are,

$$\omega_1 = \frac{1}{2}(\omega_A + \omega_B - a_3), \quad (5.31a)$$

$$\omega_2 = \frac{1}{2}(\omega_A + \omega_B + a_3), \quad (5.31b)$$

$$\omega_3 = a_3. \quad (5.31c)$$

There is no permutation or generalised symmetry between sites  $A$  and  $B$  and so although we do have persistent oscillations and a limit cycle the sites are not robustly synchronised as seen in Fig. 5.8.

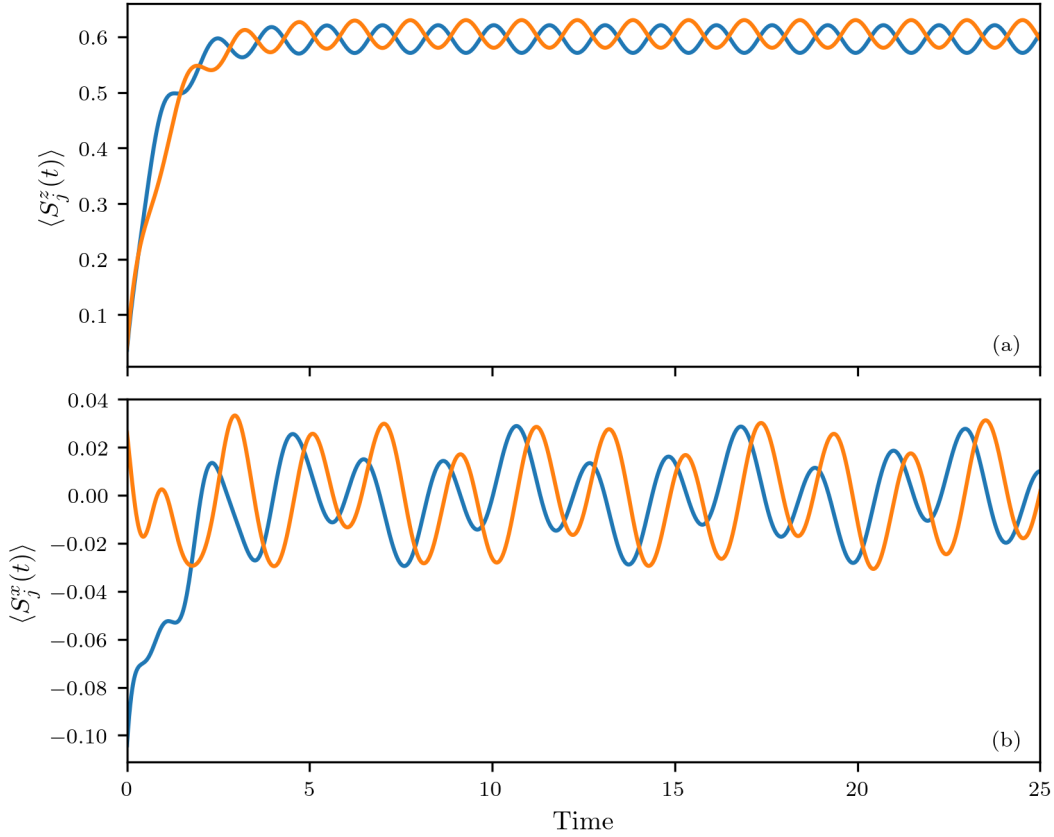


**Figure 5.8:** Evolution of  $S_j^z$  (a) and  $S_j^x$  (b) observables on sites  $A$  (blue) and  $B$  (orange) for the Spin-1, pure gain model. We have non-zero detuning and interaction,  $\Delta, \epsilon \neq 0$  and asymmetric driving,  $\gamma_A^u \neq \gamma_B^u$ . Initialising the system in a random state, we see that while persistent dynamics occur the two sites do not identically synchronise for either observable. This can be understood through the absence of generalised symmetry between sites  $A$  and  $B$ . As with the example in Sec 3.1, under a more relaxed definition the observables  $S_j^z$  could be considered synchronised.

### 3.3 Lattice models with translationally invariant non-abelian symmetries

The examples studied above have considered small systems and have been presented to demonstrate the definitions we gave and show pedagogically how our results can be applied. We will now use our results to understand synchronisation in a broad class of truly many-body models. These systems will exhibit robust stable/meta-stable synchronisation between every individual site as a direct consequence of their symmetry structure. We first discuss the heated Fermi-Hubbard model as a base case and then explore its generalisations to multi-band and higher spin versions before commenting on how the theory we have developed can be applied to existing experimental setups. We will also explain how systems can be engineered using our theory to create long-lived synchronisation.

### 3.3.1 Fermi-Hubbard model with spin agnostic heating

We first return to the Fermi-Hubbard model with spin-agnostic Lindblad operators, which we previously studied in Ch 4. This model was interesting in the previous context of dissipative time crystals because of the environmental noise-induced periodic motion from a model that otherwise evolved chaotically. We will now demonstrate that it additionally exhibits robust, stable synchronisation across all the sites.

Recall that our Hamiltonian is given by

$$H = - \sum_{\langle i,j \rangle} \sum_{s \in \{\uparrow, \downarrow\}} (c_{i,s}^\dagger c_{j,s} + \text{h.c.}) + \sum_j U_j n_{j,\uparrow} n_{j,\downarrow} + \sum_j \epsilon_j n_j + \frac{B_j}{2} (n_{j,\uparrow} - n_{j,\downarrow}) \quad (5.32)$$

and we introduce Lindblad operators

$$L_j^- = \gamma_j^- c_{j,\downarrow} c_{j,\uparrow} \quad (5.33a)$$

$$L_j^+ = \gamma_j^+ c_{j,\uparrow}^\dagger c_{j,\downarrow}^\dagger \quad (5.33b)$$

$$L_j^z = \gamma_j^z n_j, \quad (5.33c)$$

on each site. Compared with our previous treatment in Ch 4 we have now included on-site dephasing through the  $L_j^z$  terms which importantly do not affect the strong dynamical symmetry structure of the model. These Lindblad operators represent the dominant standard 2-body loss, gain and dephasing processes, naturally realised in optical lattice setups [302, 359–363].

As we discussed before, when the magnetic field is homogeneous,  $B_j = B$ , the total spin raising operator  $S^+ = \sum_j c_{j,\uparrow}^\dagger c_{j,\downarrow}$  is a strong dynamical symmetry with,

$$[H, S^+] = BS^+, \quad [L_j^\alpha, S^+] = 0. \quad (5.34)$$

For  $\gamma_j^- = \gamma_j^+$  we also have

$$\sum_{\alpha,j} [L_j^\alpha, (L_j^\alpha)^\dagger] = 0, \quad (5.35)$$

so we find the map is unital. Provided that  $S^+$  and its conjugate  $S^-$  are the only operator satisfying the conditions of Thm 2, as is generically the case unless  $\gamma_j^- = \gamma_j^+ = \gamma_j^z = 0$ , we may apply Thm 7 and conclude that every site is stably, robustly synchronised with every other site because  $S^+$  and  $S^-$  have complete permutation invariance. We remark that the on-site potentials,  $\epsilon_j$ , and interactions,  $U_j$ , need not be the same in this case. This explicitly demonstrates how our theory can be applied non-perturbatively to non-identical subsystems. As with the dissipative time crystal case discussed before, metastability can be achieved by, for example, allowing detuning between the on-site magnetic field and considering perturbations from the average value  $\bar{B}$ , i.e. taking  $B_j = \bar{B} + \delta_j$ , or by introducing weak next-nearest neighbour interactions. We illustrate these principles in Fig 5.9.

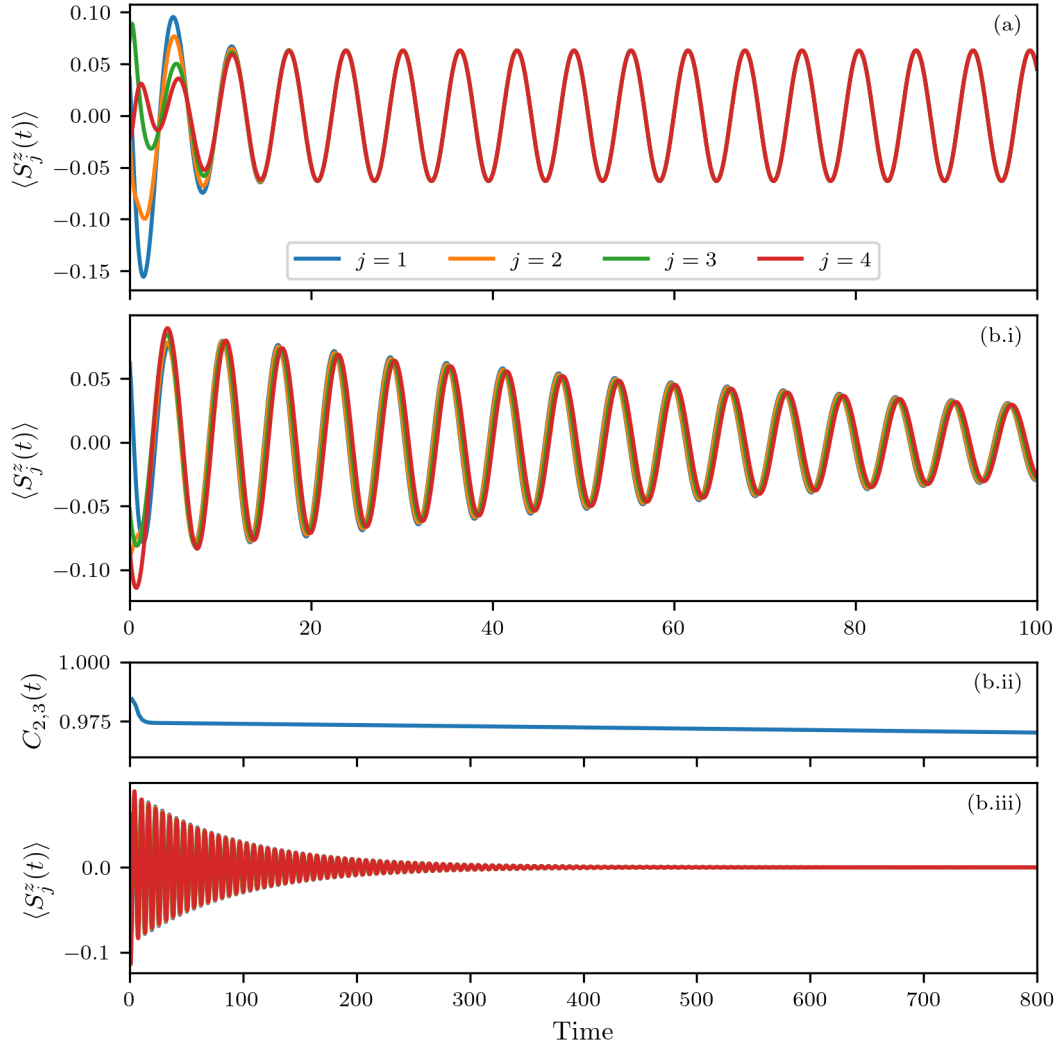


**Figure 5.9:** (a) We plot the transverse spin on each site of a 4-site Fermi-Hubbard model periodic boundary conditions, spin agnostic heating and a homogeneous magnetic field when evolved from a random initial state, and observe complete stable robust synchronisation. (b) We perturb the same system by introducing random spatial inhomogeneities in the magnetic field. In (b.i) we plot the transverse spin and observe that the perfect synchronisation is broken and that the oscillations are metastable. In (b.iii) we show this decay more clearly over longer times and in (b.ii) show the slow decay of the Pearson indicator between sites 2 and 3.

### 3.3.2 An algebraic framework for constructing models which exhibit quantum synchronisation

The heated Fermi-Hubbard model above hints at a general framework to construct more elaborate examples of systems that exhibit quantum synchronisation based on their symmetry structure. To understand this we make the following observations:

- (i) In the absence of a magnetic field and potential,  $B_j = \epsilon_j = 0$ , the Hubbard model has a symmetry group  $G = SU(2) \times SU(2)/\mathbb{Z}_2$ , coming from the

independent spin and  $\eta$  symmetries [311].

- (ii) Further, the representation of these symmetries are permutation invariant, that is

$$[S^\alpha, P_{j,k}] = [\eta^\alpha, P_{j,k}] = 0, \quad \alpha = x, y, z.$$

- (iii) Introduction of the magnetic field,  $BS^z$ , which corresponds to the unique element of the Cartan subalgebra of the spin- $SU(2)$  symmetry, breaks the spin symmetry. Consequently, the remaining elements,  $S^+$ ,  $S^-$  of the spin- $\mathfrak{su}(2)$  algebra become dynamical symmetries.
- (iv) Choosing a unital set of Lindblad operators,  $L_\mu$ , from the complementary  $\eta$  symmetry guarantees that  $[L_\mu, S^\pm] = 0$  so that the spin operators are strong dynamical symmetries as required for Thm 2. Also, since the choice of Lindblad operators do not all commute with the  $\eta^\alpha$  operators, there can be no further strong dynamical symmetries. Finally, since these strong dynamical symmetries have complete permutation invariance the synchronisation is robust, as per Cor 3.

These principles can be applied more widely to models with more elaborate symmetry structures to guarantee quantum synchronisation. In the following section, we will follow this framework to explore synchronisation in generalised  $SU(N)$  models, which have previously been explored in cold atoms [364–367].

### 3.3.3 Generalised Fermi-Hubbard model with $SU(N)$ symmetry and experimental applications

For concreteness, we will first consider the model studied in [367] describing fermionic alkaline-earth atoms in an optical lattice. These atoms are often studied as they have a meta-stable  $^3P_0$  excited state, which is coupled to the  $^1S_0$  ground state through an ultra-narrow doubly-forbidden transition [368]. We will refer to these levels as  $g$  (ground) and  $e$  (excited). We will further label the nuclear Zeeman levels as  $m = -I, \dots, I$  on-site  $i$ , where  $N = 2I + 1$  is the total number of Zeeman levels of the atoms. For example,  $^{87}\text{Sr}$  has  $N = 10$ . It is further known that in these atoms, the nuclear spin is almost completely decoupled from the electronic angular momentum in the two states  $\{g, e\}$  [368]. Thus to a good level of approximation, one can describe a system of these atoms in an optical trap using a two-orbital single-band Hubbard Hamiltonian [367],

$$\begin{aligned} H = & - \sum_{\langle i,j \rangle} \sum_{s,m} J_s (c_{i,s,m}^\dagger c_{j,s,m} + c_{j,s,m}^\dagger c_{i,s,m}) \\ & + \sum_{j,s} U_{ss} n_{j,s} (n_{j,s} - 1) + V \sum_j n_{j,g} n_{j,e} \\ & + V_{ex} \sum_{j,m,m'} c_{j,g,m}^\dagger c_{j,e,m'}^\dagger c_{j,g,m'} c_{j,e,m}. \end{aligned} \quad (5.36)$$

Here the  $c_{i,s,m}$  operator annihilates a state with nuclear spin  $m$  and electronic orbital state  $s \in \{g, e\}$  on site  $i$ . Further  $n_{j,s} = \sum_m c_{j,s,m}^\dagger c_{j,s,m}$  counts the number of atoms with electronic orbital state  $s$  on site  $j$ . This model assumes that the scattering and trapping potential are independent of nuclear spin, which gives rise to a large  $SU(N)$  symmetry.

Defining the nuclear spin permutation operators as

$$S_n^m = \sum_{j,s} c_{j,s,n}^\dagger c_{j,s,m}, \quad (5.37)$$

which obey the  $SU(N)$  algebra,

$$[S_n^m, S_q^p] = \delta_{mq} S_n^p - \delta_{np} S_q^m, \quad (5.38)$$

we find that the Hamiltonian in equation (5.36) has full  $SU(N)$  symmetry,

$$[H, S_n^m] = 0 \quad \forall n, m. \quad (5.39)$$

We can also introduce the electron orbital operators as,

$$T^\alpha = \sum_{j,s,s',m} c_{j,s,m}^\dagger \sigma_{ss'}^\alpha c_{j,s',m}, \quad (5.40)$$

where  $\alpha = x, y, z$  and  $\sigma^\alpha$  are the Pauli matrices in the  $g, e$  basis. These operators obey the usual  $SU(2)$  algebra and are independent of the nuclear spin operators,  $[T^\alpha, S_n^m] = 0$ . In the specific case  $J_e = J_g$ ,  $U_{ee} = U_{gg} = V$ ,  $V_{ex} = 0$  these are also a global symmetry of the system,  $[H, T^\alpha] = 0$ .

If we now introduce dephasing of the nuclear spin levels via the on-site Lindblad operators

$$L_j^{(m)} = \gamma_j^{(m)} S_m^m \quad (5.41)$$

we break the  $SU(N)$  nuclear-spin symmetry, while the electronic orbital symmetry is promoted to a strong symmetry [111] since the operators  $T^\alpha$  all commute with the Lindblad operators. This may be accomplished experimentally by scattering with incoherent light that does not distinguish between various energy levels of the internal degree of freedom  $s$  [359, 369]. In particular, this represents the fact that the light has transmitted information to the environment about the location of an atom, but not its internal degree of freedom that remains coherent. The rates  $\gamma_j^{(m)}$  can be made larger by introducing more light scattering.

In the presence of a field that only couples to the electronic degrees of freedom,

$$H_{\text{field}} = \omega T^z \quad (5.42)$$



the electronic orbital  $SU(2)$  symmetry is broken to a dynamical symmetry with frequency  $\omega$ . Since the  $T^\pm$  operators are translationally independent, all the conditions of Cor 3 are satisfied to guarantee robust, stable synchronisation between all pairs of sites.

In realistic setups, this strict symmetry structure is unlikely to be perfectly maintained. In particular, certain cold atom species may have a finite exchange term  $V_{ex}$  between the spin levels, e.g. [370, 371]. Thus we would expect metastable synchronisation to be present when the conditions  $J_e = J_g$ ,  $U_{ee} = U_{gg} = V$ ,  $V_{ex} = 0$  do not hold perfectly or there are some inhomogeneities in the additional field. More generally, we could consider cases of interacting systems where the nuclear and electronic degrees of freedom are coupled through scattering processes, such as in the experiment conducted by [372]. Generically such systems will lack the symmetries required for robust, stable quantum synchronisation, and thus the timescale over which synchronisation can be maintained will be a measure of how much these symmetries are broken through these imperfections.

One possible approach for achieving metastable synchronisation in more complex systems is to proceed as follows. Ignoring interactions, we can diagonalise the single site Hamiltonians to obtain eigenstates  $|n\rangle_j$  and energy levels  $E_{n,j}$  for each site,  $j$ . These give trivial onsite dynamical symmetries  $A_j^{n,m} = |n\rangle\langle m|_j$  for  $E_{n,j} \neq E_{m,j}$ . We then introduce dephasing operators on each site which break all but a few of these dynamical symmetries. When we reintroduce interactions between neighbouring sites, we search for translationally invariant linear combinations of the remaining on-site strong dynamical symmetries, which are as close as possible to dynamical symmetries of the whole model. These linear combinations can, in principle, be further optimised by adjusting the experimental parameters of the system. These considerations emphasise the importance of our theory when engineering long-lived synchronisation in more complex systems. Our theory tells us that in order to produce quantum systems that exhibit long-lived synchronisation, it is the symmetries that must be carefully controlled.

Another aspect of our theory that can be applied to these more complicated systems, even if they do not admit the symmetries required for synchronisation, is to give the scalings of decay rates and frequencies of the meta-stable oscillations. As an example we consider the experimental set up investigated by [372, 373], where fermionic atoms with nuclear spin-9/2 were confined to a deep optical lattice. In their experiment they initialised the system so that every site contained two atoms, one with  $m = 9/2$  and the second with  $m = 1/2$ , and observed oscillations across the whole system between this initial state and the state in which the two atoms had spins  $m = 7/2$  and  $m = 3/2$ . These oscillations were most pronounced in the limit where the optical lattice was very deep, corresponding to minimal hopping. It

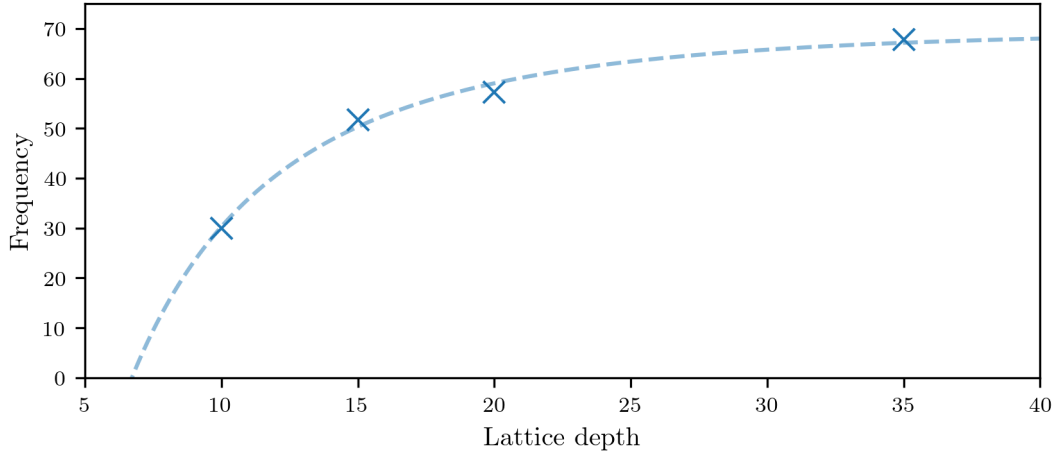


**Figure 5.10:** The crosses mark the experimental results from [372] for the oscillation frequencies of an effective 1D lattice of fermionic spinor atoms. We compare the experimental data (crosses) with the prediction (dashed line) of Eq. (5.45) where  $\omega_0$  and  $\lambda$  are obtained by fitting to the data, and see remarkable agreement.

is known that deep optical lattices can often cause dephasing processes to occur, so it is likely that in the limit of no hopping, the system also experiences strong dephasing processes. Thus we apply the results of Ch 3 Sec 3.1 to predict that as the trap becomes shallower the frequency should vary as,

$$\omega = \omega_0 + \frac{\lambda}{\gamma} + o(1/\gamma) \quad (5.43)$$

for some constant  $\lambda$ , where  $\gamma = U/J$  is the ratio between the interaction strength and the hopping. This ratio is known to be related to the lattice depth in a 1D sinusoidal lattice in the deep lattice limit as [362],

$$\gamma \sim \exp\left(\sqrt{V_0}\right) \quad (5.44)$$

for  $V_0$  the lattice depth, measured in units of  $E_r$ . The 1D approximation is valid because the other two dimensions of the optical lattice are kept at very deep values  $V_{\perp} = 35E_r$  [372]. Thus we obtain

$$\omega(V_0) = \omega_0 + \lambda \exp\left(-\sqrt{V_0}\right). \quad (5.45)$$

We compare this prediction with the experimental data from [372] in Fig 5.10. This simple result appears to be in better agreement with the experimental measurements than the numerical simulations in [372].

## 4 Conclusions

This chapter builds upon the results from Ch 3 regarding Liouvillian eigenvalues to present a general theory of spontaneous synchronisation in many-body quantum systems. The advantage of this theory is that it provides an algebraic framework based primarily on dynamical symmetries from which to study quantum synchronisation in many-body systems systematically.

We used this theory to study several examples, both new ones and from existing literature, and to provide a framework for algebraically constructing models which exhibit synchronisation. We also discussed how these results relate to experimental setups and demonstrated why robust quantum synchronisation requires careful engineering and symmetry selective controlling of experimental imperfections. Apart from higher symmetry fermionic quantum gases, similar considerations can also be directly applied to other complex cold atom systems with high degrees of symmetry and a large number of degrees of freedom, such as quantum spinor gases [374–376]. This demonstrates how our theory provides a guideline for achieving synchronisation that would be difficult to predict without resorting to using our algebraic perspective.

Our results provide several illuminating insights which are helpful for generating models that exhibit synchronisation. The first is that the most straightforward way to synchronise quantum many-body systems is to use unital maps, most obviously dephasing. This is because we may reduce the problem to eliminating dynamical symmetries that lack the required permutation symmetry structure for synchronisation. Our results also indicate the importance of interactions. For instance, if a model has only quadratic ‘interacting’ terms corresponding to hopping or on-site fields, dynamical symmetries that are not translationally invariant are possible [120]. In particular free-fermion models admit a host of non-translationally invariant conservation laws and these ruin the translation invariance in the long-time limit [286]. Adding interactions generally leaves only translationally invariant  $A$  operators.

Interestingly, there has been recent debate about the related phenomenon of limit cycles in driven-dissipative systems with finite local Hilbert space dimensions, particularly spin-1/2 systems. Mean-field methods find evidence of limit cycles [171], whereas when quantum correlations are included using numerical methods, studies seem to indicate an absence of limit cycle phases in the same models [377, 378]. Alternative methods [379], however, do show limit cycles in the fully quantum system, making the issue controversial. Since limit cycles correspond to persistent dynamics and purely imaginary eigenvalues of the corresponding quantum Liouvillians, our general algebraic theory, particularly the results from Ch 3, should apply to these systems and could be used to prove either presence or absence of limit cycles.

We also remark again that it would be very desirable to develop corresponding results to those of Ch 3 for periodically driven open systems. In the synchronisation context, such results would allow us to study driven synchronisation which is the natural next step having characterised sponanteous synchronisation in many body systems. This could also lead to connection between our theory and the field of Synergetics. As we mentioned in Ch 4 recent results of [277] have made progress in this direction but much work still remains to be done.

# 6

## Engineering superconductivity through symmetries

Used in cutting edge physical experiments such as particle accelerators, tokamaks, and quantum computers, as well as more widely in MRI machines and maglev trains, superconducting materials are at the heart of all manner of modern technologies. Unfortunately, current superconducting materials only transition to their superconducting phase in extreme conditions such as very low temperatures or very high pressures. Even the more recent ‘high- $T_c$ ’ superconductors have a critical temperature of  $-170^\circ\text{C}$  at atmospheric pressure, and the cost of cooling to such temperatures renders many novel applications prohibitively expensive.

As a potential solution, there has been substantial interest in studying ‘induced’ superconductivity, where the superconducting material transitions to its superconducting phase in response to some stimulation. In particular, certain materials have been demonstrated to exhibit superconducting properties well above their critical temperature after being excited by laser driving.

This chapter will propose a theory to explain these recent experimental results. Our explanation will rely only on well-established principles of quantum thermalisation and the existence of an approximate electron pairing symmetry which is often present in lattice models of strongly interacting electrons. We will then use our ideas to propose a mechanism for stabilising the superconducting state, which relies, counter-intuitively, either on the system’s interaction with an environment or external driving. While not all aspects of the theory have been rigorously proven or tested, and there are still unanswered questions, we will argue that our proposed theory gives verifiable agreement with experiments and provides an explanation that can be applied to most known examples of light-induced superconductivity.

# 1 Conventional vs. light-induced superconductivity

Superconductivity was one of the earliest observed macroscopic quantum phenomena, first studied by Onnes in 1911 when he found that the electrical resistance of mercury vanishes below 4.2 K [139]. In 1957, Bardeen, Cooper, and Schrieffer presented their explanation of superconductivity in terms of Cooper pairs and their interactions with lattice phonons [140]. Their theory accurately describes what is now referred to as *conventional superconductivity* which occurs at temperatures  $T \lesssim 10$  K.

Materials in a superconducting phase have two fundamental properties, which both have substantial technological benefits. Firstly the electrical resistivity of a superconducting material vanishes, as originally witnessed by Onnes. This has clear applications for the lossless transmission of electrical energy, particularly at high power. The vanishing resistivity of superconducting wires has also been exploited to develop superconducting magnets. These are electromagnets made from coils of superconducting wires, which can carry much higher currents than conventional wires and thus generate a more intense magnetic field. Secondly, weak magnetic fields cannot penetrate a superconducting material and instead, they remain at the surface. This phenomenon, known as the Meissner effect, was first observed by Meissner and Ochsenfeld in 1933 [380] and is understood through the London equation for the penetration depth [381]. The Meissner effect has been used to create frictionless bearings [382, 383] and mounts which reduce vibrations [384].

Unfortunately, conventional superconductors only transition to their superconducting phase at very low temperatures or very high pressures, severely limiting their application. Even so-called ‘high-temperature’ superconductors, which are beyond the regime of BCS theory, have a critical temperature of around 80 - 100 K. This is still too low for most applications due to the high cost of cooling. Consequently, there has been a sustained effort to develop novel materials that become superconducting at room temperatures and pressures, possibly after some stimulation protocol. One successful line of research in this direction has been light-induced superconductivity, where transient out-of-equilibrium superconducting states are excited via light driving at temperatures above  $T_c$  [385–389].

The experiments we consider excite the sample material using short laser pulses with drive times of approximately 10-100 fs. Following the short pulse, reflectivity is probed using THz laser pulses, which can be directly connected to the optical conductivity via Drude-Lorenz theory. It is signatures in the optical conductivity that are usually used to determine whether or not the sample material is in a superconducting state. The sample materials that provide the best superconducting response have been found to be cuprates, or certain organic salts [388, 390–393].

In these experiments, signatures of superconductivity at temperatures much higher than  $T_c$  were observed for an unexpectedly long time. For instance, a recent experiment in an organic  $K_3C_{60}$  found lifetimes on the order of milliseconds at a temperature  $T = 100\text{K} > T_c = 20\text{K}$  [387]. For comparison, electrons in normal matter usually have energies around 10eV, which corresponds to attosecond durations, while the screened hopping times are on the order of picoseconds. Hence the superconducting state has a lifetime far longer than the relevant Hamiltonian time scales of the electrons. This behaviour also seems to contradict theoretical results regarding thermalisation [35, 318, 394], which predicts thermalisation within 1-2 orders of magnitude of the hopping times for a spatially homogenous out-of-equilibrium state, and that the thermalised state should not be superconducting. Even considering the fact that the laser pulse is not homogenous in space but has a wavelength of  $1\text{ }\mu\text{m}$ , an electron needs at most  $10^3\text{ ps}$  to “smooth out” the inhomogeneity. The experimental evidence suggests that thermalisation seems to be delayed by between one to eight orders of magnitude depending on the material, and explanations for this have so far been lacking.

Surprisingly, these results have been observed in various compounds, all at significantly higher temperatures than critical, indicating that the phenomenon results from general mechanisms with minimal dependence on the microscopic details. Unfortunately, the transient superconducting states do not yet last long enough to have technological applications. Understanding the general underlying mechanism which governs these experiments has so far been challenging theoretically but is of crucial importance for achieving a superconducting state at high temperature that is stable for useful lifetimes. Several arguments have been previously proposed to explain these experiments, primarily based on diagrammatic field theory calculations [395] and numerical simulations [396, 397]. While these methods have provided reasonable explanations for some of the observed phenomena, they are still unsatisfactory in several ways. Firstly, the models corresponding to the materials examined have strongly repulsive electronic structure making the validity of the perturbation theory used in diagrammatic field theory calculations questionable. Further, most numerical calculations assume charge conservation, but as we will argue in Sec 2.2 below, due to locality out-of-equilibrium protocols cannot both conserve electron number and induce the off-diagonal long-range order thought to be responsible for superconductivity if the system is initially in a clustering state [398]. Another approach that proved fruitful in our understanding of ordinary superconductivity is density functional theory [399, 400]. However, its application and domain of validity are not precisely understood out of equilibrium.

## 2 Theoretical background

Before expounding our theory and explaining its relation to the experiments, we first review some technical background. In particular, why off-diagonal long-range order (ODLRO) and  $\eta$ -pairing are generally believed to be related to superconductivity and also some fundamental principles of prethermalisation and their consequences for ODLRO and superconductivity.

### 2.1 ODLRO and superconductivity

The relation between off-diagonal long-range order and superconductivity was first understood by Yang in his 1962 work [401] where he directly showed that ODLRO implies magnetic flux quantisation - a hallmark of superconductivity. This result has been confirmed and extended in subsequent studies to also include the prediction of the Meissner effect [402–404]. ODLRO in a fermionic system is understood as long-range order in the two-body correlation matrix, i.e.

$$\langle c_{i,\uparrow}^\dagger c_{i,\downarrow}^\dagger c_{j,\uparrow} c_{j,\downarrow} \rangle = \text{Const.} \quad \forall i, j, \quad (6.1)$$

where  $c_{i,s}$  annihilates a fermion on site  $i$  with spin  $s$ . Importantly the sites  $i$  and  $j$  can be arbitrarily far apart. Note that the operators

$$\eta_i^+ = e^{i\theta_i} c_{i,\uparrow}^\dagger c_{i,\downarrow}^\dagger, \quad \eta_i^- = -e^{-i\theta_i} c_{i,\uparrow} c_{i,\downarrow}, \quad (6.2)$$

are associated with  $\eta$ -symmetry in single band Fermi-Hubbard models, where the phases  $\theta_i$  depend on the lattice geometry. For this reason ODLRO in fermionic models is often referred to as  $\eta$ -pairing.

In his 1986 paper [405], Yang showed that there exist eigenstates of the 1D Hubbard model that exhibit ODLRO. These states are given by

$$|\eta^N\rangle \propto \left(\eta^+\right)^N |0\rangle, \quad (6.3)$$

where

$$\eta^+ = \sum_k \eta_k^+, \quad (6.4)$$

is the global  $\eta^+$  operator, and  $|0\rangle$  is the vacuum state. Unfortunately, these states are highly excited, and their long-range order is usually undetectable by experiments that study thermal or ground state properties. However, many subsequent studies have explored  $\eta$ -pairing superconductivity in the Hubbard and similar models, and it is generally accepted that  $\eta$ -pairs can be a valid mechanism for superconductivity provided they can be excited and sustained for sufficiently long times. We finally note that finite Drude weight in superconductors has only been demonstrated under additional model-specific assumptions, such as in standard BCS theory [406] and that Meissner stiffness (implying supercurrent) and the Drude weight (implying ballistic transport) are not the same quantity [407, 408].



## 2.2 Prethermalisation

As we discussed in Ch 1, following a quench, quantum systems are generically expected to thermalise via the eigenstate thermalisation hypothesis (ETH) [35, 38, 39]. However, in cases where the microscopic Hamiltonian has a separation of scales, it is possible that the system first prethermalises on short time scales up to  $t < \tau_{\text{pre}}$  before thermalising fully at times  $t \gg \tau_{\text{pre}}$ .

More specifically consider a Hamiltonian of the form

$$H = H_0 + \gamma H_1, \quad (6.5)$$

where  $\gamma$  is a perturbative parameter that separates the time scales of  $H$ . Provided the thermalisation time of  $H_0$  is not too long the system will equilibrate under  $H_0$  and reach a prethermal state described by  $\rho_{\text{pre}}$  which lasts for times  $t < \tau_{\text{pre}}$ . The time  $\tau_{\text{pre}}$  is controlled by the parameter  $\lambda$  and generically given by [394]

$$\tau_{\text{pre}} = \mathcal{O}(1/\gamma^2). \quad (6.6)$$

Note that when we say the system is described by the prethermal state  $\rho_{\text{pre}}$  we mean this in the usual sense that a Gibbs ensemble can be used to accurately describe observables of a thermalised system even if the true quantum state remains pure. It is generally expected that the prethermal state is given by a generalised Gibbs state (GGE)

$$\rho_{\text{GGE}} = \frac{e^{-\sum_k \lambda_k Q_k}}{\text{Tr} \left[ e^{-\sum_k \lambda_k Q_k} \right]}, \quad (6.7)$$

where  $\{Q_k\}$  are the local/quasi-local conserved quantities, or symmetries, of  $H_0$ . If there exist extensive dynamical symmetries of  $H_0$  then the system instead equilibrates to a time-dependent generalised Gibbs state (tGGE)

$$\rho_{\text{GGE}} = \frac{e^{-\sum_k \lambda_k Q_k + \sum_k \mu_k(t) A_k + \mu_k(t)^* A_k^\dagger}}{\text{Tr} \left[ e^{-\sum_k \lambda_k Q_k + \sum_k \mu_k(t) A_k + \mu_k(t)^* A_k^\dagger} \right]}, \quad (6.8)$$

where  $[H_0, A_k] = -\omega_k A_k$  and

$$\mu_k(t) = e^{-i\omega_k t}. \quad (6.9)$$

In essence, prethermalisation can be understood as conserving quantities on short time scales before the symmetry breaking dynamics take over on longer time scales.

An important property related to thermalisation is *clustering* [394, 409]. A state  $\rho$  is said to have clustering if for all strictly local observables  $O_k(x)$  which only have support in some finite region around the location  $x$ ,

$$\lim_{|x-y| \rightarrow \infty} \langle O_1(x) O_2(y) \rangle = \langle O_1(x) \rangle \langle O_2(y) \rangle. \quad (6.10)$$

It is known that states with clustering include finite temperature states of one-dimensional systems, ground states of gapped 1D systems and thermal states of higher dimensional systems at sufficiently high temperature [394] where it is always assumed that the Hamiltonians of these systems are local and do not contain any long range interaction or hopping terms. In these same systems, we can use the Lieb-Robinson bounds [307], which prove that systems with local Hamiltonians cannot propagate correlations faster than some fixed velocity, to conclude that time evolution preserves clustering, i.e

$$\begin{aligned} \lim_{|x-y| \rightarrow \infty} \langle O_1(x, 0) O_2(y, 0) \rangle &= \langle O_1(x, 0) \rangle \langle O_2(y, 0) \rangle \\ &\Rightarrow \\ \lim_{|x-y| \rightarrow \infty} \langle O_1(x, t) O_2(y, t) \rangle &= \langle O_1(x, t) \rangle \langle O_2(y, t) \rangle. \end{aligned} \tag{6.11}$$

One may worry about the validity of the system size becoming infinite in a real experiment where only finite samples are used. However, experiments with single layer cuprates use samples with lengths on the order of 0.1 mm while the lattice spacing is on the order of 1 Å, and so with respect to the lattice spacing the separations of distant sites is so large that no qualitatively new behaviour is expected as the system size increases further. We can now make an important observation about the production of  $\eta$ -pairing by driving thermal states. If an initial thermal state has clustering and no off-diagonal long-range order, evolution under a local Hamiltonian that conserves particle number cannot lead to the emergence of off-diagonal long-range order. Importantly for our discussion of light-induced  $\eta$ -paired superconductivity, this observation implies that if the light driving is to induce off-diagonal long-range order in a system initially in a thermal state, then it cannot conserve the number of electrons, at least in the superconducting band. This immediately questions most previous explanations of this phenomenon that consider exclusively single band models.

### 3 Possible explanation of experimentally observed superconductivity

We now return to considering the experimental observations of light-induced superconductivity, focusing primarily on single-layer cuprates. This restriction is made for simplicity and so that we can compare directly with available experimental results. Importantly our proposed explanation will not directly rely on any equilibrium superconducting properties, and thus we are able to study single-layer cuprates even though equilibrium superconductivity in these materials is not yet understood. However, the general principles of our argument carry across to other materials.

### 3.1 Description of underlying Hamiltonian

#### 3.1.1 The generic Hamiltonian

For our theory, we assume that the material can be well described by a general strongly repulsive Hamiltonian. As such, we start with the most general possible electronic Hamiltonian with phonon coupling,

$$H = H_{el} + H_{ph} + H_{el-ph}. \quad (6.12)$$

For our electronic Hamiltonian, we will focus on a general  $p - d$  multiband model that is generally used for the cuprates we are interested in [410, 411]. Additionally this Hamiltonian is also applicable to organic Mott insulators which have also been found to exhibit light induced superconductivity. Specifically we take

$$H_{el} = \sum_{ij\lambda\lambda'\sigma\sigma'} t_{ij}^{\lambda\lambda'} c_{i\lambda\sigma}^\dagger c_{j\lambda'\sigma} + V_{ij}^{\lambda\lambda'} n_{i\lambda\sigma} n_{j\lambda'\sigma} + (\varepsilon_{i\lambda} - \mu) n_{i\lambda\sigma}, \quad (6.13)$$

where  $c_{j\lambda\sigma}$  annihilates an electron/hole on lattice site  $j$  in orbital  $\lambda$  with spin  $\sigma$  and  $n_{j\lambda\sigma} = c_{j\lambda\sigma}^\dagger c_{j\lambda\sigma}$  is the corresponding local particle number. This Hamiltonian is dominated by the on-site inner-band interaction term,  $V_{ii}^{\lambda\lambda}$ , since we assume that the electrons are strongly correlated. Importantly, we will also assume that this Hamiltonian is local and thus the sum only runs over sites  $i, j$  with finite separation. The term  $H_{el-ph}$  is a standard electron-phonon interaction, which we assume to be well described by the Fröhlich Hamiltonian [412–414], and  $H_{ph}$  is the phonon Hamiltonian,

$$H_{ph} = \sum_{\mathbf{q}, n} \hbar\omega_{\mathbf{q}n} (b_{\mathbf{q},n}^\dagger b_{\mathbf{q},n} + 1/2) \quad (6.14)$$

$$H_{el-ph} = \sum_{\mathbf{k}, \mathbf{q}, n, \lambda, \lambda'} g_{\lambda, \lambda', n}(\mathbf{k}, \mathbf{q}) c_{\mathbf{k}+\mathbf{q}, \lambda\sigma}^\dagger c_{\mathbf{k}, \lambda'\sigma} (b_{\mathbf{q}, n} + b_{-\mathbf{q}, n}^\dagger), \quad (6.15)$$

where we have moved to momentum space and  $b_{\mathbf{q}, n}$  is the boson annihilation operator for a phonon with momentum  $\mathbf{q}$  and in branch  $n$ . Note that, apart from when describing polar materials,  $g_{\lambda, \lambda', n}(\mathbf{k}, \mathbf{q})$  is local in space [414]. For our work, we will follow the usual assumption that the effective dynamics of the electrons are also local.

#### 3.1.2 Hamiltonian symmetries

It was asserted in [401] that the origins of superconductivity at high temperatures could be related to the off-diagonal long range order, which can arise due to the existence of non-abelian symmetries, such as the  $SU(2)$   $\eta$ -symmetry of the Hubbard model studied by Yang and discussed above in Sec 2.1. In realistic situations, such symmetries are, however, not exact. This means that the density operator describing the state of the system will not be stationary and will instead eventually reach

the thermal state. Therefore such symmetries are not so relevant at equilibrium. However, driving the system out of equilibrium can, in general, lead to the onset of the off-diagonal order, which typically decays on very long, possibly exponential in the symmetry breaking parameter  $\gamma$  [415], timescales. This is similar to the meta-stable dissipative time crystal in Ch 4 where the weakly broken strong dynamical symmetry led to a meta-stable dynamical phase of matter. On shorter timescales, before the weak symmetry breaking has been able to influence the dynamics, we therefore expect the emergence of superconductivity due to the existence of a non-abelian symmetry and consequently off diagonal long range order.

We can identify such symmetries in some of the materials which exhibit light-induced superconductivity, such as the  $\eta$ -pairing in single layer cuprates as described by the Hubbard model in Eq. (6.13). In the simplest example of a 1D system with a single band the symmetry is given by

$$\eta^+ = \sum_x (-1)^x c_{x,\uparrow}^\dagger c_{x,\downarrow}^\dagger, \quad (6.16)$$

as we have seen before in Chs 4 & 5. In 2D bipartite lattices, with multiple electron bands, analogous  $SU(2)$  symmetries can be found. Further, in models of other materials, superconductivity has been asserted to arise as a consequence of other symmetries, such as in theories of  $SO(5)$  superconductivity [416]. Importantly, in all models where the superconductivity can be related to a non-abelian symmetry, if the symmetry breaking in those materials is expected to be small compared to, say, on-site repulsion and nearest neighbour hopping, then we can expect the superconductivity to be stable for some transient time. For instance, in single-layer cuprates, the on-site repulsion is expected to be one or even two orders of magnitude higher than the other parameters [417]. Similarly, in the organic Mott insulators, the on-site repulsion significantly exceeds the symmetry-breaking terms  $U_\lambda > 4V_{ii+1}$ .

## 3.2 Microscopic description of the laser pulse and the induction of ODLRO

### 3.2.1 Microscopic description of the laser pulse

We now consider the effect of driving the material with light. Since the pulse interacts weakly with the system, at least compared to the Hamiltonian energy scales, we can express the driving Hamiltonian as

$$H_{\text{drive}} = H + \epsilon h, \quad (6.17)$$

where  $h$  represents the interaction between the light and the material. Since the laser is only active for a short time in the experiments, which we label  $\Delta t$ , we

can work perturbatively in time. Following our discussion of clustering, since we assume the effective dynamics for the electrons are local, it is sufficient to consider the evolution of  $\langle \eta^+(t) \rangle$  during the laser pulse in order to determine whether the state has ODLRO immediately after the pulse. As discussed previously, we assume that the material is initially described by a clustering state  $\rho_0$ , which has no off-diagonal long-range order and is a stationary state of the undriven Hamiltonian. It is also reasonable to assume that we can express this initial state as a series in the small symmetry-breaking parameter,  $\gamma$ , as

$$\rho_0 = R_0 + \gamma R_1 + \mathcal{O}(\gamma^2). \quad (6.18)$$

We can then perturbatively expand  $\langle \eta^+(\Delta t) \rangle$  as

$$\langle \eta^+(\Delta t) \rangle = \text{Tr} \left( \eta^+ e^{(-iH_{\text{drive}}\Delta t)} \rho_0 e^{(iH_{\text{drive}}\Delta t)} \right) \quad (6.19a)$$

$$= \text{Tr} \left( \eta^+ \left( \rho_0 - i\Delta t [H_{\text{drive}}, \rho_0] - \frac{1}{2} \Delta t^2 [H_{\text{drive}}, [H_{\text{drive}}, \rho_0]] \right) \right) + \mathcal{O}(\Delta t^3) \quad (6.19b)$$

$$= -i\Delta t \text{Tr} \left( \eta^+ [H_0 + \gamma H_1 + \epsilon h, \rho_0] \right) \quad (6.19c)$$

$$- \frac{1}{2} \Delta t^2 \text{Tr} ([H_0 + \gamma H_1 + \epsilon h, [H_0 + \gamma H_1 + \epsilon h, \rho_0]]) \\ + \mathcal{O}(\Delta t^3)$$

$$= -i\Delta t \text{Tr} \left( \eta^+ [\epsilon h, R_0 + \gamma R_1] \right) \quad (6.19d)$$

$$- \frac{1}{2} \Delta t^2 \text{Tr} ([H_0 + \gamma H_1 + \epsilon h, [\epsilon h, R_0 + \gamma R_1]]) \\ + \mathcal{O}(\gamma^2 \Delta t, \Delta t^3)$$

$$= -i\Delta t \epsilon \gamma \text{Tr} \left( \eta^+ [h, R_1] \right) \quad (6.19e)$$

$$- \frac{1}{2} \Delta t^2 \epsilon^2 \text{Tr} \left( \eta^+ [h, [h, R_0]] \right) \\ + \mathcal{O}(\gamma^2 \Delta t, \gamma \epsilon \Delta t^2, \Delta t^3)$$

$$:= \delta_1 \epsilon \Delta t \gamma + \delta_2 \epsilon^2 \Delta t^2. \quad (6.19f)$$

In this calculation, we have used the requirement that the initial state is a stationary state of the undriven Hamiltonian and made repeated use of the identity  $\text{Tr}(A[B, C]) = 0$  when any two of  $A, B, C$  commute. We have assumed that the relative strengths and time scales satisfy  $\gamma \ll \epsilon \ll \Delta t$ , which is justified for the materials and experimental parameters in question. The quantities  $\delta_{1,2}$  can both be seen to depend on the material and the laser-material coupling. Importantly we see that the change in  $\langle \eta^+ \rangle$  is a function of  $F = \epsilon \Delta t$  which corresponds to the *fluency* of the laser pulse. We will discuss this further in Sec 3.4.

### 3.2.2 Induction of ODLRO from preformed pairs

From our previous discussion of clustering, we have established that to induce ODLRO in a given electron band, which we will refer to as the superconducting band, the light driving cannot conserve electron number in this band. This argument extends naturally to the case of multiple superconducting bands. Subsequently, there are two possible routes within the model for the laser pulse to induce ODLRO:

1. The laser could directly couple the superconducting band with some other electron band and transfer electrons between these two bands.
2. The laser could couple to the phonon modes via the generalised Fröhlich Hamiltonian [414], leading to a change in the expectation value of  $\langle b_{\mathbf{q},n} \rangle$  for some mode. This could proceed via a possibly non-linear phonon-phonon interaction. Importantly, since the phonon degrees of freedom admit a mean-field treatment, we can observe that in the electron-phonon Hamiltonian,  $H_{el-ph}$ , this change in  $\langle b_{\mathbf{q},n} \rangle \rightarrow \langle b_{\mathbf{q},n} \rangle + \Delta b_{\mathbf{q},n}$  leads to an effective modification of the electron hopping,

$$\begin{aligned}
 g_{\lambda,\lambda',n}(\mathbf{k}, \mathbf{q}) c_{\mathbf{k}+\mathbf{q}\lambda\sigma}^\dagger c_{\mathbf{k}\lambda'\sigma} & \left( b_{\mathbf{q},n} + b_{-\mathbf{q},n}^\dagger \right) \\
 & \rightarrow g_{\lambda,\lambda',n}(\mathbf{k}, \mathbf{q}) c_{\mathbf{k}+\mathbf{q}\lambda\sigma}^\dagger c_{\mathbf{k}\lambda'\sigma} \left( \langle b_{\mathbf{q},n} \rangle + \langle b_{-\mathbf{q},n}^\dagger \rangle \right) \\
 & \quad + 2g_{\lambda,\lambda',n}(\mathbf{k}, \mathbf{q}) \mathbb{R}e \{ \Delta b_{\mathbf{q},n} \} (c_{\mathbf{k}+\mathbf{q}\lambda\sigma}^\dagger c_{\mathbf{k}\lambda'\sigma}).
 \end{aligned} \tag{6.20}$$

This modification again allows electrons to be transferred between the superconducting band and some other electron band. To make the energy transfer to the phonons appreciable so that this effective coupling between electron bands is strong, the phonons must be driven close to resonance.

In either case, we see that the laser-material coupling must drive electron transfer between two different electron bands. However, it is essential to note that laser driving cannot introduce or remove electrons, so the total electron number across all the bands must remain conserved. Consequently, to induce  $\eta$  pairs in the superconducting band, finite off-diagonal expectation values in the initial state are required. To see this, we need focus only on the electronic degrees of freedom. Let  $\{|i\rangle\}$  be the electron number basis across all the electron bands and assume that our state before the pulse,  $\rho$ , is diagonal so that

$$\rho_0 = \sum_i \rho^{(i)} |i\rangle \langle i|. \tag{6.21}$$

Let the action of the pulse be described by some unitary,  $U$ , so that after the pulse that state becomes

$$\tilde{\rho} = U \rho_0 U^\dagger. \tag{6.22}$$

Then we can calculate the expected value of  $\eta_{x,\nu}^+$  where  $\nu$  indicates the superconducting band,

$$\langle \eta_{x,\nu}^+ \rangle_{\tilde{\rho}} = \text{Tr} \left( c_{x,\nu,\uparrow}^\dagger c_{x,\nu,\downarrow}^\dagger \tilde{\rho} \right) \quad (6.23)$$

$$= \sum_i \langle i | c_{x,\nu,\uparrow}^\dagger c_{x,\nu,\downarrow}^\dagger U \rho_0 U^\dagger | i \rangle \quad (6.24)$$

$$= \sum_{i,j} \rho^{(j)} \langle i | c_{x,\nu,\uparrow}^\dagger c_{x,\nu,\downarrow}^\dagger U | j \rangle \langle j | U^\dagger | i \rangle. \quad (6.25)$$

Since  $U$  must conserve the total electron number we see that  $\langle i | c_{x,\nu,\uparrow}^\dagger c_{x,\nu,\downarrow}^\dagger U | j \rangle$  and  $\langle i | U | j \rangle$  cannot *both* be non-zero. Hence the initial state must have non-zero off diagonal terms to induce non-zero  $\langle \eta^+ \rangle$ .

In other words, the material must initially have off-diagonal preformed electron pairs, although these pairs will not be true  $\eta$ -pairs as the material is not initially superconducting. This is in agreement with experimental results, which have so far only observed transient light-induced superconductivity for initial states which are believed to contain preformed pairs [417]. Finally, since no further superselection rules are preventing a change of  $\langle \eta^+ \rangle$  to a finite value, it will generically happen, and hence the constants  $\delta_{1/2}$  in Eq. (6.19f) are expected to be  $\mathcal{O}(1)$ . For the case of strongly repulsive systems, this may be mediated via on-site electron-electron correlations hybridising with the driving.

### 3.3 Superconductivity following the laser pulse

So far, we have established that in order to induce ODLRO within our model, the material must contain preformed pairs and be driven in such a way that electrons are transferred between bands. If these conditions are met, then after the laser pulse, our material is in some state,  $\tilde{\rho}$ , with

$$\langle \eta^+ \rangle_{\tilde{\rho}} = \delta_1 \epsilon \Delta t \gamma + \delta_2 \epsilon^2 \Delta t^2, \quad (6.26)$$

at leading order. We now study the behaviour of the system following the pulse.

#### 3.3.1 Description of prethermal state

As we discussed above, quantum systems with approximate symmetries are generically expected to rapidly relax to the prethermal time-dependent generalised Gibbs ensemble. Therefore we can deduce that following the pulse, when the system Hamiltonian is once again described by Eq. (6.12) and thus admits the decomposition in Eq. (6.5), the material prethermalises and after the very short pre-relaxation time can be described by the tGGE state

$$\rho_{PT}(t) \approx \frac{\exp(-\beta' H_0 + \mu(t) \eta^+ + \mu^*(t) \eta^-)}{\text{Tr} [\exp(-\beta' H_0 + \mu(t) \eta^+ + \mu^*(t) \eta^-)]}, \quad \mu(t) = \mu_0 e^{-i\omega t}, \quad (6.27)$$

where  $\omega$  is a frequency determined by the on-site electronic potentials and  $\mu_0$  is a Lagrange multiplier fixed by the initial expectation value  $\langle \eta^+ \rangle_{\bar{\rho}}$  which is being preserved by the prethermalisation. The exact relation between  $\mu_0$  and  $\langle \eta^+ \rangle$  at generic temperatures is usually impossible to calculate but for a standard  $N$ -site, 1D Hubbard model with interaction strength  $U$  and hopping amplitude  $t$  at leading order in inverse temperature we have

$$\frac{\langle \eta^+ \rangle}{N} = \frac{1}{8} U \beta' \cosh(\mu_0) \tanh\left(\frac{\mu_0}{2}\right) \text{sech}^2\left(\frac{\mu_0}{2}\right) + \mathcal{O}(\beta'^2). \quad (6.28)$$

Note that the inverse temperature,  $\beta'$ , is not necessarily the same as before the pulse, and is expected to generically decrease as the pulse transfers energy to the system thus heating it up. We remark here that it may also include additional conservation laws or dynamical symmetries for which  $[H_0, A_\kappa] = -\omega_\kappa A_\kappa$ , such as charge number or the spin  $\text{SU}(2)$  algebra, but these are orthogonal to  $\{\eta^+, \eta^-\}$  and will not change the value of the relevant superconducting pairing function.

Importantly, provided the temperature is sufficiently high, the tGGE state satisfies clustering and so we can decompose

$$\langle \eta_j^+ \eta_k^- \rangle_{\rho_{PT}(t)} = \langle \eta_j^+ \rangle_{\rho_{PT}(t)} \langle \eta_k^- \rangle_{\rho_{PT}(t)}. \quad (6.29)$$

Since our model Hamiltonian is translationally invariant the tGGE state is spatially homogeneous in the thermodynamic limit, it suffices the focus on the relevant extensive quantity

$$|\langle \eta^+ \rangle| = \langle \eta_j^+ \rangle V, \quad (6.30)$$

where  $V$  is the number of electron sites in the material and  $j$  can be taken as any lattice site. To reiterate, we are assuming that the experimental samples excited by the laser are sufficiently large that these thermodynamic arguments can be justified to a sufficient accuracy.

### 3.3.2 Superconductivity of the prethermal state

We now examine the superconductivity properties of the prethermal state. In particular, we will calculate the Meissner stiffness, or superconducting weight, as a function of  $\mu_0$  at high temperatures for a 1D ring of fixed finite radius. The Meissner stiffness,  $n_s$ , is defined through the London equation, which states that for small magnetic fields with vector potential  $\mathbf{A}$  the current response satisfies

$$\langle \mathbf{J} \rangle = -n_s \mathbf{A}. \quad (6.31)$$

We assume that introducing a gauge field modifies the system Hamiltonian by introducing a Peierls phase to the electron hopping. Focusing for simplicity on



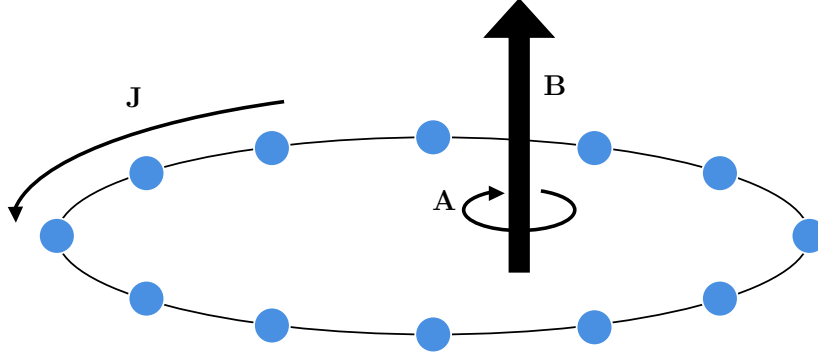


**Figure 6.1:** We consider a 1D periodic ring of  $N$  lattice sites so that the current flows around the ring. The magnetic field is transverse to the plane of the ring and we choose the gauge in which the magnetic potential is tangential to the ring.

a single band Hubbard model on a 1D ring with  $N$  sites and a fixed radius  $R$ . Note that in this geometry, we must take  $N$  to be even in order to define an  $\eta$ -pairing operator. The magnetic field is taken to be perpendicular to the plane of the 1D ring, as illustrated in Fig 6.1, and we work in the gauge where the magnetic potential is tangential to the ring.

The corresponding Hamiltonian, in units of the hopping amplitude, is

$$H_0[\mathbf{A}] = H_{\text{kin}} + H_U \quad (6.32a)$$

$$H_0[\mathbf{A}] = - \sum_{j,a \in \{\uparrow, \downarrow\}} (e^{i\lambda_{j,j+1}} c_{j,a}^\dagger c_{j+1,a} + e^{-i\lambda_{j,j+1}} c_{j+1,a}^\dagger c_{j,a}) \quad (6.32b)$$

$$+ U \sum_j n_{j,\uparrow} n_{j,\downarrow}$$

where the Peierls phase, assuming there are sufficiently many lattice sites, is given by

$$\lambda_{j,j+1} = \frac{2\pi R}{N} |\mathbf{A}| = \frac{\Phi_B}{N}, \quad (6.33)$$

where  $\Phi_B$  is the total flux through the ring. Note that this simplification captures the key features of the prethermal state that we believe are sufficient to understand the superconductivity properties of the material following the pulse, in particular  $\eta$ -pairing in a model of electron hopping.

When we turn on the external magnetic field in order to observe the Meissner effect, by the usual assumptions of prethermalisation, the prethermal state adjusts on time scales that are much shorter than the final relaxation time giving,

$$\rho_{PT}[A] \approx \frac{\exp(-\beta' H_0[\mathbf{A}] + \mu(t)\eta^+ + \mu^*(t)\eta^-)}{\text{Tr}[\exp(-\beta' H_0[\mathbf{A}] + \mu(t)\eta^+ + \mu^*(t)\eta^-)]}. \quad (6.34)$$

Crucially the strictly local hopping terms with the added Peierls phase cannot change macroscopically the expectation value of  $|\langle \eta^+ \rangle|$  because they conserve total particle number.

Taking the current operator to have the usual form corresponding to electron conservation,

$$J[A] = -i \sum_{j,s \in \{\uparrow, \downarrow\}} \left( e^{i\lambda_{j,j+1}} c_{j,s}^\dagger c_{j+1,s} - \text{c.c.} \right) \quad (6.35)$$

we can calculate the Meissner stiffness as

$$n_s = - \left. \frac{d}{dA} \right|_{A=0} \langle J \rangle \quad (6.36a)$$

$$= - \text{Tr}(J'[0] \rho_{PT}[0] + J[0] \rho'_{PT}[0]) \quad (6.36b)$$

$$= \frac{1}{N} \left( \langle H_{\text{kin}} \rangle - \beta' \langle J \rangle^2 + \beta' \int_0^1 ds \text{Tr}(J \rho_{PT}^{(1-s)} J \rho_{PT}^s) \right), \quad (6.36c)$$

where in the final line all terms are evaluated at zero gauge field. This agrees with the results of [418] where the Meissner stiffness is defined as the second derivative of the free energy with respect to the flux, up to some multiplicative factors. While we cannot exactly evaluate the right hand side of Eq. (6.36c), progress can be made if we assume that at high temperatures  $n_s$  has an asymptotic series expansion. Under this assumption we calculate the leading order term in  $\beta'$  as,

$$n_s = - \frac{2\pi R \beta'}{N Z(0, \mu_0)} \left( \text{Tr}(H_{\text{kin}} H e^{\hat{\Delta}}) - \frac{\text{Tr}(H_{\text{kin}} e^{\hat{\Delta}}) \text{Tr}(H e^{\hat{\Delta}})}{Z(0, \mu_0)} + \text{Tr}(J e^{\hat{\Delta}})^2 \right. \\ \left. - \int_0^1 ds \text{Tr}(J e^{(1-s)\hat{\Delta}} J e^{s\hat{\Delta}}) \right) + \mathcal{O}(\beta'^2). \quad (6.37)$$

where  $Z(\beta', \mu_0) = \text{Tr}(e^{-\beta H_0 + \mu(\eta^+ + \eta^-)})$ . Evaluating each term for fixed system size,  $N$ , we arrive at

$$n_s = \frac{\Phi_B}{\cosh^2\left(\frac{\mu_0}{2}\right)} \left( \frac{\sinh(\mu_0)}{\mu_0} - 1 \right) \beta' + \mathcal{O}(\beta'^2). \quad (6.38)$$

This agrees with similar studies regarding  $\eta$ -paired superconductivity, which reported that the superconducting weight increases quadratically with the  $\eta$ -pairing parameter at leading order [419]. In particular, this argument demonstrates that provided the laser pulse induces ODLRO, the resulting prethermal state will be superconducting. However, we see in Fig 6.2 that if too much ODLRO is induced, then the Meissner stiffness decreases again. Unfortunately it is unclear whether this is an effect that could be observed experimentally as the range of realistic experimental values for  $\mu_0$  are unknown, although it can be understood intuitively by the absence of superconductivity in the infinite temperature state when  $\mu_0 \gg \beta'$ , i.e. at true infinite temperatures.

Unfortunately, the above calculation cannot be performed as easily for a 2D square lattice due to the quadratic scaling of system size, but this is a direction

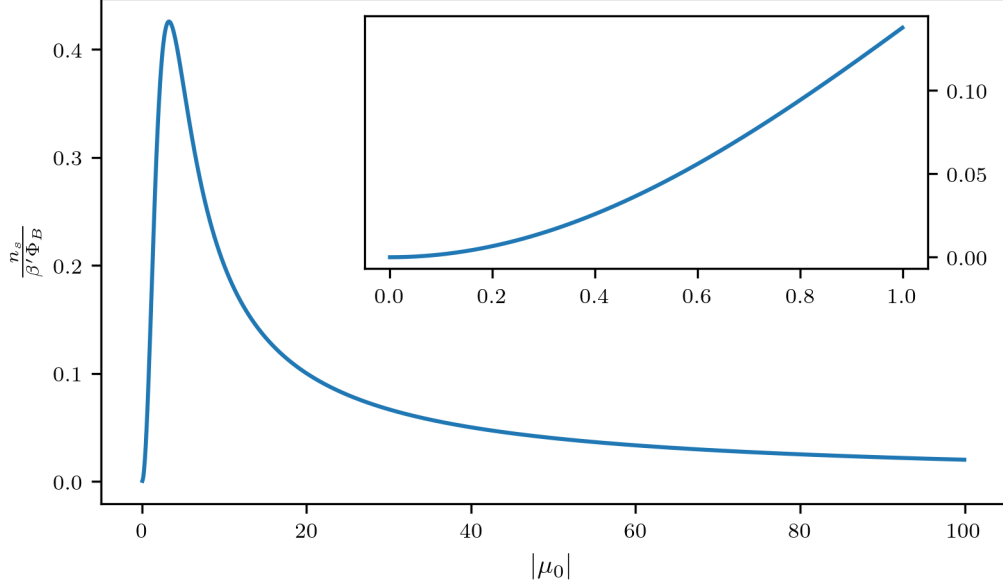


**Figure 6.2:** We plot the Meissner stiffness calculated to leading order in  $\beta$  from Eq. (6.38). The main figure shows the exponential decay with large  $|\mu_0|$ , while the inset shows the quadratic dependence for small  $|\mu_0|$ . The peak is located at  $|\mu_0| \approx 3.278$  with  $n_s \approx 0.4257\Phi_B\beta'$

that should be pursued in the future. It would also be desirable to compute higher-order corrections in  $\beta'$  or perform numerical analysis in order to verify this series expansion's validity. Finally, we remark that to make a concrete link with experiments, our theory should be used to calculate the Drude weight in a 2D geometry. Unfortunately, such calculations have proven impossible so far, but it is hoped that the recent work of Abanin [415] regarding exponential stability in strongly correlated models could be used to demonstrate a non-zero Drude weight for our theory, at least in the strongly interacting limit.

### 3.3.3 Decay of the prethermal state

We must now examine how the prethermal state decays in order to understand how long the material will remain superconducting. Since we have been assuming generic behaviour throughout, the decay can be modelled by a simple Pauli master equation once we move first to a co-rotating frame to eliminate the trivial time-dependence of  $\rho_{PT}(t)$ . In this basis the state is,

$$\rho'_{PT} \approx \frac{\exp(-\beta' H_0 + \mu_0(\eta^+ + \eta^-))}{\text{Tr} [\exp(-\beta' H_0 + \mu_0(\eta^+ + \eta^-))]}, \quad (6.39)$$

which is a stationary state of the new Hamiltonian in the co-rotating frame. We may now formally diagonalise  $\rho'_{PT}$  in the energy eigenbasis of  $H_0$ . In this basis,

which can be chosen so that  $\rho'_{PT}$  is also diagonal, we have

$$\rho'_{PT} = \sum_j P_j |\varphi_j\rangle \langle \varphi_j|. \quad (6.40)$$

We write the components as a vector  $\mathbf{P} = P_j$ , and then use [394] to obtain a simple master equation for this vector,

$$\frac{d\mathbf{P}}{dt} = W\mathbf{P}, \quad (6.41)$$

where  $W$  is a Markovian transition matrix in the interaction picture and its elements are given by Fermi's golden rule for weak perturbation,

$$W_{nm} \approx 2\pi\gamma^2 |\langle \varphi_n | H_1 | \varphi_m \rangle|^2 \delta(E_n^0 - E_m^0). \quad (6.42)$$

Here  $E_n^0$  are the energies of  $H_0$  with  $|\varphi_n\rangle$  the corresponding eigenstates. This is simply a standard Pauli master equation, which is well-established in perturbation theory.

This master equation cannot be directly solved since we do not know the exact expression for  $W$ . We can deduce, however, that generically the decay will be given by the eigenvalue of  $W$  that has a maximal finite real part,

$$\Lambda_1 = \max_j [-\operatorname{Re}(\lambda_j)], \quad (6.43)$$

where  $\lambda_j$  are the eigenvalues of  $W$  that have  $\operatorname{Re}(\lambda_j) < 0$ . This is often called the gap and determines an exponential relaxation rate in the long-time limit, similar to the Liouvillian gap from Ch 2. In a macroscopically large system, it is not unreasonable to assume that this eigenvalue is degenerate and has corresponding eigenstates  $\{\mathbf{P}_k^{(1)}\}$ .

In the models relevant to the experiments we are concerned with, it is in fact natural to assume that we have two sources of perturbation with differing strengths that we write compactly as

$$W = \tilde{W} + \kappa w, \quad \gamma \gg \kappa > 0, \quad (6.44)$$

representing a hierarchy of timescales. Here  $\tilde{W}$  is the dominant perturbation while  $w$  is the secondary perturbation. A standard example of this behaviour is when the lattice geometry does not support  $\eta^+$  as a (dynamical) symmetry because it is not bipartite. This produces the large perturbation,  $\tilde{W}$ , while the secondary weaker perturbation,  $w$ , comes from coupling to phonon modes of the relevant band(s). Using further perturbation theory, under the assumption that  $\Lambda_1$  is degenerate, it will typically split

$$\Lambda_2 = \Lambda_1 + \mathcal{O}(\kappa^2). \quad (6.45)$$

Thus we have two or more dominant relaxation rates, leading to a double-exponential decay

$$\langle \eta^+ \rangle \sim A \exp(-\Lambda_1 t) + B \exp(-\Lambda_2 t) + \dots \quad (6.46)$$

A double exponential decay has been observed in the experiments of [387]. Within our model and proposal, such phenomenology can be explained by degeneracies in the hierarchy of perturbations and a non-closing of the gap. While the validity of these assumptions has not yet been verified rigorously, the experimental observation of double exponential decay combined with the existence of several perturbations with different timescales seem to suggest that this or some similar mechanism is at work.

### 3.4 Predictions of the theory and agreement with experimental evidence

We now summarise this theory's key insights and predictions and discuss their agreement with experimental results where possible.

**Requirement of strong interactions** The fundamental assumption that underpins our theory is the separation of the full Hamiltonian into a part that respects  $\eta$ -pairing symmetry and a much weaker part that does not. The most common terms which respect  $\eta$ -pairing symmetry are nearest neighbour hopping and on-site interaction. This suggests that the materials in which light-induced superconductivity is observed should be strongly correlated. Indeed, as [415] indicates,  $\eta$ -pairs in the Hubbard model are exponentially stable for large on-site interactions. This prediction is corroborated by current experimental evidence, where light-induced superconductivity has been observed in cuprates and organic salts, all of which are strongly interacting.

**Electron conservation** The second prediction of our theory comes from our discussion in Sec. 2.2, where we argued that the laser pulse responsible for inducing ODLRO must couple multiple electron bands and break electron conservation within each band. This is an important observation because it questions many previous attempts at explaining these experiments, which focused exclusively on single-band electronic Hamiltonians. It is also important to understand this requirement when engineering future mechanisms to induce  $\eta$ -paired superconductivity.

**Necessity of preformed pairs** We also argued in Sec. 3.2 that because the laser pulse must conserve total electron number across all the bands, there must already exist off-diagonal terms in the initial state. These correspond to preformed pairs which do not have the correct phases to be coherent BSC or  $\eta$ -pairs. This is corroborated by current experimental evidence, which suggests light-induced superconductivity occurs only in states with preformed pairs.

**Lifetime of superconducting state** Using general arguments related to perturbation theory, we saw that the pre-thermal state could decay according to a double-exponential under certain assumptions. Thus the experimental results of [387] are not outside our model.

**Dependence of the resistivity on fluency** Finally, we can use our theory to predict the behaviour of the materials resistivity while in the superconducting phase. Assuming that the supercurrent is proportional to this pairing function, as is widely argued [401, 419] and agrees with our discussion in Sec. 3.3.2, the scaling of the resistivity is given by simple Ohm's law,

$$R \propto \frac{1}{I} \quad (6.47)$$

$$\propto \frac{1}{I_n + I_S} \quad (6.48)$$

$$\propto \frac{1}{I_n + bF^2 + cF^3}, \quad (6.49)$$

where  $F$  represents the *fluency* of the laser pulse. Here  $I_n$  is the normal component of the current, and we have expanded the superconducting current,  $I_S$  in the leading two orders of fluency using Eq. (6.19f). The coefficients  $b$  and  $c$  are given by

$$b = \delta_1 \gamma, \quad c = \delta_2 \delta_1 \gamma, \quad (6.50)$$

where we recall that  $\delta_j$  are material dependent constants of order 1 while  $\gamma$  is the symmetry breaking parameter. This is consistent with experimental measurements of the resistivity in light-driven  $K_3C_{60}$  [387], as we show in Fig 6.3.

## 4 Stabilising the superconducting state

Having presented our theory to explain the experimental observations of light-induced superconductivity, we will now demonstrate how this general structure admits a mechanism for stabilising the superconducting state. To do so, we will utilise the Zeno effect, which offers theoretically arbitrarily long stabilisation.

### 4.1 Stabilisation from the quantum Zeno effect

It is well-established that external dissipation from a bath or incoherent driving, which is either strong [243, 244, 420] or such that the bath is at high temperature compared to the system [421] will induce the quantum Zeno effect. This has the effect of partially freezing some dynamics of the system.

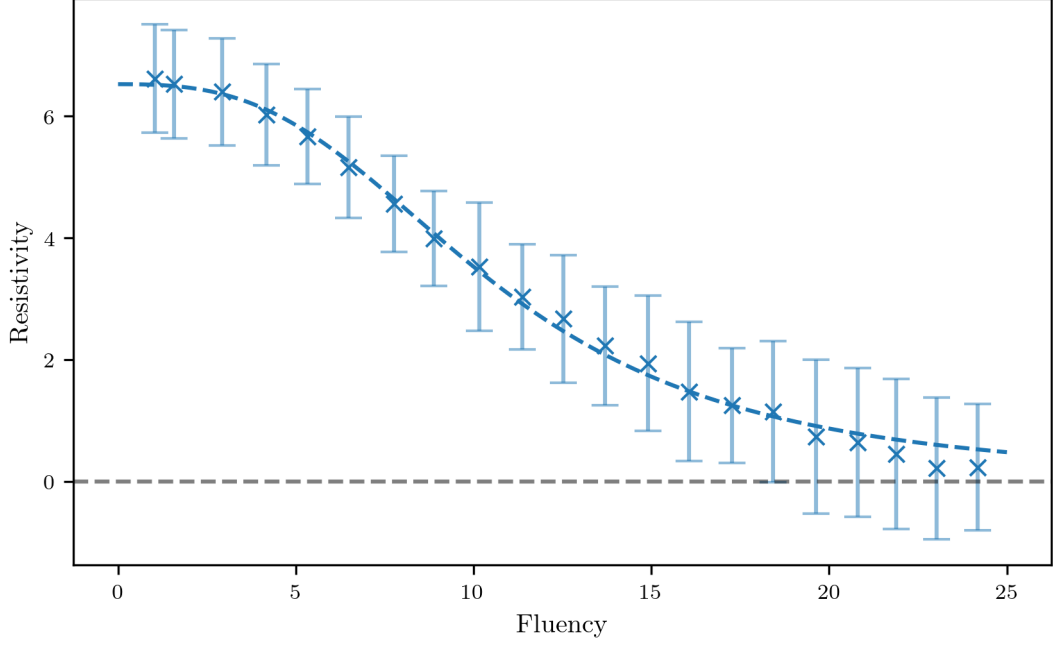


**Figure 6.3:** The crosses and error bars show the experimental data for the dependence of resistivity on fluency from [387] for  $K_3C_{60}$ . The dashed curve shows the prediction of our theory by fitting the data to Eq. (6.49). The agreement is impressive and well within experimental errors. The fitted parameters are  $I_n = 0.153$ ,  $b = 1.05 \times 10^{-4}$ ,  $c = 1.20 \times 10^{-4}$ , which is in agreement with our derivation where  $b$  &  $c$  should be of the order  $\gamma$  which should be small.

As in Sec. 3.3.2, we will simplify our discussion to only consider a single band model so as to remove redundant indices in our equations, but the generalisation is immediate. Defining the on-site spin operators as

$$s_j^+ = c_{j,\uparrow}^\dagger c_{j,\downarrow}, \quad s_j^z = n_{j,\uparrow} - n_{j,\downarrow}, \quad s_j^- = (s_j^+)^\dagger, \quad (6.51)$$

where  $n_{j,\sigma} = c_{j,\sigma}^\dagger c_{j,\sigma}$  is the on-site particle number operator, we see that these operators all commute with the on-site  $\eta_j^+$  pairing operators. If we introduce a strong additional term so that our Hamiltonian becomes

$$H' = H_0 + \gamma H_1 + \Gamma \sum_{j,\alpha} B_j^\alpha \otimes s_j^z, \quad (6.52)$$

where  $\gamma \ll \Gamma$  and  $B_j^\alpha$  are a set of external effective bath operators, then the quantum Zeno effect will be induced [420]. Alternatively, we could introduce high-frequency time dependent driving on each site through a term such as

$$H_z(t) = \sum_j \chi_j(t) s_j^z. \quad (6.53)$$

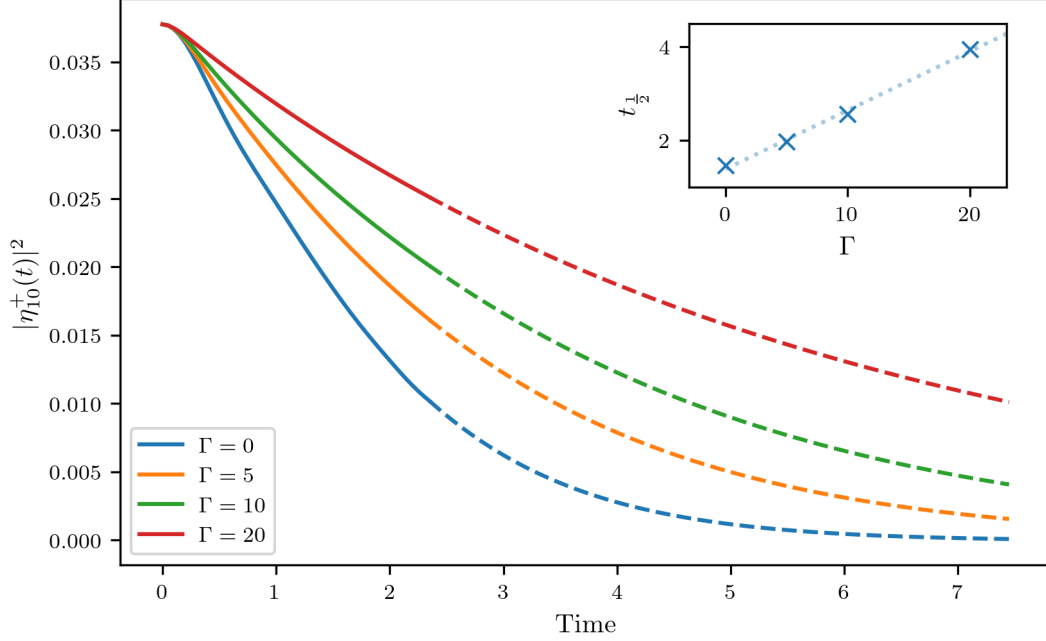


**Figure 6.4:** We simulate the decay of  $\eta$ -pairing in a single band Hubbard model with next nearest neighbour hopping. The two site hopping breaks  $\eta$ -symmetry leading to decay. However this can be stabilised by introducing on-site spin dephasing Lindblad operators  $L_k = \sqrt{\Gamma} s_j^z$ . As  $\Gamma$  is increased the lifetime of the  $\eta$ -pairing is extended. The solid lines show numerical data while the dashed lines show extrapolation assuming double exponential decay. The inset shows the linear relationship between the half-life of the  $\eta$ -pairs,  $t_{1/2}$  and the dissipation strength,  $\Gamma$ .

At leading order, the effective dynamics for large  $\Gamma$  are governed by [243, 244]

$$H_{\text{eff}} = \sum_j P_j (H_0 + \gamma H_1) P_j, \quad (6.54)$$

where  $P_j$  are projectors to the local joint eigenspaces of  $s_j^\alpha$ . Crucially, this means that any term in  $H_1$  that changes local spin on-site  $j$  will vanish in  $H_{\text{eff}}$ . We can interpret this as the strong driving suppressing processes that change the spin degrees of freedom. Moreover, the Zeno dynamics conserve  $\eta_k^+$  because  $[\eta_k^+, P_j] = 0$ . Therefore  $\eta^+$  will be stabilised against all processes that change local on-site spin values, an obvious example of which is electron hopping. We demonstrate this effect in Fig. 6.4 where we stabilise the decay of the prethermal state in a 1D Hubbard model against next nearest-neighbour hopping using strong dephasing baths.

Importantly, we expect that the dominant contribution to  $H_1$  that destroys  $\eta^+$  will be charge-phonon coupling. This follows from a mean-field treatment of the Fröhlich Hamiltonian as in Eq. (6.20) which shows the phonon contribution to the electronic Hamiltonian can be written as

$$H_{el-ph} \sim \sum_{i,j,\sigma} f(b_{i,j}) \sum_{\langle ij \rangle, \sigma} c_{i,\sigma}^\dagger c_{j,\sigma}, \quad (6.55)$$



where  $f(b_{i,j})$  is some function of the phonon degrees of freedom. This is effectively a hopping-like interaction and therefore our quantum Zeno stabilisation suppresses charge-phonon coupling.

Unfortunately, we do not expect the signatures of superconductivity to be measurable during the stabilisation as dissipative effects generically lead to diffusive transport. Additionally, our calculations in Sec 3.3.2 indicate that in an infinite temperature state, which is where our stabilisation will generically drive the system, the Meissner effect vanishes.

## 4.2 Possible realisations

We now briefly outline some possible routes for experimentally realising this proposed Zeno stabilisation effect.

- The most theoretically straightforward method is to follow [422] and embed a cuprate parent material into recently realised terahertz cavities, which will strongly couple to magnetic fluctuations. The essential idea, as discussed by Ashida et al. in [422] is that spin-orbit coupling cannot be neglected in the case of a cavity, leading in the large  $U$  limit to an effective model of spin dynamics. As recently shown by Ashida and collaborators at leading order, this introduces a light-magnon interaction of the form,

$$H_{\text{int}} \propto \sum_{\langle i,j \rangle, \ell} (-1)^\ell \hat{E}^z \mathbf{s}_{i,\ell} \cdot \mathbf{s}_{j,\ell}, \quad (6.56)$$

where the sum is over nearest neighbour lattice sites  $i$  and  $j$  and  $\hat{E}^z$  is an electric field operator in the  $z$ -direction. By treating the driving of  $\hat{E}^z$  in the mean-field limit, we can assume that the driving simply introduces a spin-spin interaction term with strength  $\Delta = \langle \hat{E}^z \rangle$ . In the Zeno limit of taking  $\Delta$  to be very large, this means that the lifetime of the prethermal state,  $\rho_{PT}$ , scales as  $\Delta^2$ , while also possibly heating the state to arbitrarily high effective temperature,  $\beta' \rightarrow 0$ .

- Alternatively, it may be possible to stabilise the  $\eta$ -pairing superconducting order parameter against perturbations by driving a phonon mode that strongly couples to the spin degrees of freedom in  $H_0$ . This means that, as we discussed for the pulse inducing the superconducting state, we drive at a different frequency to excite a phonon mode that has strong spin coupling. While such optically active phonon modes with strong spin coupling have not been observed in single-layer cuprates, they may exist in other materials.

- Finally, one could subject the system to a strong inhomogeneous external magnetic field that is evolving randomly in time and is effectively white noise. Such a magnetic field introduces on-site spin dephasing Lindblad operators, which will stabilise the  $\eta$ -pairing as in Fig 6.4. Unfortunately, the magnetic fields required to achieve this are likely at the edge of, if not beyond, those that can currently be achieved experimentally.

## 5 Conclusions

To summarise, this chapter has proposed a new theory to explain recent experimental evidence of light-induced superconductivity at temperatures well above critical. The theory asserts that a laser pulse induces ODLRO in the material, which is approximately conserved during a prethermalisation regime due to the material's Hamiltonian being dominated by a term that admits an  $\eta$ -symmetry. The proposal makes three key predictions that agree with experimental observations: (i) that the material must have preformed pairs, (ii) that the material must be strongly correlated and (iii) that the resistivity should at leading order be a function of the fluency, as in Eq. (6.49). The ideas have been developed with minimal model-specific assumptions and are based almost exclusively on well-established principles of symmetries and thermalisation.

We have also presented a theoretical proposal for stabilising the prethermal superconducting state by employing the quantum Zeno effect. It requires strongly driving the spin degrees of freedom so that they become effectively frozen and cannot contribute to the decay of the  $\eta$ -pairing. In Sec. 4.2 we gave possible routes for experimentally realising this effect. This is an obvious avenue for future research since the ability to stabilise superconducting states could have far-reaching technological applications.

This work does not make predictions of exact values for particular quantities. Instead, we have predicted general scaling arguments that are independent of the specific model parameters. This is both a blessing and a curse. On the one hand, our ideas cannot be used to a priori determine precisely which experimental parameters will yield the best results or to calibrate set-ups using quantitative theoretical prediction. However, our theory exposes the general mechanisms that are potentially at work in these experiments and gives indications of approaches that may or may not be successful.

Finally, it is essential to expound upon the areas of our work that still require further study. The most pressing issue is rigorously demonstrating the prethermal state's superconductivity in a 2D lattice model. While the calculation in Sec 3.3.2 may be possible for a 2D model, therefore implying the Meissner effect, it would

also be desirable to demonstrate a non-zero Drude weight rigorously. To this end, we envisage using the results of [415] to obtain an effective Hamiltonian in the strong coupling limit and then constructing an appropriate Mazur bound. Efforts should also be made to understand in more detail the induction of ODLRO through light driving, ideally to establish a quantitative relation between the properties of the pulse and the amount of ODLRO induced. In particular, it would be beneficial to study possible toy models of the materials in question with approximately known physical parameters and to carry out a detailed numerical analysis of our theory. Such details would be incredibly beneficial for both verifying our predictions and for influencing future experimental studies. Finally, our arguments regarding the double exponential decay should be examined with more rigour to understand precisely which spectral properties are required in the thermodynamic limit.

# 7

## Conclusions and outlook

This thesis revealed new analytic insights into the dynamics of non-equilibrium many-body quantum systems by considering the constraints that non-abelian symmetries place on the evolution. In particular, we utilised algebraic techniques to understand better the behaviour of several dynamical phenomena in quantum matter. These techniques were applied to several diverse topical areas of research, specifically transport in integrable models, time crystals, synchronisation and light-induced superconductivity, and our results can be applied to experimentally relevant systems. In this final chapter, we will summarise the key results of our work and evaluate the degree to which we have achieved our ambitious aims. We will also discuss the future work to which this thesis naturally leads.

In chapter 2 we studied integrable systems in the presence of dissipation. Integrable systems provide the most natural setting for studying the dynamical constraints of symmetries due to their rich algebraic structure. Our principal result was to develop a method for analytically calculating the Liouvillian spectrum for integrable systems in the presence of particular forms of loss. This method relies on the pseudo-Hamiltonian resembling an integrable model with complex parameters. We discussed how each integrable model admits some form of dissipation under which it is soluble via our method.

We chose to study in detail the example of an XXZ spin chain with boundary loss at one end. Our method allowed us to directly identify phase transitions in the Liouvillian spectrum and calculate the Liouvillian gap. We were also able to link the observed domain wall formation, and a dissipative phase transition to the existence of boundary bound states which effectively insulated the bulk of the system from the boundary in the easy axis regime.

While we demonstrated the analytic insight that our method can provide to the dynamics of lossy integrable systems, the scope of this method is somewhat

limited for two key reasons. Firstly it relies on solving a set of Bethe equations, which is notoriously tricky in general, although, as in our example, progress can be made within certain limits. Secondly, our method can only access the Liouvillian eigenvalues and not the corresponding eigenstates. It is possible that the expressions we gave for the eigenstates of the boundary loss XXZ model may reduce in some limits, but it is unclear how much advantage this would give.

We then discussed the challenges involved in using the thermodynamic Bethe ansatz to extend our method to the thermodynamic limit. These challenges are mainly related to issues of holomorphicity and the location of poles in the complex plane. This led us to consider alternative techniques to studying the dynamics of dissipative integrable systems using generalised hydrodynamics. Here we highlighted two possible avenues for future study, specifically localised loss in an XXZ model and localised dephasing in a Lieb-Liniger model. Given the recent successes of GHD, we expect this to be an exciting and fruitful path for future research to follow.

In chapter 3 we moved away from the restriction of integrability to study more general models. We presented several very general results which completely characterised the purely imaginary eigenvalues of a Liouvillian algebraically. Most notably, we proved that when the Liouvillian has a full rank non-equilibrium steady state, the purely imaginary eigenmodes are completely determined by the strong dynamical symmetries of the system. This result improves upon previous works, which showed strong dynamical symmetries to be sufficient for purely imaginary eigenvalues. We were also able to prove results regarding the absence of purely imaginary eigenvalues and the behaviour of purely imaginary eigenvalues when the system is perturbed.

These results have a wide range of applications and represent a notable development in the understanding of quantum Liouvillians in general. Additionally, because they are formulated in terms of the algebra of the symmetries of the Liouvillian, it is possible to apply them to larger systems that are beyond numerical treatment. However, some theoretical questions still remained unanswered, in particular the two<sup>1</sup> conjectures regarding the non-existence of purely imaginary eigenvalues when the NESS is unique and the characterisation of purely imaginary eigenvalues of the discrete-time evolution operator for time-dependent Liouvillians. These conjectures provide a clear direction for future work.

Chapters 4 & 5 demonstrated the applicability of the formal results from chapter 3 by using them to study time crystals and quantum synchronisation respectively. In particular, in Ch 4 we studied a novel type of time crystal which we called a dissipative time crystal, where the time crystallinity only occurs in the presence of dissipation. We analysed this behaviour in the Hubbard model with electron pair loss

---

<sup>1</sup>Note that one conjecture was given in Ch 3 and a second in Ch 4.

and gain and explained how the model could be realised experimentally. This work is closely related to the idea of boundary time crystals, and the links between these two phenomena should be explored in more detail. We finally adapted our model by introducing a time-dependent magnetic field so that the system displayed *discrete* dissipative time crystal behaviour. These models showed impressive stability to temporal noise, possibly indicating that they are good candidates for experimental study. Future work regarding discrete dissipative time crystals is likely to be connected to our conjectured characterisation of purely imaginary eigenvalues of the discrete-time evolution operator.

Using our complete characterisation of the purely imaginary Liouvillian eigenvalues from Ch 3, in chapter 5 we gave sufficient conditions for many-body quantum systems to exhibit robust spontaneous synchronisation. Again, these conditions were formulated in terms of algebraic properties, making them incredibly useful for studying many-body systems where existing techniques struggle. We used these conditions to study several examples of spontaneous synchronisation in quantum systems and presented several general principles for engineering quantum synchronisation that our results elucidate. In particular, we found that unital Liouvillians appeared to be the best candidates for models which exhibit synchronisation. This is because we may reduce the problem to eliminating dynamical symmetries that lack the required permutation symmetry structure for synchronisation. We were also able to use our general principles to explain experimental observations of the dynamics of fermionic spinor atoms in optical lattices.

These results provide the previously absent theory of spontaneous synchronisation in many-body quantum systems and have far-reaching applications to theoretical and experimental studies. The most obvious extension to this work is to study driven synchronisation. This would again follow from a study of our conjecture for time dependent Liouvillians and could also lead to a connection between our theory and the field of Synergetics.

Finally, in chapter 6, we studied  $\eta$ -paired superconductivity as a possible explanation for the recent experimental evidence of light-induced superconductivity. We presented a very general theory to explain these findings, which relied only on well-established principles of thermalisation and  $\eta$ -pairing symmetry. Using minimal model-specific assumptions, our theory asserts that a laser pulse induces ODLRO in the material, which is approximately conserved during a prethermalisation regime due to the material's Hamiltonian being dominated by a term that admits an  $\eta$ -symmetry. The proposal has several key predictions that agree with experimental observations and does not suffer from some of the flaws of other theories.

However, our proposal still has its own unanswered questions that warrant further investigation. The most pressing issue is to rigorously demonstrate superconductivity

of our proposed prethermal state in a 2D lattice model that resembles one of the materials used in experiments. This is a challenging problem, but we envisage making progress using work regarding the exponential stability of strongly interacting Hubbard models. Alternatively, it would be desirable to experimentally verify that  $\eta$ -pairs are responsible for the observed superconductivity, although it is unclear how this could be achieved. Efforts should also be made to understand in more detail the induction of ODLRO through light driving, ideally to establish a quantitative relation between the properties of the pulse and the levels of ODLRO, and by extension superconductivity, induced.

In summary, this thesis demonstrated the utility of algebraic approaches for studying the dynamics of non-equilibrium many-body quantum systems. The algebraic nature of these results and methods make them useful for many-body systems as they avoid the need for expensive or impossible computations in exponentially growing Hilbert spaces and instead require only an understanding of the algebra of the symmetries. Further, the ability to obtain exact analytic solutions has enabled us to provide substantial insight into transport in integrable models, time crystals, quantum synchronisation and light-induced superconductivity with results that are of both theoretical and experimental interest. Although we cannot claim to have wholly disproven Anderson's conjecture, this thesis marks a step in the right direction.

# Appendices



# A

## The Jordan-Wigner transformation

Several of the models used as examples in this thesis were models of spinful fermions and were constructed using the on-site fermionic creation and annihilation operators. These operators obey the canonical anticommutation relation

$$\{c_{\mathbf{x},\sigma}, c_{\mathbf{y},s}\} = \{c_{\mathbf{x},\sigma}^\dagger, c_{\mathbf{y},s}^\dagger\} = 0, \quad \{c_{\mathbf{x},\sigma}, c_{\mathbf{y},s}^\dagger\} = \delta_{\mathbf{x},\mathbf{y}}\delta_{\sigma,s}, \quad (\text{A.1})$$

where  $\mathbf{x}$  labels the lattice position and  $s \in \{\uparrow, \downarrow\}$  labels the spin. In order to perform numerical calculations these operators must be mapped to matrices in  $\mathbb{C}^{4^N \times 4^N}$  where  $N$  is the total number of lattice sites. In one dimension, this can be achieved using the Jordan-Wigner transformation [423] which we will now outline, although generalisations have been studied and exist in higher dimensions [424–427].

In one dimension, the Jordan-Wigner transformation provides a one-to-one mapping between spinful fermionic operators on  $N$  lattice sites and Pauli spin-1/2 operators on  $2N$  lattices arranged in a ladder of length  $N$  as illustrated in Figure A.1. We label Pauli operators on the top chain as  $\sigma_{j,t}^\alpha$  and those on the bottom as  $\sigma_{j,b}^\alpha$ . Each vertical rung, containing two spin-1/2 sites, is then associated with a single spinful fermion site through the mapping,

$$c_{j,\uparrow} = \left( \prod_{i < j} \sigma_{i,t}^z \sigma_{i,b}^z \right) \sigma_{j,t}^- \quad (\text{A.2})$$

$$c_{j,\downarrow} = \left( \prod_{i \leq j} \sigma_{i,t}^z \sigma_{i,b}^z \right) \sigma_{j,b}^- \quad (\text{A.3})$$

with the creation operators given by taking the Hermitian conjugate. The operators

$$F_k = \sigma_{k,t}^z \sigma_{k,b}^z, \quad (\text{A.4})$$

are sometimes referred to as the  $F$ -operators or Jordan-Wigner operators and are Hermitian, involutory operators.

This mapping is non-local, as the operator  $c_{k,\uparrow}$ , for instance, contains  $F$ -operators on all sites preceding  $k$ . One might worry that this breaks the locality of any Hamiltonian or local observable constructed from these fermionic operators. However

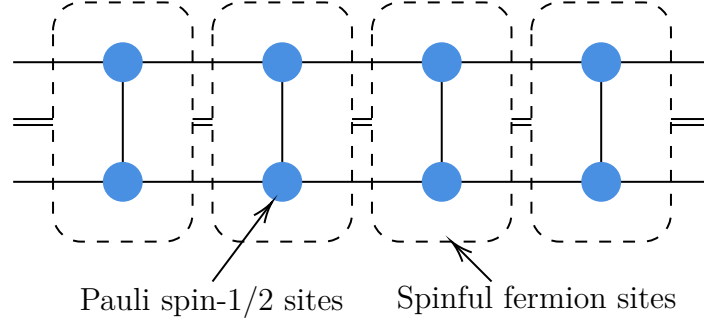


**Figure A.1:** The Jordan-Wigner ladder for a 1D Jordan-Wigner transformation between spinful fermions and Pauli spin-1/2 operators. The blue sites represent Pauli spin-1/2 sites while the dashed boxes indicate the spinful fermion sites.

fermionic operators must appear in pairs to conserve fermionic parity and we see that any pair of fermion operators has support only on the sites between them as the  $F$ -operators cancel each other. For example,

$$c_{j,\uparrow}^\dagger c_{k,\downarrow} = \left( \prod_{i<j} F_i \right) \sigma_{j,t}^+ \left( \prod_{i\leq k} F_i \right) \sigma_{k,b}^- \quad (\text{A.5})$$

$$= \sigma_{j,t}^+ \left( \prod_{j\leq i\leq k} F_i \right) \sigma_{k,b}^-. \quad (\text{A.6})$$

Alternatively, one can view this the other way as locality requiring that fermionic operators come in pairs, thus conserving fermionic parity.

# B

## Matrix product state calculations

As we discussed in Ch 1, exact numerical simulation of a many-body quantum system is extremely computationally expensive as a result of the exponentially growing Hilbert space with system size. The most widely used approach to mitigate this hurdle is to describe many-body quantum states using tensor networks. Here we will briefly outline the use of matrix product states (MPS) and matrix product operators (MPO) for simulating the evolution of closed one-dimensional many-body quantum systems. This discussion will be limited only to the essential details, and for further information the reader is directed to [26, 28, 428–432] and the references therein.

### 1 The MPS ansatz

At the heart of one dimensional tensor network methods for many-body quantum systems is the matrix product state ansatz. Suppose that our system consists of  $N$  sites each with a local Hilbert space  $\mathcal{H}_{\text{loc}}$  that has dimension  $d$ . In principal the local Hilbert spaces need not be identical but we focus on this case for simplicity. Choosing a local basis for each site as  $\{|i\rangle\}_{i=1}^d$  a general state of the full system can be expressed as

$$|\psi\rangle = \sum_{i_1, i_2, \dots, i_N} \Psi_{i_1, i_2, \dots, i_N} |i_1, i_2, \dots, i_N\rangle, \quad (\text{B.1})$$

where  $\Psi_{i_1, i_2, \dots, i_N}$  is a tensor with  $\mathcal{O}(d^N)$  complex entries. The MPS ansatz decomposes  $\Psi_{i_1, i_2, \dots, i_N}$  as a ‘train’ of smaller tensors,

$$\Psi_{i_1, i_2, \dots, i_N} = \sum_{b_1, b_2, \dots, b_{N-1}} A[i_1]_{b_1} A[i_2]_{b_2}^{b_1} A[i_3]_{b_3}^{b_2} \dots A[i_{N-1}]_{b_{N-1}}^{b_{N-2}} A[i_N]^{b_{N-1}}, \quad (\text{B.2})$$

which we visualise as

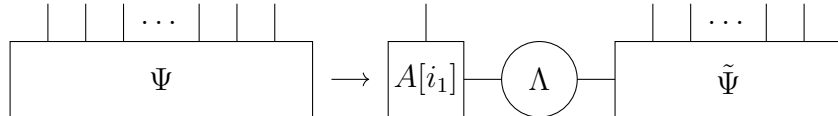
$$|\psi\rangle = \begin{array}{c} |i_1 \\ \boxed{A[i_1]} \\ b_1 \end{array} \text{---} \begin{array}{c} |i_2 \\ \boxed{A[i_2]} \\ b_2 \end{array} \text{---} \begin{array}{c} |i_3 \\ \boxed{A[i_3]} \\ b_3 \end{array} \text{---} \dots \text{---} \begin{array}{c} |i_{N-1} \\ \boxed{A[i_{N-1}]} \\ b_{N-1} \end{array} \text{---} \begin{array}{c} |i_N \\ \boxed{A[i_N]} \end{array} \quad (\text{B.3})$$

The labels on each link or *bond* between the sites indicate an index which is contracted between the two adjacent tensors, while the labels on the ‘free’ links indicate the site index which runs over the local basis states. We then require that each bond has a fixed maximum dimension  $\chi$ , called the bond dimension, so that  $b_j$  runs over  $1, \dots, \chi$  for each site  $j$ . Using this representation, we have  $\mathcal{O}(Nd\chi^2)$  complex parameters, which for fixed  $\chi$  scales only linearly with the system size. It is important to note that when simulating models with conservation laws, the MPS ansatz can be adapted to only express states on the relevant manifolds within  $\mathcal{H}$ , thus reducing the complexity further.

For sufficiently large  $\chi$  at fixed  $N$  the MPS ansatz can express all states in  $\mathcal{H}$ . To see this we can take a general state with wavefunction  $\Psi_{i_1, i_2, \dots, i_N}$  and consider this a matrix of dimension  $i_1 \times (i_2 i_3 \dots i_N)$ . We then perform a singular value decomposition to express

$$\Psi_{i_1, i_2, \dots, i_N} = A[i_1]^{b_1} \Lambda_{b_1}^a \tilde{\Psi}_{a, i_2, i_3, \dots, i_N}, \quad (\text{B.4})$$

where  $\Lambda$  is a diagonal matrix containing the singular values. Pictorially we can view this as



$$\Psi \rightarrow A[i_1] - \Lambda - \tilde{\Psi} \quad (\text{B.5})$$

Repeating this procedure as a sweep across all the lattice sites and absorbing the diagonal  $\Lambda$  matrix into the right-hand tensor yields an expression in the form of Eq. (B.3). However, this immediately negates any benefit from using the ansatz as in order to achieve this  $\chi$  must scale exponentially with  $N$ . Instead, we can limit the maximum bond dimension by only keeping the  $\chi$  greatest singular values in each singular value decomposition. This approximation limits the entanglement and long-range correlations. Fortunately, states with limited entanglement and only short-range correlations are exactly the typical states that arise when considering the evolution of a system under local Hamiltonians with only short-range interactions. Hence, we can be confident that the MPS ansatz will generally give a good approximation for the dynamics, provided we take the bond dimensions to be large enough. In practice, one generally increases the bond dimension incrementally until the solution converges sufficiently.

## 2 Matrix product operators

Having outlined how to describe pure quantum states using the MPS ansatz, we must also indicate how to represent operators, such as the Hamiltonian or other observables of interest. In the same basis we used above, we can express a generic operator,  $O$ , as

$$O = \sum_{\substack{i_1, i_2, \dots, i_N \\ j_1, j_2, \dots, j_N}} O_{i_1, i_2, \dots, i_N}^{j_1, j_2, \dots, j_N} |i_1, i_2, \dots, i_N\rangle \langle j_1, j_2, \dots, j_N|. \quad (\text{B.6})$$

We can then use the analogous decomposition as for the MPS ansatz to express

$$O_{i_1, i_2, \dots, i_N}^{j_1, j_2, \dots, j_N} = \sum_{b_1, b_2, \dots, b_{N-1}} O[i_1, j_1]_{b_1} O[i_2, j_2]_{b_2}^{b_1} \dots O[i_{N-1}, j_{N-1}]_{b_{N-1}}^{b_{N-2}} O[i_N, j_N]^{b_{N-1}}, \quad (\text{B.7})$$

which is pictorially represented by

$$O = \begin{array}{c} |i_1 \\ \boxed{O[i_1, j_1]} \\ |j_1 \end{array} \text{---}_{b_1} \begin{array}{c} |i_2 \\ \boxed{O[i_2, j_2]} \\ |j_2 \end{array} \text{---}_{b_2} \dots \text{---}_{b_{N-2}} \begin{array}{c} |i_{N-1} \\ \boxed{O[i_{N-1}, j_{N-1}]} \\ |j_{N-1} \end{array} \text{---}_{b_{N-1}} \begin{array}{c} |i_N \\ \boxed{O[i_N, j_N]} \\ |j_N \end{array} \quad (\text{B.8})$$

The action of applying an operator to a state is then performed by contracting the relevant indices as

$$O |\psi\rangle = \begin{array}{c} \begin{array}{c} |i_1 \\ \boxed{O[i_1, j_1]} \\ |j_1 \end{array} \text{---}_{b_1} \begin{array}{c} |i_2 \\ \boxed{O[i_2, j_2]} \\ |j_2 \end{array} \text{---}_{b_2} \dots \text{---}_{b_{N-2}} \begin{array}{c} |i_{N-1} \\ \boxed{O[i_{N-1}, j_{N-1}]} \\ |j_{N-1} \end{array} \text{---}_{b_{N-1}} \begin{array}{c} |i_N \\ \boxed{O[i_N, j_N]} \\ |j_N \end{array} \\ \begin{array}{c} |j_1 \\ \boxed{A[j_1]} \\ |b'_1 \end{array} \text{---}_{b'_1} \begin{array}{c} |j_2 \\ \boxed{A[j_2]} \\ |b'_2 \end{array} \text{---}_{b'_2} \dots \text{---}_{b'_{N-2}} \begin{array}{c} |j_{N-1} \\ \boxed{A[j_{N-1}]} \\ |b'_{N-1} \end{array} \text{---}_{b'_{N-1}} \begin{array}{c} |j_N \\ \boxed{A[j_N]} \end{array} \end{array} \quad (\text{B.9a})$$

$$= \begin{array}{c} |i_1 \\ \boxed{A'[i_1]} \\ |b''_1 \end{array} \text{---}_{b''_1} \begin{array}{c} |i_2 \\ \boxed{A'[i_2]} \\ |b''_2 \end{array} \text{---}_{b''_2} \dots \text{---}_{b''_{N-2}} \begin{array}{c} |i_{N-1} \\ \boxed{A'[i_{N-1}]} \\ |b''_{N-1} \end{array} \text{---}_{b''_{N-1}} \begin{array}{c} |i_N \\ \boxed{A'[i_N]} \end{array} \quad (\text{B.9b})$$

Note that when performing these contractions, it is usually necessary to perform a sweep of singular value decompositions to ensure that the bonds still have maximum dimension  $\chi$ .

Finally we can calculate the overlap between two states, and by extension the expectation values of observables or norms of states, by conjugating and contracting



contracting the observable with the tensors for that site as

$$\langle O_k \rangle = \begin{array}{c} \begin{array}{|c|} \hline A[i_k]^* \\ \hline \end{array} \\ | \\ \begin{array}{|c|} \hline O \\ \hline \end{array} \\ | \\ \begin{array}{|c|} \hline A[i_k] \\ \hline \end{array} \end{array} \quad (B.14)$$

By extension, careful positioning of the orthogonality centre can improve the efficiency of computing the expectation value of any observable with finite support.

### 3 Time evolution operators

The matrix product state ansatz was initially developed to study the ground states of many-body systems. However, under the assumption that the system does not become too entangled as it evolves, the MPS ansatz can also be used to study dynamics. In particular, these methods are most effective for time-independent Hamiltonians with finite range interactions.

Consider the Schrodinger equation

$$\frac{d}{dt} |\psi\rangle = -iH |\psi\rangle, \quad |\psi(0)\rangle = |\psi_0\rangle, \quad (B.15)$$

which can be solved as

$$|\psi(t)\rangle = e^{-itH} |\psi_0\rangle. \quad (B.16)$$

For small  $\delta t$  we can approximate

$$U(\delta t) = e^{-i\delta t H} = \mathbb{1} - i\delta t H - \frac{\delta t^2}{2} H^2 + \dots \quad (B.17)$$

where we truncate the series at some finite order. If we have expressed  $H$  as an MPO then by the above expansion we can also calculate an MPO approximation to  $U(\delta t)$  from which we can compute

$$|\psi(n\delta t)\rangle = U(\delta t)^n |\psi_0\rangle. \quad (B.18)$$

In practice, for a general Hamiltonian, it is usually only computationally feasible to calculate the expansion in Eq. (B.17) to second or possibly third order. However, techniques have been developed to calculate  $U(\delta t)$  up to order  $k$  without calculating  $H^k$  directly. A widely used method, and the one used for simulations in this thesis where applicable, is the Suzuki-Trotter decomposition [15, 21]. For this

method, we assume that the 1D Hamiltonian contains only on-site and nearest neighbour terms and can be written as

$$H = \sum_k k_k, \quad (\text{B.19})$$

where  $h_k$  acts only on sites  $k$  and  $k + 1$ . This can be decomposed as

$$H = \sum_{\text{even } l} h_l + \sum_{\text{odd } k} h_k = F + G \quad (\text{B.20})$$

where  $[h_l, h_k] = 0$  for  $l$  even and  $k$  odd. We can then use the Trotter expansion to write<sup>1</sup>

$$e^{-i\delta t H} = e^{-i\delta t F/2} e^{-i\delta t G} e^{-i\delta t F/2} + \mathcal{O}(\delta t^3). \quad (\text{B.21})$$

Finally we notice that

$$e^{\lambda F} = \prod_{\text{even } l} e^{\lambda h_l}, \quad (\text{B.22})$$

and similarly for  $G$  since the terms in  $F$  and  $G$  all commute. The operator  $e^{\lambda h_l}$  is a two site operator which can either be calculated exactly or easily approximated to a very high accuracy.

It is important to remark that several other tensor-network algorithms for simulating the evolution of closed many-body quantum systems exist and further details can be found in the review of [23] and the references therein.

---

<sup>1</sup>Higher order approximations can be constructed. See [433] for details.





# Tensor network methods for the dynamics of open systems

We now outline two methods that extend the MPS based methods discussed above in Appdx B to study the evolution of open many-body quantum systems when described by the Lindblad equation.

## 1 Quantum Monte-Carlo

Also known as quantum trajectories or quantum jumps, this method uses Monte-Carlo sampling to simulate the evolution of a pure initial state under the Lindblad equation [84, 85, 434, 435]. The method proceeds as follows. Given a Lindblad equation

$$\frac{d}{dt}\rho(t) = -i[H, \rho] + \sum_k 2L_k\rho L_k^\dagger - \{L_k^\dagger L_k, \rho\}, \quad (\text{C.1})$$

we define

$$H_{\text{eff}} = H - i\sum_k L_k^\dagger L_k. \quad (\text{C.2})$$

The algorithm then defines a stochastic evolution for a sample trajectory  $|\psi_i(t)\rangle$  as follows. Given the state at time  $t_0$  choose a random number  $r$  uniformly from  $[0, 1]$ . Then solve the equation

$$\|e^{-it_1 H_{\text{eff}}} |\psi_i(t_0)\rangle\|^2 = r, \quad (\text{C.3})$$

for  $t_1$  using any numerical integration method. The time  $t_1$  indicates the time at which a ‘jump’ will occur. For  $t \in [t_0, t_1]$  the trajectory is given by

$$|\psi_i(t)\rangle = \frac{e^{-i(t-t_0)H_{\text{eff}}} |\psi_i(t_0)\rangle}{\|e^{-i(t-t_0)H_{\text{eff}}} |\psi_i(t_0)\rangle\|}. \quad (\text{C.4})$$

Now let

$$|\phi_-\rangle = \frac{e^{-i(t_1-t_0)H_{\text{eff}}} |\psi_i(t_0)\rangle}{\|e^{-i(t_1-t_0)H_{\text{eff}}} |\psi_i(t_0)\rangle\|}, \quad (\text{C.5})$$

be the state of the trajectory immediately before the jump and calculate

$$p_m = \langle \phi_- | L_m^\dagger L_m | \phi_- \rangle. \quad (\text{C.6})$$

We now draw a second random number,  $s$ , uniformly from  $[0, 1]$  and find the smallest  $k$  such that

$$s < \frac{p_k}{\sum_m p_m}. \quad (\text{C.7})$$

We then define

$$|\psi_i(t_1)\rangle = \frac{L_k |\phi_- \rangle}{\|L_k |\phi_- \rangle\|}, \quad (\text{C.8})$$

and repeat the procedure. Once we have computed  $M$  such trajectories independently, the state of the system is approximated as

$$\rho(t) = \frac{1}{M} \sum_{i=1}^M |\psi_i(t)\rangle \langle \psi_i(t)|, \quad (\text{C.9})$$

and this approximation is then used to calculate expectation values of observables.

This method can be implemented using the MPS ansatz we outlined above and is particularly convenient for computation as the individual trajectories are calculated independently and can therefore be naturally parallelised. However, the method is limited by requiring the initial state to be pure. In principle one can calculate the evolution of a general mixed state,  $\rho_0 = \sum_k |\psi_k\rangle \langle \psi_k|$ , by evolving each component,  $|\psi_k\rangle$ , but this can rapidly become impractical, especially for thermal states.

## 2 Ancilla MPS description

The second method used in this thesis for simulating the Lindblad equation is the ancilla method. Recall that an operator on  $\mathcal{H}$  can be described as an MPO, and thus we can write the density operator describing our state as

$$\rho = \begin{array}{c} | \\ \boxed{\rho_1} \\ | \end{array} - \begin{array}{c} | \\ \boxed{\rho_2} \\ | \end{array} - \dots - \begin{array}{c} | \\ \boxed{\rho_{N-1}} \\ | \end{array} - \begin{array}{c} | \\ \boxed{\rho_N} \\ | \end{array} \quad (\text{C.10})$$

We can then move the downward facing legs to the top which creates a MPS with  $2N$  legs

$$|\rho\rangle\rangle = \begin{array}{c} | \quad | \\ \boxed{\rho_1} \\ | \quad | \end{array} - \begin{array}{c} | \quad | \\ \boxed{\rho_2} \\ | \quad | \end{array} - \dots - \begin{array}{c} | \quad | \\ \boxed{\rho_N} \\ | \quad | \end{array} \quad (\text{C.11})$$

$$= \begin{array}{c} | \\ \boxed{\rho_1} \\ | \end{array} - \begin{array}{c} | \\ \boxed{\rho'_1} \\ | \end{array} - \begin{array}{c} | \\ \boxed{\rho_2} \\ | \end{array} - \begin{array}{c} | \\ \boxed{\rho'_2} \\ | \end{array} - \dots - \begin{array}{c} | \\ \boxed{\rho_N} \\ | \end{array} - \begin{array}{c} | \\ \boxed{\rho'_N} \\ | \end{array} \quad (\text{C.12})$$

In the second line we have used a singular value decomposition to separate the pairs of legs into single ‘ancilla’ sites. This is equivalent to working in Fock-Liouville space with

$$|\rho\rangle\rangle = \sum_{\substack{i_1, i_2, \dots, i_N \\ j_1, j_2, \dots, j_N}} \rho_{i_1, j_1, i_2, \dots, i_N, j_N} |i_1, j_1, \dots, i_N, j_N\rangle\rangle. \quad (\text{C.13})$$

We then write the Liouvillian superoperator as an MPO on the  $2N$  legs and calculate the time evolution using similar techniques to Appdx B. When considering fermionic systems, care must be taken to place the  $F$ -operators from the Jordan-Wigner transformation on the correct legs.

This method can work with both pure or mixed initial states, so it is well suited to studying the dynamics of thermal initial states. However, in this naive implementation, there is no guarantee that the MPS will continue to describe a density operator throughout the evolution, and so at each step one must enforce hermicity and renormalise so that the trace remains 1. More careful implementation can be restricted to the manifold of density operators, thus avoiding this problem. In general, this method will require a higher bond dimension,  $\chi$ , to achieve a given accuracy than when working with closed systems, and it remains to be understood thoroughly how justified the MPS ansatz is for describing density states.

# References

- [1] P. W. Anderson. “More Is Different”. In: *Science* 177.4047 (1972), pp. 393–396. DOI: 10.1126/science.177.4047.393.
- [2] Z. E. Musielak and B. Quarles. “The Three-Body Problem”. In: *Rep. Prog. Phys.* 77.6 (2014), p. 065901. DOI: 10.1088/0034-4885/77/6/065901.
- [3] Weimin Zheng. “Research Trend of Large-Scale Supercomputers and Applications from the TOP500 and Gordon Bell Prize”. In: *Sci. China Inf. Sci.* 63.7 (2020), p. 171001. DOI: 10.1007/s11432-020-2861-0.
- [4] *June 2021 / TOP500*. 2021. URL: <https://www.top500.org/lists/top500/2021/06/>.
- [5] M. Fannes, B. Nachtergaele, and R. F. Werner. “Finitely Correlated States on Quantum Spin Chains”. In: *Commun.Math. Phys.* 144.3 (1992), pp. 443–490. DOI: 10.1007/BF02099178.
- [6] A. Klümper, A. Schadschneider, and J. Zittartz. “Matrix Product Ground States for One-Dimensional Spin-1 Quantum Antiferromagnets”. In: *EPL* 24.4 (1993), pp. 293–297. DOI: 10.1209/0295-5075/24/4/010.
- [7] B. Pirvu et al. “Matrix Product Operator Representations”. In: *New J. Phys.* 12.2 (2010), p. 025012. DOI: 10.1088/1367-2630/12/2/025012.
- [8] F. Verstraete and J. I. Cirac. “Renormalization Algorithms for Quantum-Many Body Systems in Two and Higher Dimensions”. In: (2004).
- [9] J. Jordan et al. “Classical Simulation of Infinite-Size Quantum Lattice Systems in Two Spatial Dimensions”. In: *Physical Review Letters* 101.25 (2008). DOI: 10.1103/PhysRevLett.101.250602.
- [10] I. V. Oseledets. “Tensor-Train Decomposition”. In: *SIAM J. Sci. Comput.* 33.5 (2011), pp. 2295–2317. DOI: 10.1137/090752286.
- [11] Steven R. White. “Density Matrix Formulation for Quantum Renormalization Groups”. In: *Phys. Rev. Lett.* 69.19 (1992), pp. 2863–2866. DOI: 10.1103/PhysRevLett.69.2863.
- [12] Steven R. White. “Density-Matrix Algorithms for Quantum Renormalization Groups”. In: *Phys. Rev. B* 48.14 (1993), pp. 10345–10356. DOI: 10.1103/PhysRevB.48.10345.
- [13] Stellan Östlund and Stefan Rommer. “Thermodynamic Limit of Density Matrix Renormalization”. In: *Phys. Rev. Lett.* 75.19 (1995), pp. 3537–3540. DOI: 10.1103/PhysRevLett.75.3537.
- [14] M. B. Hastings. “Solving Gapped Hamiltonians Locally”. In: *Phys. Rev. B* 73.8 (2006), p. 085115. DOI: 10.1103/PhysRevB.73.085115.
- [15] Guifré Vidal. “Efficient Simulation of One-Dimensional Quantum Many-Body Systems”. In: *Phys. Rev. Lett.* 93.4 (2004), p. 040502. DOI: 10.1103/PhysRevLett.93.040502.
- [16] Steven R. White and Adrian E. Feiguin. “Real-Time Evolution Using the Density Matrix Renormalization Group”. In: *Phys. Rev. Lett.* 93.7 (2004), p. 076401. DOI: 10.1103/PhysRevLett.93.076401.

- [17] A. J. Daley et al. “Time-Dependent Density-Matrix Renormalization-Group Using Adaptive Effective Hilbert Spaces”. In: *J. Stat. Mech.* 2004.04 (2004), P04005. DOI: 10.1088/1742-5468/2004/04/P04005.
- [18] Ulrich Schollwöck. “The Density-Matrix Renormalization Group in the Age of Matrix Product States”. In: *Annals of Physics*. January 2011 Special Issue 326.1 (2011), pp. 96–192. DOI: 10.1016/j.aop.2010.09.012.
- [19] Jutho Haegeman et al. “Time-Dependent Variational Principle for Quantum Lattices”. In: *Phys. Rev. Lett.* 107.7 (2011), p. 070601. DOI: 10.1103/PhysRevLett.107.070601.
- [20] Jutho Haegeman et al. “Unifying Time Evolution and Optimization with Matrix Product States”. In: *Phys. Rev. B* 94.16 (2016), p. 165116. DOI: 10.1103/PhysRevB.94.165116.
- [21] Masuo Suzuki. “Generalized Trotter’s Formula and Systematic Approximants of Exponential Operators and Inner Derivations with Applications to Many-Body Problems”. In: *Commun.Math. Phys.* 51.2 (1976), pp. 183–190. DOI: 10.1007/BF01609348.
- [22] Chris C. Paige, Beresford N. Parlett, and Henk A. van der Vorst. “Approximate Solutions and Eigenvalue Bounds from Krylov Subspaces”. In: *Numerical Linear Algebra with Applications* 2.2 (1995), pp. 115–133. DOI: 10.1002/nla.1680020205.
- [23] Sebastian Paeckel et al. “Time-Evolution Methods for Matrix-Product States”. In: *Annals of Physics* 411 (2019), p. 167998. DOI: 10.1016/j.aop.2019.167998.
- [24] Karen A. Hallberg. “New Trends in Density Matrix Renormalization”. In: *Advances in Physics* 55.5-6 (2006), pp. 477–526. DOI: 10.1080/00018730600766432.
- [25] F. Verstraete, J. J. García-Ripoll, and J. I. Cirac. “Matrix Product Density Operators: Simulation of Finite-Temperature and Dissipative Systems”. In: *Phys. Rev. Lett.* 93.20 (2004), p. 207204. DOI: 10.1103/PhysRevLett.93.207204.
- [26] Román Orús. “Tensor Networks for Complex Quantum Systems”. In: *Nat Rev Phys* 1.9 (2019), pp. 538–550. DOI: 10.1038/s42254-019-0086-7.
- [27] Guifré Vidal. “Efficient Classical Simulation of Slightly Entangled Quantum Computations”. In: *Phys. Rev. Lett.* 91.14 (2003), p. 147902. DOI: 10.1103/PhysRevLett.91.147902.
- [28] Román Orús. “A Practical Introduction to Tensor Networks: Matrix Product States and Projected Entangled Pair States”. In: *Annals of Physics* 349 (2014), pp. 117–158. DOI: 10.1016/j.aop.2014.06.013.
- [29] Michael Zwolak and Guifré Vidal. “Mixed-State Dynamics in One-Dimensional Quantum Lattice Systems: A Time-Dependent Superoperator Renormalization Algorithm”. In: *Phys. Rev. Lett.* 93.20 (2004), p. 207205. DOI: 10.1103/PhysRevLett.93.207205.
- [30] A. W. Sandvik and G. Vidal. “Variational Quantum Monte Carlo Simulations with Tensor-Network States”. In: *Phys. Rev. Lett.* 99.22 (2007), p. 220602. DOI: 10.1103/PhysRevLett.99.220602.

- [31] F. Verstraete and J. I. Cirac. “Continuous Matrix Product States for Quantum Fields”. In: *Phys. Rev. Lett.* 104.19 (2010), p. 190405. DOI: 10.1103/PhysRevLett.104.190405.
- [32] Norbert Schuch et al. “Computational Complexity of Projected Entangled Pair States”. In: *Phys. Rev. Lett.* 98.14 (2007), p. 140506. DOI: 10.1103/PhysRevLett.98.140506.
- [33] J. von Neumann. “Proof of the Ergodic Theorem and the H-theorem in Quantum Mechanics”. In: *EPJ H* 35.2 (2010), pp. 201–237. DOI: 10.1140/epjh/e2010-00008-5.
- [34] S. Goldstein et al. “Long-Time Behavior of Macroscopic Quantum Systems”. In: *EPJ H* 35.2 (2010), pp. 173–200. DOI: 10.1140/epjh/e2010-00007-7.
- [35] Luca D’Alessio et al. “From Quantum Chaos and Eigenstate Thermalization to Statistical Mechanics and Thermodynamics”. In: *Advances in Physics* 65.3 (2016), pp. 239–362. DOI: 10.1080/00018732.2016.1198134.
- [36] J. M. Deutsch. “Quantum Statistical Mechanics in a Closed System”. In: *Phys. Rev. A* 43.4 (1991), pp. 2046–2049. DOI: 10.1103/PhysRevA.43.2046.
- [37] M. L. Mehta. *Random Matrices*. Amsterdam; San Diego, CA: Elsevier/Academic Press, 2004. URL: <https://www.sciencedirect.com/science/book/9780120884094>.
- [38] Mark Srednicki. “Chaos and Quantum Thermalization”. In: *Phys. Rev. E* 50.2 (1994), pp. 888–901. DOI: 10.1103/PhysRevE.50.888.
- [39] Mark Srednicki. “The Approach to Thermal Equilibrium in Quantized Chaotic Systems”. In: *J. Phys. A: Math. Gen.* 32.7 (1999), pp. 1163–1175. DOI: 10.1088/0305-4470/32/7/007.
- [40] Javier Duoandikoetxea. *Fourier Analysis*. Providence, R.I: American Mathematical Society, 2001.
- [41] Marcos Rigol, Vanja Dunjko, and Maxim Olshanii. “Thermalization and Its Mechanism for Generic Isolated Quantum Systems”. In: *Nature* 452.7189 (2008), pp. 854–858. DOI: 10.1038/nature06838.
- [42] Marcos Rigol. “Breakdown of Thermalization in Finite One-Dimensional Systems”. In: *Phys. Rev. Lett.* 103.10 (2009), p. 100403. DOI: 10.1103/PhysRevLett.103.100403.
- [43] Heinz-Peter Breuer and Francesco Petruccione. *The Theory of Open Quantum Systems*. Oxford: Oxford University Press, 2007. DOI: 10.1093/acprof:oso/9780199213900.001.0001.
- [44] Robert Alicki and Mark Fannes. *Quantum Dynamical Systems*. Oxford: Oxford University Press, 2001. DOI: 10.1093/acprof:oso/9780198504009.001.0001.
- [45] Daniel Manzano. “A Short Introduction to the Lindblad Master Equation”. In: *AIP Advances* 10.2 (2020), p. 025106. DOI: 10.1063/1.5115323.
- [46] W. Forrest Stinespring. “Positive Functions on C\*-Algebras”. In: *Proceedings of the American Mathematical Society* 6.2 (1955), pp. 211–216. DOI: 10.2307/2032342.

- [47] Philip Pechukas. “Reduced Dynamics Need Not Be Completely Positive”. In: *Phys. Rev. Lett.* 73.8 (1994), pp. 1060–1062. DOI: 10.1103/PhysRevLett.73.1060.
- [48] Christopher J. Wood. “Non-Completely Positive Maps: Properties and Applications”. Bachelor of Science with Honours. Macquarie University, 2009. arXiv: 0911.3199. URL: <http://arxiv.org/abs/0911.3199>.
- [49] Hilary A. Carteret, Daniel R. Terno, and Karol Życzkowski. “Dynamics beyond Completely Positive Maps: Some Properties and Applications”. In: *Phys. Rev. A* 77.4 (2008), p. 042113. DOI: 10.1103/PhysRevA.77.042113.
- [50] F. Strocchi. *An Introduction to the Mathematical Structure of Quantum Mechanics: A Short Course for Mathematicians*. 2nd ed. edition. New Jersey: World Scientific Publishing Company, 2008.
- [51] I. E. Segal. “Irreducible Representations of Operator Algebras”. In: *Bulletin of the American Mathematical Society* 53.2 (1947), pp. 73–88. URL: <https://projecteuclid.org/journals/bulletin-of-the-american-mathematical-society/volume-53/issue-2/Irreducible-representations-of-operator-algebras/bams/1183510397.full>.
- [52] Jacques Dixmier. *C\*-Algebras*. Amsterdam: North Holland, 2011.
- [53] Robert S. Doran and American Mathematical Society. *C\*-Algebras: 1943-1993 : A Fifty Year Celebration : AMS Special Session Commemorating the First Fifty Years of C\*-Algebra Theory, January 13-14, 1993, San Antonio, Texas*. American Mathematical Society, 1994.
- [54] Israel Gelfand and Mark Naimark. “On the Imbedding of Normed Rings into the Ring of Operators in Hilbert Space”. In: (1943).
- [55] I.E. Segal. *Decompositions of Operator Algebras, 1 and 2*. Providence, UNITED STATES: American Mathematical Society, 1951. URL: <http://ebookcentral.proquest.com/lib/oxford/detail.action?docID=3113552>.
- [56] Mark M. Wilde. *Quantum Information Theory*. Second. Cambridge: Cambridge University Press, 2017. DOI: 10.1017/9781316809976.
- [57] G. Lindblad. “On the Generators of Quantum Dynamical Semigroups”. In: *Commun.Math. Phys.* 48.2 (1976), pp. 119–130. DOI: 10.1007/BF01608499.
- [58] A. G. Redfield. “The Theory of Relaxation Processes”. In: *Advances in Magnetic and Optical Resonance*. Ed. by John S. Waugh. Vol. 1. Advances in Magnetic Resonance. Academic Press, 1965, pp. 1–32. DOI: 10.1016/B978-1-4832-3114-3.50007-6.
- [59] Daniel A. Lidar, Zolt Bihary, and K. Birgitta Whaley. “From Completely Positive Maps to the Quantum Markovian Semigroup Master Equation”. In: *Chemical Physics* 268.1 (2001), pp. 35–53. DOI: 10.1016/S0301-0104(01)00330-5.
- [60] Michael M. Wolf and J. Ignacio Cirac. “Dividing Quantum Channels”. In: *Commun. Math. Phys.* 279.1 (2008), pp. 147–168. DOI: 10.1007/s00220-008-0411-y.
- [61] Ángel Rivas, Susana F. Huelga, and Martin B. Plenio. “Quantum Non-Markovianity: Characterization, Quantification and Detection”. In: *Rep. Prog. Phys.* 77.9 (2014), p. 094001. DOI: 10.1088/0034-4885/77/9/094001.

- [62] Marvin Rausand and Arnljot Hoyland. *System Reliability Theory: Models, Statistical Methods, and Applications*. 2nd edition. Hoboken, NJ: Wiley-Interscience, 2004.
- [63] Valerio Scarani et al. “Thermalizing Quantum Machines: Dissipation and Entanglement”. In: *Phys. Rev. Lett.* 88.9 (2002), p. 097905. DOI: 10.1103/PhysRevLett.88.097905.
- [64] Mário Ziman, Peter Štelmachovič, and Vladimír Bužek. “Description of Quantum Dynamics of Open Systems Based on Collision-Like Models”. In: *Open Syst. Inf. Dyn.* 12.01 (2005), pp. 81–91. DOI: 10.1007/s11080-005-0488-0.
- [65] Mário Ziman and Vladimír Bužek. “All (Qubit) Decoherences: Complete Characterization and Physical Implementation”. In: *Phys. Rev. A* 72.2 (2005), p. 022110. DOI: 10.1103/PhysRevA.72.022110.
- [66] Luigi Accardi, Alberto Frigerio, and John T. Lewis. “Quantum Stochastic Processes”. In: *Publ. Res. Inst. Math. Sci.* 18.1 (1982), pp. 97–133. DOI: 10.2977/prims/1195184017.
- [67] Heinz-Peter Breuer, Elsi-Mari Laine, and Jyrki Piilo. “Measure for the Degree of Non-Markovian Behavior of Quantum Processes in Open Systems”. In: *Phys. Rev. Lett.* 103.21 (2009), p. 210401. DOI: 10.1103/PhysRevLett.103.210401.
- [68] Steffen Wißmann, Heinz-Peter Breuer, and Bassano Vacchini. “Generalized Trace-Distance Measure Connecting Quantum and Classical Non-Markovianity”. In: *Phys. Rev. A* 92.4 (2015), p. 042108. DOI: 10.1103/PhysRevA.92.042108.
- [69] Bassano Vacchini. “A Classical Appraisal of Quantum Definitions of Non-Markovian Dynamics”. In: *J. Phys. B: At. Mol. Opt. Phys.* 45.15 (2012), p. 154007. DOI: 10.1088/0953-4075/45/15/154007.
- [70] Dariusz Chruściński and Filip A. Wudarski. “Non-Markovian Random Unitary Qubit Dynamics”. In: *Physics Letters A* 377.21 (2013), pp. 1425–1429. DOI: 10.1016/j.physleta.2013.04.020.
- [71] Inés de Vega and Daniel Alonso. “Dynamics of Non-Markovian Open Quantum Systems”. In: *Rev. Mod. Phys.* 89.1 (2017), p. 015001. DOI: 10.1103/RevModPhys.89.015001.
- [72] S. Chaturvedi and F. Shibata. “Time-Convolutionless Projection Operator Formalism for Elimination of Fast Variables. Applications to Brownian Motion”. In: *Z Physik B* 35.3 (1979), pp. 297–308. DOI: 10.1007/BF01319852.
- [73] Bassano Vacchini. “Generalized Master Equations Leading to Completely Positive Dynamics”. In: *Phys. Rev. Lett.* 117.23 (2016), p. 230401. DOI: 10.1103/PhysRevLett.117.230401.
- [74] Stephen M. Barnett and Stig Stenholm. “Hazards of Reservoir Memory”. In: *Phys. Rev. A* 64.3 (2001), p. 033808. DOI: 10.1103/PhysRevA.64.033808.
- [75] Alex W. Chin, Susana F. Huelga, and Martin B. Plenio. “Quantum Metrology in Non-Markovian Environments”. In: *Phys. Rev. Lett.* 109.23 (2012), p. 233601. DOI: 10.1103/PhysRevLett.109.233601.
- [76] Elsi-Mari Laine, Heinz-Peter Breuer, and Jyrki Piilo. “Nonlocal Memory Effects Allow Perfect Teleportation with Mixed States”. In: *Sci Rep* 4.1 (2014), p. 4620. DOI: 10.1038/srep04620.



- [77] B. Bylicka, D. Chruściński, and S. Maniscalco. “Non-Markovianity and Reservoir Memory of Quantum Channels: A Quantum Information Theory Perspective”. In: *Sci Rep* 4.1 (2014), p. 5720. DOI: 10.1038/srep05720.
- [78] Guo-Yong Xiang et al. “Memory Assisted Entanglement Distribution in Optical Fibers”. In: *Research in Optical Sciences (2014), Paper QTu3A.3*. Optical Society of America, 2014, QTu3A.3. DOI: 10.1364/QIM.2014.QTu3A.3.
- [79] George F. Simmons. *Differential Equations with Applications and Historical Notes*. 3rd edition. Boca Raton London New York: Chapman and Hall/CRC, 2016.
- [80] Vasily E. Tarasov. “Chapter 22 Quantum Dynamical Methods”. In: *Monograph Series on Nonlinear Science and Complexity*. Ed. by Vasily E. Tarasov. Vol. 7. Quantum Mechanics of Non-Hamiltonian and Dissipative Systems. Elsevier, 2008, pp. 463–474. DOI: 10.1016/S1574-6917(07)00022-0.
- [81] Hans-Jürgen Briegel and Berthold-Georg Englert. “Quantum Optical Master Equations: The Use of Damping Bases”. In: *Phys. Rev. A* 47.4 (1993), pp. 3311–3329. DOI: 10.1103/PhysRevA.47.3311.
- [82] Frank Verstraete, V. Murg, and J. I. Cirac. “Matrix Product States, Projected Entangled Pair States, and Variational Renormalization Group Methods for Quantum Spin Systems”. In: *ADVANCES IN PHYSICS* 57.2 (2008), pp. 143–224. DOI: 10.1080/14789940801912366.
- [83] Regina Finsterhölzl et al. “Using Matrix-Product States for Open Quantum Many-Body Systems: Efficient Algorithms for Markovian and Non-Markovian Time-Evolution”. In: *Entropy* 22.9 (2020), p. 984. DOI: 10.3390/e22090984.
- [84] Andrew J. Daley. “Quantum Trajectories and Open Many-Body Quantum Systems”. In: *Advances in Physics* 63.2 (2014), pp. 77–149. DOI: 10.1080/00018732.2014.933502.
- [85] Jean Dalibard, Yvan Castin, and Klaus Mølmer. “Wave-Function Approach to Dissipative Processes in Quantum Optics”. In: *Phys. Rev. Lett.* 68.5 (1992), pp. 580–583. DOI: 10.1103/PhysRevLett.68.580.
- [86] B. Bidégaray, A. Bourgeade, and D. Reignier. “Introducing Physical Relaxation Terms in Bloch Equations”. In: *Journal of Computational Physics* 170.2 (2001), pp. 603–613. DOI: 10.1006/jcph.2001.6752.
- [87] Michael Riesch and Christian Jirauschek. “Analyzing the Positivity Preservation of Numerical Methods for the Liouville-von Neumann Equation”. In: *Journal of Computational Physics* 390 (2019), pp. 290–296. DOI: 10.1016/j.jcp.2019.04.006.
- [88] David E Evans and Harald Hanche-Olsen. “The Generators of Positive Semigroups”. In: *Journal of Functional Analysis* 32.2 (1979), pp. 207–212. DOI: 10.1016/0022-1236(79)90054-5.
- [89] David E. Evans. “Irreducible Quantum Dynamical Semigroups”. In: *Commun.Math. Phys.* 54.3 (1977), pp. 293–297. DOI: 10.1007/BF01614091.
- [90] P. D. Nation et al. “Iterative Solutions to the Steady-State Density Matrix for Optomechanical Systems”. In: *Phys. Rev. E* 91.1 (2015), p. 013307. DOI: 10.1103/PhysRevE.91.013307.

- [91] Victor V. Albert and Liang Jiang. “Symmetries and Conserved Quantities in Lindblad Master Equations”. In: *Phys. Rev. A* 89.2 (2014), p. 022118. DOI: 10.1103/PhysRevA.89.022118.
- [92] E. Noether. “Invariante Variationsprobleme”. In: *Nachrichten von der Gesellschaft der Wissenschaften zu Göttingen, Mathematisch-Physikalische Klasse* 1918 (1918), pp. 235–257. URL: <https://eudml.org/doc/59024>.
- [93] J. P. Elliott and P. G. Dawber. *Symmetry in Physics: Principles and Simple Applications: 001*. Reprint edition. New York: Oxford Univ Pr, 1985.
- [94] Martin Lorenz. *A Tour of Representation Theory*. Providence, Rhode Island: American Mathematical Society, 2018.
- [95] Masahito Hayashi. *Group Representation for Quantum Theory*. Springer International Publishing, 2017. DOI: 10.1007/978-3-319-44906-7.
- [96] P. Mazur. “Non-Ergodicity of Phase Functions in Certain Systems”. In: *Physica* 43.4 (1969), pp. 533–545. DOI: 10.1016/0031-8914(69)90185-2.
- [97] M. Suzuki. “Ergodicity, Constants of Motion, and Bounds for Susceptibilities”. In: *Physica* 51.2 (1971), pp. 277–291. DOI: 10.1016/0031-8914(71)90226-6.
- [98] Enej Ilievski and Tomaž Prosen. “Thermodynamic Bounds on Drude Weights in Terms of Almost-conserved Quantities”. In: *Commun. Math. Phys.* 318.3 (2013), pp. 809–830. DOI: 10.1007/s00220-012-1599-4.
- [99] Enej Ilievski et al. “Quasilocal Charges in Integrable Lattice Systems”. In: *J. Stat. Mech.* 2016.6 (2016), p. 064008. DOI: 10.1088/1742-5468/2016/06/064008.
- [100] Enej Ilievski, Marko Medenjak, and Tomaž Prosen. “Quasilocal Conserved Operators in the Isotropic Heisenberg Spin- $\frac{1}{2}$  Chain”. In: *Phys. Rev. Lett.* 115.12 (2015), p. 120601. DOI: 10.1103/PhysRevLett.115.120601.
- [101] Marko Medenjak. “Quasilocality and Equilibration in Quantum Systems”. PhD thesis. University of Ljubljana, Faculty of Mathematics and Physics, 2018. URL: <https://repozitorij.uni-lj.si/IzpisGradiva.php?lang=eng&id=101756>.
- [102] Tomaž Prosen and Enej Ilievski. “Families of Quasilocal Conservation Laws and Quantum Spin Transport”. In: *Phys. Rev. Lett.* 111.5 (2013), p. 057203. DOI: 10.1103/PhysRevLett.111.057203.
- [103] Benjamin Doyon. “Thermalization and Pseudolocality in Extended Quantum Systems”. In: *Commun. Math. Phys.* 351.1 (2017), pp. 155–200. DOI: 10.1007/s00220-017-2836-7.
- [104] Sanjay Moudgalya, Nicolas Regnault, and B. Andrei Bernevig. “ $\eta$ -Pairing in Hubbard Models: From Spectrum Generating Algebras to Quantum Many-Body Scars”. In: *Phys. Rev. B* 102.8 (2020), p. 085140. DOI: 10.1103/PhysRevB.102.085140.
- [105] K. Kikoin, Y. Avishai, and M. N. Kiselev. “Dynamical Symmetries in Nanophysics”. In: *arXiv:cond-mat/0407063* (2004). arXiv: cond-mat/0407063. URL: <http://arxiv.org/abs/cond-mat/0407063>.
- [106] Marko Medenjak, Berislav Buča, and Dieter Jaksch. “Isolated Heisenberg Magnet as a Quantum Time Crystal”. In: *Phys. Rev. B* 102.4 (2020), p. 041117. DOI: 10.1103/PhysRevB.102.041117.

- [107] Bruno Gruber and Takaharu Otsuka, eds. *Symmetries in Science VII: Spectrum-Generating Algebras and Dynamic Symmetries in Physics*. Softcover reprint of the original 1st ed. 1993 edition. New York: Springer, 2012.
- [108] Francesco Iachello. “Spectrum Generating Algebras and Dynamic Symmetries”. In: *Lie Algebras and Applications*. Ed. by Francesco Iachello. Lecture Notes in Physics. Berlin, Heidelberg: Springer, 2006, pp. 163–172. DOI: 10.1007/3-540-36239-8\_11.
- [109] Arno Bohm, Asim Orhan, and Yuval Ne’eman. *Dynamical Groups and Spectrum Generating Algebras*. World Scientific, 1988. URL: <https://www.worldscientific.com/worldscibooks/10.1142/0299#t=toc>.
- [110] Berislav Buca et al. “Quantum Many-Body Attractors”. In: *arXiv:2008.11166 [cond-mat, physics:nlin, physics:quant-ph]* (2020). arXiv: 2008.11166 [cond-mat, physics:nlin, physics:quant-ph]. URL: <http://arxiv.org/abs/2008.11166>.
- [111] Berislav Buča and Tomaž Prosen. “A Note on Symmetry Reductions of the Lindblad Equation: Transport in Constrained Open Spin Chains”. In: *New J. Phys.* 14.7 (2012), p. 073007. DOI: 10.1088/1367-2630/14/7/073007.
- [112] Victor V. Albert. “Lindbladians with Multiple Steady States: Theory and Applications”. PhD thesis. Yale University, 2018. arXiv: 1802.00010. URL: <http://arxiv.org/abs/1802.00010>.
- [113] Bernhard Baumgartner and Heide Narnhofer. “Analysis of Quantum Semigroups with GKS–Lindblad Generators: II. General”. In: *J. Phys. A: Math. Theor.* 41.39 (2008), p. 395303. DOI: 10.1088/1751-8113/41/39/395303.
- [114] Bernhard Baumgartner, Heide Narnhofer, and Walter Thirring. “Analysis of Quantum Semigroups with GKS–Lindblad Generators: I. Simple Generators”. In: *J. Phys. A: Math. Theor.* 41.6 (2008), p. 065201. DOI: 10.1088/1751-8113/41/6/065201.
- [115] C.-E. Bardyn et al. “Topology by Dissipation”. In: *New J. Phys.* 15.8 (2013), p. 085001. DOI: 10.1088/1367-2630/15/8/085001.
- [116] V. Popkov and R. Livi. “Manipulating Energy and Spin Currents in Non-Equilibrium Systems of Interacting Qubits”. In: *New J. Phys.* 15.2 (2013), p. 023030. DOI: 10.1088/1367-2630/15/2/023030.
- [117] Mazyar Mirrahimi et al. “Dynamically Protected Cat-Qubits: A New Paradigm for Universal Quantum Computation”. In: *New J. Phys.* 16.4 (2014), p. 045014. DOI: 10.1088/1367-2630/16/4/045014.
- [118] Daniel A. Lidar and K. Birgitta Whaley. “Decoherence-Free Subspaces and Subsystems”. In: *Irreversible Quantum Dynamics*. Ed. by Fabio Benatti and Roberto Floreanini. Lecture Notes in Physics. Berlin, Heidelberg: Springer, 2003, pp. 83–120. DOI: 10.1007/3-540-44874-8\_5.
- [119] Berislav Buča, Joseph Tindall, and Dieter Jaksch. “Non-Stationary Coherent Quantum Many-Body Dynamics through Dissipation”. In: *Nat Commun* 10.1 (2019), p. 1730. DOI: 10.1038/s41467-019-09757-y.

- [120] J. Tindall et al. “Quantum Synchronisation Enabled by Dynamical Symmetries and Dissipation”. In: *New J. Phys.* 22.1 (2020), p. 013026. DOI: 10.1088/1367-2630/ab60f5.
- [121] L.d. Faddeev. “Algebraic Aspects of the Bethe Ansatz”. In: *Int. J. Mod. Phys. A* 10.13 (1995), pp. 1845–1878. DOI: 10.1142/S0217751X95000905.
- [122] Anatoli Polkovnikov et al. “Colloquium: Nonequilibrium Dynamics of Closed Interacting Quantum Systems”. In: *Rev. Mod. Phys.* 83.3 (2011), pp. 863–883. DOI: 10.1103/RevModPhys.83.863.
- [123] Fabio Franchini. *An Introduction to Integrable Techniques for One-Dimensional Quantum Systems*. 1st ed. 2017 edition. New York, NY: Springer, 2017.
- [124] H. Bethe. “Zur Theorie der Metalle”. In: *Z. Physik* 71.3 (1931), pp. 205–226. DOI: 10.1007/BF01341708.
- [125] Mariya V. Medvedyeva, Fabian H. L. Essler, and Tomaž Prosen. “Exact Bethe Ansatz Spectrum of a Tight-Binding Chain with Dephasing Noise”. In: *Phys. Rev. Lett.* 117.13 (2016), p. 137202. DOI: 10.1103/PhysRevLett.117.137202.
- [126] Aleksandra A. Ziolkowska and Fabian Essler. “Yang-Baxter Integrable Lindblad Equations”. In: *SciPost Physics* 8.3 (2020), p. 044. DOI: 10.21468/SciPostPhys.8.3.044.
- [127] Naoyuki Shibata and Hosho Katsura. “Dissipative Spin Chain as a Non-Hermitian Kitaev Ladder”. In: *Phys. Rev. B* 99.17 (2019), p. 174303. DOI: 10.1103/PhysRevB.99.174303.
- [128] Naoyuki Shibata and Hosho Katsura. “Dissipative Quantum Ising Chain as a Non-Hermitian Ashkin-Teller Model”. In: *Phys. Rev. B* 99.22 (2019), p. 224432. DOI: 10.1103/PhysRevB.99.224432.
- [129] Jacopo De Nardis et al. “Correlation Functions and Transport Coefficients in Generalised Hydrodynamics”. In: *arXiv:2104.04462 [cond-mat, physics:math-ph]* (2021). arXiv: 2104.04462 [cond-mat, physics:math-ph]. URL: <http://arxiv.org/abs/2104.04462>.
- [130] B. Bertini et al. “Finite-Temperature Transport in One-Dimensional Quantum Lattice Models”. In: *Rev. Mod. Phys.* 93.2 (2021), p. 025003. DOI: 10.1103/RevModPhys.93.025003.
- [131] Maxime Dupont and Joel E. Moore. “Universal Spin Dynamics in Infinite-Temperature One-Dimensional Quantum Magnets”. In: *Phys. Rev. B* 101.12 (2020), p. 121106. DOI: 10.1103/PhysRevB.101.121106.
- [132] Žiga Krajnik and Tomaz Prosen. “Kardar-Parisi-Zhang Physics in Integrable Rotationally Symmetric Dynamics on Discrete Space-Time Lattice.” In: *Journal of Statistical Physics* 179.1 (2020), pp. 110–131. URL: <https://go.gale.com/ps/i.do?p=AONE&sw=w&issn=00224715&v=2.1&it=r&id=GALE%7CA619871463&sid=googleScholar&linkaccess=abs>.
- [133] Žiga Krajnik, Enej Ilievski, and Tomaž Prosen. “Integrable Matrix Models in Discrete Space-Time”. In: (2020). URL: <https://scipost.org/submissions/2003.05957v2/>.

- [134] Jacopo De Nardis et al. “Superdiffusion from Emergent Classical Solitons in Quantum Spin Chains”. In: *Phys. Rev. Lett.* 125.7 (2020), p. 070601. DOI: 10.1103/PhysRevLett.125.070601.
- [135] Bruno Bertini et al. “Transport in Out-of-Equilibrium  $XXZ$  Chains: Exact Profiles of Charges and Currents”. In: *Phys. Rev. Lett.* 117.20 (2016), p. 207201. DOI: 10.1103/PhysRevLett.117.207201.
- [136] Olalla A. Castro-Alvaredo, Benjamin Doyon, and Takato Yoshimura. “Emergent Hydrodynamics in Integrable Quantum Systems Out of Equilibrium”. In: *Phys. Rev. X* 6.4 (2016), p. 041065. DOI: 10.1103/PhysRevX.6.041065.
- [137] Anastasia Doikou et al. “Introduction to Quantum Integrability”. In: *Int. J. Mod. Phys. A* 25.17 (2010), pp. 3307–3351. DOI: 10.1142/S0217751X10049803.
- [138] Stijn J. van Tongeren. “Introduction to the Thermodynamic Bethe Ansatz”. In: *J. Phys. A: Math. Theor.* 49.32 (2016), p. 323005. DOI: 10.1088/1751-8113/49/32/323005.
- [139] Per F. Dahl. “Kamerlingh Onnes and the Discovery of Superconductivity: The Leyden Years, 1911-1914”. In: *Historical Studies in the Physical Sciences* 15.1 (1984), pp. 1–37. DOI: 10.2307/27757541.
- [140] J. Bardeen, L. N. Cooper, and J. R. Schrieffer. “Microscopic Theory of Superconductivity”. In: *Phys. Rev.* 106.1 (1957), pp. 162–164. DOI: 10.1103/PhysRev.106.162.
- [141] Christiaan Huygens. *Christiaan Huygens’ the Pendulum Clock or Geometrical Demonstrations Concerning the Motion of Pendula As Applied to Clocks*. Trans. by Richard J. Blackwell. Ames: Iowa State Pr, 1986.
- [142] Steven H. Strogatz. *Nonlinear Dynamics And Chaos: With Applications To Physics, Biology, Chemistry, And Engineering*. 1st edition. Cambridge, Mass: CRC Press, 2000.
- [143] Arkady Pikovsky et al. *Synchronization: A Universal Concept in Nonlinear Sciences*. Cambridge University Press, 2003.
- [144] Alexandre Roulet and Christoph Bruder. “Quantum Synchronization and Entanglement Generation”. In: *Phys. Rev. Lett.* 121.6 (2018), p. 063601. DOI: 10.1103/PhysRevLett.121.063601.
- [145] Alexandre Roulet and Christoph Bruder. “Synchronizing the Smallest Possible System”. In: *Phys. Rev. Lett.* 121.5 (2018), p. 053601. DOI: 10.1103/PhysRevLett.121.053601.
- [146] G. L. Giorgi et al. “Spontaneous Synchronization and Quantum Correlation Dynamics of Open Spin Systems”. In: *Phys. Rev. A* 88.4 (2013), p. 042115. DOI: 10.1103/PhysRevA.88.042115.
- [147] A. A. Michailidis et al. “Stabilizing Two-Dimensional Quantum Scars by Deformation and Synchronization”. In: *Phys. Rev. Research* 2.2 (2020), p. 022065. DOI: 10.1103/PhysRevResearch.2.022065. arXiv: 2003.02825.
- [148] Gian Luca Giorgi, Fernando Galve, and Roberta Zambrini. “Probing the Spectral Density of a Dissipative Qubit via Quantum Synchronization”. In: *Phys. Rev. A* 94.5 (2016), p. 052121. DOI: 10.1103/PhysRevA.94.052121.

- [149] G. Karpát, İ. Yalçınkaya, and B. Çakmak. “Quantum Synchronization of Few-Body Systems under Collective Dissipation”. In: *Phys. Rev. A* 101.4 (2020), p. 042121. DOI: 10.1103/PhysRevA.101.042121.
- [150] Albert Cabot, Gian Luca Giorgi, and Roberta Zambrini. “Synchronization and Coalescence in a Dissipative Two-Qubit System”. In: *Proc. R. Soc. A* 477.2249 (2021), p. 20200850. DOI: 10.1098/rspa.2020.0850. arXiv: 1912.10984.
- [151] Albert Cabot et al. “Quantum Synchronization in Dimer Atomic Lattices”. In: *Phys. Rev. Lett.* 123.2 (2019), p. 023604. DOI: 10.1103/PhysRevLett.123.023604.
- [152] B. Bellomo et al. “Quantum Synchronization as a Local Signature of Super- and Subradiance”. In: *Phys. Rev. A* 95.4 (2017), p. 043807. DOI: 10.1103/PhysRevA.95.043807.
- [153] Marco Cattaneo et al. “Bath-Induced Collective Phenomena on Superconducting Qubits: Synchronization, Subradiance, and Entanglement Generation”. In: *ANNALEN DER PHYSIK* 533.5 (2021), p. 2100038. DOI: 10.1002/andp.202100038. arXiv: 2005.06229.
- [154] Stefan Siwiak-Jaszek and Alexandra Olaya-Castro. “Transient Synchronisation and Quantum Coherence in a Bio-Inspired Vibronic Dimer”. In: *Faraday Discuss.* 216.0 (2019), pp. 38–56. DOI: 10.1039/C9FD00006B.
- [155] Göktuğ Karpát et al. “Synchronization and Non-Markovianity in Open Quantum Systems”. In: *Phys. Rev. A* 103.6 (2021), p. 062217. DOI: 10.1103/PhysRevA.103.062217. arXiv: 2008.03310.
- [156] Martin Koppenhöfer, Christoph Bruder, and Alexandre Roulet. “Quantum Synchronization on the IBM Q System”. In: *Phys. Rev. Research* 2.2 (2020), p. 023026. DOI: 10.1103/PhysRevResearch.2.023026.
- [157] Mark E. Ladd et al. “Pros and Cons of Ultra-High-Field MRI/MRS for Human Application”. In: *Progress in Nuclear Magnetic Resonance Spectroscopy* 109 (2018), pp. 1–50. DOI: 10.1016/j.pnmrs.2018.06.001.
- [158] A. P. Pljonkin. “Vulnerability of the Synchronization Process in the Quantum Key Distribution System”. In: *International Journal of Cloud Applications and Computing (IJCAC)* 9.1 (2019), pp. 50–58. DOI: 10.4018/IJCAC.2019010104.
- [159] Peng Liu et al. “Secure and Efficient Synchronization Scheme for Quantum Key Distribution”. In: *OSA Continuum, OSAC* 2.10 (2019), pp. 2883–2890. DOI: 10.1364/OSAC.2.002883.
- [160] Anton Pljonkin, Konstantin Rumyantsev, and Pradeep Kumar Singh. “Synchronization in Quantum Key Distribution Systems”. In: *Cryptography* 1.3 (2017), p. 18. DOI: 10.3390/cryptography1030018.
- [161] Frank Wilczek. “Quantum Time Crystals”. In: *Phys. Rev. Lett.* 109.16 (2012), p. 160401. DOI: 10.1103/PhysRevLett.109.160401.
- [162] Haruki Watanabe and Masaki Oshikawa. “Absence of Quantum Time Crystals”. In: *Phys. Rev. Lett.* 114.25 (2015), p. 251603. DOI: 10.1103/PhysRevLett.114.251603.

- [163] Vedika Khemani, Roderich Moessner, and S. L. Sondhi. “A Brief History of Time Crystals”. In: *arXiv e-prints* 1910 (2019), arXiv:1910.10745. URL: <http://adsabs.harvard.edu/abs/2019arXiv191010745K>.
- [164] Haruki Watanabe, Masaki Oshikawa, and Tohru Koma. “Proof of the Absence of Long-Range Temporal Orders in Gibbs States”. In: *J Stat Phys* 178.4 (2020), pp. 926–935. DOI: 10.1007/s10955-019-02471-5.
- [165] Berislav Buča. “Local Hilbert Space Fragmentation and Out-of-Time-Ordered Crystals”. In: *arXiv:2108.13411 [cond-mat, physics:math-ph, physics:quant-ph]* (2021). arXiv: 2108.13411 [cond-mat, physics:math-ph, physics:quant-ph]. URL: <http://arxiv.org/abs/2108.13411>.
- [166] Dominic V. Else, Bela Bauer, and Chetan Nayak. “Floquet Time Crystals”. In: *Phys. Rev. Lett.* 117.9 (2016), p. 090402. DOI: 10.1103/PhysRevLett.117.090402.
- [167] Achilleas Lazarides, Arnab Das, and Roderich Moessner. “Periodic Thermodynamics of Isolated Quantum Systems”. In: *Phys. Rev. Lett.* 112.15 (2014), p. 150401. DOI: 10.1103/PhysRevLett.112.150401.
- [168] Wing Chi Yu et al. “Discrete Time Crystal in Globally Driven Interacting Quantum Systems without Disorder”. In: *Phys. Rev. A* 99.3 (2019), p. 033618. DOI: 10.1103/PhysRevA.99.033618.
- [169] Achilleas Lazarides et al. “Time Crystallinity in Dissipative Floquet Systems”. In: *Phys. Rev. Research* 2.2 (2020), p. 022002. DOI: 10.1103/PhysRevResearch.2.022002.
- [170] E. I. Rodríguez Chiacchio and A. Nunnenkamp. “Dissipation-Induced Instabilities of a Spinor Bose-Einstein Condensate Inside an Optical Cavity”. In: *Phys. Rev. Lett.* 122.19 (2019), p. 193605. DOI: 10.1103/PhysRevLett.122.193605.
- [171] Ching-Kit Chan, Tony E. Lee, and Sarang Gopalakrishnan. “Limit-Cycle Phase in Driven-Dissipative Spin Systems”. In: *Phys. Rev. A* 91.5 (2015), p. 051601. DOI: 10.1103/PhysRevA.91.051601.
- [172] F. M. Gambetta et al. “Classical Stochastic Discrete Time Crystals”. In: *Phys. Rev. E* 100.6 (2019), p. 060105. DOI: 10.1103/PhysRevE.100.060105.
- [173] Toni L. Heuguel et al. “Classical Many-Body Time Crystals”. In: *Phys. Rev. Lett.* 123.12 (2019), p. 124301. DOI: 10.1103/PhysRevLett.123.124301.
- [174] R. Hurtado-Gutiérrez et al. “Building Continuous Time Crystals from Rare Events”. In: *Phys. Rev. Lett.* 125.16 (2020), p. 160601. DOI: 10.1103/PhysRevLett.125.160601.
- [175] J. Zhang et al. “Observation of a Discrete Time Crystal”. In: *Nature* 543.7644 (2017), pp. 217–220. DOI: 10.1038/nature21413.
- [176] J. Smits et al. “Observation of a Space-Time Crystal in a Superfluid Quantum Gas”. In: *Phys. Rev. Lett.* 121.18 (2018), p. 185301. DOI: 10.1103/PhysRevLett.121.185301.
- [177] Jared Rovny, Robert L. Blum, and Sean E. Barrett. “Observation of Discrete-Time-Crystal Signatures in an Ordered Dipolar Many-Body System”. In: *Phys. Rev. Lett.* 120.18 (2018), p. 180603. DOI: 10.1103/PhysRevLett.120.180603.

- [178] Hans Keßler et al. “Observation of a Dissipative Time Crystal”. In: *Phys. Rev. Lett.* 127.4 (2021), p. 043602. DOI: 10.1103/PhysRevLett.127.043602.
- [179] Xiao Mi et al. “Observation of Time-Crystalline Eigenstate Order on a Quantum Processor”. In: *arXiv:2107.13571 [cond-mat, physics:quant-ph]* (2021). arXiv: 2107.13571 [cond-mat, physics:quant-ph]. URL: <http://arxiv.org/abs/2107.13571>.
- [180] S. Autti et al. “AC Josephson Effect between Two Superfluid Time Crystals”. In: *Nat. Mater.* 20.2 (2021), pp. 171–174. DOI: 10.1038/s41563-020-0780-y.
- [181] “Time Crystal Discovery Could Change the Future of Quantum Computing”. In: *Inverse* (2020). URL: <https://www.inverse.com/innovation/time-crystals-quantum-computing-study>.
- [182] Michio Jimbo. *Yang-Baxter Equation in Integrable Systems*. World Scientific, 1990.
- [183] V. E. Korepin, N. M. Bogoliubov, and A. G. Izergin. *Quantum Inverse Scattering Method and Correlation Functions*. Cambridge: Cambridge University Press, 1997.
- [184] V. I. Arnol’d. *Mathematical Methods of Classical Mechanics (Graduate Texts in Mathematics): 60*. Trans. by K. Vogtmann and A. Weinstein. 1989. Corr. 4th edition. New York: Springer, 1997.
- [185] Mark J. Ablowitz et al. “The Inverse Scattering Transform-Fourier Analysis for Nonlinear Problems”. In: *Studies in Applied Mathematics* 53.4 (1974), pp. 249–315. DOI: 10.1002/sapm1974534249.
- [186] Vladimir A. Marchenko. “The Boundary Value Problem of Scattering Theory”. In: *Sturm-Liouville Operators and Applications*. Ed. by Vladimir A. Marchenko. Operator Theory: Advances and Applications. Basel: Birkhäuser, 1986, pp. 173–306. DOI: 10.1007/978-3-0348-5485-6\_3.
- [187] Vladimir Aleksandrovich Marchenko. “On Reconstruction of the Potential Energy from Phases of the Scattered Waves”. In: 1955.
- [188] I. Gel’fand and B. M. Levitan. “On the Determination of a Differential Equation from Its Spectral Function”. In: 1955. DOI: 10.1090/trans2/001/11.
- [189] Clifford S. Gardner et al. “Method for Solving the Korteweg-deVries Equation”. In: *Phys. Rev. Lett.* 19.19 (1967), pp. 1095–1097. DOI: 10.1103/PhysRevLett.19.1095.
- [190] Yuri I. Manin, Theo Raedschelders, and Michel Van den Bergh. *Quantum Groups and Noncommutative Geometry*. Softcover reprint of the original 2nd ed. 2018 edition. Place of publication not identified: Springer, 2018.
- [191] Rodney J. Baxter. *Exactly Solved Models in Statistical Mechanics*. Illustrated edition. Mineola, N.Y: Dover Publications Inc., 2008.
- [192] Jean-Claude Zambrini and Nenad Manojlovic. “Another Perspective on the Relation Between Classical and Quantum Integrability”. In: *Proceedings of the Third International Conference on Geometry, Integrability and Quantization 3* (2002), pp. 442–454. DOI: 10.7546/giq-3-2002-442-453.
- [193] L. D. Faddeev. *Algebraic Aspects of the Bethe Ansatz*. 1994. URL: <https://arxiv.org/abs/hep-th/9404013>.



- [194] F. C. Alcaraz et al. “Surface Exponents of the Quantum XXZ, Ashkin-Teller and Potts Models”. In: *J. Phys. A: Math. Gen.* 20.18 (1987), pp. 6397–6409. DOI: 10.1088/0305-4470/20/18/038.
- [195] N. Crampe and E. Ragoucy. “Generalized Coordinate Bethe Ansatz for Non-Diagonal Boundaries”. In: *Nuclear Physics B* 858.3 (2012), pp. 502–512. DOI: 10.1016/j.nuclphysb.2012.01.020.
- [196] Jan de Gier and Pavel Pyatov. “Bethe Ansatz for the Temperley–Lieb Loop Model with Open Boundaries”. In: *J. Stat. Mech.* 2004.03 (2004), P002–P002. DOI: 10.1088/1742-5468/2004/03/P002.
- [197] Masahiro Shiroishi and Miki Wadati. “Bethe Ansatz Equation for the Hubbard Model with Boundary Fields”. In: *J. Phys. Soc. Jpn.* 66.1 (1997), pp. 1–4. DOI: 10.1143/JPSJ.66.1.
- [198] Marius de Leeuw. “The Bethe Ansatz for  $AdS_5 \times S^5$  bound States”. In: *J. High Energy Phys.* 2009.01 (2009), pp. 005–005. DOI: 10.1088/1126-6708/2009/01/005.
- [199] Damien Simon. “Construction of a Coordinate Bethe Ansatz for the Asymmetric Simple Exclusion Process with Open Boundaries”. In: *J. Stat. Mech.* 2009.07 (2009), P07017. DOI: 10.1088/1742-5468/2009/07/P07017.
- [200] E. K. Sklyanin. “Boundary Conditions for Integrable Quantum Systems”. In: *J. Phys. A: Math. Gen.* 21.10 (1988), pp. 2375–2389. DOI: 10.1088/0305-4470/21/10/015.
- [201] Michio Jimbo. “Aq-Difference Analogue of  $U(g)$  and the Yang-Baxter Equation”. In: *Lett Math Phys* 10.1 (1985), pp. 63–69. DOI: 10.1007/BF00704588.
- [202] V. G. Drinfel’d. “Hopf Algebras and the Quantum Yang-Baxter Equation”. In: *Yang-Baxter Equation in Integrable Systems*. Vol. Volume 10. Advanced Series in Mathematical Physics. WORLD SCIENTIFIC, 1990, pp. 264–268. DOI: 10.1142/9789812798336\_0013.
- [203] C. Marboe and D. Volin. “Fast Analytic Solver of Rational Bethe Equations”. In: *J. Phys. A: Math. Theor.* 50.20 (2017), p. 204002. DOI: 10.1088/1751-8121/aa6b88.
- [204] Yunfeng Jiang and Yang Zhang. “Algebraic Geometry and Bethe Ansatz. Part I. The Quotient Ring for BAE”. In: *J. High Energy Phys.* 2018.3 (2018), p. 87. DOI: 10.1007/JHEP03(2018)087.
- [205] Michael Karbach, Kun Hu, and Gerhard Müller. “Introduction to the Bethe Ansatz II”. In: *Computers in Physics* 12.6 (1998), pp. 565–573. DOI: 10.1063/1.168740.
- [206] H. Babujian et al. “Exact Form Factors in Integrable Quantum Field Theories: The Sine-Gordon Model”. In: *Nuclear Physics B* 538.3 (1999), pp. 535–586. DOI: 10.1016/S0550-3213(98)00737-8.
- [207] Nikolai Kitanine et al. “On Determinant Representations of Scalar Products and Form Factors in the SoV Approach: The XXX Case”. In: *Journal of Physics A: Mathematical and Theoretical* 49.10 (2016), p. 104002. DOI: 10.1088/1751-8113/49/10/104002.

- [208] F. A. Smirnov. *Form Factors in Completely Integrable Models of Quantum Field Theory (Advanced Series in Mathematical Physics): 14*. Singapore ; River Edge, NJ: World Scientific Publishing Co Pte Ltd, 1990.
- [209] N. Kitanine, J. M. Maillet, and V. Terras. “Form Factors of the XXZ Heisenberg Spin-1/2 Finite Chain”. In: *Nuclear Physics B* 554.3 (1999), pp. 647–678. DOI: 10.1016/S0550-3213(99)00295-3.
- [210] O. Castro-Alvaredo and J. M. Maillet. “Form Factors of Integrable Heisenberg (Higher) Spin Chains”. In: *Journal of Physics A: Mathematical and General* 40.27 (2007), pp. 7451–7471. DOI: 10.1088/1751-8113/40/27/004.
- [211] M. Kormos, G. Mussardo, and A. Trombettoni. “One-Dimensional Lieb-Liniger Bose Gas as Nonrelativistic Limit of the Sinh-Gordon Model”. In: *Phys. Rev. A* 81.4 (2010), p. 043606. DOI: 10.1103/PhysRevA.81.043606.
- [212] Balázs Pozsgay, Willem-Victor van Gerven Oei, and Márton Kormos. “On Form Factors in Nested Bethe Ansatz Systems”. In: *J. Phys. A: Math. Theor.* 45.46 (2012), p. 465007. DOI: 10.1088/1751-8113/45/46/465007.
- [213] C. N. Yang and C. P. Yang. “Thermodynamics of a One-Dimensional System of Bosons with Repulsive Delta-Function Interaction”. In: *J. Math. Phys.* 10.7 (1969), pp. 1115–1122. DOI: 10.1063/1.1664947.
- [214] Paola Ruggiero et al. “Quantum Generalized Hydrodynamics”. In: *Phys. Rev. Lett.* 124.14 (2020), p. 140603. DOI: 10.1103/PhysRevLett.124.140603.
- [215] Daniel A. Rowlands and Austen Lamacraft. “Noisy Spins and the Richardson-Gaudin Model”. In: *Phys. Rev. Lett.* 120.9 (2018), p. 090401. DOI: 10.1103/PhysRevLett.120.090401.
- [216] Sergio Lerma-Hernández, Alvaro Rubio-García, and Jorge Dukelsky. “Trigonometric SU(N) Richardson–Gaudin Models and Dissipative Multi-Level Atomic Systems”. In: *J. Phys. A: Math. Theor.* 53.39 (2020), p. 395302. DOI: 10.1088/1751-8121/abab54.
- [217] Fabian H. L. Essler and Lorenzo Piroli. “Integrability of One-Dimensional Lindbladians from Operator-Space Fragmentation”. In: *Phys. Rev. E* 102.6 (2020), p. 062210. DOI: 10.1103/PhysRevE.102.062210.
- [218] Tomaž Prosen. “Third Quantization: A General Method to Solve Master Equations for Quadratic Open Fermi Systems”. In: *New J. Phys.* 10.4 (2008), p. 043026. DOI: 10.1088/1367-2630/10/4/043026.
- [219] Thomas H. Seligman and Tomaž Prosen. “Third Quantization”. In: *AIP Conference Proceedings* 1323.1 (2010), pp. 296–300. DOI: 10.1063/1.3537859.
- [220] Juan Mauricio Torres. “Closed-Form Solution of Lindblad Master Equations without Gain”. In: *Phys. Rev. A* 89.5 (2014), p. 052133. DOI: 10.1103/PhysRevA.89.052133.
- [221] Osamu Tsuchiya and Takashi Yamamoto. “Boundary Bound States for the Open Hubbard Chain with Boundary Fields”. In: *J. Phys. Soc. Jpn.* 66.7 (1997), pp. 1950–1953. DOI: 10.1143/JPSJ.66.1950.
- [222] S. Dür et al. “Lieb-Liniger Model of a Dissipation-Induced Tonks-Girardeau Gas”. In: *Phys. Rev. A* 79.2 (2009), p. 023614. DOI: 10.1103/PhysRevA.79.023614.

- [223] Maciej Lewenstein et al. “Ultracold Atomic Gases in Optical Lattices: Mimicking Condensed Matter Physics and Beyond”. In: *Advances in Physics* 56.2 (2007), pp. 243–379. DOI: 10.1080/00018730701223200.
- [224] Christian Gross and Immanuel Bloch. “Quantum Simulations with Ultracold Atoms in Optical Lattices”. In: *Science* 357.6355 (2017), pp. 995–1001. DOI: 10.1126/science.aal3837.
- [225] Masaya Nakagawa, Norio Kawakami, and Masahito Ueda. “Exact Liouvillian Spectrum of a One-Dimensional Dissipative Hubbard Model”. In: *Phys. Rev. Lett.* 126.11 (2021), p. 110404. DOI: 10.1103/PhysRevLett.126.110404.
- [226] C. D. Parmee and N. R. Cooper. “Phases of Driven Two-Level Systems with Nonlocal Dissipation”. In: *Phys. Rev. A* 97.5 (2018), p. 053616. DOI: 10.1103/PhysRevA.97.053616.
- [227] C. D. Parmee and N. R. Cooper. “Decay Rates and Energies of Free Magnons and Bound States in Dissipative  $XXZ$  Chains”. In: *Phys. Rev. A* 99.6 (2019), p. 063615. DOI: 10.1103/PhysRevA.99.063615.
- [228] D. Jaksch et al. “Uniting Bose-Einstein Condensates in Optical Resonators”. In: *Phys. Rev. Lett.* 86.21 (2001), pp. 4733–4736. DOI: 10.1103/PhysRevLett.86.4733.
- [229] Kristian Baumann et al. “Dicke Quantum Phase Transition with a Superfluid Gas in an Optical Cavity”. In: *Nature* 464.7293 (2010), pp. 1301–1306. DOI: 10.1038/nature09009.
- [230] Emanuele G. Dalla Torre et al. “Dissipative Preparation of Spin Squeezed Atomic Ensembles in a Steady State”. In: *Phys. Rev. Lett.* 110.12 (2013), p. 120402. DOI: 10.1103/PhysRevLett.110.120402.
- [231] Nishant Dogra et al. “Dissipation-Induced Structural Instability and Chiral Dynamics in a Quantum Gas”. In: *Science* 366.6472 (2019), pp. 1496–1499. DOI: 10.1126/science.aaw4465.
- [232] Jayson G. Cosme, Jim Skulte, and Ludwig Mathey. “Time Crystals in a Shaken Atom-Cavity System”. In: *Phys. Rev. A* 100.5 (2019), p. 053615. DOI: 10.1103/PhysRevA.100.053615.
- [233] Alan O. Jamison, Benjamin Plotkin-Swing, and Subhadeep Gupta. “Advances in Precision Contrast Interferometry with Yb Bose-Einstein Condensates”. In: *Phys. Rev. A* 90.6 (2014), p. 063606. DOI: 10.1103/PhysRevA.90.063606.
- [234] Sigmund Kohler and Fernando Sols. “Oscillatory Decay of a Two-Component Bose-Einstein Condensate”. In: *Phys. Rev. Lett.* 89.6 (2002), p. 060403. DOI: 10.1103/PhysRevLett.89.060403.
- [235] Kilian Seibold, Riccardo Rota, and Vincenzo Savona. “Dissipative Time Crystal in an Asymmetric Nonlinear Photonic Dimer”. In: *Phys. Rev. A* 101.3 (2020), p. 033839. DOI: 10.1103/PhysRevA.101.033839.
- [236] E. M. Graefe, H. J. Korsch, and A. E. Niederle. “Mean-Field Dynamics of a Non-Hermitian Bose-Hubbard Dimer”. In: *Phys. Rev. Lett.* 101.15 (2008), p. 150408. DOI: 10.1103/PhysRevLett.101.150408.

- [237] C. Lledó, Th. K. Mavrogordatos, and M. H. Szymańska. “Driven Bose-Hubbard Dimer under Nonlocal Dissipation: A Bistable Time Crystal”. In: *Phys. Rev. B* 100.5 (2019), p. 054303. DOI: 10.1103/PhysRevB.100.054303.
- [238] Wim Casteels and Michiel Wouters. “Optically Bistable Driven-Dissipative Bose-Hubbard Dimer: Gutzwiller Approaches and Entanglement”. In: *Phys. Rev. A* 95.4 (2017), p. 043833. DOI: 10.1103/PhysRevA.95.043833.
- [239] Jon Links and Katrina E. Hibberd. “Bethe Ansatz Solutions of the Bose-Hubbard Dimer”. In: *SIGMA. Symmetry, Integrability and Geometry: Methods and Applications* 2 (2006), p. 095. DOI: 10.3842/SIGMA.2006.095.
- [240] V. Z. Enol’skii et al. “Alternate Quantizations of the Discrete Self-Trapping Dimer”. In: *Phys. Scr.* 43.3 (1991), pp. 229–235. DOI: 10.1088/0031-8949/43/3/002.
- [241] J. Dukelsky, S. Pittel, and G. Sierra. “Colloquium: Exactly Solvable Richardson-Gaudin Models for Many-Body Quantum Systems”. In: *Rev. Mod. Phys.* 76.3 (2004), pp. 643–662. DOI: 10.1103/RevModPhys.76.643.
- [242] TOHRU KOMA and BRUNO NACHTERGAELE. “The Spectral Gap of the Ferromagnetic XXZ-Chain”. In: *Letters in Mathematical Physics* 40.1 (1997), pp. 1–16. DOI: 10.1023/A:1007351803403.
- [243] P. Facchi and S. Pascazio. “Quantum Zeno Subspaces”. In: *Phys. Rev. Lett.* 89.8 (2002), p. 080401. DOI: 10.1103/PhysRevLett.89.080401.
- [244] P. Facchi and S. Pascazio. “Quantum Zeno Dynamics: Mathematical and Physical Aspects”. In: *J. Phys. A: Math. Theor.* 41.49 (2008), p. 493001. DOI: 10.1088/1751-8113/41/49/493001.
- [245] Paolo Zanardi and Lorenzo Campos Venuti. “Coherent Quantum Dynamics in Steady-State Manifolds of Strongly Dissipative Systems”. In: *Phys. Rev. Lett.* 113.24 (2014), p. 240406. DOI: 10.1103/PhysRevLett.113.240406.
- [246] Vladislav Popkov et al. “Effective Quantum Zeno Dynamics in Dissipative Quantum Systems”. In: *Phys. Rev. A* 98.5 (2018), p. 052110. DOI: 10.1103/PhysRevA.98.052110.
- [247] Alan Beardon and Lisa Lorentzen. “Approximants of Śleszyński–Pringsheim Continued Fractions”. In: *Journal of Computational and Applied Mathematics* 132.2 (2001), pp. 467–477. DOI: 10.1016/S0377-0427(00)00448-9.
- [248] Mario Collura, Andrea De Luca, and Jacopo Viti. “Analytic Solution of the Domain-Wall Nonequilibrium Stationary State”. In: *Phys. Rev. B* 97.8 (2018), p. 081111. DOI: 10.1103/PhysRevB.97.081111.
- [249] Oleksandr Gamayun, Yuan Miao, and Enej Ilievski. “Domain-Wall Dynamics in the Landau-Lifshitz Magnet and the Classical-Quantum Correspondence for Spin Transport”. In: *Phys. Rev. B* 99.14 (2019), p. 140301. DOI: 10.1103/PhysRevB.99.140301.
- [250] Grégoire Misguich, Nicolas Pavloff, and Vincent Pasquier. “Domain Wall Problem in the Quantum XXZ Chain and Semiclassical Behavior Close to the Isotropic Point”. In: *SciPost Physics* 7.2 (2019), p. 025. DOI: 10.21468/SciPostPhys.7.2.025.

- [251] Mario Collura et al. “Domain Wall Melting in the Spin- $\frac{1}{2}$  XXZ Spin Chain: Emergent Luttinger Liquid with a Fractal Quasiparticle Charge”. In: *Phys. Rev. B* 102.18 (2020), p. 180409. DOI: 10.1103/PhysRevB.102.180409.
- [252] Marko Medenjak and Jacopo De Nardis. “Domain Wall Melting in Spin-1 XXZ Chains”. In: *Phys. Rev. B* 101.8 (2020), p. 081411. DOI: 10.1103/PhysRevB.101.081411.
- [253] E. M. Kessler et al. “Dissipative Phase Transition in a Central Spin System”. In: *Phys. Rev. A* 86.1 (2012), p. 012116. DOI: 10.1103/PhysRevA.86.012116.
- [254] Birger Horstmann, J. Ignacio Cirac, and Géza Giedke. “Noise-Driven Dynamics and Phase Transitions in Fermionic Systems”. In: *Phys. Rev. A* 87.1 (2013), p. 012108. DOI: 10.1103/PhysRevA.87.012108.
- [255] Elliott H. Lieb and Werner Liniger. “Exact Analysis of an Interacting Bose Gas. I. The General Solution and the Ground State”. In: *Phys. Rev.* 130.4 (1963), pp. 1605–1616. DOI: 10.1103/PhysRev.130.1605.
- [256] Elliott H. Lieb. “Exact Analysis of an Interacting Bose Gas. II. The Excitation Spectrum”. In: *Phys. Rev.* 130.4 (1963), pp. 1616–1624. DOI: 10.1103/PhysRev.130.1616.
- [257] Elliott H. Lieb, Robert Seiringer, and Jakob Yngvason. “One-Dimensional Bosons in Three-Dimensional Traps”. In: *Phys. Rev. Lett.* 91.15 (2003), p. 150401. DOI: 10.1103/PhysRevLett.91.150401.
- [258] Minoru Takahashi and Masuo Suzuki. “One-Dimensional Anisotropic Heisenberg Model at Finite Temperatures”. In: *Progress of Theoretical Physics* 48.6 (1972), pp. 2187–2209. DOI: 10.1143/PTP.48.2187.
- [259] Jacopo De Nardis et al. “Delta-Bose Gas on a Half-Line and the Kardar–Parisi–Zhang Equation: Boundary Bound States and Unbinding Transitions”. In: *J. Stat. Mech.* 2020.4 (2020), p. 043207. DOI: 10.1088/1742-5468/ab7751.
- [260] Sebastian Grijalva, Jacopo De Nardis, and Veronique Terras. “Open XXZ Chain and Boundary Modes at Zero Temperature”. In: (2019). URL: <https://scipost.org/submissions/1901.10932v4/>.
- [261] Paul Fendley. “Strong Zero Modes and Eigenstate Phase Transitions in the XYZ/Interacting Majorana Chain”. In: *J. Phys. A: Math. Theor.* 49.30 (2016), 30LT01. DOI: 10.1088/1751-8113/49/30/30LT01.
- [262] Benjamin Doyon. “Lecture Notes on Generalised Hydrodynamics”. In: *SciPost Physics Lecture Notes* (2020), p. 018. DOI: 10.21468/SciPostPhysLectNotes.18.
- [263] International Centre for Theoretical Sciences. *Generalised Hydrodynamics Lectures by Benjamin Doyon*. 2019. URL: <https://www.youtube.com/watch?v=p0WnKXJhQ3o>.
- [264] Benjamin Doyon, Herbert Spohn, and Takato Yoshimura. “A Geometric Viewpoint on Generalized Hydrodynamics”. In: *Nuclear Physics B* 926 (2018), pp. 570–583. DOI: 10.1016/j.nuclphysb.2017.12.002.
- [265] Benjamin Doyon and Takato Yoshimura. “A Note on Generalized Hydrodynamics: Inhomogeneous Fields and Other Concepts”. In: *SciPost Physics* 2.2 (2017), p. 014. DOI: 10.21468/SciPostPhys.2.2.014.

- [266] Alvise Bastianello, Vincenzo Alba, and Jean-Sébastien Caux. “Generalized Hydrodynamics with Space-Time Inhomogeneous Interactions”. In: *Phys. Rev. Lett.* 123.13 (2019), p. 130602. DOI: 10.1103/PhysRevLett.123.130602.
- [267] Alvise Bastianello, Jacopo De Nardis, and Andrea De Luca. “Generalized Hydrodynamics with Dephasing Noise”. In: *Phys. Rev. B* 102.16 (2020), p. 161110. DOI: 10.1103/PhysRevB.102.161110.
- [268] Frederik S. Møller and Jörg Schmiedmayer. “Introducing iFluid: A Numerical Framework for Solving Hydrodynamical Equations in Integrable Models”. In: (2020). URL: <https://scipost.org/submissions/2001.02547v1/>.
- [269] Isabelle Bouchoule, Benjamin Doyon, and Jerome Dubail. “The Effect of Atom Losses on the Distribution of Rapidities in the One-Dimensional Bose Gas”. In: *SciPost Physics* 9.4 (2020), p. 044. DOI: 10.21468/SciPostPhys.9.4.044.
- [270] B. Davies and V. E. Korepin. “Higher Conservation Laws for the Quantum Non-Linear Schroedinger Equation”. In: *arXiv:1109.6604 [cond-mat, physics:math-ph]* (2011). arXiv: 1109.6604 [cond-mat, physics:math-ph]. URL: <http://arxiv.org/abs/1109.6604>.
- [271] Michael Grady. “Infinite Set of Conserved Charges in the Ising Model”. In: *Phys. Rev. D* 25.4 (1982), pp. 1103–1113. DOI: 10.1103/PhysRevD.25.1103.
- [272] D. Salgado and J. L. Sanchez-Gomez. “Lindbladian Evolution with Selfadjoint Lindblad Operators as Averaged Random Unitary Evolution”. In: *arXiv:quant-ph/0208175* (2002). arXiv: quant-ph/0208175. URL: <http://arxiv.org/abs/quant-ph/0208175>.
- [273] Alvise Bastianello, Jacopo De Nardis, and Andrea De Luca. “Generalized Hydrodynamics with Dephasing Noise: Supplemental Material”. In: *Phys. Rev. B* 102.16 (2020), p. 161110. DOI: 10.1103/PhysRevB.102.161110.
- [274] Jamir Marino. *Personal Communications*. 2021.
- [275] Michael M. Wolf. *Quantum Channels & Operations: A Guided Tour*. 2012. URL: <https://www-m5.ma.tum.de/foswiki/pub/M5/Allgemeines/MichaelWolf/QChannelLecture.pdf>.
- [276] D. Burgarth et al. “Ergodic and Mixing Quantum Channels in Finite Dimensions”. In: *New J. Phys.* 15.7 (2013), p. 073045. DOI: 10.1088/1367-2630/15/7/073045.
- [277] Koki Chinzei and Tatsuhiko N. Ikeda. “Time Crystals Protected by Floquet Dynamical Symmetry in Hubbard Models”. In: *Phys. Rev. Lett.* 125.6 (2020), p. 060601. DOI: 10.1103/PhysRevLett.125.060601.
- [278] Victor V. Albert et al. “Geometry and Response of Lindbladians”. In: *Phys. Rev. X* 6.4 (2016), p. 041031. DOI: 10.1103/PhysRevX.6.041031.
- [279] Alberto Frigerio. “Quantum Dynamical Semigroups and Approach to Equilibrium”. In: *Lett Math Phys* 2.2 (1977), pp. 79–87. DOI: 10.1007/BF00398571.
- [280] Alberto Frigerio. “Stationary States of Quantum Dynamical Semigroups”. In: *Commun.Math. Phys.* 63.3 (1978), pp. 269–276. DOI: 10.1007/BF01196936.
- [281] Katarzyna Macieszczak et al. “Towards a Theory of Metastability in Open Quantum Dynamics”. In: *Phys. Rev. Lett.* 116.24 (2016), p. 240404. DOI: 10.1103/PhysRevLett.116.240404.

- [282] Tosio Kato. *Perturbation Theory for Linear Operators*. Second. Classics in Mathematics. Berlin Heidelberg: Springer-Verlag, 1995. DOI: 10.1007/978-3-642-66282-9.
- [283] N. D. Mermin and H. Wagner. “Absence of Ferromagnetism or Antiferromagnetism in One- or Two-Dimensional Isotropic Heisenberg Models”. In: *Phys. Rev. Lett.* 17.22 (1966), pp. 1133–1136. DOI: 10.1103/PhysRevLett.17.1133.
- [284] John Cardy. *Scaling and Renormalization in Statistical Physics*. Cambridge Lecture Notes in Physics. Cambridge: Cambridge University Press, 1996. DOI: 10.1017/CB09781316036440.
- [285] Lev Vidmar and Marcos Rigol. “Generalized Gibbs Ensemble in Integrable Lattice Models”. In: *J. Stat. Mech.* 2016.6 (2016), p. 064007. DOI: 10.1088/1742-5468/2016/06/064007.
- [286] Fabian H. L. Essler and Maurizio Fagotti. “Quench Dynamics and Relaxation in Isolated Integrable Quantum Spin Chains”. In: *J. Stat. Mech.* 2016.6 (2016), p. 064002. DOI: 10.1088/1742-5468/2016/06/064002.
- [287] Pablo Sala et al. “Ergodicity Breaking Arising from Hilbert Space Fragmentation in Dipole-Conserving Hamiltonians”. In: *Phys. Rev. X* 10.1 (2020), p. 011047. DOI: 10.1103/PhysRevX.10.011047.
- [288] Dominik Hahn, Paul A. McClarty, and David J. Luitz. “Information Dynamics in a Model with Hilbert Space Fragmentation”. In: (2021). URL: <https://scipost.org/submissions/2104.00692v4/>.
- [289] Loïc Herviou, Jens H. Bardarson, and Nicolas Regnault. “Many-Body Localization in a Fragmented Hilbert Space”. In: *Phys. Rev. B* 103.13 (2021), p. 134207. DOI: 10.1103/PhysRevB.103.134207.
- [290] Krzysztof Sacha and Jakub Zakrzewski. “Time Crystals: A Review”. In: *Rep. Prog. Phys.* 81.1 (2017), p. 016401. DOI: 10.1088/1361-6633/aa8b38.
- [291] Krzysztof Giergiel et al. “Topological Time Crystals”. In: *New J. Phys.* 21.5 (2019), p. 052003. DOI: 10.1088/1367-2630/ab1e5f.
- [292] D. A. Ivanov et al. “Feedback-Induced Quantum Phase Transitions Using Weak Measurements”. In: *Phys. Rev. Lett.* 124.1 (2020), p. 010603. DOI: 10.1103/PhysRevLett.124.010603.
- [293] Guido Homann, Jayson G. Cosme, and Ludwig Mathey. “Higgs Time Crystal in a High- $T_c$  Superconductor”. In: *Phys. Rev. Research* 2.4 (2020), p. 043214. DOI: 10.1103/PhysRevResearch.2.043214.
- [294] F. M. Gambetta et al. “Discrete Time Crystals in the Absence of Manifest Symmetries or Disorder in Open Quantum Systems”. In: *Phys. Rev. Lett.* 122.1 (2019), p. 015701. DOI: 10.1103/PhysRevLett.122.015701.
- [295] Bihui Zhu et al. “Dicke Time Crystals in Driven-Dissipative Quantum Many-Body Systems”. In: *New J. Phys.* 21.7 (2019), p. 073028. DOI: 10.1088/1367-2630/ab2afe.
- [296] Reuben R. W. Wang et al. “Period Doubling in Period-One Steady States”. In: *Phys. Rev. E* 97.2 (2018), p. 020202. DOI: 10.1103/PhysRevE.97.020202.

- [297] Michel Fruchart et al. “Non-Reciprocal Phase Transitions”. In: *Nature* 592.7854 (2021), pp. 363–369. DOI: 10.1038/s41586-021-03375-9.
- [298] Valerii K. Kozin and Oleksandr Kyriienko. “Quantum Time Crystals from Hamiltonians with Long-Range Interactions”. In: *Phys. Rev. Lett.* 123.21 (2019), p. 210602. DOI: 10.1103/PhysRevLett.123.210602.
- [299] Andrea Pizzi, Johannes Knolle, and Andreas Nunnenkamp. “Period- $n$  Discrete Time Crystals and Quasicrystals with Ultracold Bosons”. In: *Phys. Rev. Lett.* 123.15 (2019), p. 150601. DOI: 10.1103/PhysRevLett.123.150601.
- [300] Krzysztof Giergiel, Arkadiusz Kuroś, and Krzysztof Sacha. “Discrete Time Quasicrystals”. In: *Phys. Rev. B* 99.22 (2019), p. 220303. DOI: 10.1103/PhysRevB.99.220303.
- [301] Soonwon Choi et al. “Observation of Discrete Time-Crystalline Order in a Disordered Dipolar Many-Body System”. In: *Nature* 543.7644 (2017), pp. 221–225. DOI: 10.1038/nature21426.
- [302] Michael Schreiber et al. “Observation of Many-Body Localization of Interacting Fermions in a Quasirandom Optical Lattice”. In: *Science* 349.6250 (2015), pp. 842–845. DOI: 10.1126/science.aaa7432.
- [303] D. A. Lidar, I. L. Chuang, and K. B. Whaley. “Decoherence-Free Subspaces for Quantum Computation”. In: *Phys. Rev. Lett.* 81.12 (1998), pp. 2594–2597. DOI: 10.1103/PhysRevLett.81.2594.
- [304] F. Iemini et al. “Boundary Time Crystals”. In: *Phys. Rev. Lett.* 121.3 (2018), p. 035301. DOI: 10.1103/PhysRevLett.121.035301.
- [305] Luis Fernando dos Prazeres, Leonardo da Silva Souza, and Fernando Iemini. “Boundary Time Crystals in Collective  $d$ -Level Systems”. In: *Phys. Rev. B* 103.18 (2021), p. 184308. DOI: 10.1103/PhysRevB.103.184308. arXiv: 2102.03374.
- [306] Carlos Sánchez Muñoz et al. “Non-Stationary Dynamics and Dissipative Freezing in Squeezed Superradiance”. In: *arXiv:1903.05080 [cond-mat, physics:physics, physics:quant-ph]* (2019). arXiv: 1903.05080 [cond-mat, physics:physics, physics:quant-ph]. URL: <http://arxiv.org/abs/1903.05080>.
- [307] Elliott H. Lieb and Derek W. Robinson. “The Finite Group Velocity of Quantum Spin Systems”. In: *Commun.Math. Phys.* 28.3 (1972), pp. 251–257. DOI: 10.1007/BF01645779.
- [308] Thomas Gorin et al. “Dynamics of Loschmidt Echoes and Fidelity Decay”. In: *Physics Reports* 435.2 (2006), pp. 33–156. DOI: 10.1016/j.physrep.2006.09.003.
- [309] Markus Heyl. “Dynamical Quantum Phase Transitions: A Review”. In: *Rep. Prog. Phys.* 81.5 (2018), p. 054001. DOI: 10.1088/1361-6633/aaaf9a.
- [310] F.J. Harris. “On the Use of Windows for Harmonic Analysis with the Discrete Fourier Transform”. In: *Proceedings of the IEEE* 66.1 (1978), pp. 51–83. DOI: 10.1109/PROC.1978.10837.
- [311] Fabian H. L. Essler et al. *The One-Dimensional Hubbard Model*. Cambridge: Cambridge University Press, 2005. DOI: 10.1017/CB09780511534843.



- [312] T. Barthel and U. Schollwöck. “Dephasing and the Steady State in Quantum Many-Particle Systems”. In: *Phys. Rev. Lett.* 100.10 (2008), p. 100601. DOI: 10.1103/PhysRevLett.100.100601.
- [313] Roy M. Howard. *A Signal Theoretic Introduction to Random Processes*. Hoboken, UNITED STATES: John Wiley & Sons, Incorporated, 2015. URL: <http://ebookcentral.proquest.com/lib/oxford/detail.action?docID=1895995>.
- [314] Hendra I. Nurdin. “Quantum Stochastic Processes and the Modelling of Quantum Noise”. In: *Encyclopedia of Systems and Control*. Ed. by John Baillieul and Tariq Samad. London: Springer, 2019, pp. 1–8. DOI: 10.1007/978-1-4471-5102-9\_100160-1.
- [315] Vedika Khemani, Roderich Moessner, and S. L. Sondhi. “Comment on “Quantum Time Crystals from Hamiltonians with Long-Range Interactions””. In: *arXiv:2001.11037 [cond-mat, physics:quant-ph]* (2020). arXiv: 2001.11037 [cond-mat, physics:quant-ph]. URL: <http://arxiv.org/abs/2001.11037>.
- [316] A. Kshetrimayum et al. “Quantum Time Crystals with Programmable Disorder in Higher Dimensions”. In: *Phys. Rev. B* 103.22 (2021), p. 224205. DOI: 10.1103/PhysRevB.103.224205.
- [317] Vedika Khemani et al. “Phase Structure of Driven Quantum Systems”. In: *Phys. Rev. Lett.* 116.25 (2016), p. 250401. DOI: 10.1103/PhysRevLett.116.250401.
- [318] Christian Gogolin and Jens Eisert. “Equilibration, Thermalisation, and the Emergence of Statistical Mechanics in Closed Quantum Systems”. In: *Rep. Prog. Phys.* 79.5 (2016), p. 056001. DOI: 10.1088/0034-4885/79/5/056001.
- [319] Fabien Alet and Nicolas Laflorencie. “Many-Body Localization: An Introduction and Selected Topics”. In: *Comptes Rendus Physique. Quantum Simulation / Simulation Quantique* 19.6 (2018), pp. 498–525. DOI: 10.1016/j.crhy.2018.03.003.
- [320] Hans Keßler et al. “From a Continuous to a Discrete Time Crystal in a Dissipative Atom-Cavity System”. In: *New J. Phys.* 22.8 (2020), p. 085002. DOI: 10.1088/1367-2630/ab9fc0.
- [321] Hossein Taheri et al. “All-Optical Dissipative Discrete Time Crystals”. In: *arXiv:2012.07927 [cond-mat, physics:nlin, physics:physics]* (2021). arXiv: 2012.07927 [cond-mat, physics:nlin, physics:physics]. URL: <http://arxiv.org/abs/2012.07927>.
- [322] Albert C. J. Luo. “A Theory for Synchronization of Dynamical Systems”. In: *Communications in Nonlinear Science and Numerical Simulation* 14.5 (2009), pp. 1901–1951. DOI: 10.1016/j.cnsns.2008.07.002.
- [323] Albert C. J. Luo. *Dynamical System Synchronization*. Nonlinear Systems and Complexity. New York: Springer-Verlag, 2013. DOI: 10.1007/978-1-4614-5097-9.
- [324] K. Pyragas. “Properties of Generalized Synchronization of Chaos”. In: *NAMC* 3.1 (1998), pp. 101–129. DOI: 10.15388/NA.1998.3.0.15261.
- [325] H. Haken. “A Nonlinear Theory of Laser Noise and Coherence. I”. In: *Z. Physik* 181.1 (1964), pp. 96–124. DOI: 10.1007/BF01383921.

- [326] H. Haken. “Cooperative Phenomena in Systems Far from Thermal Equilibrium and in Nonphysical Systems”. In: *Rev. Mod. Phys.* 47.1 (1975), pp. 67–121. DOI: 10.1103/RevModPhys.47.67.
- [327] H Haken. “Analogy between Higher Instabilities in Fluids and Lasers”. In: *Physics Letters A* 53.1 (1975), pp. 77–78. DOI: 10.1016/0375-9601(75)90353-9.
- [328] H. Haken. “Synergetics: An Overview”. In: *Rep. Prog. Phys.* 52.5 (1989), pp. 515–553. DOI: 10.1088/0034-4885/52/5/001.
- [329] Peter Schuster, ed. Springer Series in Synergetics. URL: <http://www.springer.com/series/712>.
- [330] Hermann Haken and Michael Stadler, eds. *Synergetics of Cognition: Proceedings of the International Symposium at Schloß Elmau, Bavaria, June 4–8, 1989*. Springer Series in Synergetics. Berlin Heidelberg: Springer-Verlag, 1990. DOI: 10.1007/978-3-642-48779-8.
- [331] Louis M. Pecora and Thomas L. Carroll. “Synchronization in Chaotic Systems”. In: *Phys. Rev. Lett.* 64.8 (1990), pp. 821–824. DOI: 10.1103/PhysRevLett.64.821.
- [332] K. Pyragas. “Weak and Strong Synchronization of Chaos”. In: *Phys. Rev. E* 54.5 (1996), R4508–R4511. DOI: 10.1103/PhysRevE.54.R4508.
- [333] J. H. Peng et al. “Synchronizing Hyperchaos with a Scalar Transmitted Signal”. In: *Phys. Rev. Lett.* 76.6 (1996), pp. 904–907. DOI: 10.1103/PhysRevLett.76.904.
- [334] T. Kapitaniak. “Synchronization of Chaos Using Continuous Control”. In: *Phys. Rev. E* 50.2 (1994), pp. 1642–1644. DOI: 10.1103/PhysRevE.50.1642.
- [335] Meng Zhan et al. “Complete Synchronization and Generalized Synchronization of One-Way Coupled Time-Delay Systems”. In: *Phys. Rev. E* 68.3 (2003), p. 036208. DOI: 10.1103/PhysRevE.68.036208.
- [336] N. DeTal, H. Taheri, and K. Wiesenfeld. “Synchronization Behavior in a Ternary Phase Model”. In: *Chaos* 29.6 (2019), p. 063115. DOI: 10.1063/1.5097237.
- [337] Erik Mosekilde, Yuri Maistrenko, and Dmitry Postnov. *Chaotic Synchronization: Applications to Living Systems*. Vol. 42. World Scientific Series on Nonlinear Science Series A. WORLD SCIENTIFIC, 2002. DOI: 10.1142/4845.
- [338] Carsten Schäfer et al. “Synchronization in the Human Cardiorespiratory System”. In: *Phys. Rev. E* 60.1 (1999), pp. 857–870. DOI: 10.1103/PhysRevE.60.857.
- [339] Haixia Wang, Qishao Lu, and Qingyun Wang. “Bursting and Synchronization Transition in the Coupled Modified ML Neurons”. In: *Communications in Nonlinear Science and Numerical Simulation* 13.8 (2008), pp. 1668–1675. DOI: 10.1016/j.cnsns.2007.03.001.
- [340] H. G. Enjieu Kadji, J. B. Chabi Orou, and P. Wofo. “Synchronization Dynamics in a Ring of Four Mutually Coupled Biological Systems”. In: *Communications in Nonlinear Science and Numerical Simulation* 13.7 (2008), pp. 1361–1372. DOI: 10.1016/j.cnsns.2006.11.004.

- [341] Fernando Galve, Gian Luca Giorgi, and Roberta Zambrini. “Quantum Correlations and Synchronization Measures”. In: *Lectures on General Quantum Correlations and Their Applications*. Ed. by Felipe Fernandes Fanchini, Diogo de Oliveira Soares Pinto, and Gerardo Adesso. Quantum Science and Technology. Cham: Springer International Publishing, 2017, pp. 393–420. DOI: 10.1007/978-3-319-53412-1\_18.
- [342] S. Boccaletti et al. “The Synchronization of Chaotic Systems”. In: *Physics Reports* 366.1 (2002), pp. 1–101. DOI: 10.1016/S0370-1573(02)00137-0.
- [343] Gonzalo Manzano Paule. “Transient Synchronization and Quantum Correlations”. In: *Thermodynamics and Synchronization in Open Quantum Systems*. Ed. by Gonzalo Manzano Paule. Springer Theses. Cham: Springer International Publishing, 2018, pp. 179–200. DOI: 10.1007/978-3-319-93964-3\_4.
- [344] Gian Luca Giorgi et al. “Quantum Correlations and Mutual Synchronization”. In: *Phys. Rev. A* 85.5 (2012), p. 052101. DOI: 10.1103/PhysRevA.85.052101.
- [345] N. K. Pareek, Vinod Patidar, and K. K. Sud. “Discrete Chaotic Cryptography Using External Key”. In: *Physics Letters A* 309.1-2 (2003), pp. 75–82. URL: [https://www.academia.edu/28738386/Discrete\\_chaotic\\_cryptography\\_using\\_external\\_key](https://www.academia.edu/28738386/Discrete_chaotic_cryptography_using_external_key).
- [346] N. K. Pareek, Vinod Patidar, and K. K. Sud. “Cryptography Using Multiple One-Dimensional Chaotic Maps”. In: *Communications in Nonlinear Science and Numerical Simulation* 10.7 (2005), pp. 715–723. DOI: 10.1016/j.cnsns.2004.03.006.
- [347] Arman Kiani-B et al. “A Chaotic Secure Communication Scheme Using Fractional Chaotic Systems Based on an Extended Fractional Kalman Filter”. In: *Communications in Nonlinear Science and Numerical Simulation* 14.3 (2009), pp. 863–879. DOI: 10.1016/j.cnsns.2007.11.011.
- [348] Kia Fallahi, Reza Raoufi, and Hossein Khoshbin. “An Application of Chen System for Secure Chaotic Communication Based on Extended Kalman Filter and Multi-Shift Cipher Algorithm”. In: *Communications in Nonlinear Science and Numerical Simulation* 13.4 (2008), pp. 763–781. DOI: 10.1016/j.cnsns.2006.07.006.
- [349] J. A. Martínez-Nonthé et al. “Cryptosystem with One Dimensional Chaotic Maps”. In: *Computational Intelligence in Security for Information Systems*. Ed. by Álvaro Herrero and Emilio Corchado. Lecture Notes in Computer Science. Berlin, Heidelberg: Springer, 2011, pp. 190–197. DOI: 10.1007/978-3-642-21323-6\_24.
- [350] J. M. Gonzalez-Miranda. “Amplitude Envelope Synchronization in Coupled Chaotic Oscillators”. In: *Phys. Rev. E* 65.3 (2002), p. 036232. DOI: 10.1103/PhysRevE.65.036232.
- [351] Yuxiang Yang, Giulio Chiribella, and Masahito Hayashi. “Quantum Stopwatch: How to Store Time in a Quantum Memory”. In: *Proceedings of the Royal Society A: Mathematical, Physical and Engineering Sciences* 474.2213 (May 31, 2018), p. 20170773. DOI: 10.1098/rspa.2017.0773. URL: <https://royalsocietypublishing.org/doi/10.1098/rspa.2017.0773>.

- [352] Gian Luca Giorgi, Albert Cabot, and Roberta Zambrini. “Transient Synchronization in Open Quantum Systems”. In: *Advances in Open Systems and Fundamental Tests of Quantum Mechanics*. Ed. by Bassano Vacchini, Heinz-Peter Breuer, and Angelo Bassi. Cham: Springer International Publishing, 2019, pp. 73–89.
- [353] H. Eneriz et al. “Degree of Quantumness in Quantum Synchronization”. In: *Sci Rep* 9.1 (2019), p. 19933. DOI: 10.1038/s41598-019-56468-x.
- [354] Noufal Jaseem et al. “Generalized Measure of Quantum Synchronization”. In: *Phys. Rev. Research* 2.4 (2020), p. 043287. DOI: 10.1103/PhysRevResearch.2.043287.
- [355] Davide Nigro. “Invariant Neural Network Ansatz for Weakly Symmetric Open Quantum Lattices”. In: *Phys. Rev. A* 103.6 (2021), p. 062406. DOI: 10.1103/PhysRevA.103.062406.
- [356] Katarzyna Macieszczak and Dominic C. Rose. “Quantum Jump Monte Carlo Approach Simplified: Abelian Symmetries”. In: *Phys. Rev. A* 103.4 (2021), p. 042204. DOI: 10.1103/PhysRevA.103.042204.
- [357] Zh Zhang et al. “Stationary State Degeneracy of Open Quantum Systems with Non-Abelian Symmetries”. In: *J. Phys. A: Math. Theor.* 53.21 (2020), p. 215304. DOI: 10.1088/1751-8121/ab88e3.
- [358] Álvaro Parra-López and Joakim Bergli. “Synchronization in Two-Level Quantum Systems”. In: *Phys. Rev. A* 101.6 (2020), p. 062104. DOI: 10.1103/PhysRevA.101.062104.
- [359] S. Sarkar et al. “Light Scattering and Dissipative Dynamics of Many Fermionic Atoms in an Optical Lattice”. In: *Phys. Rev. A* 90.2 (2014), p. 023618. DOI: 10.1103/PhysRevA.90.023618.
- [360] K. Sponselee et al. “Dynamics of Ultracold Quantum Gases in the Dissipative Fermi–Hubbard Model”. In: *Quantum Sci. Technol.* 4.1 (2018), p. 014002. DOI: 10.1088/2058-9565/aadccd.
- [361] N. Syassen et al. “Strong Dissipation Inhibits Losses and Induces Correlations in Cold Molecular Gases”. In: *Science* 320.5881 (2008), pp. 1329–1331. DOI: 10.1126/science.1155309.
- [362] Immanuel Bloch, Jean Dalibard, and Wilhelm Zwerger. “Many-Body Physics with Ultracold Gases”. In: *Rev. Mod. Phys.* 80.3 (2008), pp. 885–964. DOI: 10.1103/RevModPhys.80.885.
- [363] Michael Köhl et al. “Fermionic Atoms in a Three Dimensional Optical Lattice: Observing Fermi Surfaces, Dynamics, and Interactions”. In: *Phys. Rev. Lett.* 94.8 (2005), p. 080403. DOI: 10.1103/PhysRevLett.94.080403.
- [364] Lindsay Sonderhouse et al. “Thermodynamics of a Deeply Degenerate SU(N)-Symmetric Fermi Gas”. In: *Nat. Phys.* 16.12 (2020), pp. 1216–1221. DOI: 10.1038/s41567-020-0986-6.
- [365] I. Titvinidze et al. “Magnetism and Domain Formation in SU(3)-Symmetric Multi-Species Fermi Mixtures”. In: *New J. Phys.* 13.3 (2011), p. 035013. DOI: 10.1088/1367-2630/13/3/035013.

- [366] Carsten Honerkamp and Walter Hofstetter. “Ultracold Fermions and the  $\mathrm{SU}(N)$  Hubbard Model”. In: *Phys. Rev. Lett.* 92.17 (2004), p. 170403. DOI: 10.1103/PhysRevLett.92.170403.
- [367] A. V. Gorshkov et al. “Two-Orbital  $\mathrm{SU}(N)$  Magnetism with Ultracold Alkaline-Earth Atoms”. In: *Nature Phys* 6.4 (2010), pp. 289–295. DOI: 10.1038/nphys1535.
- [368] Martin M. Boyd et al. “Nuclear Spin Effects in Optical Lattice Clocks”. In: *Phys. Rev. A* 76.2 (2007), p. 022510. DOI: 10.1103/PhysRevA.76.022510.
- [369] H. Pichler, A. J. Daley, and P. Zoller. “Nonequilibrium Dynamics of Bosonic Atoms in Optical Lattices: Decoherence of Many-Body States Due to Spontaneous Emission”. In: *Phys. Rev. A* 82.6 (2010), p. 063605. DOI: 10.1103/PhysRevA.82.063605.
- [370] B. Abeln et al. “Interorbital Interactions in an  $\mathrm{SU}(2)$ -Symmetric Fermi-Fermi Mixture”. In: *Phys. Rev. A* 103.3 (2021), p. 033315. DOI: 10.1103/PhysRevA.103.033315.
- [371] A. Guttridge et al. “Interspecies Thermalization in an Ultracold Mixture of Cs and Yb in an Optical Trap”. In: *Phys. Rev. A* 96.1 (2017), p. 012704. DOI: 10.1103/PhysRevA.96.012704.
- [372] Jasper S. Krauser et al. “Coherent Multi-Flavour Spin Dynamics in a Fermionic Quantum Gas”. In: *Nature Phys* 8.11 (2012), pp. 813–818. DOI: 10.1038/nphys2409.
- [373] J. S. Krauser et al. “Giant Spin Oscillations in an Ultracold Fermi Sea”. In: *Science* 343.6167 (2014), pp. 157–160. DOI: 10.1126/science.1244059.
- [374] Dan M. Stamper-Kurn and Masahito Ueda. “Spinor Bose Gases: Symmetries, Magnetism, and Quantum Dynamics”. In: *Rev. Mod. Phys.* 85.3 (2013), pp. 1191–1244. DOI: 10.1103/RevModPhys.85.1191.
- [375] Maximilian Prüfer et al. “Observation of Universal Dynamics in a Spinor Bose Gas Far from Equilibrium”. In: *Nature* 563.7730 (2018), pp. 217–220. DOI: 10.1038/s41586-018-0659-0.
- [376] Z. Chen et al. “Quantum Quench and Nonequilibrium Dynamics in Lattice-Confined Spinor Condensates”. In: *Phys. Rev. Lett.* 123.11 (2019), p. 113002. DOI: 10.1103/PhysRevLett.123.113002.
- [377] J. J. Mendoza-Arenas et al. “Beyond Mean-Field Bistability in Driven-Dissipative Lattices: Bunching-antibunching Transition and Quantum Simulation”. In: *Phys. Rev. A* 93.2 (2016), p. 023821. DOI: 10.1103/PhysRevA.93.023821.
- [378] E. T. Owen et al. “Quantum Correlations and Limit Cycles in the Driven-Dissipative Heisenberg Lattice”. In: *New J. Phys.* 20.4 (2018), p. 045004. DOI: 10.1088/1367-2630/aab7d3.
- [379] Haggai Landa, Marco Schiró, and Grégoire Misguich. “Multistability of Driven-Dissipative Quantum Spins”. In: *Phys. Rev. Lett.* 124.4 (2020), p. 043601. DOI: 10.1103/PhysRevLett.124.043601.

- [380] W. Meissner and R. Ochsenfeld. “Ein neuer Effekt bei Eintritt der Supraleitfähigkeit”. In: *Naturwissenschaften* 21.44 (1933), pp. 787–788. DOI: 10.1007/BF01504252.
- [381] F. London, H. London, and Frederick Alexander Lindemann. “The Electromagnetic Equations of the Supraconductor”. In: *Proceedings of the Royal Society of London. Series A - Mathematical and Physical Sciences* 149.866 (1935), pp. 71–88. DOI: 10.1098/rspa.1935.0048.
- [382] Tadashi Kitamura and Mochimitsu Komori. “Levitational Bearing Systems by Meissner Effect”. In: *Micro System Technologies 90*. Ed. by Herbert Reichl. Berlin, Heidelberg: Springer, 1990, pp. 826–831. DOI: 10.1007/978-3-642-45678-7\_119.
- [383] Ashok K. Agarwala. “Bearing System Employing a Superconductor Element”. US5126317A. 1992. URL: <https://patents.google.com/patent/US5126317/en>.
- [384] Xinning Hu et al. “Device and Method for Inhibiting Vibration of Superconducting Magnetic Suspension Rotor”. US20130285624A1. 2013. URL: <https://patents.google.com/patent/US20130285624/da>.
- [385] M. Mitrano et al. “Possible Light-Induced Superconductivity in K3C60 at High Temperature”. In: *Nature* 530.7591 (2016), pp. 461–464. DOI: 10.1038/nature16522.
- [386] Jure Demsar. “Light-Induced Superconductivity”. In: *Nature Phys* 12.3 (2016), pp. 202–203. DOI: 10.1038/nphys3687.
- [387] M. Budden et al. “Evidence for Metastable Photo-Induced Superconductivity in K3C60”. In: *Nat. Phys.* 17.5 (2021), pp. 611–618. DOI: 10.1038/s41567-020-01148-1.
- [388] M. Buzzi et al. “Phase Diagram for Light-Induced Superconductivity in  $\kappa\text{-ET}_{x/2}\text{-X}$ ”. In: *Phys. Rev. Lett.* 127.19 (2021), p. 197002. DOI: 10.1103/PhysRevLett.127.197002.
- [389] Stefan Kaiser. “Light-Induced Superconductivity in High-Tc Cuprates”. In: *Phys. Scr.* 92.10 (2017), p. 103001. DOI: 10.1088/1402-4896/aa8201.
- [390] D. Fausti et al. “Light-Induced Superconductivity in a Stripe-Ordered Cuprate”. In: *Science* 331.6014 (2011), pp. 189–191. DOI: 10.1126/science.1197294.
- [391] W. Hu et al. “Optically Enhanced Coherent Transport in YBa2Cu3O6.5 by Ultrafast Redistribution of Interlayer Coupling”. In: *Nature Mater* 13.7 (2014), pp. 705–711. DOI: 10.1038/nmat3963.
- [392] M. Buzzi et al. “Photomolecular High-Temperature Superconductivity”. In: *Phys. Rev. X* 10.3 (2020), p. 031028. DOI: 10.1103/PhysRevX.10.031028.
- [393] B. Liu et al. “Pump Frequency Resonances for Light-Induced Incipient Superconductivity in  $\text{YBa}_2\text{Cu}_3\text{O}_{6.5}$ ”. In: *Phys. Rev. X* 10.1 (2020), p. 011053. DOI: 10.1103/PhysRevX.10.011053.
- [394] Takashi Mori et al. “Thermalization and Prethermalization in Isolated Quantum Systems: A Theoretical Overview”. In: *J. Phys. B: At. Mol. Opt. Phys.* 51.11 (2018), p. 112001. DOI: 10.1088/1361-6455/aabcdf.

- [395] Mehrtash Babadi et al. “Theory of Parametrically Amplified Electron-Phonon Superconductivity”. In: *Phys. Rev. B* 96.1 (2017), p. 014512. DOI: 10.1103/PhysRevB.96.014512.
- [396] J. R. Coulthard et al. “Enhancement of Superexchange Pairing in the Periodically Driven Hubbard Model”. In: *Phys. Rev. B* 96.8 (2017), p. 085104. DOI: 10.1103/PhysRevB.96.085104.
- [397] J. Tindall et al. “Dynamical Order and Superconductivity in a Frustrated Many-Body System”. In: *Phys. Rev. Lett.* 125.13 (2020), p. 137001. DOI: 10.1103/PhysRevLett.125.137001.
- [398] Ola Bratteli and Derek William Robinson. *Operator Algebras and Quantum Statistical Mechanics: Equilibrium States. Models in Quantum Statistical Mechanics*. 2nd edition. New York: Springer, 1997.
- [399] L. N. Oliveira, E. K. U. Gross, and W. Kohn. “Density-Functional Theory for Superconductors”. In: *Phys. Rev. Lett.* 60.23 (1988), pp. 2430–2433. DOI: 10.1103/PhysRevLett.60.2430.
- [400] M. Lüders et al. “Ab Initio Theory of Superconductivity. I. Density Functional Formalism and Approximate Functionals”. In: *Phys. Rev. B* 72.2 (2005), p. 024545. DOI: 10.1103/PhysRevB.72.024545.
- [401] C. N. Yang. “Concept of Off-Diagonal Long-Range Order and the Quantum Phases of Liquid He and of Superconductors”. In: *Rev. Mod. Phys.* 34.4 (1962), pp. 694–704. DOI: 10.1103/RevModPhys.34.694.
- [402] Geoffrey L. Sewell. “Off-Diagonal Long-Range Order and the Meissner Effect”. In: *J Stat Phys* 61.1 (1990), pp. 415–422. DOI: 10.1007/BF01013973.
- [403] H. T. Nieh, Gang Su, and Bao-Heng Zhao. “Off-Diagonal Long-Range Order: Meissner Effect and Flux Quantization”. In: *Phys. Rev. B* 51.6 (1995), pp. 3760–3764. DOI: 10.1103/PhysRevB.51.3760.
- [404] Geoffrey L. Sewell. “Off-Diagonal Long Range Order and Superconductive Electrodynamics”. In: *Journal of Mathematical Physics* 38.4 (1997), pp. 2053–2071. DOI: 10.1063/1.532193.
- [405] Chen Ning Yang. “ $\eta$  Pairing and Off-Diagonal Long-Range Order in a Hubbard Model”. In: *Phys. Rev. Lett.* 63.19 (1989), pp. 2144–2147. DOI: 10.1103/PhysRevLett.63.2144.
- [406] Michael Tinkham. *Introduction to Superconductivity*. Courier Corporation, 2004.
- [407] Raffaele Resta. “Drude Weight and Superconducting Weight”. In: *J. Phys.: Condens. Matter* 30.41 (2018), p. 414001. DOI: 10.1088/1361-648X/aade19.
- [408] Douglas J. Scalapino, Steven R. White, and Shoucheng Zhang. “Insulator, Metal, or Superconductor: The Criteria”. In: *Phys. Rev. B* 47.13 (1993), pp. 7995–8007. DOI: 10.1103/PhysRevB.47.7995.
- [409] Spyros Sotiriadis and Pasquale Calabrese. “Validity of the GGE for Quantum Quenches from Interacting to Noninteracting Models”. In: *J. Stat. Mech.* 2014.7 (2014), P07024. DOI: 10.1088/1742-5468/2014/07/P07024.

- [410] “From the Cuprate Compounds to the Hubbard Model”. In: *Quantum Electron Liquids and High-Tc Superconductivity*. Ed. by José González et al. Lecture Notes in Physics Monographs. Berlin, Heidelberg: Springer, 1995, pp. 127–149. DOI: 10.1007/978-3-540-47678-8\_6.
- [411] W. Hanke et al. “The 3-Band Hubbard-model versus the 1-Band Model for the High-Tc Cuprates: Pairing Dynamics, Superconductivity and the Ground-State Phase Diagram”. In: *Eur. Phys. J. Spec. Top.* 188.1 (2010), pp. 15–32. DOI: 10.1140/epjst/e2010-01294-y.
- [412] Herbert Fröhlich and Nevill Francis Mott. “Theory of Electrical Breakdown in Ionic Crystals”. In: *Proceedings of the Royal Society of London. Series A - Mathematical and Physical Sciences* 160.901 (1937), pp. 230–241. DOI: 10.1098/rspa.1937.0106.
- [413] J. T. Devreese. “Fröhlich Polarons. Lecture Course Including Detailed Theoretical Derivations – 10th Edition”. In: *arXiv:1611.06122 [cond-mat]* (2020). arXiv: 1611.06122 [cond-mat]. URL: <http://arxiv.org/abs/1611.06122>.
- [414] Feliciano Giustino. “Electron-Phonon Interactions from First Principles”. In: *Rev. Mod. Phys.* 89.1 (2017), p. 015003. DOI: 10.1103/RevModPhys.89.015003.
- [415] Dmitry Abanin et al. “A Rigorous Theory of Many-Body Prethermalization for Periodically Driven and Closed Quantum Systems”. In: *Commun. Math. Phys.* 354.3 (2017), pp. 809–827. DOI: 10.1007/s00220-017-2930-x.
- [416] Shou-Cheng Zhang. “A Unified Theory Based on SO(5) Symmetry of Superconductivity and Antiferromagnetism”. In: *Science* 275.5303 (1997), pp. 1089–1096. DOI: 10.1126/science.275.5303.1089.
- [417] M. Buzzi. *Personal Communications*. 2021.
- [418] Thierry Giamarchi and B. Sriram Shastry. “Persistent Currents in a One-Dimensional Ring for a Disordered Hubbard Model”. In: *Phys. Rev. B* 51.16 (1995), pp. 10915–10922. DOI: 10.1103/PhysRevB.51.10915.
- [419] Jiajun Li et al. *Long-Range  $\eta$ -Pairing in Photodoped Mott Insulators*. Aug. 23, 2019. arXiv: 1908.08693 [cond-mat]. URL: <http://arxiv.org/abs/1908.08693>.
- [420] Daniel Burgarth et al. “Quantum Zeno Dynamics from General Quantum Operations”. In: *Quantum* 4 (2020), p. 289. DOI: 10.22331/q-2020-07-06-289.
- [421] B. Militello, M. Scala, and A. Messina. “Quantum Zeno Subspaces Induced by Temperature”. In: *Phys. Rev. A* 84.2 (2011), p. 022106. DOI: 10.1103/PhysRevA.84.022106.
- [422] Yuto Ashida et al. “Quantum Electrodynamic Control of Matter: Cavity-Enhanced Ferroelectric Phase Transition”. In: *Phys. Rev. X* 10.4 (2020), p. 041027. DOI: 10.1103/PhysRevX.10.041027.
- [423] P. Jordan and E. Wigner. “Über das Paulische Äquivalenzverbot”. In: *Z. Physik* 47.9 (1928), pp. 631–651. DOI: 10.1007/BF01331938.
- [424] C. P. Burgess, C. A. Lütken, and F. Quevedo. “Bosonization in Higher Dimensions”. In: *Physics Letters B* 336.1 (1994), pp. 18–24. DOI: 10.1016/0370-2693(94)00963-5.



- [425] Luis Huerta and Jorge Zanelli. “Bose-Fermi Transformation in Three-Dimensional Space”. In: *Phys. Rev. Lett.* 71.22 (1993), pp. 3622–3624. DOI: 10.1103/PhysRevLett.71.3622.
- [426] Hoi Chun Po. “Symmetric Jordan-Wigner Transformation in Higher Dimensions”. In: *arXiv:2107.10842 [cond-mat, physics:hep-lat, physics:hep-th]* (2021). arXiv: 2107.10842 [cond-mat, physics:hep-lat, physics:hep-th]. URL: <http://arxiv.org/abs/2107.10842>.
- [427] Djordje Radicevic. “Spin Structures and Exact Dualities in Low Dimensions”. In: *arXiv:1809.07757 [cond-mat, physics:hep-lat, physics:hep-th, physics:math-ph]* (2019). arXiv: 1809.07757 [cond-mat, physics:hep-lat, physics:hep-th, physics:math-ph]. URL: <http://arxiv.org/abs/1809.07757>.
- [428] Shi-Ju Ran et al. *Tensor Network Contractions: Methods and Applications to Quantum Many-Body Systems*. 1st ed. 2020 edition. Springer, 2020.
- [429] Pietro Silvi et al. “The Tensor Networks Anthology: Simulation Techniques for Many-Body Quantum Lattice Systems”. In: *SciPost Physics Lecture Notes* (2019), p. 008. DOI: 10.21468/SciPostPhysLectNotes.8.
- [430] Jacob C. Bridgeman and Christopher T. Chubb. “Hand-Waving and Interpretive Dance: An Introductory Course on Tensor Networks”. In: *J. Phys. A: Math. Theor.* 50.22 (2017), p. 223001. DOI: 10.1088/1751-8121/aa6dc3.
- [431] Mikel Sanz Ruiz. “Tensor Networks in Condensed Matter”. PhD thesis. Max-Planck-Institut für Quantenoptik: Technische Universität München, 2011.
- [432] Ignacio Cirac et al. “Matrix Product States and Projected Entangled Pair States: Concepts, Symmetries, and Theorems”. In: *arXiv:2011.12127 [cond-mat, physics:hep-th, physics:quant-ph]* (2021). arXiv: 2011.12127 [cond-mat, physics:hep-th, physics:quant-ph]. URL: <http://arxiv.org/abs/2011.12127>.
- [433] Masuo Suzuki. “General Theory of Fractal Path Integrals with Applications to Many-body Theories and Statistical Physics”. In: *J. Math. Phys.* 32.2 (1991), pp. 400–407. DOI: 10.1063/1.529425.
- [434] Klaus Mølmer, Yvan Castin, and Jean Dalibard. “Monte Carlo Wave-Function Method in Quantum Optics”. In: *J. Opt. Soc. Am. B, JOSAB* 10.3 (1993), pp. 524–538. DOI: 10.1364/JOSAB.10.000524.
- [435] R. Dum, P. Zoller, and H. Ritsch. “Monte Carlo Simulation of the Atomic Master Equation for Spontaneous Emission”. In: *Phys. Rev. A* 45.7 (1992), pp. 4879–4887. DOI: 10.1103/PhysRevA.45.4879.